



The
University
Of
Sheffield.

MRC

Centre for Developmental
and Biomedical Genetics

The role of the transcription factor *klf2a* in vascular biology

Peter Novodvorsky

Thesis submitted for the degree of Doctor of

Philosophy

University of Sheffield

Department of Cardiovascular Science

July 2014

post *viva voce* amendments made in December 2014

Acknowledgements

I would like to thank my supervisors, Dr Tim Chico and Dr Freek van Eeden for their continuous support, guidance and courage they provided to me during the whole course of this project. Tim and Freek are both wonderful people and I was very lucky to be their student. I am thankful to MRC who funded my clinical fellowship.

Next I would like to thank to Michaela, my wife who has supported me not only emotionally but also practically given her experience in the world of science. I still remember that Sunday afternoon back in January 2011 when she taught me in her Nottingham lab how to hold a pipette and how to make serial dilutions correctly. I have come a long way since then and I am thankful to everybody who helped me to grow scientifically and personally.

I am especially thankful to Rob Wilkinson, Stone Elworthy, Caroline Gray, Oliver Watson, Huw Jones, Richard Beniston, Eleanor Markham and everybody in the D38 and D18 labs which are great places not only to do research but also to meet extraordinary people who became friends along the way.

Abstract

Introduction: The zinc-finger transcription factor Krüppel-like factor 2 (*KLF2*) transduces physical forces of blood flow into molecular signals responsible for a wide range of biological responses. *KLF2* maintains a healthy, quiescent endothelial phenotype. I studied the expression and function of the zebrafish *KLF2* ortholog *klf2a* in vascular biology.

Materials and Methods: Expression patterns of genes were observed using Whole-mount in situ hybridisation (WISH) technique. Relative expressions of genes were investigated using reverse transcription quantitative polymerase chain reaction (RT-qPCR). Particle imaging velocimetry (PIV) method was used to measure blood flow velocities. Blood flow in zebrafish embryos was manipulated genetically and pharmacologically. Transcription Activator-Like Effector Nucleases (TALEN) were used to generate a stable *klf2a* mutant line. Western blot, mass spectrometry and immunoprecipitation techniques were used in Klf2a protein studies. *klf2a* mutant lines were crossed with several transgenic reporter lines to study the role of *klf2a* in vascular development and transcription.

Results: I reproduced and extended previous studies of spatial and temporal *klf2a* expression patterns by showing strong vascular *klf2a* expression at 3dpf and by detecting *klf2a* mRNA in subintestinal veins, the hepatic vein and neuromasts. I confirmed that this expression is dependent on blood flow. Morpholino-mediated *klf2a* knockdown had no effect on cardiac output but induced upregulation of both *cxcr4a* and *dll4* in embryonic zebrafish vasculature, although without detectable effects on vascular Notch signalling.

I generated a stable *klf2a* mutant line using TALEN mutagenesis. *klf2a* mutants are viable to adulthood and fertile and display a subtle phenotype with faster heart rate and slower aortic blood flow velocity at 3dpf when compared to controls. However, *klf2a* mutation did not reproduce published morphant phenotypes nor did it affect *cxcr4a* or *dll4* expression. The explanation for the differences between the observed *klf2a* morphant and mutant phenotypes remains unclear.

Table of Contents

Acknowledgements	i
Abstract	iii
Table of contents	v
Table of figures	x
Index of tables	xii
Abbreviations	xiii
CHAPTER 1 INTRODUCTION.....	1
1.1 ENDOTHELIAL CELLS AND SHEAR STRESS	2
1.2 THE KLF FAMILY OF TRANSCRIPTION FACTORS.....	3
1.2.1 KLF2.....	3
1.2.1.1 <i>KLF2</i> expression in human and mouse	4
1.2.1.2 <i>klf2a</i> expression in zebrafish and comparison with <i>klf2b</i>	5
1.3 MECHANOTRANSDUCTION AND <i>KLF2</i> EXPRESSION	8
1.4 FLOW DEPENDENT REGULATION OF <i>KLF2</i> EXPRESSION	11
1.5 NON FLOW-DEPENDENT REGULATION OF <i>KLF2</i>	14
1.5.1 Factors stimulating <i>KLF2</i> expression.....	14
1.6 FACTORS INHIBITING <i>KLF2</i> EXPRESSION.....	17
1.7 FUNCTIONS OF <i>KLF2</i>	18
1.7.1 Maintenance of endothelial homeostasis.....	18
1.7.1.1 Vasoregulation	21
1.7.1.2 Thromboprotection	21
1.7.1.3 Inflammation	23
1.7.1.4 Complement activation	25
1.7.1.5 Endothelial barrier function	25
1.7.1.6 Endothelial morphology and intercellular gap junctions	26
1.7.1.7 Oxidative stress	27
1.7.1.8 MicroRNA production	28
1.7.2 Haematopoietic stem cell development	28
1.7.3 T-cell and B-cell biology	29
1.7.4 Monocyte and macrophage biology	31
1.7.5 Vasculogenesis and angiogenesis.....	32
1.7.6 Valvulogenesis	37
1.8 <i>KLF4</i> AND ITS ROLE IN VASCULAR BIOLOGY	38
1.8.1 <i>klf4a</i> and <i>klf4b</i> expression patterns and functions	39
1.9 CHEMOKINE RECEPTOR CXCR4 IS INVOLVED IN COLLATERAL VESSEL FORMATION.....	40

1.10 HYPOXIA INDUCIBLE FACTOR (HIF) AND VON HIPPEL - LINDAU PROTEIN (PVHL) IN HYPOXIC SIGNALLING	41
1.11 NOTCH SIGNALLING.....	43
1.12 ZEBRAFISH AS A MODEL FOR CARDIOVASCULAR STUDIES	44
1.13 AIMS OF MY RESEARCH	47
1.14 HYPOTHESES	47
1.15 OBJECTIVES	48
CHAPTER 2 MATERIALS AND METHODS	49
2.1 ZEBRAFISH HUSBANDRY	50
2.1.1 Home Office regulations.....	50
2.1.2 Wild type zebrafish strains	50
2.1.3 Mutant zebrafish lines	50
2.1.4 Transgenic reporter lines	51
2.2 MANIPULATION WITH ZEBRAFISH.....	51
2.2.1 Embryo collection and storage.....	51
2.2.1.1 E3 medium	52
2.2.2 Morpholino microinjections.....	52
2.2.2.1 Splice blocking <i>klf2a</i> morpholino (SB <i>klf2a</i> MO)	53
2.2.2.2 Translation-blocking <i>klf2a</i> morpholino (ATG <i>klf2a</i> MO)	57
2.2.3 Tricaine treatment for anaesthesia or temporary blockage of embryonic heart contractions	60
2.2.4 Dechoriation	60
2.2.5 Fin-clipping of adult zebrafish	61
2.2.6 Fin-clipping of zebrafish embryos at 3dpf	61
2.2.7 Phenylthiourea (PTU) treatment to inhibit embryonic pigment formation	62
2.2.8 Microscopy	62
2.2.8.1 Light Microscopy	62
2.2.8.2 Fluorescence Microscopy	62
2.3 STATISTICAL ANALYSIS.....	63
2.4 MOLECULAR BIOLOGY METHODS.....	63
2.4.1 Primers design	63
2.4.2 RNA extraction	64
2.4.3 cDNA synthesis by reverse transcription (RT) of RNA	65
2.4.4 Real-time reverse transcription polymerase chain reaction (RT-qPCR).....	65
2.4.4.1 Analysis of RT-qPCR data	66
2.4.5 <i>klf2a</i> ^{sh317} mutant line cDNA sequencing.....	66
2.4.6 Genomic DNA extraction.....	67
2.4.7 <i>vhl</i> ^{hu2117} genotyping	68
2.4.8 DNA sequencing	69

2.5 MEASUREMENT OF CARDIOVASCULAR PARAMETERS	69
2.5.1 Measurement of heart rates	69
2.5.2 Blood flow velocity analysis.....	70
2.5.3 Digital motion analysis	71
2.5.4 Calculations of retrograde flow fraction (RFF)	71
2.5.5 Endothelial nuclei quantification.....	71
2.5.6 Measurements of mean fluorescence in <i>Tg(CSL:venus)qmc61</i> zebrafish line	72
2.6 WHOLE MOUNT IN SITU HYBRIDISATION (WISH).....	72
2.6.1 Synthesis of <i>klf2a</i> riboprobe.....	72
2.6.2 Synthesis of <i>klf2b</i> , <i>klf4a</i> and <i>biklf/klf4b/klf17</i> riboprobes	74
2.6.3 WISH protocol	76
2.7 TRANSCRIPTION ACTIVATOR-LIKE EFFECTOR NUCLEASES (TALEN) MUTAGENESIS PROTOCOL	78
2.7.1 Choosing a TALEN target site and TALEN design	79
2.7.2 TALEN assembly	81
2.7.2.1 TALEN assembly stage 1	81
2.7.2.2 TALEN assembly stage 2	82
2.7.3 Capped mRNA synthesis and injections into zebrafish embryos	82
2.7.4 Mutation analysis of injected embryos	83
2.7.4.1 PCR and restriction enzyme test used in <i>klf2a</i> TALEN mutagenesis	83
2.7.5 Screening for founder fish	84
2.7.6 Screening for F1 generation of heterozygous carriers.....	84
2.7.7 Experiments on F2 and F3 generation of <i>klf2a</i> mutant line	85
2.8 KLF2A PROTEIN ANALYSIS	86
2.8.1 Western blot analysis	86
2.8.2 Klf2a protein immunoprecipitation (IP).....	87
2.8.3 Mass Spectrometry	88
CHAPTER 3 KLF2A EXPRESSION PATTERNS AND MORPHOLINO - MEDIATED	
KLF2A KNOCKDOWN EXPERIMENTS	89
3.1 INTRODUCTION	90
3.2 RESULTS.....	91
3.2.1 <i>klf2a</i> expression patterns in developing zebrafish embryos	91
3.2.2 <i>klf2a</i> vascular expression is blood flow dependent.....	96
3.2.2.1 SB <i>klf2a</i> MO and ATG <i>klf2a</i> MO do not impair cardiac performance of zebrafish embryos at 48hpf	98
3.2.3 <i>cxcr4a</i> vascular expression is upregulated in a proportion of SB <i>klf2a</i> MO and ATG <i>klf2a</i> MO injected morphants at 48hpf	100
3.2.3.1 RT-qPCR data do not show any significant increase in relative <i>cxcr4a</i> expression in SB <i>klf2a</i> MO and ATG <i>klf2a</i> MO morphants at 48hpf	102

3.2.4 Does <i>klf2a</i> play a role in flow dependent regulation of Notch signalling in embryonic zebrafish vasculature?	104
3.2.4.1 <i>klf2a</i> MO morphants do not exhibit increased CSL:venus fluorescence in DA at 48hpf and 72hpf	106
3.3 DISCUSSION	108
CHAPTER 4 GENERATION OF A STABLE <i>KLF2A</i> MUTANT LINE	114
4.1 INTRODUCTION	115
4.2 RESULTS	115
4.2.1 <i>klf2a</i> targeted mutagenesis by Transcription Activator-Like Effector Nucleases (TALEN)	115
4.2.1.1 <i>klf2a</i> TALEN design	116
4.2.1.2 Test PCR across the <i>klf2a</i> TALEN target site and XcmI digest	116
4.2.1.3 <i>klf2a</i> TALEN assembly and mRNA synthesis	119
4.2.1.4 <i>klf2a</i> TALEN mRNA injections and mutation analysis of injected embryos	119
4.2.1.5 Screening for potential founder fish and identification of 4 <i>klf2a</i> mutant alleles	122
4.2.1.6 Generation of <i>klf2a</i> TALEN mutant lines	125
4.2.2 Assessment of the effects of <i>klf2a</i> mutation on <i>klf2a</i> mRNA transcription and Klf2a protein translation	128
4.2.2.1 <i>klf2a</i> ^{sh317} cDNA sequencing	128
4.2.2.2 Klf2a Western blot	130
4.2.2.3 Identification of Klf2a proteins by Mass spectrometry analysis	130
4.2.2.4 Maternal <i>klf2a</i> mRNA is not present in unfertilised zebrafish eggs	133
4.3 DISCUSSION	135
CHAPTER 5 CHARACTERISATION OF THE <i>KLF2A</i> MUTANT ZEBRAFISH LINE	139
5.1 INTRODUCTION	140
5.2 RESULTS	140
5.2.1 <i>klf2a</i> mutant zebrafish do not show any morphological abnormalities	140
5.2.2 Characterisation of cardiovascular system	143
5.2.2.1 <i>klf2a</i> mutant embryos exhibit normal vascular patterning	143
5.2.2.2 <i>klf2a</i> mutants exhibit normal AA5x angiogenesis	145
5.2.2.3 <i>klf2a</i> mutation does not affect endothelial cell numbers in ISVs and DLAV	148
5.2.2.4 <i>klf2a</i> mutant embryos exhibit decreased blood flow velocities and increased heart rates at 72hpf.	150
5.2.2.5 <i>klf2a</i> mutant embryos do not show increased vascular <i>cxcr4a</i> expression	155
5.2.2.6 Flow dependent regulation of Notch signalling is not affected in <i>klf2a</i> mutant zebrafish embryos	157
5.2.2.7 Blood flow mechanotransduction critical for aberrant angiogenic phenotype of <i>vhl</i> mutants in not affected in <i>klf2a</i> mutant zebrafish embryos	160
5.2.2.8 Blood flow dependent HSC maturation is not affected in <i>klf2a</i> mutant zebrafish embryos	162

5.2.2.9 <i>klf2b</i> is detected in vasculature of a proportion of WT and <i>klf2a</i> mutant zebrafish embryos	165
5.2.2.10 AA5x angiogenesis is not affected in <i>klf2a</i> ^{sh317} mutant embryos injected with <i>klf2b</i> MO	170
5.2.2.11 <i>klf4a</i> and <i>biklf/klf4b/klf17</i> are not expressed in the vasculature of wild type or <i>klf2a</i> mutant embryos	172
5.3 DISCUSSION	174
CHAPTER 6 GENERAL DISCUSSION	182
CHAPTER 7 REFERENCES.....	193

Table of figures

Figure 1.1 Molecular mechanisms involved in regulation of endothelial <i>KLF2</i> expression.	13
Figure 1.2 Effects of KLF2 on endothelial homeostasis.	20
Figure 2.1 Verification of <i>klf2a</i> splice-blocking morpholino, as per Nicoli, Standley et al. 2010..	55
Figure 2.2 Verification of <i>klf2a</i> splice-blocking morpholino	56
Figure 2.3 Verification of ATG <i>klf2a</i> morpholino	58
Figure 2.4 Structure of a TALEN.....	80
Figure 3.1 <i>klf2a</i> expression patterns in AB WT embryos at 24 to 48hpf.	93
Figure 3.2 <i>klf2a</i> expression patterns in AB WT embryos at 3 to 5dpf.	94
Figure 3.3 Cross sections of an AB WT zebrafish embryo at 48hpf after <i>klf2a</i> WISH.....	95
Figure 3.4 <i>klf2a</i> vascular expression is blood flow dependent.	97
Figure 3.5 Comparison of heart rates and blood flow velocities of cont MO, SB <i>klf2a</i> MO and ATG <i>klf2a</i> MO morphants at 48hpf	99
Figure 3.6 <i>cxcr4a</i> vascular expression is upregulated in a proportion of SB <i>klf2a</i> MO and ATG <i>klf2a</i> MO morphants at 48hpf.....	101
Figure 3.7 RT-qPCR from whole embryonic cDNA comparing relative expression of <i>cxcr4a</i> at 48hpf.	103
Figure 3.8 <i>dll4</i> vascular expression is upregulated in a proportion of SB <i>klf2a</i> MO and ATG <i>klf2a</i> MO morphants at 48hpf.	105
Figure 3.9 Comparison of the mean venus fluorescence in dorsal wall of DA between SB <i>klf2a</i> MO and cont MO morphants at 48hpf and 72hpf.	107
Figure 4.1 <i>klf2a</i> TALEN mutagenesis	117
Figure 4.2 Test PCR across <i>klf2a</i> TALEN mutagenesis target site.....	118
Figure 4.3 <i>klf2a</i> TALEN assembly. Control enzymatic digests and capped mRNA synthesis .	120
Figure 4.4 <i>klf2a</i> TALEN F0 generation mutation analysis.	121
Figure 4.5 Screening for potential <i>klf2a</i> TALEN founder fish.....	123
Figure 4.6 Identification of 4 <i>klf2a</i> mutant alleles.....	124
Figure 4.7 Genotyping of <i>klf2a</i> mutant zebrafish	127
Figure 4.8 <i>klf2a</i> ^{sh317} cDNA sequencing	129
Figure 4.9 Klf2a Western blot	132
Figure 4.10 Test for the presence of maternal mRNA in unfertilised zebrafish eggs	134
Figure 5.1 Comparison of wild type and <i>klf2a</i> mutant zebrafish embryos	141
Figure 5.2 Comparison of morphology of zebrafish embryonic structures with high <i>klf2a</i> expression	142
Figure 5.3 Vascular anatomy of a WT and <i>klf2a</i> ^{sh317} embryo at 3dpf	144
Figure 5.4 AA5x angiogenesis is blood flow dependent but is unaffected in <i>klf2a</i> ^{sh317} mutants	146

Figure 5.5 Quantification of endothelial cell nuclei in a region of 4 ISVs and corresponding part of DLAV: <i>klf2a</i> ^{sh317} versus WT at 3dpf	149
Figure 5.6 Comparison of heart rates and blood flow velocities of Nacre WT and <i>klf2a</i> ^{sh317} mutants at 48hpf	151
Figure 5.7 Comparison of heart rates and blood flow velocities of Nacre WT and <i>klf2</i> ^{sh317} mutants at 72hpf	152
Figure 5.8 Comparison of transvalvular blood flow patterns in Nacre WT and <i>klfa2</i> ^{sh317} embryos with retrograde flow fraction (RFF) quantifications	153
Figure 5.9 <i>klf2a</i> ^{sh317} mutant embryos do not show increased <i>cxcr4a</i> vascular expression at 48hpf.	156
Figure 5.10 <i>klf2a</i> ^{sh306/sh317} mutant embryos do not show any changes in vascular activity of Notch transcription factor CSL Venus.	158
Figure 5.11 <i>klf2a</i> ^{sh317} mutant embryos do not show increased <i>dll4</i> vascular expression at 48hpf	159
Figure 5.12 Blood flow mechanotransduction critical for <i>vhl</i> ^{-/-} angiogenic phenotype is unaffected in <i>klf2a</i> ^{sh317} mutant embryos.....	161
Figure 5.13 <i>klf2a</i> mutants do not show differences in expression of HSC marker <i>runx1</i> at 36hpf	163
Figure 5.14 <i>klf2a</i> mutants do not show differences in expression of HSC marker <i>cmyb</i> at 36hpf	164
Figure 5.15 <i>klf2b</i> expression patterns in Nacre WT and <i>klf2a</i> ^{sh317} mutants at 48hpf.....	167
Figure 5.16 <i>klf2b</i> expression patterns in Nacre WT and <i>klf2a</i> ^{sh317} mutants at 72hpf.....	169
Figure 5.17 Comparison of heart rates and AA5x angiogenesis in <i>klf2b</i> MO injected homozygous and heterozygous <i>klf2a</i> ^{sh317} carriers.....	171
Figure 5.18 Expression patterns of <i>klf4a</i> and <i>biklf/klf4b/klf17</i> in Nacre WT and <i>klf2a</i> ^{sh317} mutants at 48hpf	173
Figure 6.1 Gene tree showing phylogenetic relations of zebrafish <i>klf2a</i>	192

Index of tables

Table 1 Morpholino (MO) sequences and mechanism of action	53
Table 2 List of primers	63
Table 3 PCR programme used for <i>vhl</i> ^{hu2117} genotyping	68
Table 4 WISH riboprobes	75
Table 5 WISH reagents	77
Table 6 PCR programme used for genotyping in <i>klf2a</i> TALEN mutagenesis	84

Abbreviations

$\bar{/}$	homozygous
$+/$	heterozygous
$+/+$	wild type
3' UTR	3 prime untranslated region
AA	aortic arch / amino acid
ACE	angiotensin-converting enzyme
AD	Alzheimer's disease
AGM	aorta-gonad-mesonephros
ALM	anterior lateral mesoderm
AMPK	AMP-activated protein kinase
Ang-1/-2	angiopoietin-1/angiopoietin-2
AP-1	activator protein-1
ATF2	activating transcription factor 2
AV	atrioventricular
BDM	2,3-butanedione 2-monoxime
BMPER	bone morphogenic protein endothelial precursor cell-derived regulator
°C	degrees centigrade
CAT	catalase
CCL5	chemokine (C-C motif) ligand 5
CD	cluster of differentiation
cDNA	complementary DNA
CHT	caudal haematopoietic tissue
CNP	C-natriuretic peptide
CoDA	context-dependent assembly
CRISPR/Cas9	clustered regularly interspaced short palindromic repeats/CRISPR associated systems
CSL	CBF1/Suppressor of Hairless/LAG-1
CX37	connexin 37
CXCR4 C-X-C	chemokine receptor type 4
CV	caudal vein
DA	dorsal aorta
DEPC	dyethylpyrocarbonate
DLAV	dorsal longitudinal anastomotic vessel
DLL4 (<i>dll4</i>)	delta like ligand 4
DNA	deoxyribonucleic acid
dpf	days post fertilization
E	embryonic day (in murine embryonic development)
EC(s)	endothelial cell(s)
eGFP	enhanced green fluorescent protein
EMT	epithelial-to-mesenchymal transformation
eNOS	endothelial nitric oxide synthase
ERG	ETS-related gene
ERK5	extracellular signal-regulated kinase 5
EST	expressed sequence tag
ET1	endothelin-1
ETS	E26 transformation-specific (family of transcription factors)
F	forward
FAK	focal adhesion kinase
FLK1 (<i>flk1</i>)	fetal liver kinase
FOXO1	forkhead box protein O1
GAPDH	glyceraldehyde-3-phosphate dehydrogenase
GCLM	glutamate-cysteine ligase modifier subunit
gDNA	genomic DNA

GFP	green fluorescent protein
GGPP	geranylgeranyl pyrophosphate
GKLF	gut-enriched KLF
HAoECs	human aortic endothelial cells
HDAC5	histone deacetylase 5
HIF	hypoxia inducible factor
HMG-CoA	3-hydroxy-3-methylglutaryl-coenzyme A reductase
hnRNP-D	heterogenous nuclear ribonucleoprotein D
HO-1	heme oxygenase 1
hpf	hours post fertilisation
HSC	haematopoietic stem cell
HUVECs	human umbilical vein endothelial cells
ICM	intermediate cell mass
IFN- γ	interferon gamma
IgG	immunoglobulin G
IL-1/6/8	interleukin-1/6/8
IP	immunoprecipitation
ISH	in situ hybridisation
kDa	kilodalton
<i>kdr1</i>	kinase insert domain receptor like
KLF	Krüppel-like factor
L	left
LDL	low-density lipoprotein
LPS	lipopolysaccharide
M	molar
MABT	maleic acid buffer with tween 20 (0.1%)
mM	milimolar
μ M	micromolar
μ m	micrometer
MC	mural cell
MAPK	mitogen activated protein kinase
MCP	monocyte chemotactic protein
MEF2	myocyte enhancer factor 2
MEK5	mitogen-activated protein kinase kinase 5
min	minute
MIRL	membrane inhibitor of reactive lysis / CD59
miRs	micro RNAs
MO	morpholino
mRNA	messenger RNA
MS	mass spectrometry
NEB	New England Biolabs
NHEJ	non-homologous end joining
NICD	Notch intercellular domain
NO	nitric oxide
NQO1	NAD(P)H dehydrogenase quinone 1
oxLDL	oxidised low-density lipoprotein
PACs	proangiogenic cells
PAI-1	plasminogen activator inhibitor-1
PAR-1	protease-activated receptor-1
PCAF	p300/CBP associated factor
PCR	polymerase chain reaction
PCV	posterior cardinal vein
PDGF	platelet-derived growth factor
PECAM	platelet endothelial cell adhesion molecule
PI3K	phosphatidylinositol 3-kinase
PIV	particle imaging velocimetry
PTU	1-phenyl 2-thiourea
pVHL	von Hippel - Lindau protein

R	reverse/right
RANTES	regulated on activation, normal T-cell expressed and secreted
RFF	retrograde flow fraction
RFP	red fluorescent protein
RhoA	Ras homolog gene family member A
RNA	ribonucleic acid
RT	room temperature
RT-PCR	reverse transcription polymerase chain reaction
RT-qPCR	reverse transcription - quantitative polymerase chain reaction
RVD	repeat-variable di-residue
SDF1 α	stromal cell derived factor 1 α
SDS-PAGE	sodium dodecyl sulphate polyacrylamide gel electrophoresis
sec	second
SIRT1	sirtuin-1
SIVs	subintestinal veins
SP	single-positive
<i>tardpb</i>	transactive response DNA-binding protein
TALEN	Transcription Activator-Like Effector Nucleases
TF	tissue factor
Tgf β	transforming growth factor β
TM	thrombomodulin
TNF α	tumour necrosis factor alpha
tPA	tissue plasminogen activator inhibitor
Tregs	T regulatory cells
TXNIP	thioredoxin interacting protein
VCAM	vascular cell adhesion molecule
VE-cadherin	vascular endothelial cell cadherin
VEGF-A	vascular endothelial growth factor A
VEGFR2	vascular endothelial growth factor receptor 2
VHL	von Hippel - Lindau
VSMC	vascular smooth muscle cells
vWF	von Willebrand factor
WISH	whole mount in situ hybridisation
WT	weight/wild type
ZMP	zebrafish mutation project
ZFN	zinc finger nuclease

Gene and protein nomenclature used in this thesis follow the current nomenclature guidelines for zebrafish (ZFIN Zebrafish Nomenclature Guidelines), mouse (Mouse Genome Informatics – MGI) and human (HUGO Gene Nomenclature Committee – HGN)

Chapter 1

Introduction

Substantial parts of this chapter were published in **Genetics of Cardiovascular Disease, Vol 124, The Role of the Transcription Factor KLF2 in Vascular Development and Disease, Drs. Novodvorsky, Chico, pp. 155-188, copyright Elsevier, 2014**. Reproduced with kind permission from Elsevier Limited.

1.1 Endothelial cells and shear stress

The endothelium is critically important for maintaining vascular homeostasis and plays an important role in processes such as regulation of vascular tone, inflammation, thrombosis, vasculogenesis/angiogenesis and atherosclerosis (Folkman and Haudenschild 1980; Gimbrone 1999; Ross 1999). Endothelium forms the interface between circulating blood and the inner layers of the vessel wall and surrounding tissue. Due to this location and function, endothelial phenotype can be affected by both biomechanical or biochemical factors such as blood flow, (Topper and Gimbrone 1999) endogenous factors such as cytokines or acetylcholine (Busse, Trogisch et al. 1985; Schleef, Bevilacqua et al. 1988) or pharmacological agents (Parmar, Nambudiri et al. 2005).

Blood flow generates physical forces that act on the vessel wall. These have two major components. Shear stress is a frictional force exerted on the vessel wall with its vector parallel to the direction of flow whereas tensile stress represents a dilating force on the vessel wall with its vector perpendicular to the direction of flow (White and Frangos 2007).

It has been shown that it is not only the absolute magnitude of the shear stress but also, and more importantly, the flow pattern resulting in different shear stress wave forms that is important for the actual effects of shear stress on endothelial phenotype (Parmar, Larman et al. 2006). Atherosclerotic lesions occur in a non-random pattern and their distribution correlates with distinct types of shear stress waveforms. Arterial branch points and areas of major curvatures are associated with turbulent oscillatory flow patterns and significantly higher rates of atherosclerotic lesions when compared to sites exposed to pulsatile blood flow with laminar shear stress pattern (Gimbrone 1999; Parmar, Larman et al. 2006).

1.2 The KLF family of transcription factors

Krüppel-like factors (KLFs) are zinc finger transcription factors which were identified by their homology to the *Drosophila melanogaster* protein Krüppel (Miller and Bieker 1993). The mammalian KLF family comprises 17 members so far (van Vliet, Crofts et al. 2006). Each has 3 tandem C₂H₂ (cysteine-histidine type) zinc fingers in the C terminus of the protein with a consensus amino acid sequence F/Y-X-C-X₂₋₄-C-X₃-F-X₅-L-X₂-H-X-R/K-X-H (X represents any amino acid, underscored C and H bind zinc atoms) connected by a characteristic linker T/S-G-E-R/K-P within the deoxyribonucleic acid (DNA) binding domain. These sequences are highly conserved in the KLF gene family (Ruppert, Kinzler et al. 1988; Oates, Pratt et al. 2001). In contrast to this similarity in their DNA-binding domains, the non-DNA-binding N-termini have some common conserved motifs that act as transactivation or repression domains, but exhibit much less similarity in their primary structure (Anderson, Kern et al. 1995; Oates, Pratt et al. 2001). KLFs act as transcriptional activators and repressors and are expressed in various types of tissues (Turner and Crossley 1999). Their zinc-finger motifs are able to bind to CG-rich sites of general structure CCN CNC CCN, such as CACCC-boxes in various promoters and enhancers (Klevit 1991; Miller and Bieker 1993).

1.2.1 KLF2

The majority of previous experimental work on KLF2 in relation to vascular biology has been performed in human and mouse with some work recently done on zebrafish animal model. *KLF2* genomic structure and expression patterns in these species will be therefore briefly detailed.

KLF2 was firstly characterised in 1995 through its homology with *EKLF/KLF1* in mice (Anderson, Kern et al. 1995), followed by its characterisation in humans in 1999 (Wani,

Conkright et al. 1999) and zebrafish in 2001 (Oates, Pratt et al. 2001). Due to its high expression in murine lung it was originally termed lung Krüppel-like factor (*LKLF*). The murine and human *KLF2* proteins are >90% identical in primary structure (Wani, Conkright et al. 1999). Zebrafish have two *KLF2* paralogs, *klf2a* and *klf2b* reflecting the partial genome duplication of the zebrafish genome after divergence of the teleost lineage during evolution (Taylor, Braasch et al. 2003). Zebrafish *klf2a* and *klf2b* are structurally related but exhibit different expression patterns and were reported to have different functions in developing zebrafish (Oates, Pratt et al. 2001). Zebrafish *klf2a* is considered to be the ortholog of human and murine *KLF2* and like these, its expression in the zebrafish vasculature is blood-flow dependent (Oates, Pratt et al. 2001).

In addition to the zinc finger containing DNA binding domain (AA 268-354) described in Section 1.2, work on murine *Klf2* constructs localised a transcriptional activation domain between amino acids (AA) 1-110 and an inhibitory domain between AA 111-267. This inhibitory domain directly interacts with the E3 ubiquitin ligase WWP1 which mediates ubiquitination and proteasomal degradation of *KLF2* (Conkright, Wani et al. 2001; Zhang, Srinivasan et al. 2004).

1.2.1.1 *KLF2* expression in human and mouse

Northern blot analysis of adult human tissues detected *KLF2* messenger ribonucleic acid (mRNA) in heart, lungs, skeletal muscle, pancreas and placenta (but not brain, liver or kidney), however, vascular tissues were not examined (Wani, Conkright et al. 1999). Human and murine *KLF2* expression patterns are generally similar (Wani, Conkright et al. 1999). Further experiments confirmed *KLF2* expression in myeloid (Das, Kumar et al. 2006) and lymphoid cells (Riley, Mao et al. 2002). ISH performed on human vascular tissues from donors of various age (13 months to 76 years) and from different anatomical sites show that *KLF2* is expressed in all sections of vasculature tested, but the signal strength differs with the predicted patterns of flow and levels of

shear stress at these sites; decreased *KLF2* expression is seen at aortic bifurcations (Dekker, van Thienen et al. 2005). These sites are generally exposed to lower shear stress levels and disturbed flow patterns with atheroprone waveforms. *KLF2* expression levels negatively correlate with the presence of neointima in human iliac vessels (Dekker, van Thienen et al. 2005). Within the vessel wall, *KLF2* is selectively expressed in endothelium (Dekker, van Soest et al. 2002; Dekker, van Thienen et al. 2005; Parmar, Larman et al. 2006). Later work showed that *KLF2* is not only expressed in endothelium of large and medium-sized vessels but also in the hepatic, duodenal and glomerular microvasculature (Gracia-Sancho, Russo et al. 2011; Kobus, Kopycinska et al. 2012; Slater, Ramnath et al. 2012).

Northern blot analysis of adult murine tissues shows highest *Klf2* expression in lungs, with some expression detected in the heart, spleen, thymus, skeletal muscle, white and brown adipose tissue and testes (Anderson, Kern et al. 1995; Kuo, Veselits et al. 1997; Banerjee, Feinberg et al. 2003). The site and level of *Klf2* expression in murine embryonic endothelial cells corresponds to the predicted pattern of shear forces in the developing vasculature and remains shear stress dependent in adult murine endothelium (Dekker, van Thienen et al. 2005; Lee, Yu et al. 2006). *Klf2* expression is detectable in endothelial cells from embryonic day 8.5 (E8.5). With onset of pulsatile blood flow between E8.5 and E10.5, *Klf2* expression rises sharply in endothelial and endocardial cells – in a pattern corresponding to elevated shear. *Klf2* expression becomes detectable only on the flow sides of the developing heart valves at E14.5, by E18.5 also in the endocardium lining the intraventricular papillary muscles (Lee, Yu et al. 2006).

1.2.1.2 *klf2a* expression in zebrafish and comparison with *klf2b*

klf2a is located on chromosome 22, has 3 exons and 2 small introns, transcript length of 2180bp, and codes for a 380 AA protein. Zebrafish *klf2a* and human *KLF2* have 49%

protein identity. The level of identity is much higher in the region of 3 tandem zinc fingers - 78% for nucleotide identity and 90% for the primary protein structure. At sphere to 30% epiboly stage, *klf2a* can be detected in the extraembryonic enveloping layer. At 70% epiboly *klf2a* becomes expressed in the ventral, animal portion of the epiblast. Expression of *klf2a* at these very early stages is under control of the transcription factor Pou5f1/Oct1 (Oates, Pratt et al. 2001; Kotkamp, Mossner et al. 2014). In later stages of epiboly *klf2a* expression extends vegetally. At 24 hours post fertilisation (hpf) *klf2a* expression is detectable in the anus, in small clusters of superficial cells lateral to the most posterior notochord, in the cells closely associated with the axial vessels (pronephric ducts), in head vessels and in the heart. This expression persists until 48hpf, when a faint signal is also detected in the distal margin of the caudal fin (the tail) and in the mesenchymal interior of the pectoral fin buds (Oates, Pratt et al. 2001; Wang, Zhang et al. 2011). Embryonic heart expression of *klf2a* becomes restricted to the AV canal in later stages (48-58hpf) (Vermot, Forouhar et al. 2009).

klf2a expression in embryonic zebrafish vasculature is, like human and mouse *KLF2*, blood flow dependent. Vascular expression of *klf2a* can be detected in trunk vasculature from around 36hpf and is still present at 48hpf – the embryonic zebrafish heart begins to contract at 24-26hpf (Kimmel, Ballard et al. 1995). Whilst endothelial *klf2a* is clearly detectable in wild type (WT) embryos, it is lost in embryos with impaired blood flow, such as troponin t2 morphant (*tnnt2*) zebrafish which have a non-contractile heart or in embryos where flow was impaired pharmacologically with the local anaesthetic Tricaine or with the myosin ATPase inhibitor 2,3-butanedione 2-monoxime (BDM) (Stainier, Fouquet et al. 1996; Sehnert, Huq et al. 2002; Parmar, Larman et al. 2006; Wang, Zhang et al. 2011).

klf2b is located on chromosome 18, has 3 exons, transcript length of 3626bp and codes for a 363 AA protein. A high degree of similarity exists between *klf2b* and *klf2a* (61% identity in both nucleotide sequences and in primary protein structure) and *klf2b* expression patterns partially overlap with *klf2a* during very early developmental stages. Later expression patterns become more distinct. Generally, *klf2b* has been far less studied than *klf2a*. *klf2b* can be detected in the ventral, animal portion of the epiblast from 30% epiboly and this expression becomes stronger in time. At 70% epiboly *klf2b* expression in ventral ectoderm is much stronger than *klf2a*. At the end of epiboly, *klf2b* expression diminishes in the animal-most one third and increases in a lateral band around the embryo. Similarly to *klf2a*, *klf2b* expression at these stages is under control of Pou5f1/Oct1 (Oates, Pratt et al. 2001; Kotkamp, Mossner et al. 2014). From 24hpf *klf2b* is expressed in large squamous epidermal cells but this expression decreases significantly by 36hpf. At this stage *klf2b* mRNA can be detected in 2 cords of superficial cells anteriorly and ventrally to pectoral fin buds. At 48hpf *klf2b* is expressed in the mesenchymal interior of the fin bud and in the cleithrum. Later on *klf2b* expression decreases in the proximal portion of the fin bud, but persists in the distal portion of the mesenchymal part of the fin to 5 days post fertilisation (dpf) (Oates, Pratt et al. 2001; Thisse 2001). *klf2b* expression in the pectoral fin bud, but not in cleithrum is under control of transcription factor *sox9* (Yokoi, Yan et al. 2009). Cardiac or vascular expression of *klf2b* has not been reported at any developmental stage.

Little is known about *klf2b* function apart from its role (together with *klf2a* and *klf4b*) in differentiation of the extraembryonic enveloping layer and ectoderm in early zebrafish developmental stages (Kotkamp, Mossner et al. 2014).

1.3 Mechanotransduction and *KLF2* expression

The term mechanotransduction refers to multiple mechanisms by which cells convert mechanical forces applied at the cell surface into alteration of gene expression and subsequent changes in cellular signalling (Mammoto, Mammoto et al. 2012). Mechanotransduction is not yet fully understood but comprises multiple components localised in cellular membranes or in the cytosol to activate several cell signalling cascades that each interact. The final cellular response is based on the character of the mechanical stimulus. Mechanical forces acting on the apical surface of an endothelial cell are transmitted through 3D-changes of microtubular cytoskeleton to cell-cell and cell-matrix junctions consisting of multiple protein complexes that transduce signals from mechanical forces further into the cell (Davies 1997). One such complex consisting of platelet endothelial cell adhesion molecule (PECAM), vascular endothelial cell cadherin (VE-cadherin) and vascular endothelial growth factor 2 receptor (VEGFR2) leads subsequently to conformational activation of integrins that mediate the alignment of endothelial cells under laminar flow conditions but also activation of the proinflammatory NF- κ B pathway (Tzima, del Pozo et al. 2001; Tzima, Del Pozo et al. 2002; Tzima, Irani-Tehrani et al. 2005).

Primary cilia are likely to play an accessory and signal-amplifying role in endothelial mechanotransduction. Primary non-motile cilia are present in ECs only exposed to low and disturbed flow patterns; ECs exposed to laminar flow shed primary cilia within several hours (Iomini, Tejada et al. 2004). Primary cilia increase EC response to laminar shear stress measured by induction of *KLF2* which is significantly higher in ciliated ECs versus non-ciliated ECs (Hierck, Van der Heiden et al. 2008). Consistent with the central role of cytoskeleton in mechanotransduction, ECs chemically depleted of microtubules (Colchicine) or ECs where the microtubular network is stabilized (Taxol/Paclitaxel) show decreased or increased *KLF2* induction by shear stress

(Hierck, Van der Heiden et al. 2008). Ultrastructurally, two ciliary proteins POLYCYSTIN-1 and POLARIS are necessary for correct shear sensing by primary cilia in ECs, resulting in changes of intracellular calcium and nitric oxide (NO) levels within the range of several seconds (Nauli, Kawanabe et al. 2008).

Other cellular components that could serve as direct shear stress sensors include the glycocalyx, adhesion molecules such as integrins, cell membrane proteins (receptor tyrosine kinases such as VEGFR2 or G protein coupled receptors), caveolae and ion channels. All these 'primary' sensors are able to transduce the signal further either biochemically through cytoplasm or through the cytoskeleton (Tarbell, Weinbaum et al. 2005; Ando and Yamamoto 2009). Immediate further steps include phosphorylation of various proteins that activate secondary signalling pathways (Davies 2009). Of particular interest in view of *KLF2* are the mitogen activated protein kinases (MAPKs) that comprise 4 signalling routes: extracellular signal-regulated kinase (ERK)1/2, ERK5, Jun NH₂-terminal kinase (JNK) and p38. MAPKs play essential roles in regulating multiple cellular processes and are responsible for transducing extracellular signals into the cells (Roberts, Holmes et al. 2009). The ERK5 signalling pathway plays a role in flow-mediated induction of *KLF2* in endothelium as detailed later.

Finally, a recent theory sees endothelial mechanotransduction as a two-step process: the first, immediate step includes ciliary bending with subsequent intracellular calcium increase and release of NO, endothelin and other vasoactive substances. In the later, prolonged response cytoskeletal deformations lead to changes in gene expression levels such as *KLF2* which then orchestrate endothelial adaptation to mechanical force (Poelmann, Van der Heiden et al. 2008).

At the time that *KLF2* was found to be regulated by flow it was the first endothelial transcription factor reported to have this characteristic (Dekker, van Soest et al. 2002). In human umbilical vein endothelial cells (HUVECs) exposed to 24 hours of laminar

flow (25 dyne/cm²) *KLF2* was one of 12 genes (from 18 000) identified to have at least 5-fold increased expression compared to static culture. Following this, HUVECs were exposed to unidirectional pulsatile flow (19 ±12 dyne/cm²) for another 7 days and only 3 of these 12 genes sustained at least 5-fold increased expression, including *KLF2* (the remaining two being cytochrome P450 1B1 and diaphorase 4). The fact that pulsatile flow resulted in an additional 3-fold increase in *KLF2* expression indicates that not only the absolute size of shear stress but also the flow pattern determines *KLF2* expression (Dekker, van Soest et al. 2002). Further experiments confirmed that regulation of *KLF2* depends on the pattern of flow. HUVECs exposed to 24 hours of pulsatile shear with large net forward direction (12±4 dyne/cm²) exhibit a significant increase in *KLF2* expression. HUVECs exposed to oscillatory, atheroprone flow (1Hz 0.5±4 dyne/cm²) with low shear stress magnitude and little net forward direction show only a transient increase, followed by a continuous suppression of *KLF2* expression (Wang, Miao et al. 2006).

These *in vitro* findings have been confirmed by *in vivo* experiments in several species. *KLF2* levels in human adult vasculature correspond to local shear stress patterns as mentioned above. Similar findings are reported in mice implanted with carotid artery collars (Dekker, van Thienen et al. 2005) and in zebrafish embryos where preventing or stopping blood flow causes significant *klf2a* downregulation (Parmar, Larman et al. 2006). *Klf2* is highly expressed in rat aorta and on the medial aspect of the coeliac artery (areas exposed to high levels of laminar shear stress), but is low on the lateral aspect of coeliac artery at the branching point with aorta with atheroprone flow patterns (Wang, Miao et al. 2006). Taken together these findings confirm blood flow dependent regulation of *KLF2* in all models and species examined.

1.4 Flow dependent regulation of *KLF2* expression

Figure 1.1 summarises the mechanisms of regulation of *KLF2* transcription. The critical region required for shear stress induced expression of *KLF2* lies -157 to -95bp upstream from the transcription start site and is highly conserved across species (Huddleson, Srinivasan et al. 2004). This region contains a single consensus myocyte enhancer factor 2 (MEF2) binding site (Kumar, Lin et al. 2005). MEF2 binding to this site is not significantly affected by exposure to flow. MEF2 transactivation through its phosphorylation is however critical for shear stress induced *KLF2* upregulation and is mediated via its upstream mitogen-activated protein kinase ERK5 (Parmar, Larman et al. 2006). ERK5 is in turn specifically upregulated by its activating kinase MEK5 (also known as mitogen-activated protein kinase kinase 5) (Parmar, Larman et al. 2006). Another factor necessary for activation of the MEK5/ERK5/MEF2 pathway is AMP-activated protein kinase (AMPK). AMPK lies upstream of MEK5/ERK5/MEF2 and its activation is critical for shear stress induced phosphorylation of ERK5 and MEF2 (Young, Wu et al. 2009).

Other co-factors involved in shear stress mediated *KLF2* regulation include p300/CBP associated factor (PCAF), heterogenous nuclear ribonucleoprotein D (hnRNP-D) and nucleolin (Huddleson, Ahmad et al. 2005; Huddleson, Ahmad et al. 2006). PCAF and hnRNP-D induce *KLF2* promoter chromatin remodelling via acetylation of histones H3 and H4 with resulting promotion of *KLF2* expression. PCAF and hnRNP-D act through a phosphatidylinositol 3-kinase (PI3K)-dependent, but Akt-independent pathway (Huddleson, Ahmad et al. 2005).

Under static conditions or disturbed flow, histone deacetylase 5 (HDAC5) is bound to MEF2 on the *KLF2* promoter and inhibits MEF2 transcriptional activity. Sufficiently high laminar shear stress (12 dyne/cm²) phosphorylates HDAC5 in a Ca²⁺/calmodulin dependent manner resulting in its dissociation from MEF2, allowing increased flow-

dependent *KLF2* transcription (Wang, Ha et al. 2010). Oscillatory shear stress promotes expression of class I HDAC (HDAC1/2/3) and class II HDAC (HDAC3/5/7) and their association with MEF2 via PI3K/Akt pathway thus leading to downregulation of *KLF2* expression, whereas pulsatile shear stress induces phosphorylation-dependent class II HDAC (HDAC5/7) nuclear export leading to induction of *KLF2* expression (Lee, Lee et al. 2012).

Endothelial thioredoxin interacting protein (*TXNIP*) is downregulated by steady laminar flow which leads to upregulation of thioredoxin activity and subsequent inhibition of EC inflammatory response to tumour necrosis factor α (TNF α) (Yamawaki, Pan et al. 2005). Conversely, *TXNIP* is upregulated by disturbed flow and this promotes endothelial-leukocyte adhesion. *TXNIP* binds to shear responsive region of *KLF2* promoter (-157bp to -78bp) where it forms a part of a transcriptional repressing complex and inhibits *KLF2* expression (Wang, Nigro et al. 2012).

MicroRNAs (*miRs*) are small (18-24bp long) single-stranded non-coding RNAs that bind to 3 prime untranslated region (3'UTR) of their target mRNAs and thus regulate gene expression at the posttranscriptional level, either via translational inhibition or by degradation of mRNAs (Bartel 2004; Bartel 2009; Chekulaeva and Filipowicz 2009). *miRs* play a role in flow-mediated regulation of *KLF2* expression as evidenced by the fact that knockdown of the critical component of *miRs* biosynthesis pathway Dicer in HUVECs increases *KLF2* expression. 3'UTR region of *KLF2* contains a *miR-92a* binding site and it was shown that laminar flow downregulates *miR-92a* and induces *KLF2* expression, while *miR-92a* overexpression decreases expression of *KLF2* (Bonauer, Carmona et al. 2009) (**Figure 1.1**).

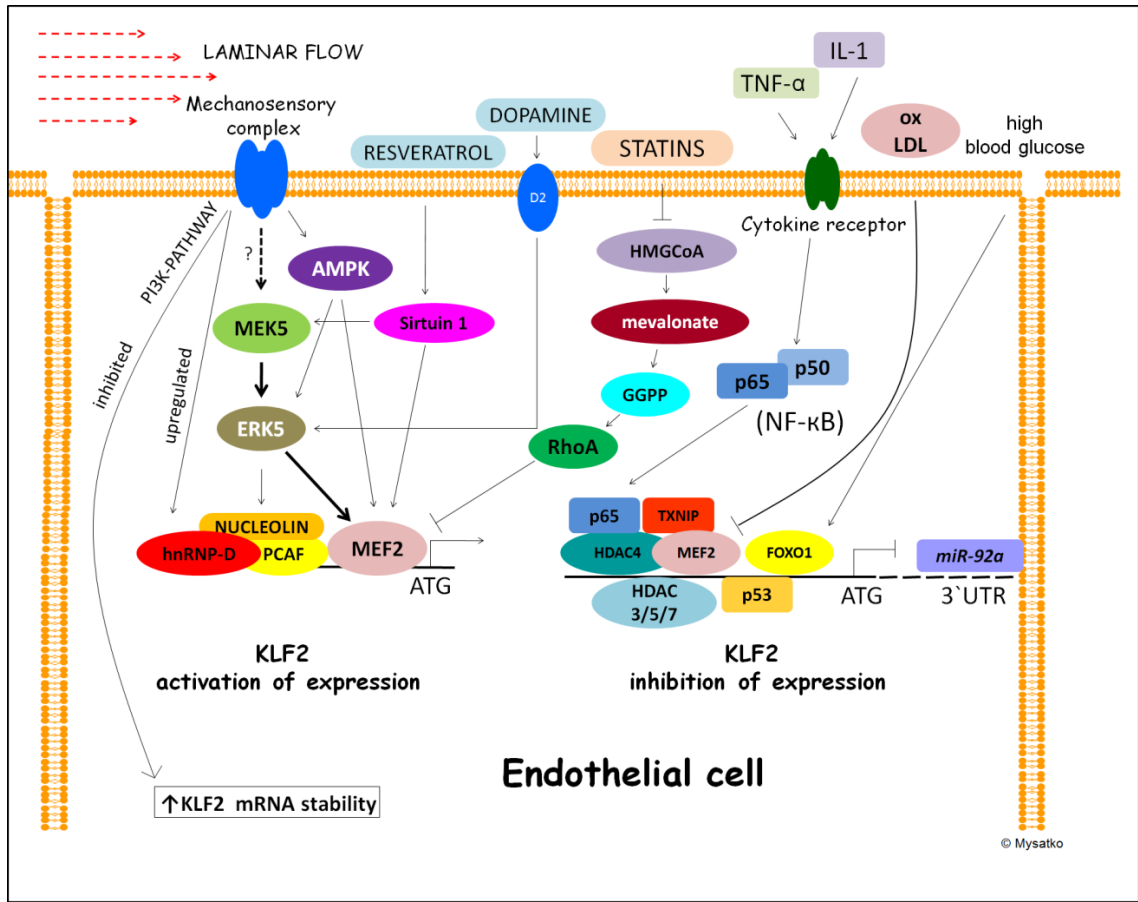


Figure 1.1 Molecular mechanisms involved in regulation of endothelial *KLF2* expression.

Schematic diagram showing factors that stimulate (left side of diagram) and suppress (right side of diagram) endothelial *KLF2* expression. Abbreviations: *KLF2*: Krüppel-like factor 2, MEK5: mitogen-activated protein kinase kinase 5, ERK5: extracellular signal-regulated kinase 5, MEF2: myocyte enhancer factor 2, AMPK: AMP-activated protein kinase, PCAF: p300/CBP associated factor, hnRNP-D: heterogeneous nuclear ribonucleoprotein D, HMG-CoA : 3-hydroxy-3-methylglutaryl-coenzyme A reductase, GGPP: geranylgeranyl pyrophosphate, RhoA: Ras homolog gene family member A, TNF α : tumour necrosis factor alpha, IL-1: interleukin-1, oxLDL- oxidised LDL lipoprotein, TXNIP: thioredoxin interacting protein, FOXO1: forkhead box protein O1, HDAC3/4/5/7: histone deacetylase 3/4/5/7, *miR-92a*: microRNA-92a.

1.5 Non flow-dependent regulation of KLF2

1.5.1 Factors stimulating *KLF2* expression

Statins are lipid-lowering drugs widely used in clinical practice. It has been suggested that their beneficial effects exceed those expected from lipid lowering alone (Bellosto, Ferri et al. 2000). Several statins induce *KLF2* expression in a dose-dependent manner and *KLF2* mediates the induction of endothelial NO synthase (*eNOS*), thrombomodulin (*TM*) and heme-oxygenase-1 (*HO-1*) by statins (Parmar, Nambudiri et al. 2005; Sen-Banerjee, Mir et al. 2005).

Statins are inhibitors of 3-hydroxy-3-methylglutaryl-coenzyme A (HMG-CoA) reductase, a crucial enzyme in cholesterol synthesis. As a result of this, cells are depleted of mevalonate which is a precursor of isoprenoid intermediates such as farnesyl pyrophosphate and geranylgeranyl pyrophosphate (GGPP). Isoprenoids function as membrane anchors for various proteins, for example small GTPases from the Rho family. One of them, Ras homolog gene family member A (RhoA) undergoes posttranslational modification by geranylgeranylation and is then able to inhibit *KLF2* expression (Sen-Banerjee, Mir et al. 2005). Taken together, statins inhibit the mevalonate pathway and thus production of functionally active RhoA and the absence of RhoA has a positive effect on *KLF2* expression (Sen-Banerjee, Mir et al. 2005) (**Figure 1.1**).

Prolonged shear stress induces *KLF2*-mediated expression of *eNOS* and *TM* more than statins because shear stress is able to stabilize *KLF2* mRNA via inhibition of PI3K. Specific inhibition of PI3K by LY294002 results in higher stability and thus higher levels of *KLF2* mRNA (van Thienen, Fledderus et al. 2006). This negative role of PI3K-pathway contradicts the described positive effect of PI3K-pathway on shear-specific nuclear binding of several factors that promote *KLF2* transcription mentioned

elsewhere in this chapter. Shear stress and statins combined have an additive, not synergistic effect on *KLF2*, *eNOS* and *TM* expression in human endothelial cells (Rossi, Rouleau et al. 2010).

Statins exert their pleiotropic effects via *KLF2* not only in endothelial cells but also in macrophages and lymphocytes. Human macrophages treated with simvastatin exhibit upregulation of *KLF2* expression and downregulation of several proinflammatory chemokines such as monocyte chemoattractant protein-1 (MCP-1), macrophage inflammatory proteins-1 α and β , interleukin-2 receptor- β , lymphotoxin β , vascular cell adhesion molecule 1 (VCAM-1) and tissue factor (TF) (Tuomisto, Lumivuori et al. 2008). Human T-cells treated with simvastatin show significantly increased *KLF2* expression with decreased interferon gamma (IFN- γ) secretion and diminished T-cell proliferation (Bu, Tarrío et al. 2010).

Several lines of evidence therefore suggest that some clinical effects of statins occur via upregulation of *KLF2*. Addition of simvastatin to the cold storage solution in which explanted healthy or steatotic rat livers are stored maintains *Klf2* expression with resulting prevention of endothelial dysfunction (Russo, Gracia-Sancho et al. 2012; Gracia-Sancho, Garcia-Caldero et al. 2013). Atorvastatin increases *Klf2* and decreases protease-activated receptor-1 (*Par-1*) expression in aortae of *ApoE*^{-/-} mice in keeping with its antiinflammatory effects (Yang, Zhou et al. 2013).

Resveratrol, a polyphenol produced naturally in some plants and present in red wine (Baur and Sinclair 2006) is a potent inducer of *KLF2* in HUVECs. This induction is mediated via NAD⁺-dependent deacetylase Sirtuin-1 (SIRT1) which in turn activates MEK5 and MEF2 (Gracia-Sancho, Villarreal et al. 2010) (**Figure 1.1**).

Recently, the structurally and functionally abnormal tumour vasculature (Hanahan and Folkman 1996; Jain 2005; Hamzah, Jugold et al. 2008; Fukumura, Duda et al. 2010) was found to lack sympathetic innervation and dopamine regulation (Chakroborty, Sarkar et al. 2011). Exogenous administration of dopamine acting through D2

receptors can normalize abnormal tumour vessel morphology and leakiness resulting in improved blood flow and reduced tumour hypoxia. This effect may be explained by dopamine's ability to upregulate *KLF2* expression in tumour ECs and HUVECs through upregulation of ERK5 (**Figure 1.1**). Dopamine also directly upregulates angiotensin-1 (*Ang-1*) expression in tumour endothelial pericytes. This could be of therapeutic relevance because administration of DA increases concentration of chemotherapeutic agents in tumour tissues (Chakroborty, Sarkar et al. 2011).

Rapamycin (sirolimus) is one of the drugs commonly eluted from coronary stents to reduce the recurrence of the vessel narrowing, the so-called restenosis. The effect of rapamycin on the endothelium is complex. Its potentially prothrombotic profile (Luscher, Steffel et al. 2007; Muldowney, Stringham et al. 2007; Jin, Ahn et al. 2009) might be counteracted by its ability to increase *KLF2* expression in HUVECs (Ma, Nie et al. 2012). The authors of this study postulate that *KLF2* might be a downstream target of the PI3K/AKT/mTOR pathway. This is based on the fact that rapamycin inhibits the PI3K/AKT/mTOR pathway by inhibition of the mammalian target of rapamycin (mTOR) (Hay and Sonenberg 2004) and there have been reports showing that specific inhibition of PI3K by LY2940002 results in stabilisation of *KLF2* mRNA (van Thienen, Fledderus et al. 2006). This is however in conflict with studies suggesting that a shear stress dependent binding of several co-factors necessary for *KLF2* transcription is PI3K-dependent (Huddleson, Ahmad et al. 2005).

Even more surprisingly, the same group of researchers who initially suggested positive effect of rapamycin on *KLF2* expression in HUVECs (Ma, Nie et al. 2012) soon after published another work suggesting the opposite effect of rapamycin on murine *Klf2* mRNA and protein expression *in vivo*. Here, the rapamycin-induced inhibition of *Klf2* expression in mice resulted in a significantly shorter time to FeCl₃-induced murine carotid artery thrombotic occlusion (Nie, Su et al. 2013).

1.6 Factors inhibiting *KLF2* expression

Several inflammatory cytokines potently inhibit *KLF2* expression. Exposure of HUVECs to interleukin 1 β (IL-1 β) results in a 4.7-fold decrease in *KLF2* expression (SenBanerjee, Lin et al. 2004), and *KLF2* expression is also reduced by treatment with TNF α (Lin, Kumar et al. 2005). TNF α -mediated repression of *KLF2* occurs via the NF- κ B pathway, but does not depend on direct NF- κ B binding to the *KLF2* promoter. The p65 subunit of NF- κ B cooperates with histone deacetylase 4 (HDAC4) to bind to the *KLF2* promoter and inhibits MEF2-mediated induction of *KLF2* (Kumar, Lin et al. 2005) (**Figure 1.1**).

Normal and oxidised low-density lipoprotein (LDL and oxLDL) particles potently inhibit *KLF2* expression *in vitro* in HUVECs (Li, Wang et al. 2011; Kumar, Kumar et al. 2013) (**Figure 1.1**). LDL particles exert their inhibitory effect on *KLF2* expression epigenetically via stimulation of DNA methyltransferase1 - induced CpG dinucleotide methylation. Methylated CpG islands decrease MEF2 occupancy of the *KLF2* promoter and promote assembly of a transcriptional repressor complex consisting of methyl-CpG-binding protein 2 and histone methyltransferase enhancer of zeste homolog 2 (Kumar, Kumar et al. 2013).

High glucose levels (35 mmol/L) suppress *KLF2* and *eNOS* expression levels in HUVECs and in carotid arteries of diabetic rats (Lee, Youn et al. 2012). This suppression of *KLF2* is mediated by the forkhead box protein O1 (FOXO1) that directly binds to the *KLF2* promoter (**Figure 1.1**). This could represent one possible mechanism of endothelial dysfunction in diabetics (Lee, Youn et al. 2012). Atorvastatin inhibits the negative effects of FOXO1 on *KLF2* and *eNOS* and restores *KLF2* and *eNOS* expression in HUVECs incubated in high glucose. Similar findings were observed *in vivo* in diabetic rats. Mechanistically, atorvastatin deactivates FOXO1 by its phosphorylation resulting in its translocation from nucleus into cytoplasm (Lee,

Youn et al. 2013). Interestingly, active FOXO1 completely prevents *KLF2* induction by atorvastatin (Lee, Youn et al. 2013).

The adaptor protein p66shc promotes cellular oxidative stress (Migliaccio, Giorgio et al. 1999) and has pro-apoptotic (Pacini, Pellegrini et al. 2004), pro-atherogenic (Napoli, Martin-Padura et al. 2003) and pro-angiogenic (De, Razorenova et al. 2005) effects. p66shc downregulates *MEF2A* expression resulting in downregulation of *KLF2* and *TM* mRNA and protein. Conversely, p66shc knockdown increases *KLF2* and *TM* mRNA and protein levels and decreases hydrogen peroxide levels in HUVECs (Kumar, Hoffman et al. 2009).

p53 is a tumour suppressor gene which plays a crucial role in regulating the cell cycle, DNA repair and apoptosis (Levine 1997). p53 inhibits *KLF2* expression in HUVECs through recruiting HDAC and binding to its p53 response element in *KLF2* promoter (**Figure 1.1**) with resulting H3 histone hypoacetylation and subsequent transcriptional repression of *KLF2* (Kumar, Kim et al. 2011).

1.7 Functions of KLF2

Below I summarise the existing literature on the functions of KLF2 in the vasculature (**Figure 1.2**). Because of the large number of studies and our increasingly complex understanding of how KLF2 influences vascular homeostasis I have divided this into sections, although as will be apparent, much overlap exists.

1.7.1 Maintenance of endothelial homeostasis

KLF2 plays a critical role in flow mediated upregulation of multiple genes in endothelium. 15% of all genes known to be upregulated by flow (109 out of 716) are KLF2-dependent (Parmar, Larman et al. 2006). Later data suggest that KLF2 together

with nuclear factor erythroid2-related factor 2 (Nrf2) control expression of about 70% of shear stress-induced endothelial genes (Fledderus, Boon et al. 2008). KLF2 modulates expression of genes critical in regulating vascular tone, haemostasis and thrombosis, inflammation and regulates endothelial barrier function and its antioxidative capacity (**Figure 1.2**). KLF2 acts as a molecular switch between healthy inactivated and activated atheroprone phenotype with direct effects on pathogenesis of atherosclerosis (Parmar, Larman et al. 2006; Atkins, Wang et al. 2008). Hemizygous deficient *Klf2*^{+/-} mice in *ApoE*^{-/-} background exhibit increased diet-induced atherosclerosis (Atkins, Wang et al. 2008). Levels of *Klf2* expression in vulnerable aortic plaques are significantly decreased when compared to the *Klf2* levels in stable plaques of *ApoE*^{-/-} mice (Yang, Zhou et al. 2013). KLF2 has distinct roles in developmental and adult vasculogenesis, angiogenesis and heart formation as detailed in separate sections.

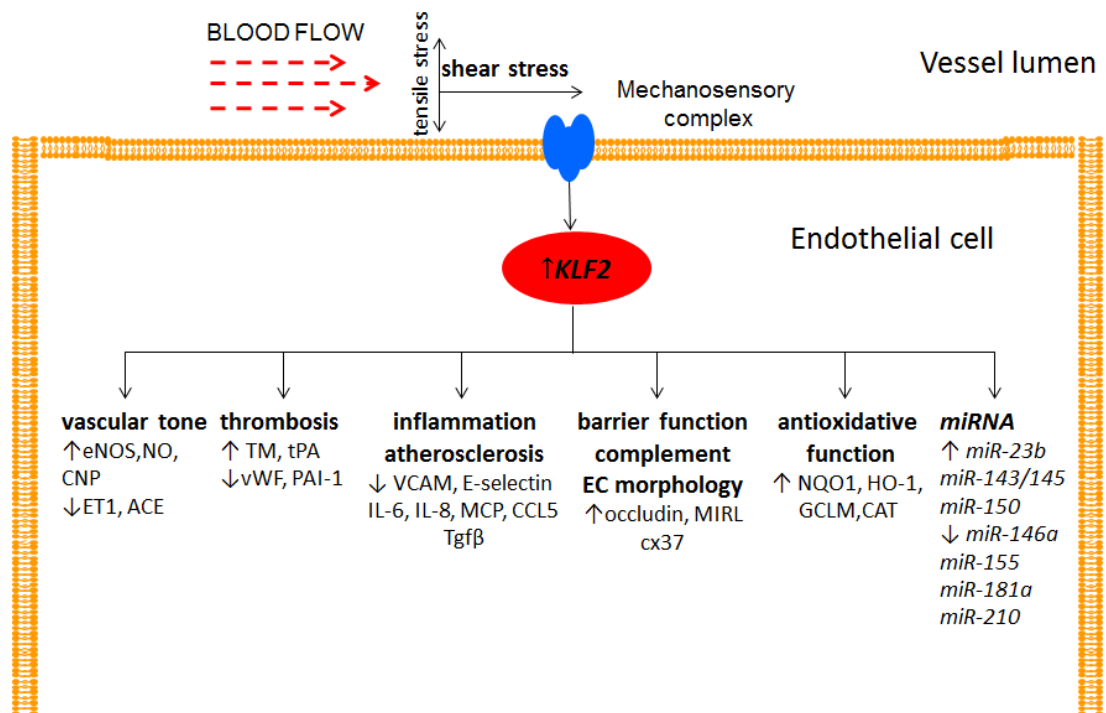


Figure 1.2 Effects of KLF2 on endothelial homeostasis.

Laminar and pulsatile blood flow induces *KLF2* expression in endothelial cells. *KLF2* regulates expression of important endothelial genes involved in endothelial homeostasis. Abbreviations: *KLF2*: Krüppel-like factor 2, eNOS: endothelial nitric oxide synthase, NO: nitric oxide, CNP: C-natriuretic peptide, ET1: endothelin-1, ACE: angiotensin-converting enzyme, TM: thrombomodulin, tPA: tissue plasminogen activator inhibitor, vWF: von Willebrand factor, PAI-1: plasminogen activator inhibitor 1, VCAM: vascular cell adhesion molecule, IL-6 and IL-8: interleukin 6 and 8, MCP: monocyte chemotactic protein, CCL5: chemokine (C-C motif) ligand 5, Tgfβ: transforming growth factor β, MIRL: membrane inhibitor of reactive lysis, also known as CD59, cx37: connexin 37, NQO1: NAD(P)H dehydrogenase quinone 1, HO-1: heme oxygenase 1, GCLM: glutamate-cysteine ligase modifier subunit, CAT: catalase.

1.7.1.1 Vasoregulation

Healthy endothelium is able to effectively regulate vascular tone. ECs produce several vasodilators such as NO from endothelial nitric oxide synthase (eNOS), C-natriuretic peptide (CNP) and adrenomedullin, or vasoconstrictive factors such as endothelin-1 (ET1) and angiotensin-converting enzyme (ACE) (Malek, Greene et al. 1993; Drexler and Hornig 1999; Chauhan, Nilsson et al. 2003). KLF2 potently induces expression of eNOS and CNP and inhibits expression of ET1, angiotensin-converting enzyme (ACE) and adrenomedullin (SenBanerjee, Lin et al. 2004; Dekker, van Thienen et al. 2005). KLF2 directly binds to the eNOS promoter to increase its transcriptional activity and downregulates caveolin-1, a negative regulator of eNOS activity (Razani, Engelman et al. 2001; Parmar, Larman et al. 2006).

eNOS and NO have multiple effects on endothelium. Apart from being a vasodilator, NO is antiinflammatory via inhibition of endothelial adhesion molecules ICAM-1 and VCAM-1 (De Caterina, Libby et al. 1995; Kaminski, Pohl et al. 2004) and antithrombotic (Tziros and Freedman 2006). Flow-mediated induction of eNOS through KLF2 therefore represents an important mechanism by which shear stress mediates its effects on endothelium.

1.7.1.2 Thromboprotection

KLF2 regulates expression of key endothelial thrombotic factors and generally has an antithrombotic effect. Overexpression of *KLF2* in HUVECs significantly increases expression and activity of antithrombotic thrombomodulin (*TM*) and mildly increased expression of tissue plasminogen activator (*tPA*). *TM* is a key cofactor in the thrombin-induced activation of the anticoagulant protein C. KLF2 directly binds to the *TM* promoter to increase its expression. *KLF2* overexpression inhibits expression of prothrombotic factors plasminogen activator inhibitor 1 (*PAI-1*) and Von Willebrand

factor (*vWF*) (Lin, Kumar et al. 2005). *KLF2* overexpression inhibits cytokine-mediated induction of TF and PAI-1 and prevents TM inhibition (Lin, Kumar et al. 2005). *In vitro* assays show that perfusion of native human blood over HUVECs overexpressing *KLF2* significantly increases clotting time (Lin, Kumar et al. 2005), while *KLF2* knockdown has the opposite effect with reduction of antithrombotic gene expression and induction of procoagulant factors (Lin, Kumar et al. 2005).

Interestingly, in contrast to the above, another group observed approximately 2-fold induction of *vWF* mRNA and protein levels following lentiviral *KLF2* overexpression in HUVECs. Following stimulation with thrombin and forskolin, both inducers of *vWF* release, a corresponding 2-fold increase of *vWF* protein was detected (Dekker, Boon et al. 2006). Additionally, several changes were observed in Weibel-Palade bodies, the storage organelles for *vWF* and other bioactive compounds. Weibel-Palade bodies in HUVECs overexpressing *KLF2* are shorter, have lower content of proinflammatory angiopoietin-2 (Ang-2) and interleukin-8 (IL-8), but are more equally distributed with larger average number per cell across the population of HUVECs when compared to controls (Dekker, Boon et al. 2006; van Agtmaal, Bierings et al. 2012).

KLF2 is involved in pathogenesis of the antiphospholipid syndrome (APS) characterised by production of antiphospholipid antibodies, particularly against β 2-glycoprotein 1 (β 2GP1) resulting in thrombosis and recurrent miscarriage (Rand 2003). β 2GP1 together with anti- β 2GP1 cause endothelial cell activation that is central to APS pathogenesis (Simantov, LaSala et al. 1995; De Martin, Hoeth et al. 2000). β 2GP1/anti- β 2GP1 inhibit, via yet unknown mechanisms, expression of *KLF2* and *KLF4*. In the presence of low levels of *KLF2* and *KLF4*, CBP/p300, a transcriptional co-activator of both *NF- κ B* and *KLFs*, gets preferentially bound to *NF- κ B*. This results in increased *NF- κ B* signalling and endothelial activation (Allen, Hamik et al. 2011).

1.7.1.3 Inflammation

Adenovirally overexpressed *KLF2* in HUVECs inhibits IL-1 β , TNF- α and lipopolysaccharide (LPS)-mediated induction of adhesion molecules VCAM-1 and E-selectin (Parmar, Larman et al. 2006). As a consequence, T-cell attachment and rolling is markedly attenuated. *KLF2* also inhibits IL-1 β -mediated production of inflammatory cytokines (Parmar, Larman et al. 2006). *KLF2* exerts antiinflammatory functions through competition for a transcriptional coactivator CBP/p300 with NF- κ B pathway and subsequent decrease of NF- κ B activity (SenBanerjee, Lin et al. 2004). Thrombin also mediates its proinflammatory effects via the NF- κ B pathway. *KLF2* inhibits expression of thrombin receptor *PAR-1* and consequently thrombin-mediated NF- κ B nuclear accumulation and DNA binding (Lin, Hamik et al. 2006).

Decreased expression of *KLF2* as a result of proinflammatory signalling activation (TNF- α through NF- κ B) decreases levels of the antiinflammatory factor bone morphogenic protein endothelial precursor cell-derived regulator (*BMPER*). Low levels of *BMPER* enable increased expression of proinflammatory bone morphogenic protein 2 (*BMP2*) resulting in decreased *eNOS* and increased *ICAM-1* and *VCAM* expression and in induced leukocyte adhesion and extravasation. Overexpression of *KLF2* in HUVECs increases *BMPER* expression and prevents TNF- α induced *BMPER* downregulation, providing another line of evidence for the antiinflammatory effects of *KLF2* on endothelium (Helbing, Rothweiler et al. 2011).

Antiinflammatory effects of prolonged shear stress have been linked to inhibition of certain MAPK pathways (Berk, Abe et al. 2001). JNK is an upstream kinase that activates both activator protein-1 (AP-1) components - activating transcription factor 2 (ATF2) and c-Jun. AP-1 together with NF- κ B and other co-activators like CBP/p300 forms a transcriptional complex that potently induces expression of proinflammatory genes in endothelium in response to inflammatory cytokines and is therefore

considered as proinflammatory and proatherogenic (Kracht and Saklatvala 2002). *ATF2* is constitutively expressed in human endothelium but is found in high amounts in its active phosphorylated form in endothelial cells overlying early atherosclerotic lesions. The observation that prolonged shear stress inhibits *ATF2* function by inhibiting nuclear localisation of phosphorylated *ATF2* that is mediated by *KLF2* (Fledderus, van Thienen et al. 2007) was later expanded by the same group when they showed that the anti-inflammatory effects of *KLF2* are mediated through actin cytoskeleton changes and require several days to reach full effect (Boon, Leyen et al. 2010). In this model *KLF2* inhibits phosphorylation of focal adhesion kinase (FAK) involved in actin cytoskeleton regulation (Kaunas, Usami et al. 2006) and in phosphorylation of JNK (together with actin filaments) (Shaik, Soltau et al. 2009). As a result JNK is not activated via phosphorylation and cannot activate both AP-1 components *ATF2* and c-Jun. The same effect can be observed following disruption of actin cytoskeleton by cytochalasin D confirming the link between *KLF2* and inhibition of the JNK pathway via the actin cytoskeleton (Boon, Leyen et al. 2010).

Regulation of *KLF2* expression may differ at different developmental stages and may also depend on the animal model used. This is shown by the interplay between shear stress, *KLF2* and transforming growth factor β ($Tgf\beta$) signalling in HUVECs or human aortic endothelial cells (HAoECs) and murine embryonic endothelial cells on the other hand (Boon, Fledderus et al. 2007; Egorova, Van der Heiden et al. 2011). $Tgf\beta$ signalling in non-embryonic endothelial cells is considered to have proatherogenic effects because $Tgf\beta$ induces PAI-1, MCP-1 and endothelial oxidized-LDL receptor. Shear stress increases *KLF2* expression in these cells and *KLF2* subsequently inhibits $Tgf\beta$ signalling in two separate ways. Firstly, *KLF2* induces Smad7 that inhibits phosphorylation of Smad2 and transcriptional activity of Smad3/4 which are all members of $Tgf\beta$ signalling pathway acting through the $Tgf\beta$ receptor Alk5. Secondly, *KLF2* inhibits another $Tgf\beta$ signalling pathway by inhibiting phosphorylation of one of

the AP-1 components c-Jun (Boon, Fledderus et al. 2007). On the other hand, in murine embryonic endothelial cells increased shear stress activates Tgf β /Alk5 signalling. Alk5 in turn activates the MEK5/ERK5/MEF2 pathway and increases *Klf2* expression (Egorova, Van der Heiden et al. 2011).

Thus in mouse embryonic endothelial cells shear stress-mediated *Klf2* induction lies downstream of Tgf β /Alk5/MEK5/ERK5 signalling. In HUVECs and HAoECs shear stress-mediated *KLF2* induction is MEK5/ERK5/MEF2-dependent and KLF2 is upstream of Tgf β /Alk5 signalling on which KLF2 has an inhibitory effect.

1.7.1.4 Complement activation

Endothelial exposure to laminar but not oscillatory shear stress leads to significant upregulation of membrane attack complex inhibitory protein CD59 (MIRL) on the endothelial surface with resulting decreased complement-mediated lysis of flow-conditioned ECs. This effect of shear stress is mediated via ERK5/*Klf2* signalling (Kinderlerer, Ali et al. 2008).

1.7.1.5 Endothelial barrier function

Klf2^{+/-} mice show increased endothelial leakage in response to an inflammatory stimulus (Lin, Kumar et al. 2005). This corresponds with *in vitro* experiments showing a protective effect of *KLF2* overexpression in HUVECs on thrombin, H₂O₂ and histamine-induced endothelial leakage. KLF2 upregulates expression of a key tight-junction protein occludin and decreases phosphorylation of myosin light chain which is a fundamental event in cell contraction (Lin, Natesan et al. 2010). Protective effects of *Klf2* on endothelial barrier function were confirmed independently in a murine stroke model. Transient middle cerebral artery occlusion was induced in *Klf2*^{-/-} mice, *Klf2* overexpressing mice and control mice and subsequently infarct volume and blood barrier function were analysed. *Klf2*^{-/-} mice exhibited significantly larger infarct volume

and impaired blood-brain barrier function due to decreased expression of occludin. Overexpression of *Klf2* reduced infarct volume and blood-brain barrier function was preserved (Shi, Sheng et al. 2013).

Recent reports suggest that decreased KLF2 might be involved in pathogenesis of Alzheimer's disease (AD) (Wu, Li et al. 2013). Blood-brain barrier dysfunction and impaired endothelial permeability have been implicated in pathogenesis of AD for some time (Strazielle, Ghersi-Egea et al. 2000). *Klf2* mRNA and protein levels in Tg2576 mouse model of AD are significantly reduced due to accumulation of amyloid beta. Amyloid beta acts through increased p53 levels that subsequently inhibit *Klf2* expression. Overexpression of *KLF2* in human brain ECs completely rescues amyloid beta-mediated impairment of occludin expression which is in keeping with the reported role of KLF2 in endothelial barrier function (Wu, Li et al. 2013). It must be noted however that potent KLF2 inducers statins have failed to decrease incidence of AD in randomised controlled trials in humans (McGuinness and Passmore 2010).

1.7.1.6 Endothelial morphology and intercellular gap junctions

It has been known that flow and shear stress influence endothelial actin cytoskeleton rearrangement and cell shape for more than two decades (Kim, Langille et al. 1989; Davies, Barbee et al. 1997). The central role of KLF2 in the cytoskeleton changes has now been elucidated. HUVECs exposed to shear stress (19 ± 17 dyne/cm² for 4 days) align in the direction of flow. This alignment is abrogated after siRNA-mediated *KLF2* silencing, whereas HUVECs overexpressing *KLF2* exhibit a stretched shape as a result of reorganisation of the cytoskeleton with formation of stress fibres even in the absence of flow (Boon, Leyen et al. 2010). HUVECs overexpressing *KLF2* also show increased cell density and decreased migration following wounding (Dekker, Boon et al. 2006).

ECs from healthy arteries or ECs cultured under high laminar shear stress conditions exhibit high expression of connexin 37 (*CX37*) and its deletion in *ApoE*^{-/-} mice

accelerates atherosclerosis (Kwak, Mulhaupt et al. 2002; Wong, Christen et al. 2006). cx37 is a transmembrane protein that forms a gap junction in the form of two hexameric hemichannels on adjacent cells. Gap junctions represent a specialized intercellular connection that link the cytoplasm of two cells enabling direct communication through exchange of ions and small metabolites (Saez, Berthoud et al. 2003). KLF2 regulates CX37 expression in response to shear stress or simvastatin by directly binding its promoter. Deletion of *KLF2* decreases passage of small molecules and ions through gap junctions in a EC monolayer, confirming the function of KLF2 in intercellular communication (Pfenniger, Wong et al. 2012).

1.7.1.7 Oxidative stress

HUVECs overexpressing *KLF2* show upregulation of antioxidant genes such as NAD(P)H dehydrogenase quinone 1 (*NQO1*), heme oxygenase (*HO-1*), glutamate-cysteine ligase modifier subunit (*GCLM*) and catalase (*CAT*) which are all target genes of Nrf2; one of the main antioxidant transcription factors upregulated by atheroprotective blood flow (Arai, Ohashi et al. 1998; Dekker, Boon et al. 2006; Lee, Youn et al. 2012). KLF2 promotes Nrf2 nuclear localization and activation necessary for its function and augments Nrf2-mediated protection against oxidative stress (Fledderus, Boon et al. 2008).

Heme oxygenase 1 (*HO-1*) is the rate-limiting enzyme in heme catabolism that catalyses heme degradation into biliverdin, carbon monoxide and free iron (Ryter, Alam et al. 2006). Products of this pathway have antioxidant (Brunt, Fenrich et al. 2006), antiinflammatory (Otterbein, Zuckerbraun et al. 2003) and antiapoptotic (Brouard, Otterbein et al. 2000) effects on vasculature. Statins act as potent inducers of *HO-1* expression in a KLF2-dependent manner and their antioxidant effects have been shown to act through generation of biliverdin and ferritin following *HO-1* activation (Ali, Hamdulay et al. 2007).

1.7.1.8 MicroRNA production

HUVECs overexpressing *KLF2* were examined for expression of *miRs* known to play roles in vascular homeostasis. Expression levels of *miR-23b* and *miR-150* (which both have regulatory role in cell migration) were significantly increased. Expression levels of *miR-146a* and *miR155* (role in inflammation), *miR-181a* (endothelial cell fate), and *miR-210* (angiogenesis and hypoxia response) were on the contrary reduced (Hergenreider, Heydt et al. 2012). Interestingly, expression of *miR143/145* which has an atheroprotective effect on vascular smooth muscle cells (VSMC) was upregulated in HUVECs under shear stress and lentiviral overexpression of *KLF2* (Hergenreider, Heydt et al. 2012). A novel mechanism has been described in which shear stress and/or *KLF2* increases production of extracellular vesicles (ectosomes) in HUVECs expressing high levels of *miR143/145* and these are secreted from HUVECs to induce a paracrine atheroprotective VSMC phenotype (Hergenreider, Heydt et al. 2012). This communication between endothelial cells and SMC might explain the deleterious effect of endothelial *Klf2* knockdown on VSMC observed a decade earlier (Kuo, Veselits et al. 1997; Wu, Bohanan et al. 2008).

1.7.2 Haematopoietic stem cell development

All vertebrates undergo 2 waves of haematopoiesis. In zebrafish, primitive haematopoiesis starts at around 11hpf in anterior lateral mesoderm (ALM) and intermediate cell mass (ICM) and its marker is the presence of embryonic globin proteins. Haematopoiesis in the ICM diminishes with onset of circulation at 24hpf. At around 26hpf definitive haematopoietic stem cells (HSCs) begin to emerge from the hemogenic endothelial cells from the ventral wall of dorsal aorta (DA) in the aorta-gonad-mesonephros region (AGM). At approximately 48hpf HSCs migrate to caudal haematopoietic tissue (CHT) that represents another site of transient haematopoiesis

and also to the kidney marrow which will be the site of definitive adult haematopoiesis that gives rise to all blood lineages. Lymphoid progenitor cells migrate from AGM at approximately 54hpf to seed the thymus which will be the site of T cells maturation (Jing and Zon 2011). It has been recently shown that blood flow plays an important role in maintenance of HSC programming (Wang, Zhang et al. 2011). Zebrafish embryos without flow show normal primitive erythropoiesis, but expression of HSC markers *runx1* and *cmyb* is downregulated in AGM and CHT from 36hpf onwards when compared to controls. Expression of thymic T cell marker *rag1* is also diminished at 4dpf in embryos lacking blood flow. It has been postulated that this blood flow dependent maturation of HSC is mediated via *klf2a* and subsequent NO signalling. ATG *klf2a* MO mediated *klf2a* knockdown resulted in decreased *runx1* and *cmyb* expression in AGM and CHT from 36hpf onwards and was claimed to be partially rescued by administration of capped *klf2a* mRNA (Wang, Zhang et al. 2011).

1.7.3 T-cell and B-cell biology

T and B lymphocytes play distinct roles in atherosclerosis (Mallat, Taleb et al. 2009; Perry, Bender et al. 2012). I will therefore briefly describe the role of KLF2 in lymphocyte biology especially in regard to vascular pathophysiology. Klf2 plays an important role in maintaining a quiescent, non-activated T-cell phenotype. *Klf2* expression is developmentally induced in quiescent single-positive (SP) T-cells (either CD4⁺ or CD8⁺), but is rapidly decreased following T-cell activation. Additionally, *Klf2*-deficient chimeric mice develop a massive reduction in peripheral single-positive T-cells which show a spontaneously activated cell surface phenotype and increased Fas-mediated apoptosis (Kuo, Veselits et al. 1997). Klf2 maintains T-cell quiescence at least partially via negative regulation of the proto-oncogene *c-Myc* (Buckley, Kuo et al. 2001). Maintenance of a quiescent T-cell phenotype by Klf2 might be physiologically

important due to the role of activated CD8⁺ T-lymphocytes in promotion of vulnerable atherosclerotic plaques in *ApoE*^{-/-} mice (Kyaw, Winship et al. 2013). Additionally, Klf2 is necessary for peripheral T-cell recirculation. *Klf2*-deficient SP T-cells show impaired thymic emigration and deficient T-cell trafficking; the majority of *Klf2*^{-/-} T-cells are found in the spleen with almost none in the blood or lymph nodes. Klf2 was subsequently shown to regulate thymocyte and T-cell trafficking into peripheral lymph organs by inducing expression of receptors critical for these processes, such as *CD62L*, β -integrin, *CCR7* (T-cell trafficking) and *S1P1* (thymocyte emigration) (Carlson, Endrizzi et al. 2006).

A particular subset of T-cells, the CD4⁺CD25⁺Fox3p⁺ T regulatory cells (Tregs) known to have a role in maintaining immunological tolerance have inhibitory effects on development and progression of atherosclerosis (Ait-Oufella, Salomon et al. 2006; Mor, Planer et al. 2007). Tregs are able to upregulate *KLF2* expression in HUVECs previously treated with oxidised LDL in a manner requiring direct cell contact (Li, Wang et al. 2011).

Klf2 knockdown in B-cells also leads to decreased expression of trafficking molecules *CD62L* and β -integrin, but expression of *S1P1* receptor remains almost unaffected. *Klf2* deficiency also causes impaired B-cell subset differentiation with increased number of marginal zone B cells and massively reduced number of atheroprotective B1 B cells (Kyaw, Tay et al. 2011).

The antiatherogenic effects of *KLF2* expression in lymphocytes are supported by the observation that simvastatin significantly increases *KLF2* expression in murine and human T-cells *in vitro* and *in vivo* with resulting decreased IFN- γ secretion and diminished T-cell proliferation (Bu, Tarrío et al. 2010).

1.7.4 Monocyte and macrophage biology

KLF2 is expressed in primary human monocytes, but its expression is reduced by cytokine or LPS activation or differentiation into macrophages. *KLF2* expression is reduced by about 30% in monocytes of patients with extensive atherosclerosis compared to healthy controls (Das, Kumar et al. 2006). This is significant because monocyte activation and recruitment plays important roles in atherosclerosis (Libby 2002).

In mice, conditional *Klf2* knockout in myeloid cell lineage in an atheroprone LDL receptor deficient background causes increased atherosclerosis (Lingrel, Pilcher-Roberts et al. 2012) in keeping with increased atherosclerosis seen in *Klf2*^{+/-} *ApoE*^{-/-} mice (Atkins, Wang et al. 2008). Myeloid *Klf2* knockout increases monocyte and neutrophil adhesion to endothelial cells with resulting increased accumulation and activity in atherosclerotic plaques (Lingrel, Pilcher-Roberts et al. 2012), but this did not confirm increased lipid accumulation by macrophages as observed in *Klf2*^{+/-} *ApoE*^{-/-} mice (Atkins, Wang et al. 2008).

Overexpression studies show that *KLF2* inhibits LPS-mediated activation of monocytes as evidenced by reduced secretion of cyclooxygenase 2, tissue factor, IL-1, IL-8, TNF- α and MCP-1. Overexpressed *KLF2* also decreases phagocytic activity and surprisingly does not inhibit but rather increases recruitment of monocytes to sites of inflammation. Conversely, *KLF2* knockdown increases monocyte expression of *MCP-1*, *TF* and cyclooxygenase 2. *KLF2* exerts its antiinflammatory effects in monocytes by inhibiting the NF- κ B and AP-1 signalling pathways (Das, Kumar et al. 2006). *KLF2* does not alter *NF- κ B* or *AP-1* expression, nuclear accumulation or DNA binding, but reduces *NF- κ B* and *AP-1* transcriptional activities by interacting with the co-activator PCAF (Das, Kumar et al. 2006).

Macrophages represent a heterogeneous cell population: M1 macrophages (activated by GM-CSF, TNF or LPS) represent a proinflammatory phenotype whereas M2 macrophages are generally antiinflammatory, contributing to tissue repair but with a higher capacity to accumulate oxidized LDL due to higher number of scavenger receptors (Goerdts and Orfanos 1999; Peiser and Gordon 2001; Mantovani, Garlanda et al. 2009). *KLF2* expression is higher in M2 than M1 macrophages. However, after exposure to oxidized LDL, *KLF2* expression decreases in M2 but remains unchanged in M1 macrophages. *KLF2* knockdown in M2 macrophages leads to increased secretion of MCP-1 (van Tits, Stienstra et al. 2011). Overall, the above data suggest that *KLF2* plays an antiinflammatory and antiatherogenic role in monocyte and macrophage biology.

1.7.5 Vasculogenesis and angiogenesis

Homozygous *Klf2* deficient mice die between E12.5-14.5 from intra-embryonic and intraamniotic haemorrhaging associated with normal vascular patterning, but defects in blood vessel morphology - endothelial necrosis, cuboidal VSMCs, abnormally thin tunica media and aneurysms. *Klf2*^{-/-} mice exhibit defective VSMCs and pericyte migration to endothelial tubes during vasculogenesis with subsequent loss of their stabilising and modulatory functions and failure to organize into a compact tunica media (Kuo, Veselits et al. 1997; Wu, Bohanan et al. 2008). There are however conflicting data about the effect of homozygous *Klf2* deletion on murine embryonic development. Another group were able to confirm the stage of lethality in *Klf2*^{-/-} embryos (E11.5-13.5) and reported retarded growth, craniofacial abnormalities, signs of anaemia and abdominal bleeding, but could not detect vessel wall abnormalities (Wani, Means et al. 1998). Mouse embryos with conditional endothelial or smooth and cardiac muscle *Klf2* deletion confirm that endothelial *Klf2* deletion is responsible for the

embryonic mortality around E14 (Lee, Yu et al. 2006). The cause of death was reported to be high-output cardiac failure caused by loss of smooth muscle tone and vasodilation. The reasoning that *Klf2* deletion was responsible for the observed phenotype was supported by data obtained from *klf2a* morphant zebrafish embryos. These exhibited increased aortic blood velocity and pericardial oedema (Lee, Yu et al. 2006).

Vascular endothelial growth factor (VEGF-A) is a key regulator of physiologic and pathologic vasculogenesis and angiogenesis (Leung, Cachianes et al. 1989). VEGF-A also promotes vascular permeability, EC migration and survival, but can also act as a proinflammatory cytokine (Senger, Galli et al. 1983; Kim, Moon et al. 2001; Ferrara, Gerber et al. 2003; Maharaj and D'Amore 2007). VEGF-A effects are mediated by its receptor tyrosine kinases, of which VEGFR2 is the most important in endothelium (Waltenberger, Claesson-Welsh et al. 1994). The following sections describe the relationship of KLF2 to VEGF-A signalling showing these two factors act in various and context-dependent manners.

klf2a (upregulated by flow) plays a positive role in angiogenesis in zebrafish by inducing expression of an endothelial-specific microRNA *miR-126* which inhibits a VEGF signalling inhibitor *spred-1*. This therefore allows VEGF-A/VEGFR2 (fetal liver kinase 1 (*flk1*) or kinase insert domain receptor like (*kdr1*) in zebrafish) mediated angiogenesis to proceed. In the absence of flow, *klf2a* and *miR-126* are down-regulated and *spred-1* inhibits angiogenesis by inhibiting VEGF-A/VEGFR2 signalling. This pathway was demonstrated on AA5x vessel angiogenesis which connects 5th and 6th aortic arch vessels to lateral dorsal aortae. This pathway thus connects flow with *klf2a* and VEGF-A/VEGFR2 via *mir-126* and suggests a stimulatory role of *klf2a* on VEGF-A/VEGFR2 signalling (Nicoli, Standley et al. 2010).

The link between KLF2 and VEGF through *miR-126* has been confirmed in human duodenal vasculature when duodenal biopsies from cirrhotic patients were compared to

healthy individuals. Increased duodenal angiogenesis in cirrhotic patients was demonstrated by increased capillary density in duodenal villi and by increased presence of endothelial markers CD31 and CD34 (Kobus, Kopycinska et al. 2012). Increased *KLF2*, *miR-126*, VEGF but also Ang-2 were detected in duodenal samples from cirrhotic patients suggesting *KLF2* might play a role in formation of porto-systemic collateral vessels as a consequence of increased intrahepatic resistance and increased blood flow (Kobus, Kopycinska et al. 2012).

Similarly, in embryonic endothelial cells of *Xenopus*, expression of *Flk1* is independently activated by *Klf2* and by one of the ETS transcription factors ETS-related gene (ERG). *Klf2* and ERG directly bind to *Flk1* enhancer within the first intron of the *Flk1* gene (Meadows, Salanga et al. 2009). Mutation of ERG or KLF binding sites results in complete or significant reduction of *Flk1* expression respectively. *Klf2* knockdown inhibits *Flk1* expression and causes significant defects in vasculogenesis. Additionally, *Klf2* and ERG can form a protein complex with synergistic effects on *Flk1* expression in *Xenopus* embryonic endothelial cells (Meadows, Salanga et al. 2009).

Vegf-1 is expressed in adult murine arterial ECs but not venous or capillary endothelium (dela Paz, Walshe et al. 2012). Shear stress potently activates VEGF signalling in HUVECs on various levels by increasing *VEGF-A* mRNA and protein levels and also increases expression and activation of VEGFR2 (dela Paz, Walshe et al. 2012). Increased VEGF-A/VEGFR2 signalling mediated via shear-dependent induction of *KLF2* expression has protective effects on HUVECs by decreasing apoptosis compared to HUVECs in static conditions (dela Paz, Walshe et al. 2012). This is contradictory to previous work suggesting an inhibitory role of *Klf2* on VEGF-A/VEGFR2(FLK1) signalling in adult endothelial cells (Bhattacharya, Senbanerjee et al. 2005; Dekker, Boon et al. 2006).

Klf2 overexpression in a nude mouse model markedly attenuates VEGF-A-mediated angiogenesis and oedema. *KLF2* overexpression in HUVECs also potently inhibits

VEGF-A mediated endothelial activation. KLF2 inhibits expression of *VEGFR2* by directly competing with Sp1 for a binding site in the *VEGFR2* promoter (Bhattacharya, Senbanerjee et al. 2005). Overexpression of *KLF2* inhibits endothelial migration, most likely due to induction of an antimigratory factor semaphorin-3F and to some extent to a less pronounced induction of *VEGFR2* (Dekker, Boon et al. 2006). These differences in the observed relationship between KLF2 and VEGF signalling may be explained by the different developmental stages and model organisms used (zebrafish and *Xenopus* embryonic angiogenesis and human adult angiogenesis versus murine adult angiogenesis).

Consistent with an inhibitory role of *KLF2* in adult angiogenesis is that KLF2 inhibits expression and function of hypoxia-inducible factor 1 (HIF-1) which is a central regulator of the hypoxic response and angiogenesis in many cell types. Under hypoxic conditions, *KLF2* overexpressed in HUVECs inhibits (and *KLF2* knockdown increases) expression of HIF-1 target genes such as IL-8, Ang-2 or VEGF and also inhibits endothelial tube formation on Matrigel (Kawanami, Mahabeleshwar et al. 2009). KLF2 prevents the hypoxia-mediated accumulation of HIF-1 α subunit of HIF and thus prevents HIF-1 α translocation into the cell nucleus where it associates with oxygen insensitive HIF-1 β subunit to form a functional HIF molecule. KLF2 inhibits HIF-1 α interaction with its chaperone Hsp90 and thus promotes its proteasomal degradation (Kawanami, Mahabeleshwar et al. 2009).

Angiopoietin-1 (Ang-1) and its receptor tyrosine kinase Tie2 are involved in maintaining vascular quiescence and angiogenesis (Wong, Haroon et al. 1997; Peters, Kontos et al. 2004). The ability to exert these distinct and opposite functions resides in the fact that in the presence of cell-cell contacts, Ang-1 induces *trans*-association of Tie2 and preferentially activates the Akt pathway, leading to vascular quiescence. In the absence of cell-cell contact Ang-1 induces Tie2 anchoring to intracellular matrix that preferentially activates the ERK1/2 pathway to promote angiogenesis (Fukuhara, Sako

et al. 2008; Saharinen, Eklund et al. 2008). *KLF2* is one of the factors induced by *trans*-associated Tie2 in the presence of cell-cell contacts promoting vascular quiescence. Ang-1/Tie2-mediated *KLF2* induction depends on PI3K/Akt pathway which in turn activates transcriptional activity of MEF2 (Sako, Fukuhara et al. 2009).

The Grb2-associated binder family docking proteins (Gab1-Gab3) play crucial roles in transmitting signals that control cell growth, differentiation and function from multiple receptors (Gu and Neel 2003). Gab1 has proangiogenic properties and plays a crucial role in postischaemic angiogenesis and arteriogenesis in mice. In this pathway hepatocyte growth factor stimulates Gab1 association with SHP2 (Src homology-2 domain-containing protein tyrosine phosphatase2) and PI3K subunit p85. This complex positively regulates migration, proliferation and stabilisation of ECs via distinct MAPK pathways. Interestingly, Gab1/SHP2 stimulates *KLF2* expression through ERK5 that might be contributing to the stabilising effects of this signalling cascade on EC (Shioyama, Nakaoka et al. 2011). Conversely, *Gab1* conditional endothelial knockout in the *ApoE*^{-/-} background decreases *Klf2* and *Klf4* expression, increases production of proinflammatory TNF α , IL-1 β and IL-6 and endothelial expression of *VCAM-1* with resulting accelerated angiotensin 2 - mediated atherosclerosis and aortic aneurysm formation (Higuchi, Nakaoka et al. 2012).

Proangiogenic cells (PACs), also known as endothelial progenitor cells are bone marrow-derived cells which circulate in the blood stream and are able to take part in angiogenesis (Asahara, Murohara et al. 1997). PACs numbers and their neovascularisation properties are negatively affected by risk factors for ischaemic heart disease such as age, hypertension or smoking (Vasa, Fichtlscherer et al. 2001). *KLF2* overexpression in human PACs increases their number by 60% *in vitro* and improves neovascularisation abilities of aged murine PACs in an ischaemic hind limb model *in vivo* (Boon, Urbich et al. 2011). A particular subset of PAC, endothelial colony-forming cells have the ability to form *de novo* vessels *in vivo* and react to laminar and pulsatile

flow in a similar manner to adult EC, with increased *KLF2* and decreased *ET1* and *VCAM1* expression (Egorova, DeRuiter et al. 2012).

1.7.6 Valvulogenesis

Cardiac valves form in vertebrates from endocardial cushions arising in the atrioventricular (AV) canal. Formation of endocardial cushions involves several steps starting with specification of a subset of endocardial cells in the AV canal and ending in their epithelial-to-mesenchymal transformation (EMT). Endocardial cushions then go on to form the AV complex and after further remodelling become functional valve leaflets (Armstrong and Bischoff 2004). There are several lines of evidence that suggest *KLF2* plays an important role in EMT.

Before functional valves develop, anterograde and retrograde (reversing) blood flows exist between atrium and ventricle. Eventually with development of mature valves only anterograde flows become possible. Experiments with alteration of the proportion of retrograde flow to the length of a cardiac cycle (the so-called retrograde flow fraction (RFF)) showed that decreased RFF was linked with severe defects in valve formation in zebrafish (Vermot, Forouhar et al. 2009). *klf2a* is upregulated by retrograde flow in the AV canal of zebrafish hearts and conversely is downregulated when RFF decreases. Interestingly, *klf2a* knockdown results in valvular defects similar to those observed in zebrafish with decreased RFF suggesting an important role of *klf2a* and its target genes *notch1b* (zebrafish Notch homolog), *bmp4*, *edn1* and *nrg1* in blood flow dependent valvulogenesis (Vermot, Forouhar et al. 2009).

Another line of evidence that *klf2a* might be involved in heart valve formation comes through identification of a novel zebrafish mutant with defective endocardial cushion formation named *bungee* (*bng*^{jh177}) with a deactivating mutation in protein kinase 2 (*pkd2*) that leads to impaired phosphorylation of Hdac5. Hdac5 thus remains in its

active state bound to the *klf2a* promoter and inhibits *klf2a* expression in the AV region leading to decreased *notch1b* signalling and defective valve formation (Just, Berger et al. 2011).

Interestingly, the role of KLF2 in murine cardiac valve development is strain-specific. FVB/N *Klf2*^{-/-} mice exhibit defective EMT and delayed formation of the atrial septum whereas C57BL/6 *Klf2*^{-/-} mice experience delayed atrial septal formation but their AV cushions develop normally. FVB/N *Klf2*^{-/-} mice at E9.5 show multiple layers of dysmorphic endothelial cells lining the AV cushions that fail to undergo the EMT properly resulting in hypocellular AV cushions at E10.5 and abnormal cardiac function. Mechanistically, KLF2 regulates several genes involved in AV cushion development such as *Gata4*, *Tbx5*, *Sox9* and *Ugdh* (Chiplunkar, Lung et al. 2013).

1.8 KLF4 and its role in vascular biology

KLF4/GKLF (gut-enriched KLF) was initially named epithelial transcription factor (Shields, Christy et al. 1996). KLF4 has functions in terminal differentiation and regulation of growth of gut and skin epithelium (Shields, Christy et al. 1996; Segre, Bauer et al. 1999; Katz, Perreault et al. 2005). *Klf4* null mouse newborns die soon after birth due to loss of skin barrier function and subsequent dehydration (Segre, Bauer et al. 1999). *KLF4* endothelial expression was suggested by cloning from a human vascular endothelial cell complementary DNA (cDNA) library (Yet, McA'Nulty et al. 1998). KLF4 was identified as another blood flow dependent transcription factor *in vitro* and *in vivo* in human and mouse endothelial cells (McCormick, Eskin et al. 2001; Hamik, Lin et al. 2007). *KLF4* endothelial expression is similarly to *KLF2* upregulated by laminar shear stress and statins, but is also upregulated by proinflammatory cytokines TNF α , IL-1 β and IFN γ (Hamik, Lin et al. 2007; Ohnesorge, Viemann et al.

2010). KLF4 strongly induces antiinflammatory and antithrombotic eNOS, TM and tPA and inhibits proinflammatory and procoagulant factors MCP-1, regulated on activation, normal T-cell expressed and secreted (RANTES), PAI-1 and IL-6. Conversely, KLF4 knockdown enhanced TNF α - mediated induction of VCAM-1, E-selectin and TF (Hamik, Lin et al. 2007; Methe, Balcells et al. 2007). To sum up, the phylogenetically close transcription factors KLF2 and KLF4 (Bieker 2001) have many overlapping functions in ECs. Their cooperation - together with other factors - seems to maintain functional levels of anti and proinflammatory factors in endothelium under basal and inflammatory conditions (Hamik, Lin et al. 2007).

1.8.1 *klf4a* and *klf4b* expression patterns and functions

Zebrafish have two *KLF4* paralogs termed *klf4a* and *klf4b*, however *klf4b* has been recently named *klf17* (Kotkamp, Mossner et al. 2014). *klf4a* is considered to be the zebrafish ortholog of human *KLF4*. Zebrafish *klf4a* shares approximately 67% AA similarities with human and murine *KLF4/Klf4* (Li, Chan et al. 2011). *klf4a* was shown to have antiproliferative effects in zebrafish intestinal epithelium. *klf4a* also regulates differentiation of goblet cells in zebrafish embryonic intestinal epithelium and these functions are in keeping with previously described *Klf4* functions in mice (Katz, Perreault et al. 2002; Li, Chan et al. 2011). At 48hpf *klf4a* expression was detected in epidermis, pectoral fins, pharynx, retina and olfactory bulbs. To my knowledge *klf4a* was not detected in zebrafish vasculature in any developmental stage.

Recent synteny studies showed that *klf4b* is related to *Klf17* (also called *Neptune*) in *Xenopus* and is therefore now named *klf17* (Kotkamp, Mossner et al. 2014). The original name *biklf* stands for blood island Krüppel-like factor and indicates that *biklf/klf4b/klf17* is expressed in blood islands throughout zebrafish embryogenesis and plays important role in primitive erythropoiesis (Kawahara and Dawid 2001; Oates,

Pratt et al. 2001; Gardiner, Gongora et al. 2007). *biklf/klf4b/klf17* is expressed in the hatching gland precursors (pre-polster and polster) and eventually in the hatching gland itself and is essential for its development. This transient organ secretes enzymes that help the embryos escape from its enveloping coats (Gardiner, Daggett et al. 2005). Finally, *biklf/klf4b/klf17* is strongly present in neuromasts that form the lateral line (Oates, Pratt et al. 2001). The lateral line is a sensory system that detects changes in the motion of water (Ghysen and Dambly-Chaudiere 2004). To my knowledge *biklf/klf4b/klf17* was not detected in zebrafish vasculature at any stage.

1.9 Chemokine receptor CXCR4 is involved in collateral vessel formation

Our group have previously shown that vascular expression of *cxcr4a*, a zebrafish ortholog of *CXCR4* is influenced by blood flow (Packham, Gray et al. 2009).

C-X-C chemokine receptor type 4 (*CXCR4*) is a G-protein-coupled receptor for a chemokine stromal cell derived factor 1 α (*SDF1 α*)/*CXCL12* (Bleul, Farzan et al. 1996). *CXCR4* is expressed on several cell types and *SDF1 α* /*CXCR4* system plays a role in various physiological processes such as haematopoiesis and organ development (Zou, Kottmann et al. 1998), lymphohaematopoiesis or leukocyte trafficking (Kim and Broxmeyer 1999). *CXCR4* is important in mobilisation of vascular stem/progenitor cells (Peled, Petit et al. 1999) and plays a role in collateral vessel formation in mice and zebrafish (Kim and Broxmeyer 1999; Packham, Gray et al. 2009). Importantly, *SDF1 α* /*CXCR4* system is involved in metastasis of several malignancies (Schrader, Lechner et al. 2002; Taichman, Cooper et al. 2002; Uchida, Begum et al. 2003).

Our group have shown that *cxcr4a* is expressed at similar levels in both control MO and flow deficient *tnnt2* MO morphants at 36hpf. At 48hpf *cxcr4a* is rapidly down-regulated in the embryos with intact blood flow, whereas in the absence of flow *cxcr4a* continues to be expressed in the vasculature up to 60hpf and promotes collateral vessel formation (Packham, Gray et al. 2009). This was shown by the observation that the MO-mediated *cxcr4a* knockdown in *gridlock* mutants significantly reduced their ability to restore blood flow to the occluded aorta by forming collateral vessels (Packham, Gray et al. 2009).

1.10 Hypoxia inducible factor (HIF) and Von Hippel - Lindau protein (pVHL) in hypoxic signalling

Recently published work from our group links blood flow as mechanical force to the vascular phenotype of zebrafish *vhl* mutant embryos with excessive aberrant angiogenesis and to changes in vascular expression of some components of Notch signalling (Watson, Novodvorsky et al. 2013).

Metazoan cells react to low oxygen levels by transcriptional adaptations aiming to restore homeostasis. Hypoxia inducible factor (HIF) is a key transcriptional factor involved in these adaptation processes (Semenza and Wang 1992; Kaelin 2005). HIF is a heterodimer that consists of a constitutively expressed HIF1- β subunit and a hypoxia regulated HIF1- α subunit. Under normoxic conditions HIF1- α undergoes hydroxylation and rapid proteasomal degradation by a multi-subunit E3 ubiquitin ligase complex containing pVHL. Under hypoxic conditions or in the absence of functional pVHL, HIF1- α is translocated to the nucleus where it meets with HIF1- β and forms a functional HIF (Kaelin 2005). HIF then regulates expression of multiple hypoxia-

inducible genes such as erythropoietin (Semenza and Wang 1992) or angiogenic growth factors *VEGF* (Liu, Cox et al. 1995), platelet-derived growth factor (*PDGF*) (Gleadle, Ebert et al. 1995), *PAI-1* (Kietzmann, Roth et al. 1999), angiopoietin 2 (*Ang-2*) (Oh, Takagi et al. 1999), *SDF-1* and *CXCR4* (Kryczek, Lange et al. 2005).

VHL tumour suppressor gene codes for Von Hippel-Lindau protein (pVHL) that acts as a recognition component for hydroxylated HIF1- α in the E3 ubiquitin ligase complex. Following pVHL binding, HIF- α undergoes ubiquitination and proteasomal degradation. Not surprisingly, mutations in the *VHL* gene result in states with increased erythropoiesis such as Chuvash polycythemia or VHL disease which is characterised by the presence of highly vascularised tumours in multiple organs (Ang, Chen et al. 2002; Kaelin 2005).

Vhl knockout mouse die in utero due to haemorrhagic lesions in placenta (Haase 2005). Identification of a zebrafish *VHL* ortholog *vhl* and its subsequent mutagenesis therefore created a useful tool for further *vhl* studies (van Rooijen, Voest et al. 2009). This mutant is identified as *vhl*^{hu2117} and has a nonsense mutation in the HIF1- α recognition site. *vhl*^{hu2117} are viable and fertile in heterozygous state. Homozygous *vhl*^{hu2117} mutants demonstrate features of upregulated hypoxic signalling such as increased expression of *vegfa*, *vegfa* receptors *flt1*, *kdr* (*kdr1*) and *kdr-like*, lactate dehydrogenase or erythropoietin. *vegfa* driven excessive angiogenesis demonstrates itself from 58hpf onwards by aberrant angiogenic sprouting from intersegmental vessels (ISVs) and increased number of cranial vessels (van Rooijen, Voest et al. 2010). *vhl*^{hu2117} mutants develop high-output cardiac failure from 4dpf onwards with cardiomegaly and pericardial oedema that results in the death between 8dpf and 11dpf (van Rooijen, Voest et al. 2009). Oliver Watson from our group recently showed that the excessive angiogenic sprouting in *vhl*^{hu2117} mutants is blood flow dependent. Excessive angiogenesis with increased endothelial cell numbers, increased vessel diameter and

length in *vhl*^{hu2117} mutants is abolished in embryos where blood flow has been removed without affecting normal vessel patterning. The mechanism of how blood flow influences *vhl* signalling remains unclear (Watson, Novodvorsky et al. 2013).

1.11 Notch signalling

The Notch signalling pathway is one of the major intercellular signalling pathways that is highly conserved between species (Andersson, Sandberg et al. 2011). Despite the fact that the canonical Notch signalling pathway is rather simple, Notch effects on various cell types at various developmental stages and in multitude of species are pleiotropic (Andersson, Sandberg et al. 2011). In relation to cardiovascular system Notch regulates among others the processes of arteriovenous specification and endothelial sprouting and branching during physiological and pathological angiogenesis (Gridley 2010).

Mechanistically, canonical Notch signalling refers to cell-cell interactions in a juxtacrine manner where Notch ligands Delta-like 1,3 and 4 (DLL1,DLL3 and DLL4) and Jagged1 and 2 localised on plasma membranes of signalling cells bind to transmembrane Notch receptors (NOTCH1-4) localised on adjacent (receiving) cells. This results in a series of proteolytic cleavages of the transmembrane Notch receptor with subsequent translocation of Notch intercellular domain (NICD) from the plasma membrane into the nucleus. NICD forms a transcriptional complex with CBF1/Suppressor of Hairless/LAG-1 (CSL) DNA-binding protein, Mastermind-like 1 protein and histone acetyltransferases leading to transcriptional activation of Notch target genes. In the absence of NICD in the nucleus, CSL binds to specific regulatory sequences of Notch target genes and inhibits their expression. Numerous auxiliary proteins modulate canonical Notch signalling as well (Andersson, Sandberg et al. 2011).

Additionally, various types of non-canonical Notch signalling have been described (D'Souza, Meloty-Kapella et al. 2010; Heitzler 2010). These do not require a canonical Notch ligand or the activation and proteolytic cleavage of Notch receptor for the initiation of Notch signalling. In other forms of non-canonical Notch signalling there is no CSL involvement reflecting possible involvement of other signalling pathways upstream of the NICD-CSL interaction (Heitzler 2010).

Our group have recently shown that blood flow suppresses vascular Notch signalling in developing zebrafish embryos via suppressing the expression of *dll4* (Watson, Novodvorsky et al. 2013). Cessation of flow in zebrafish embryos caused increased *dll4* expression resulting in increased activity of Notch signalling pathway at 48hpf and 72hpf. This was evidenced by increased vascular fluorescence in a transgenic zebrafish line *Tg(CSL:venus)qmc61* (expresses the yellow fluorescent protein derivative venus driven by concatemered CSL-binding sites) (Watson, Novodvorsky et al. 2013). This was the first time that blood flow as a mechanical force has been found to alter Notch signalling *in vivo*.

1.12 Zebrafish as a model for cardiovascular studies

Zebrafish (*Danio rerio*) are small freshwater fish that originate from Southeast Asia. Adult fish are able to produce several hundreds of eggs per week and these are fertilised externally by males and also develop externally independently of the mother. This, together with their optical clarity makes them very useful in studying vertebrate developmental processes *in vivo* (Chico, Ingham et al. 2008). Zebrafish embryos develop rapidly so that at 24hpf they have a contracting two-chambered heart. Functional axial vessels and blood flow that can be visualized *in vivo* by applying simple light microscopy. Genetic factors that drive zebrafish cardiovascular

development are largely conserved between mammals and zebrafish with zebrafish orthologs identified for many important genes in these processes such as Notch , Sonic hedgehog, VEGF or KLF2 (Stainier 2001; Lawson, Vogel et al. 2002). Zebrafish embryos are not dependent on oxygenation via blood circulation up to 5dpf as they are able to obtain sufficient amounts of oxygen via simple diffusion. This makes them very useful for studying the role of blood flow as a haemodynamic force on endothelial physiology, vasculogenesis and angiogenesis (Pelster and Burggren 1996; Chico, Ingham et al. 2008).

Improvements in techniques used to create stable transgenic lines (Busmann and Schulte-Merker 2011) enable creation of multiple zebrafish transgenic lines that allow *in vivo* localization of fluorescent reporters labelling cell types and tissues relevant to cardiovascular research (Quaife, Watson et al. 2012).

Methods of both forward and reverse genetics have been successfully employed in zebrafish to gain more insight into cardiovascular development. More than 100 mutants with abnormalities in cardiovascular system were identified by introduction of random mutations followed by observations for abnormal phenotypes (Chen, Haffter et al. 1996).

Gene function can also be studied in zebrafish using Morpholino oligonucleotides (MO). These are synthetic oligomers about 25bp long that bind to complementary RNA sequences and either block the initiation of translation or modify pre-mRNA splicing (GENE TOOLS). Injections of a specific MO into the fertilised zebrafish egg at very early stages of its development (1 to 4-cell stage) induces a specific, but temporary gene knockdown (MO effect wears off after 3-5 days) (Nasevicius and Ekker 2000). Unfortunately, MO-mediated gene knockdown has several disadvantages – incomplete loss of function, off-target effects and non-specific toxicity and aforementioned

temporary effect to mention the most important ones (Eisen and Smith 2008; Bill, Petzold et al. 2009).

In recent years novel methods and techniques of site-targeted mutagenesis have been developed enabling generations of stable zebrafish mutant lines. Zinc Finger Nuclease (ZFN) engineering by context-dependent assembly (CoDA) (Sander, Dahlborg et al. 2011), Transcription Activator-Like Effector Nucleases (TALEN) (Cermak, Doyle et al. 2011) and most recently Clustered Regularly Interspaced Short Palindromic Repeats/CRISPR-associated systems (CRISPR/Cas9) (Hwang, Fu et al. 2013) are powerful tools for targeted zebrafish genome editing. This enables creations of mutations that are stable and transmitted through the germ line (Cermak, Doyle et al. 2011; Sander, Dahlborg et al. 2011).

High fecundity, small size, rapid embryonic development, optical clarity, existence of many tissue-specific transgenic lines but also aquatic environment and permeability of zebrafish embryonic tissues make zebrafish embryos a useful tool for high throughput screening for novel therapeutic agents (Novodvorsky, Da Costa et al. 2012). Small molecule screens have been for example employed in a search for novel antiarrhythmics (Peal, Mills et al. 2011), inhibitors of intestinal lipid absorption (Clifton, Lucumi et al. 2010) or antiangiogenic drugs (Serbedzija, Flynn et al. 1999).

Despite above advantages zebrafish represent a non-mammalian model. Zebrafish genome underwent partial genome duplication after divergence of the teleost lineage during evolution (Taylor, Braasch et al. 2003), and has therefore in many cases two copies of a single mammalian gene. This makes the interpretation of the relevance of the results of single gene knockdown in zebrafish challenging (Chico, Ingham et al. 2008). Equally, there are substantial anatomic differences between humans and zebrafish. The zebrafish heart is two-chambered with no pulmonary circulation. The

anatomy of the zebrafish embryonic aorta differs to the one of adult human, not only by its diameter (the diameter of zebrafish embryonic aorta is 30-50µm which is similar to that of an adult human arteriole – 10-150µm) but also in the histology of both vessel walls. Human aorta contains a thick tunica media whereas in zebrafish a thin layer of mural cells forms at 72hpf (zebrafish equivalent to embryonic smooth muscle cells in higher vertebrates) (Chico, Ingham et al. 2008; Santoro, Pesce et al. 2009).

1.13 Aims of my research

My aims were to utilise the advantages of zebrafish animal model in further studies of *klf2a* functions in vascular biology.

1.14 Hypotheses

klf2a is expressed in embryonic zebrafish vasculature in response to blood flow

kf2a acts as a negative regulator of vascular *cxcr4a* expression in zebrafish

klf2a is involved in blood flow mediated regulation of vascular Notch signalling in zebrafish

klf2a acts as a link between blood flow and excessive angiogenesis observed in *vhl* mutants

Experiments on *klf2a* mutant embryos will confirm and extend the data obtained by MO-specific *klf2a* knockdown

1.15 Objectives

These hypotheses were tested by completing the following experimental objectives:

- Examine *klf2a* expression patterns in developing zebrafish embryos
- Examine *klf2a* involvement in blood flow dependent regulation of *cxcr4* expression in endothelium
- Examine *klf2a* involvement in blood flow dependent regulation of endothelial Notch signalling
- Examine *klf2a* involvement in blood flow dependent signalling leading to excessive angiogenesis observed in *vhl* mutants
- Generate a stable *klf2a* mutant zebrafish line
- Establish the phenotype of the *klf2a* mutant line especially with regards to cardiovascular system
- Compare the *klf2a* mutant phenotype to the data obtained by MO-mediated *klf2a* knockdown studies

Chapter 2

Materials and methods

2.1 Zebrafish husbandry

2.1.1 Home Office regulations

All studies performed on zebrafish were conformed to Home Office regulations and were carried out in accordance with project licence 40/3434 held by Dr T.J. Chico, project licence 40/3082 held by Dr F. van Eeden and personal licence 40/10149 held by myself. Zebrafish were raised in the Centre for Developmental and Biomedical Genetics aquaria and fed *artemia nauplii* (ZM SYSTEMS) by aquaria staff. Zebrafish were kept on a constant 14 hour on /10 hour off light cycle at 28°C.

2.1.2 Wild type zebrafish strains

AB wild type (AB WT) strain or Nacre wild type (Nacre WT) without neural crest-derived melanophores were used (Lister, Robertson et al. 1999).

2.1.3 Mutant zebrafish lines

Gridlock mutants are homozygous for a recessive *m145* allele of the *gridlock* gene coding for a transcription factor from the Hairy/Enhancer-of-split related (Hesr) protein family (Zhong, Rosenberg et al. 2000). Their blood flow to the trunk is impeded by a localised vascular defect in the anterior trunk (Weinstein, Stemple et al. 1995). *Gridlock* embryos were a kind gift of Dr Randall Peterson from Massachusetts Institute of Technology, Cambridge, Massachusetts, USA.

vhl^{hu2117} mutants have a nonsense mutation in the HIF1- α recognition site and were obtained from Hubrecht institute in Utrecht, Netherlands (van Rooijen, Voest et al. 2009).

By using TALEN mutagenesis I generated 4 novel *klf2a* mutant alleles named *klf2a*^{sh306}, *klf2a*^{sh307}, *klf2a*^{sh310} and *klf2a*^{sh317}.

2.1.4 Transgenic reporter lines

The *Tg(CSL-venus)qmc61* represents a notch reporter line that expresses the YFP derivative venus driven by 12 concatemerized CSL-binding sites. This was a kind gift from Dr M. Gering from University of Nottingham, Nottingham, UK.

vhl^{hu2117} line was crossed to *Tg(fli1:eGFP)* line which labelled endothelial cytoplasm with green fluorescence (Lawson and Weinstein 2002). This line was obtained from Zebrafish International Resource Centre, University of Oregon, USA.

klf2a^{sh317} line was crossed to a double transgenic line *Tg(kdrl:HRASmCherry;flk1:EGFP-nls)*. *Tg(kdrl:HRASmCherry)* labels endothelial cell membranes with red fluorescence (Hogan, Bos et al. 2009) and *Tg(flkl1:EGFP-nls)* labels endothelial nuclei with green fluorescence (Blum, Belting et al. 2008). These were a kind gift from Dr M. Affolter from University of Basel, Switzerland. *klf2a*^{sh317} line was also crossed to *Tg(CSL-venus)qmc61* and to *vhl*^{hu2117} ^{+/ -}; *Tg(fli1:eGFP)* lines to study the effects of *klf2a* on various signalling cascades.

2.2 Manipulation with zebrafish

2.2.1 Embryo collection and storage

To obtain clutches of embryos of mixed parentage, collection tanks consisting of an opaque plastic tank with a wire mesh separator and marbles were placed into adult fish tanks on the previous evening. For pair-mating, individual male and female adult fish were placed into a tank divided by a transparent plastic separator. Plastic separators

can be removed at a preferred time-point on the next morning to control the time when eggs are produced. Eggs were removed from the plastic tank and placed in a Petri dish (STERILIN) with 40ml fresh E3 medium at a density of 50 eggs per dish to maintain adequate aeration. Fertilised eggs were incubated in E3 medium at 28°C up to 5.2dpf when they were either euthanised using Tricaine (MS222) (SIGMA) and bleached or started on a feeding regimen under Home Office regulations.

2.2.1.1 E3 medium

1 litre of 10x stock concentration contains: 2.87g NaCl, 0.13g KCl, 0.48g CaCl₂·2H₂O, 0.82g MgSO₄·7H₂O. To make 1xE3, 100ml of 10x E3 was made up to 1 litre with filtered water (dH₂O). 3 drops of 0.5% (wt/vol) methylene blue were added in order to suppress mold growth.

2.2.2 Morpholino microinjections

Morpholinos (MOs) were custom made and purchased from GENE TOOLS and diluted to a stock concentration of 1mM. MOs were aliquoted and either stored at room temperature (RT) or at -20°C. Before injecting, MOs which were stored at -20°C were defrosted and put in a 65°C water bath for 5 -10min to overcome potential aggregation. MOs were subsequently diluted with milliQ water and phenol red (enables visualisation of injection) to the desired concentration.

MOs were injected into one-cell stage zebrafish embryos. Microinjection capillary tubes (TW100F-4 or TW120-4 by WORLD PRECISION INSTRUMENTS) were prepared on a micropipette puller (Model P-97 by SUTTER INSTRUMENTS). Capillary tubes were loaded with MOs and inserted into the micromanipulator attached to a pneumatic PicoPump PV 820 (WORLD PRECISION INSTRUMENTS). The end of the micropipette was removed by fine forceps. The exact amount of MOs injected was

quantified and adjusted using a graticule (PYSER-SGI) with a small drop of immersion oil. Selected embryos were lined up against a microscope slide and injected into the yolk-cell boundary under direct visualisation. Injected embryos were immediately placed in E3 medium and incubated at 28°C. MOs used in this project are listed in **Table 1**.

Table 1. Morpholino (MO) sequences and mechanism of action

MO name	Sequence (5`-3`)	Amount injected	Mechanism of action
control MO	CCTCTTACCTCAGTTACAATTTATA	2ng	no target
<i>tnnt2</i> MO	CATGTTTGCTCTGATCTGACACGCA	0.8-2ng	translation block
SB <i>klf2a</i> MO	CTCGCCTATGAAAGAAGAGAGGATT	0.5-2ng	pre-mRNA splice block
ATG <i>klf2a</i> MO	GGACCTGTCCAGTTCATCCTTCCAC	2ng	? (see section 2.2.2.2)
<i>klf2b</i> MO	AGTGTCAAATACTTACATCCTCCCA	2.2ng	pre-mRNA splice block

2.2.2.1 Splice blocking *klf2a* morpholino (SB *klf2a* MO)

The splice-blocking *klf2a* morpholino (further annotated as SB *klf2a* MO) was initially used by Nicoli et al. (Nicoli, Standley et al. 2010). SB *klf2a* MO binds to the exon 3 (E3) splice acceptor site of *klf2a* sequence with resulting inclusion of a 105bp long intron 2 (I2) (**Figure 2.1a**). Primers designed around *klf2a* I2 (F and R-RT-PCR *klf2a*) amplified a 293bp fragment in case of a properly spliced *klf2a* transcript, while inclusion of I2 resulted in a production of 398bp fragment. As shown in **Figure 2.1b** there was still a significant proportion of correctly spliced *klf2a* mRNA present even in embryos injected with the highest dose of SB *klf2a* MO used (2.5ng per embryo). This level of *klf2a* knockdown was however reported to be sufficient to cause a biological effect and

subsequent *klf2a* RT-qPCR demonstrated decreased levels of wild type *klf2a* transcript in SB *klf2a* MO injected morphants in comparison to controls (**Figure 2.1c**) (Nicoli, Standley et al. 2010). Unfortunately, the published sequence for R-RT-PCR primer was incorrect. A new set of primers spanning *klf2a* I2 named L and R *klf2a* E2E3 (**Table 2**) was designed (**Figure 2.2a**). These primers amplified a 562bp polymerase chain reaction (PCR) product in case of correct *klf2a* pre-mRNA splicing and this was confirmed by subsequent sequencing. Inclusion of *klf2a* I2 produced a 667bp fragment. Due to high and unpredictable levels of SB *klf2a* MO toxicity lower than published doses of SB *klf2a* MO had to be injected. Eventually a dose of 1.1ng of SB *klf2a* MO per embryo was established and used in subsequent experiments. Increasing levels of unspliced 667bp fragment were observed in embryos injected with increasing doses of SB *klf2a* MO (**Figure 2.2b**). As expected, PCR on cDNA from uninjected embryos produced a single 562bp indicating correct and complete *klf2a* intron 2 splicing in zebrafish *klf2a* mRNA. PCR on genomic DNA (gDNA) extracted from identical uninjected controls produced a single 667bp fragment correctly indicating the presence of intronic sequences in zebrafish gDNA (**Figure 2.2c**).

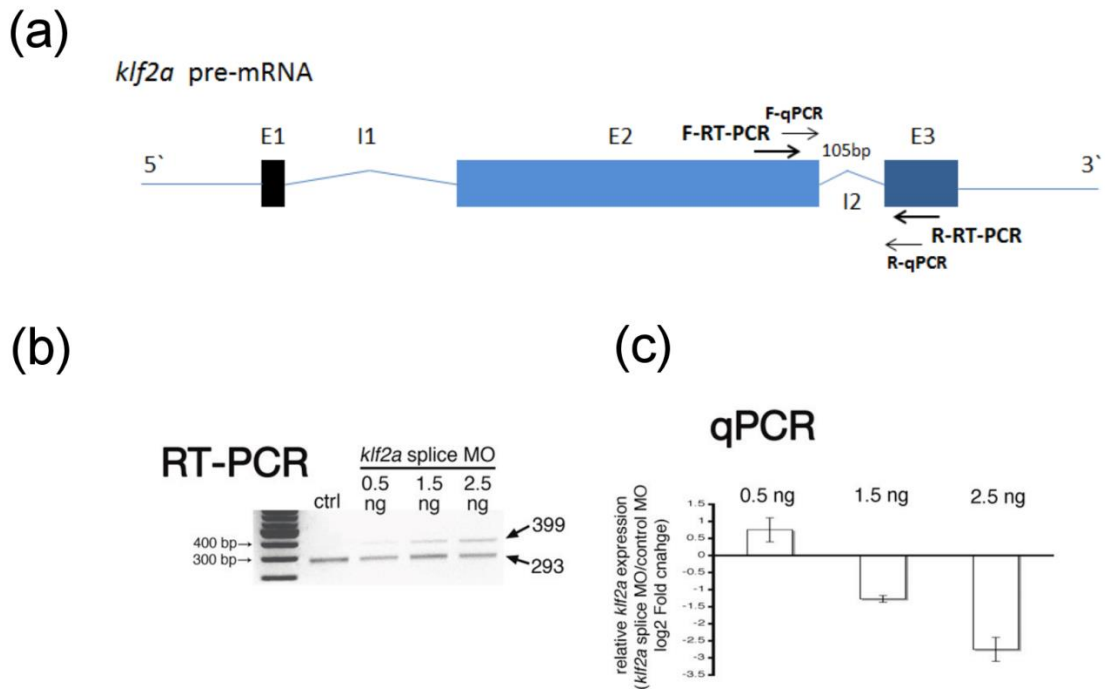


Figure 2.1 Verification of *klf2a* splice-blocking morpholino, as per Nicoli, Standley et al. 2010

(a) *klf2a* intron-exon structure with locations of primers for RT-PCR (F-RT-PCR and R-RT-PCR) and for qPCR (F-qPCR and R-qPCR). (b) RT-PCR of a fragment spanning *klf2a* intron 2 (I2). Increasing proportion of a 399bp unspliced fragment is seen with increasing amounts of SB *klf2a* MO injected per embryo but a significantly strong 293bp band representing correctly spliced *klf2a* mRNA is seen even at the highest amount of SB *klf2a* MO injected. (c) qPCR indicates decreased relative expression of correctly spliced *klf2a* in SB *klf2a* MO injected embryos when compared to controls. Adapted by permission from Macmillan Publishers Ltd: [NATURE] (Nicoli, Standley et al. 2010), copyright (2010).

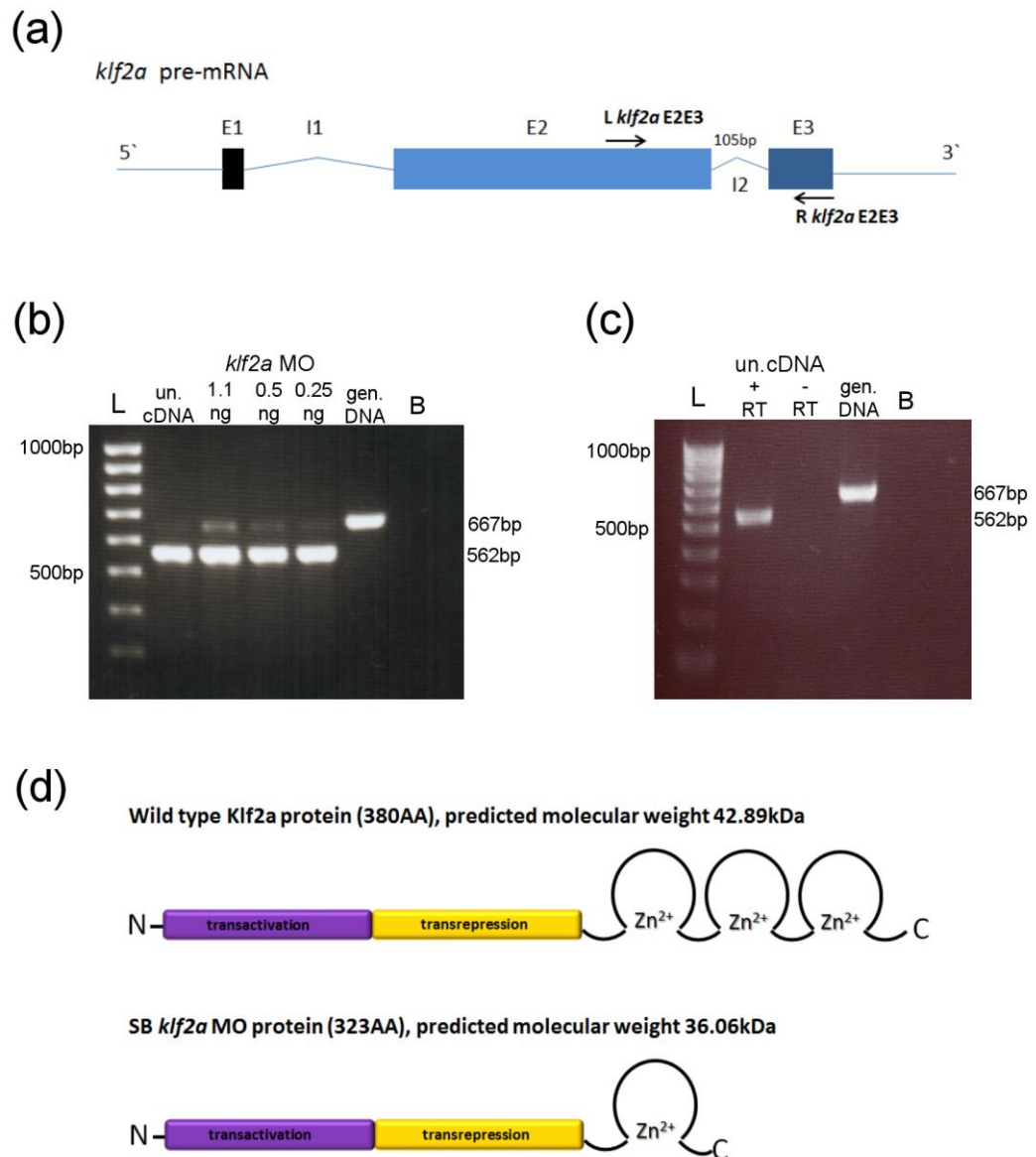


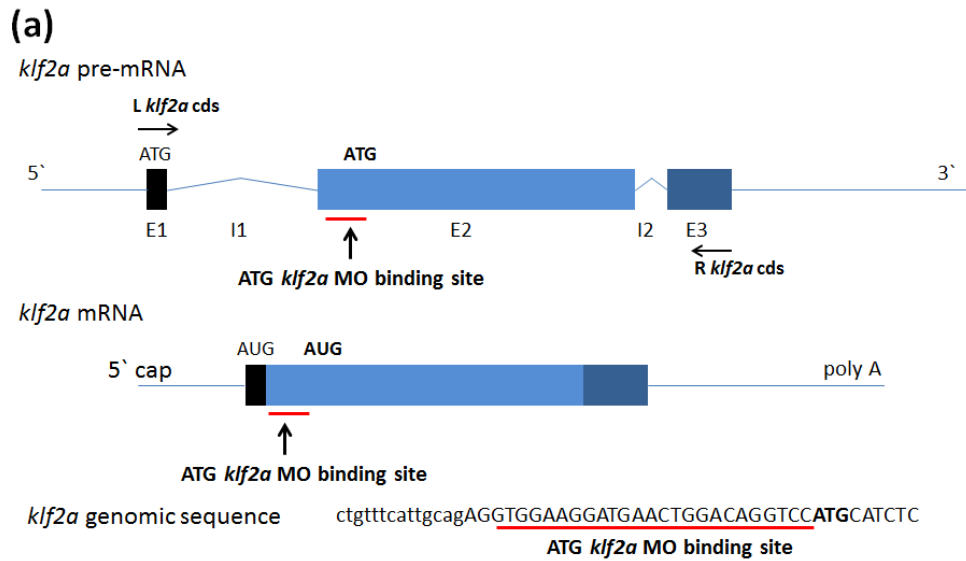
Figure 2.2 Verification of *klf2a* splice-blocking morpholino

(a) *klf2a* intron-exon structure with RT-PCR primers binding sites (L *klf2a* E2E3 and R *klf2a* E2E3). (b) Increasing amounts of a 667bp unspliced fragment are seen with increasing amounts of SB *klf2a* MO injected per embryo. (c) Reverse transcription is performed with (+RT) and without (-RT) reverse transcriptase on RNA extracted from uninjected embryos at 48hpf. Subsequent PCR with L and R *klf2a* E2E3 primers do not produce any product in case of mock RT (-RT) confirming the absence of genomic DNA contamination in cDNA samples. Abbreviations: L: Hyperladder IV (NEB), un.cDNA: complementary DNA from uninjected controls, RNA extracted at 48hpf, gen.DNA: genomic DNA extracted from wild type embryos at 48hpf, B: Blank (no template added to PCR reaction). (d) WT Klf2a and SB *klf2a* MO protein domain structures with indicated AA lengths and predicted molecular weights in kilodaltons (kDa) (free public domain http://www.bioinformatics.org/sms/prot_mw.html).

2.2.2.2 Translation-blocking *klf2a* morpholino (ATG *klf2a* MO)

The second *klf2a* morpholino I used is designed to block initiation of *klf2a* mRNA translation by binding to a region around the translational start (further annotated as ATG *klf2a* MO). This morpholino was previously used by 2 different research groups (Nicoli, Standley et al. 2010; Wang, Zhang et al. 2011). Wang et al. injected 2-10ng per embryo. I established that a dose of 4.1ng per embryo was the highest possible dose to give acceptable mortality and toxicity rates - around 20-30% death rates at 24hpf and up to 50% of healthy looking embryos with unimpeded blood circulation.

Surprisingly, later analysis of the ATG *klf2a* MO sequence showed that it does not target the region around the AUG translational start of *klf2a* mRNA as expected, but it targets a region 74 bases 3' downstream from the AUG translational start at the start of exon 2 (**Figure 2.3a**). According to GENE TOOLS, morpholinos targeted more than about 30 bases 3' to the AUG translational start site do not block translation (GENE TOOLS). Alternatively, there is an 'in frame' AUG codon in the close proximity of the ATG *klf2a* MO binding site (**Figure 2.3a**). The likelihood that this AUG represents an important alternative translational start site is low, given the fact that the first 34 amino acids (AA) of KLF2 protein (encoded between the original and putative alternative translational start) are conserved across the species (**Figure 2.3b**). In addition, this putative translational start is not present in human or mouse *KLF2/Klf2* genomic sequence in this region. Following the discussion with GENE TOOLS, an RT-PCR on RNA extracted from control MO (cont MO) and ATG *klf2a* MO morphants with primers that amplify the whole *klf2a* coding sequence (*klf2a* cds F1 and R1, see **Table 2**) was performed to detect the possibility of interference with *klf2a* pre-mRNA splicing. This revealed that ATG *klf2a* MO might be causing partial and complete inclusion of *klf2a* intron 1 (414bp) as shown in **Figure 2.3c**.



(b)

	first 34 AA of KLF2 protein	% of identity
zebrafish	MALSGTILPSISTFSAQKEKCWEN RWKDELDRSM	} 48% } 50%
mouse	MALSEPILPSFATFASPCERGLQ ERWPRNEPEAG	
human	MALSEPILPSFSTFASPCRERGLQ ERWPRAEPES	

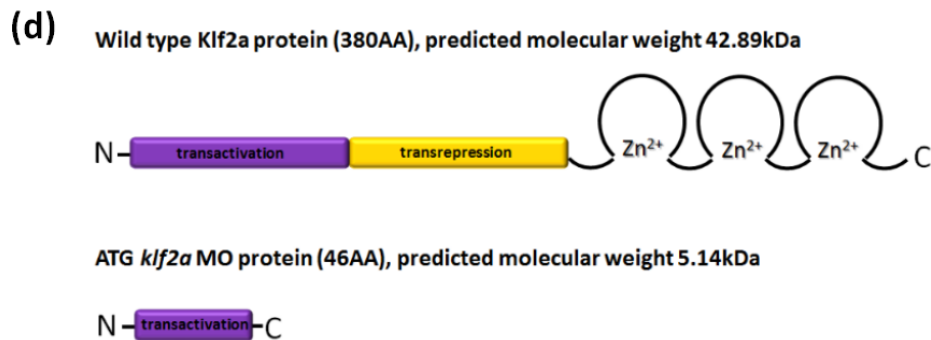
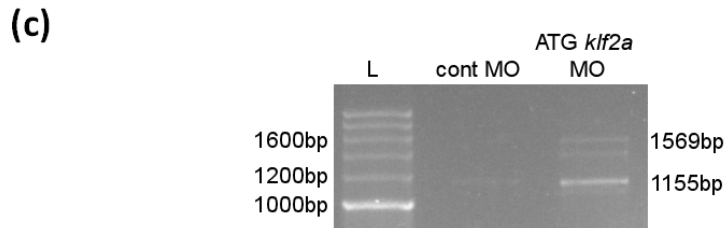


Figure 2.3 Verification of ATG *klf2a* morpholino

(a) Schematic drawing of *klf2a* intron-exon and mRNA structure with RT-PCR primers binding sites (L and R *klf2a* cds). The 2 ATGs (*klf2a* gene) and AUGs respectively (*klf2a* mRNA) indicate the original and putative translational start sites. E1-E3: exon 1-exon 3, I1-I2: intron 1- intron 2. ATG *klf2a* MO binding site is underlined in red, the 'in frame' ATG codon is highlighted in bold. **(b)** Comparison of initial 34 AAs of KLF2

proteins across the species. Translation of the coding sequence between the two AUG codons in zebrafish *klf2a* mRNA gives a 34 AA sequence (AAs coded by E1 are in black, AAs coded by E2 are in blue). Comparison of first 34 AAs of KLF2 proteins across the species shows relatively high levels of conservation. **(c)** RT-PCR on cDNA extracted from control MO and ATG *klf2a* MO morphants shows the presence of two additional bands at approx. 1400bp and 1600bp in the case of ATG *klf2a* MO likely representing the partial and complete inclusion of 414bp intron 1 sequence. A band of 1569bp would be expected in the case of complete intron 1 inclusion. 1155bp band in both cont MO and ATG *klf2a* MO lanes represents the correctly spliced *klf2a* mRNA. *klf2a* cds F and R primers that amplify the whole *klf2a* coding sequence (cds) were used. Abbreviations: L: Hyperladder II (NEB). **(d)** WT Klf2a and ATG *klf2a* MO protein domain structures with indicated AA lengths and predicted molecular weights in kilodaltons (kDa) (free public domain http://www.bioinformatics.org/sms/prot_mw.html).

2.2.3 Tricaine treatment for anaesthesia or temporary blockage of embryonic heart contractions

Tricaine (3-amino benzoic acid ethylester) was purchased in a powdered form (SIGMA). In order to make 500ml of stock concentration solution (4 mg/ml), the following was combined: 2.0 g Tricaine powder, 490ml milliQ water. The solution was buffered with 1M Trizma base (SIGMA) (pH 10) to pH 7 and stored in the fridge (4°C) for up to 2 weeks or in the freezer (-20°C) long term.

For anaesthesia, 4.2ml of Tricaine stock solution (4mg/ml) was added to 100ml of aquarium water giving a final Tricaine concentration of 0.168 mg/ml. For temporary blockage of embryonic heart contraction, Tricaine was diluted in E3 to a final concentration of 0.66mg/ml. Up to 50 embryos were put into a Petri dish with 40ml of E3 with Tricaine at 32hpf and were incubated under standard conditions (28°C) until 48hpf. This treatment reproducibly stopped erythrocyte circulation in the dorsal aortae (DA) of embryos within 30min. Embryos treated with this Tricaine concentration fully recovered circulation within 30min when put back into E3 and continued to develop normally beyond 5.2dpf. At 48hpf embryos were euthanised and used for RNA extraction or fixed for subsequent whole-mount in situ hybridisation (WISH). For AA5x angiogenesis experiments embryos were treated with the same Tricaine dilution (0.66mg/ml) in E3 medium from 46hpf until 70hpf.

2.2.4 Dechoriation

Wild type zebrafish embryos required for experiments before hatching (2-3dpf) (Kimmel, Ballard et al. 1995) were manually dechorionated under a stereomicroscope using a pair of Dumont #5 tweezers (WORLD PRECISION INSTRUMENTS). In mutant

lines or MO-injected embryos, hatching was delayed beyond this stage and these required manual dechoriation even at later developmental stages.

2.2.5 Fin-clipping of adult zebrafish

The adult zebrafish were briefly anaesthetised with Tricaine (0.168 mg/ml). The distal third of caudal fin was removed using fine scissors and placed into a marked tube. Zebrafish were immediately put into a marked tank with aquarium water.

2.2.6 Fin-clipping of zebrafish embryos at 3dpf

The progeny of an incross of 2 heterozygous carriers of the *klf2a*^{sh317} allele had to be genotyped prior to protein extraction for Western blotting at 5dpf. This protocol was developed in our centre (Wilkinson, Elworthy et al. 2013). Anaesthetized embryos were placed on the dissection surface made from petri dish lined with a strip of an autoclave tape. The tip of the caudal fin distally to blood circulation was removed under direct visual control using a stereomicroscope and a micro scalpel (WORLD PRECISION INSTRUMENTS). Individual embryos were transferred into labelled dishes. Fin biopsies were transferred into 96-well plates containing 50µl methanol (SIGMA), placed into an open PCR block and heated at 80°C until all methanol was evaporated. Next 10µl TE Tween (2.9ml TE pH 8.0 + 50µl 20% Tween) was added to each well and the block was heated to 98°C for 10min and cooled. Finally, 5µl of proteinase K (25 mg/ml) (ROCHE) was added to each well and the mixture was incubated in a PCR block at 55°C for 1 hour and at 98°C for 10min to deactivate proteinase activity. This genomic DNA solution was added directly into a PCR reaction (1-2µl).

2.2.7 Phenylthiourea (PTU) treatment to inhibit embryonic pigment formation

Addition of 1-phenyl 2-thiourea (PTU) (SIGMA-ALDRICH) into the E3 medium after shield stage, but earlier than at 24hpf, inhibited melanin formation in the skin melanophores of zebrafish embryos with resulting increased transparency for vascular imaging. 80 mg of PTU was dissolved in 25ml of phosphate buffered saline (PBS) to give a stock concentration of 3.2 mg/ml. 400µl of stock concentration PTU was added to 10ml of E3 giving final PTU concentration 0.00128% (w/v).

2.2.8 Microscopy

2.2.8.1 Light Microscopy

Visual assessment of embryos, monitoring of WISH staining and heart rate counting were performed using a Leica S6E stereo microscope (LEICA MICROSYSTEMS). Images of live embryos and WISH images were taken using a Leica M165 FC fluorescent stereo microscope with Leica DFC310 FX camera (both by LEICA MICROSYSTEMS). When imaging embryos after WISH, an external Zeiss KL1500 LCD light source (CARL ZEISS MICROSCOPY) was used and embryos were mounted in 100% glycerol in a watch glass.

2.2.8.2 Fluorescence Microscopy

Identification of fluorescent transgenic zebrafish embryos was done using a Leica M165 FC fluorescent stereo microscope (LEICA MICROSYSTEMS). Fluorescence microscopy was performed using UltraVIEW Vox spinning disc confocal microscope and Volocity v5.3.2 imaging software (both by PERKIN ELMER). Zebrafish embryos were anaesthetised with Tricaine and mounted on a cover slip in 1% low-melting point

agarose prior to imaging. Images were taken in 2µm slices across the region of interest and were then digitally processed by focal plane merging (Z stacking). Merged images were further analysed by using ImageJ software (version 1.45s public domain software <http://imagej.nih.gov/ij>).

2.3 Statistical analysis

All statistical analysis was carried out using GraphPad Prism v5.04 software. Data were presented in an appropriate graphical form as mean ± standard error of the mean (SEM). Statistical test alongside the post-test analysis used to analyse significance is annotated in the individual figure. Statistical significance was annotated as follows: ns = non-significant, * = p<0.05, ** = p<0.01, *** = p<0.001, **** = p<0.0001. Number of embryos analysed was annotated by an n number.

2.4 Molecular biology methods

2.4.1 Primers design

PCR primers were designed using Primer3 software (v.0.4.0. public domain software <http://bioinfo.ut.ee/primer3-0.4.0/primer3/>). Primers used in this project are listed in

Table 2.

Table 2. List of primers

Name	Sequence
L <i>klf2a</i> E2E3	ACGGACCTGTACGAGGAATG

R <i>klf2a</i> E2E3	TCTGATGAATTGACCCGTCA
SP6 primer	CCCAAGCTTGATTTAGGTGAC
T7 primer	AATACGACTCACTATAG
<i>klf2a</i> cds F1 (Peter F1)	GGATCCATGGCTTTGAGTGGAACG
<i>klf2a</i> cds R1 (Peter R1)	GAATTCCTACATATGACGTTTCAT
<i>klf2a</i> TAL XcmI L1	CAGGCGACTACAGAATGCAA
<i>klf2a</i> TAL XcmI R1	GCCCTCTTGTTTGACTTTGG
TAL_R2	GGCGACGAGGTGGTCGTTGG
SeqTALEN_5-1	CATCGCGCAATGCACTGAC
<i>gapdh</i> F	AGGCTTCTCACAAACGAGGA
<i>gapdh</i> R	GCCATCAGGTCACATACACG
<i>vhl</i> F	TAAGGGCTTAGCGCATGTTC
<i>vhl</i> R	CGAGTTAAACGCGTAGATAG
<i>klf2b</i> L1	CATTAACCCTCACTAAAGGGAACGTGGACATGGCTTTACCTT
<i>klf2b</i> R1	TAATACGACTCACTATAGGGATGGGAGCTTTTGGTGTACG
<i>klf4a</i> L1	CATTAACCCTCACTAAAGGGAATTGATAGCATGGCACTGAGC
<i>klf4a</i> R1	TAATACGACTCACTATAGGGCCTGCGGAAATCCAGAATAA
<i>klf4b</i> L1	CATTAACCCTCACTAAAGGGAACCCCGGACATGAATTATCA
<i>klf4b</i> R1	TAATACGACTCACTATAGGGTGTCCGGTGTGTTTCCTGTA

2.4.2 RNA extraction

RNA was extracted either from approximately 20 to 30 pooled intact zebrafish embryos or from tail sections of 30 embryos. Embryos were collected in 1.5ml Eppendorf tubes (EPPENDORF) and washed with diethylpyrocarbonate (DEPC) – treated water (LIFE TECHNOLOGIES). Next, DEPC water was removed and 250µl of TRIzol (LIFE TECHNOLOGIES) was added and tissues immediately homogenised using a 1ml syringe (PLASTIPAK BD) and 25 gauge needle (MICROLANCE 3 BD). Tail sections that were previously put into TRIzol and snap frozen in liquid Nitrogen were defrosted

on ice and homogenised as described above. Subsequently 50µl of chloroform (SIGMA ALDRICH) was added to the homogenate, mixed and left at RT for 3min and then centrifuged at 13000rpm for 15min at 4°C. The aqueous supernatant containing the RNA was carefully removed, precipitated in 85µl of isopropanol (SIGMA ALDRICH) and pelleted by centrifugation (13000rpm, 15min at 4°C). Isopropanol was then completely removed and the RNA pellet was resuspended in 15µl of RNase free water (miliQ water). RNA was quantified by spectrophotometry (Nanodrop ND100 spectrophotometer, THERMO FISHER SCIENTIFIC) and a sample was run on a gel prior to storage at -80°C.

2.4.3 cDNA synthesis by reverse transcription (RT) of RNA

cDNA synthesis was performed using the VERSO cDNA Synthesis Kit (THERMO SCIENTIFIC). A reaction was set up as follows: 5x cDNA synthesis buffer: 4µl, dNTP mix: 2µl, RNA primer (anchored oligo dT): 1µl, Verso enzyme mix: 1µl, RNA template: 1ng (1-5µl), miliQ water: up to 20µl. Reaction mix was heated to 42°C for 30min and followed by a 95°C enzyme inactivation for 2min. cDNA was quantified by spectrophotometry and stored at -20°C.

2.4.4 Real-time reverse transcription polymerase chain reaction (RT-qPCR)

All reagents and equipment for RT-qPCR assays came from LIFE TECHNOLOGIES unless stated otherwise. TaqMan Gene Expression assays were used for *cxcr4a*, *dll4* (ID: Dr03428642_m1) and *ef1* (Assay ID: Dr03432748_m1) which did not require prior primer optimisation protocols.

A reaction was set up as follows: 2x Mastermix: 10µl, 20x TaqMan gene expression assay (contains forward and reverse primers and a TaqMan probe): 1µl, cDNA sample (1µl = 50ng cDNA) and 8µl milliQ water to a final volume of 20µl. Serial dilutions of cDNA from wild type embryos (starting at 150ng) were run in duplicate for each TaqMan gene expression assay in order to calculate the efficiencies of TaqMan assays from the seven point standard curve.

The 7900HT FAST REAL-TIME PCR System (APPLIED BIOSYSTEMS) based in the Core Genomic Facility, Medical School of the University of Sheffield was used to perform the RT-qPCR reaction in a 384-well plate.

2.4.4.1 Analysis of RT-qPCR data

SDS 2.3 software was used for the initial analysis of raw data in order to set an optimal threshold value and obtain corresponding ct values. Standard curve calculations and further RT-qPCR data analysis was performed using Microsoft Excel software (MICROSOFT) and GraphPad Prism 5.04 software.

Efficiency of RT-qPCR assay was calculated by using the standard curve method. Next I used the Pfaffl method of relative quantification for calculation of fold changes of gene expression levels (Pfaffl 2001).

2.4.5 *klf2a*^{sh317} mutant line cDNA sequencing

RNA from 30 pooled embryos of the F3 generation of homozygous carriers of *klf2a*^{sh317} allele was extracted at 4dpf as described elsewhere. A set of primers named *klf2a* cds F1 and R1 that amplify the whole 1155bp long *klf2a* coding sequence (cds) were designed (**Table 2**). Following RNA extraction, cDNA was synthesised by RT reaction and *klf2a* cds was PCR amplified in a single step using Superscript III One-Step reverse transcription polymerase chain reaction (RT-PCR) kit with Platinum *Taq*

Polymerase (INVITROGEN). A reaction was set up as follows: 2x Reaction Mix: 10µl, *klf2a* cds F1 and R1 primers (10µM): 1µl each, SuperScript III RT/Platinum *Taq* Mix: 0.5µl, RNA template (c = 675ng/µl): 1µl, miliQ water up to final Volume of 20µl. This reaction was then put into a thermal cycler to undergo a following 3-step protocol (A-C): A (cDNA synthesis and pre-denaturation): one cycle of 50°C for 30min and 94 °C for 2min. B (PCR amplification): 35 cycles of: 94 °C for 2min, 56°C for 30 seconds, 68 °C for 1min. C (final extension): 68 °C for 5min. PCR product was then purified using QIAquick PCR purification kit (QIAGEN). Purified PCR product was cloned into a p-GEM T-Easy Vector (PROMEGA) using the TA cloning method. The following ligation reaction was set up: 2x Rapid Ligation Buffer: 5µl, p-GEM T-Easy Vector (c = 50ng/µl): 1µl, T4 DNA ligase (3 Weiss units/µl): 1µl, PCR product (c = 182ng/µl): 0.3µl, miliQ water up to final Volume of 10µl. The reaction was incubated at RT for 1 hour. p-GEM T-Easy Vector with cloned *klf2a* cds was transformed into 10-beta competent *E.coli* (New England Biolabs - NEB) following the manufacturer`s protocol exactly and grown on selective media (Ampicillin/X-Gal) overnight at 37°C. Next day, 23 well-separated white colonies were inoculated into LB broth with Ampicillin and grown overnight at 37°C shaking. Amplified plasmids were purified using QIAprep SpinminiPrep kit (QIAGEN) and submitted for sequencing with SP6 and T7 primers (**Table 2**).

2.4.6 Genomic DNA extraction

Genomic DNA (gDNA) extraction was performed using a modified protocol for REExtract-N-Amp™ Tissue PCR kit (SIGMA-ALDRICH). Residual ethanol (in case of resected fin tissue) or E3 medium (in case of whole embryo gDNA extraction) were completely removed because these interfere with the extraction process or subsequent PCR. 25µl of Extraction Solution and 6.25µl of Tissue Solution were added to each tissue sample and vortexed for 15 seconds. Tissues were subsequently incubated at

RT for 15min to complete the digestion process and vortexed. Next tissues were heated at 95°C for 3min to denature the digestion enzyme. Finally, 25µl of Neutralisation Solution was added per tissue sample. This solution of extracted gDNA can be directly added to a standard PCR mixture or can be long-term stored at -20°C.

2.4.7 *vhl*^{hu2117} genotyping

A 414bp region of gDNA around the site of *vhl*^{hu2117} point mutation (C/T) was PCR amplified with *vhl* F and R primers (**Table 2**) by setting up the following reaction mix: Biomix (BIOLINE): 10µl , *vhl* F and R primers: 0.5µl both, gDNA 4µl, miliQ water 5µl. For amplification, the following PCR programme was used (**Table 3**):

Table 3. PCR programme used for *vhl*^{hu2117} genotyping

Step	Temperature	Time
1. Initialisation	94°C	4min
2. Denaturation	92°C	1min
3. Annealing	56°C	30sec
4. Elongation	72°C	40sec
5. Cycle to step 2 – 39x		
6. Final elongation	72 °C	10min
7. Final hold	4 °C	hold

vhl^{hu2117} point mutation (C/T) results in a loss of restriction site for BciVI enzyme (NEB). *vhl* PCR product was incubated with BciVI enzyme (NEB) to identify wild type, heterozygous and homozygous *vhl*^{hu2117} mutants. The following reaction was set up: *vhl* PCR product: 5µl, BciVI (NEB): 0.2µl, NEBuffer IV (NEB): 1.8µl, miliQ water 13µl. This was incubated at 37°C overnight. The whole digest reaction (20µl) was then

electrophoretically separated on a 1.5% agarose gel. *vhl*^{hu2117} homozygous mutants were identified by the presence of a single 414bp band. *vhl*^{hu2117} heterozygous carriers by the presence of an undigested 414bp band as well as digested approximately 200bp long band. Wild type fish were identified by a complete BciVI (NEB) digest resulting in the presence of approx. 200bp bands on a gel.

2.4.8 DNA sequencing

DNA sequencing was performed at the Core Genomic Facility at the Medical School of the University of Sheffield. DNA samples were submitted at approximate concentrations of 50ng/μl and primers were submitted at approximate concentrations of 10 pmol/μl. DNA sequencing data were analysed using Finch TV software, version 1.4.0 public domain software <http://www.geospiza.com/Products/finchtv.shtml> .

2.5 Measurement of cardiovascular parameters

2.5.1 Measurement of heart rates

Heart rates in developing zebrafish embryos depend among other factors on environmental temperature (Barrionuevo and Burggren 1999). Embryos were therefore kept in individual dishes and removed from the 28°C incubator individually immediately before measurement took place. Heart beats were measured under direct visual control by using stereomicroscope. Beats per minute were counted for 30 seconds and then doubled to give beats per minute rate (bpm).

2.5.2 Blood flow velocity analysis

Zebrafish embryos were anesthetised with Tricaine and imaged at 10x magnification and at 300 frames/second using a high speed camera (OLYMPUS IX81) and Video Savant 4.0 digital video recording software (IO INDUSTRIES). Mounting in low melting point agarose was not necessary due to a short imaging time of approx. 1.33 second – so that 400 images in .tiff format per each embryo were recorded. A region of DA around cloaca was arbitrarily chosen as a site for measuring erythrocyte velocities due to its easy anatomical location. Images were analysed using ImageJ software in order to obtain a kymograph with lines representing movements of individual erythrocytes in real time. When a rectangle was drawn across a particular line, the width of such rectangle represented the distance that particular erythrocyte travelled and the height of a rectangle represented the time in which this distance was travelled. Knowing the ratios of pixel/ μm ($0.8 \text{ pixel}/\mu\text{m}$ or $1.25\mu\text{m}/\text{pixel}$ in 10x magnification), pixel/frame (1:1 because each rectangle drawn over the aorta will be 1 pixel high) and knowing the rate of imaging (300 frames/second), the velocity (v) was calculated by using a formula $v = \text{distance}/\text{time}$ [$\mu\text{m}/\text{sec}$]. Velocity calculated in such way represented an average erythrocyte velocity per single cardiac cycle. If this velocity exceeded certain value so that a particular kymograph is not able to capture the movement of a single erythrocyte throughout one complete cardiac cycle, erythrocyte velocity was calculated by using CORRELATOR software (custom made software by Scott Reeve). Kymograph files were imported into the CORRELATOR which calculates instantaneous erythrocyte velocities throughout the whole cardiac cycle for each embryo. An average erythrocyte velocity per single cardiac cycle was now calculated by averaging all instantaneous velocities measured in that particular cardiac cycle. This value therefore corresponded to an average erythrocyte velocity calculated in ImageJ. Additionally, when cardiac cycles of all embryos from the same treatment group were put in phase average

instantaneous erythrocyte velocities for each frame were calculated and plotted as a single velocity curve.

2.5.3 Digital motion analysis

Zebrafish embryo angiograms and images of zebrafish embryonic hearts were constructed by using particle imaging velocimetry (PIV) software DaVIS (LAVISION). Angiograms were then imported into ImageJ software and further analysed.

2.5.4 Calculations of retrograde flow fraction (RFF)

RFF calculations were performed following a protocol published by Vermot et. al (Vermot, Forouhar et al. 2009). Embryos were imaged on Leica DFC310 FX camera (LEICA MICROSYSTEMS) at 300fps and angiograms were constructed using ImageJ software. Angiograms were analysed frame by frame and erythrocyte flow direction in the AV canal between embryonic atrium and ventricle was recorded per each frame. Anterograde flow represented a flow direction from atrium to ventricle. Retrograde flow represented an erythrocyte flow from ventricle back to atrium. No erythrocyte movement in particular frame was annotated by 0. RFF was calculated as the number of frames in which the direction of flow was retrograde divided by a total number of frames per single cardiac cycle.

2.5.5 Endothelial nuclei quantification

Confocal extended images of a *Tg(kdrl:HRASmCherry;flk1:EGFP-nls)* reporter line in various genetic backgrounds were used for endothelial nuclei quantifications as an indication of the number of endothelial cells. Endothelial nuclei number was counted manually in a 3 somite region in the middle of the trunk (dorsally of cloaca) including 4

ISVs and a corresponding region of dorsal longitudinal anastomotic vessel (DLAV). Endothelial nuclei of DA were not considered.

2.5.6 Measurements of mean fluorescence in *Tg(CSL:venus)qmc61* zebrafish line

Zebrafish embryos at 2 and 3dpf were mounted laterally in 1% low-melting point agarose on a cover slip. A trunk section around the cloaca was chosen for imaging due to easy anatomical location. Embryos were imaged on confocal microscope as detailed elsewhere. Merged images were analysed using ImageJ software. Fluorescence was measured in the DA by drawing a line across the whole image to cover the longest section possible. Aortic fluorescence was normalised to fluorescence of neural tube which was also measured across the whole image to obtain representative average values. This was done due to the high variability of venus fluorescence observed among individual embryos even when from the same pair of parents.

2.6 Whole mount in situ hybridisation (WISH)

2.6.1 Synthesis of *klf2a* riboprobe

An expressed sequence tag (EST) clone IMAGp998A0510285Q containing full-length *klf2a* cDNA sequence (approx. 2.1 kB) in pT7T3D-PacI vector was purchased from IMAGENES (now LIFE SCIENCES). EST clone was stepwise amplified in selective media, checked with a restriction enzyme digest (EcoRI and NotI (NEB) and purified using QIAprep SpinminiPrep kit and HiSpeed Plasmid Midi kit (both from QIAGEN). A double enzymatic digest of EST clone with XbaI and EcoRI (both NEB) resulted in a 1144bp *klf2a* cDNA fragment. This was inserted into XbaI and EcoRI digested

Bluescript KS and subsequently used for the *klf2a* riboprobe synthesis. A shorter than full-length *klf2a* riboprobe was chosen to improve its tissue penetration.

2 restriction reactions with XbaI and EcoRI (both from NEB) were carried out. First reaction involved 4 µg of EST clone IMAGp998A0510285Q, 4µl 10x NEBuffer 4, 0.4µl 100x BSA, 1.5µl EcoRI, 1.5µl XbaI (all from NEB) and milliQ water up to final volume 40µl. Second reaction involved 10 µg of Bluescript KS vector, 4µl 10x NEBuffer 4, 0.4µl 100x BSA, 1.5µl EcoRI, 1.5µl XbaI and milliQ water up to final volume 40µl. Both restriction reactions were incubated for 4 hours at 37°C and run on a 0.8% agarose gel made up with SYBR® Safe DNA gel stain (LIFE TECHNOLOGIES). Bands of appropriate sizes were cut out from the agarose gel and purified using QIAquick Gel Extraction Kit (QIAGEN).

Next, the fragment containing first 1144bp of *klf2a* cDNA and 3kB Bluescript KS fragment were ligated. A 20µl ligation reaction was set up with following reagents: 50ng 3kB Bluescript KS fragment (vector), 5ng 1.1 kB *klf2a* cDNA fragment (insert), 2µl 10x T4 DNA ligase buffer, 1µl T4 DNA ligase (both from NEB), milliQ water up to 20µl and incubated overnight at 16°C. Ligated plasmid was purified using MinElute PCR Purification Kit (QIAGEN) and transformed into MegaX DH10B T1 Electrocomp Cells (INVITROGEN) as follows: 1µl of ligated plasmid was mixed with 25µl of Electrocomp cells (thawed on ice). This mixture was then put into a chilled 0.1cm cuvette and electroporated using Bio-Rad GenePulser II electroporator. Immediately afterwards 1ml of recovery solution (thawed to RT) was added and the solution was placed into a sterile Falcon tube and shaken at 225rpm for 1 hour at 37°C. 50µl of solution was spread on ampicillin plate with Xgal to enable for blue/white screen and was incubated overnight at 37°C. On the following morning single white colonies were picked, stepwise amplified in selective media and purified using QIAprep SpinminiPrep kit and HiSpeed Plasmid Midi kit (both from QIAGEN). Purified Bluescript KS with 1kB *klf2a* cds fragment was stored at -20°C.

Bluescript KS with 1kB *klf2a* cds fragment was subsequently linearized either with EcoRI or XbaI (both NEB) in order to obtain a template for synthesis of antisense and sense *klf2a* riboprobes, respectively. The following reactions were set up: anti-sense *klf2a* riboprobe: 1 µg of EcoRI linearized plasmid, 2µl of T7 polymerase, 2µl 10x DIG RNA labelling mix, 2µl 10x transcription buffer, 1µl RNase inhibitor (all reagents from ROCHE), and miliQ water up to final volume of 20µl. Sense *klf2a* riboprobe: 1 µg of XbaI linearized plasmid, 2µl of T3 polymerase, 2µl 10x DIG RNA labelling mix, 2µl 10x transcription buffer, 1µl RNase inhibitor (all reagents from ROCHE), and miliQ water up to final volume of 20µl. Reactions were mixed and incubated for 2 hours at 37°C. 2µl of DNase I (ROCHE) were added to each reaction and incubated at 37°C for another 30minutes. Transcribed riboprobes were purified by adding 10µl 7.5M ammonium acetate and 60µl 100% ethanol (both ice-cold) and centrifuged at 13300rpm for 15min at 4°C. Pellets were washed with 100µl 70% ethanol and centrifuged at 13300rpm for 5min. Both sense and antisense *klf2a* riboprobes were dissolved in 30µl miliQ water and 70µl formamide and stored at -80°C.

2.6.2 Synthesis of *klf2b*, *klf4a* and *biklf/klf4b/klf17* riboprobes

Total embryo RNA was extracted at 48hpf. For each gene, a set of primers was designed that amplified approximately 1000bp PCR product. T3 promoter sequence 5` CATTAAACCCTCACTAAAGGGAA 3` was added to 5` end of each of the forward (F) primers and T7 promoter sequence 5` TAATACGACTCACTATAGGG 3` was added to 5` end of each of the reverse (R) primers (**Table 2**). RT-PCR and subsequent PCR amplification of corresponding cDNA was done in a single step using Superscript III One-Step RT-PCR kit with Platinum *Taq* Polymerase (INVITROGEN). For each riboprobe 7 reactions (20µl each) were set up as follows: 2x Reaction Mix: 10µl,

corresponding F and R primer (10µm): 1µl each, SuperScript III RT/Platinum Taq Mix: 0.5µl, RNA template: approx. 500ng, miliQ water up to final volume of 20µl. These reactions were then cycled in this 3-step gradient PCR protocol (A-C): A (cDNA synthesis and pre-denaturation): one cycle of 50°C for 30min and 94 °C for 2min. B (PCR amplification): 35 cycles of: 94°C for 2min, 45-56°C for 30 seconds, 68°C for 1min. C (final extension): 68 °C for 5min. All 3 sets of primers for *klf2b*, *klf4a* and *biklf/klf4b/klf17* amplified templates across the whole annealing temperature range and PCR products could be therefore merged and purified together using QIAquick PCR purification kit (QIAGEN). In the next step sense and antisense riboprobes were synthesised as described in section 2.5.1.

Remaining riboprobes used in this project have been kindly donated by other research groups in expression plasmids. These plasmids were linearized by corresponding enzymes and riboprobes were synthesised using appropriate RNA polymerase as detailed in **Table 4**.

Table 4. WISH riboprobes

Probe	RNA polymerase	Restriction site	Reference
<i>klf2a</i>	T7	EcoRI	own riboprobe
<i>cxcr4a</i>	T7	Not1	(Knaut, Werz et al. 2003)
<i>dll4</i>	T7	SpeI	(Leslie, Ariza-McNaughton et al. 2007)
<i>runx-1</i>	T7	HindIII	(Kalev-Zylinska, Horsfield et al. 2002)
<i>c-myb</i>	T7	EcoRI	(Thompson, Ransom et al. 1998)
<i>klf2b</i>	T7	N/A	own riboprobe
<i>klf4a</i>	T7	N/A	own riboprobe
<i>biklf/klf2b/klf17</i>	T7	N/A	own riboprobe

2.6.3 WISH protocol

WISH was performed according to the protocols from Thisse and Thisse (Thisse and Thisse 2008) and from Dr Robert Wilkinson (Wilkinson 2008).

Preparation of reagents used in this protocol is detailed in **Table 5**. Dechorionated zebrafish embryos were initially fixed in 4% (wt/vol) paraformaldehyde (PFA) solution (at least) overnight at 4°C and dehydrated by incubations in successive dilutions of methanol (MeOH) in PBS (vol/vol): 5min in 25% MeOH, 5min in 75% MeOH and 5min in 100% MeOH, 100% MeOH was then changed for a fresh 100% MeOH and embryos were stored at -20°C for at least overnight.

At day 1 of the WISH protocol zebrafish embryos were rehydrated by incubations in successive dilutions of MeOH in PBT (vol/vol): 5min in 75% MeOH, 5min in 50% MeOH, 5min in 25% MeOH and 4x5min in 100% PBT. Embryos were then permeabilized by digestion with proteinase K (ROCHE) (15 µg/ml) diluted in PBT for following times depending on the age of embryos: 0min (24hpf), 15min (36hpf), 40min (48hpf), 80min (72hpf), 100min (4dpf) and 150min (5dpf). Proteinase K digestion was stopped by 2x5min rinsing with 2% glycine (SIGMA) in PBT (wt/vol) and embryos were re-fixed in 4% PFA for 20min. Embryos were rinsed 5x5min in PBT (shaking) then put into 50%PBT/50% hybridization mix+ (HM+) (vol/vol) solution for 5min and pre-hybridized in HM+ for at least 1 hour at 65°C. Subsequently embryos were put into 1:200 (vol) riboprobe solution in HM+ and hybridized overnight at 65°C.

At day 2 riboprobe solution was removed and retained for further hybridizations (can be reused several times). Embryos were then washed in pre-warmed (65°C) solutions of 75% HM-/25% 2xSSC (vol/vol), 50% HM-/50% 2xSSC (vol/vol), 25% HM-/75% 2xSSC (vol/vol) and 2xSSC for 10min each wash, and then in 0.2xSSC for 4x15min. Next, embryos were put through washes of successive dilutions of 0.2xSSC in maleic acid buffer with tween 20 (0.1%) (MABT) (vol/vol) at RT on a rocking table: 5min in 75%

0.2xSSC/25% MABT, 5min in 50% 0.2xSSC/50% MABT, 5min in 25% 0.2xSSC/75% MABT and 5min in MABT. Embryos were then incubated in 2% Blocking reagent (ROCHE) in MABT (wt/vol) for at least 1 hour. At the end of the day 2, embryos were put into 1:5000 (vol) dilution of anti-digoxigenin-AP Fab fragments (ROCHE) in 2% Blocking reagent and incubated at 4°C overnight on a rocking table protected from light.

At day 3, antibody solution was removed and embryos washed in MABT for 8x15min and subsequently equilibrated with developing buffer Bcl-III for 3x5min (all washes done on a rocking table and protected from light). For staining embryos were put into a 1:1 (vol/vol) solution of BM Purple (ROCHE) in Bcl-III buffer and kept protected from light. The level of staining was regularly checked under dissecting microscope. When the desired staining intensity was reached, the reaction was stopped with 3 brief washes with PBT. Embryos were then post-fixed in 4%PFA for 20min. When necessary, embryos (older than 24hpf) were bleached in bleaching solution for up to 30min on daylight to get rid of the pigment. After a series of 4 short washes with PBT, embryos were stepwise put through 30%, 50% and 80% glycerol in miliQ (vol/vol) for long-term storage.

Table 5. WISH reagents

Reagent	Description
Phosphate buffered saline (PBS)	One tablet (SIGMA) dissolved in 200ml of miliQ water (yields 0.01M phosphate buffer, 0.0027M potassium chloride and 0.137 M sodium chloride, pH 7.4) and then autoclaved
1M Tris-HCl	121.1 g of Trizma base (SIGMA) in 1l of miliQ water, pH is then adjusted to 9.5 with hydrochloric acid (HCl) and autoclaved
20xSSC	175.3 g sodium chloride (NaCl) and 88.2 g citric acid (both from SIGMA) dissolved in 1l miliQ water and autoclaved
PBT	add 50µl Tween20 (SIGMA) into 49.95ml PBS

Hybridization mix + (HM+)	5ml 99% formamide (SIGMA), 2.5ml 20xSSC, 10µl Tween20, 92µl 1M citric acid (filter sterilized), 5µl heparin (100mg/ml) (SIGMA), 1ml tRNA (5mg/ml) (BOEHRINGER) and milliQ water up to 10ml
Hybridization mix - (HM-)	the same as HM+ but no heparin and tRNA
Bcl-III buffer	5ml 1M Tris-HCl (ph 9.5), 1ml 5M NaCl, 5ml 0.5M magnesium chloride, 50µl Tween20, milliQ up to 50ml
Maleic acid buffer (MAB)	5.804 g maleic acid (SIGMA) and 4.383g NaCl dissolved in 400ml milliQ water, pH adjusted to 7.5 with sodium hydroxide and then milliQ added up to 500ml

2.7 Transcription Activator-Like Effector Nucleases

(TALEN) mutagenesis protocol

This protocol is based on the method and reagents published by Cermak, Doyle et al. (Cermak, Doyle et al. 2011) and was modified by Dr Stone Elworthy.

Figure 2.4 shows a structure of a TALEN. The *klf2a* TALEN used in this project has been chosen as an example. Each TALEN is a heterodimer with a left (L) and right (R) subunit. Each subunit contains a C-terminal catalytic domain of Fok1 endonuclease and an N-terminal site-specific DNA binding domain. Fok1 is functional as a dimer and therefore L and R subunits of TALEN bind to opposing DNA strands across a spacer over which the Fok1 domains come together and introduce double-strand DNA breaks (DSBs) in the specific genomic region. DSBs are repaired mainly by non-homologous end joining (NHEJ) which is error-prone with resulting small insertions and deletions (indels). This enables creations of mutations that are stable and are transmitted through the germ line (Cermak, Doyle et al. 2011; Sander, Dahlborg et al. 2011). As shown in **Figure 2.4** DNA binding specificity of TALENs is provided by transcription

activator-like (TAL) effectors (Bogdanove, Schornack et al. 2010). TAL central domain consists of tandem, 33-35 AA repeats followed by a single truncated 20 AA repeat. A polymorphic pair of adjacent AAs at positions 12 and 13, the so-called repeat-variable di-residue (RVD) specifies the target in a way that the four most common RVDs preferentially bind to one of the four nucleotide bases (**Figure 2.4**) (Boch, Scholze et al. 2009; Moscou and Bogdanove 2009; Cermak, Doyle et al. 2011).

2.7.1 Choosing a TALEN target site and TALEN design

A corresponding genomic sequence is entered into the freely accessible Old TALEN Targeter software at <https://tale-nt.cac.cornell.edu/node/add/talen-old>. Parameters are recommended to be set as follows: Spacer length should be 15-18bp and should be flanked at both ends by a T so that the final RVD for each subunit is NG (binds to T, see **Figure 2.4**). Repeat array length should be between 15 and 21.

A target site that includes a wide spanning restriction enzyme site within the spacer is preferably chosen for further easy detection of mutagenesis by loss of restriction site. PCR primers should be designed at this stage around the TALEN target site to give a 100bp to 300bp PCR product. A test digest with the wide-spanning restriction enzyme is then performed on PCR product from wild type embryonic cDNA to optimize the conditions of the digest. This method will be used for checking the efficiency of mutagenesis as well as for genotyping of individual embryos and adult fish at later stage.

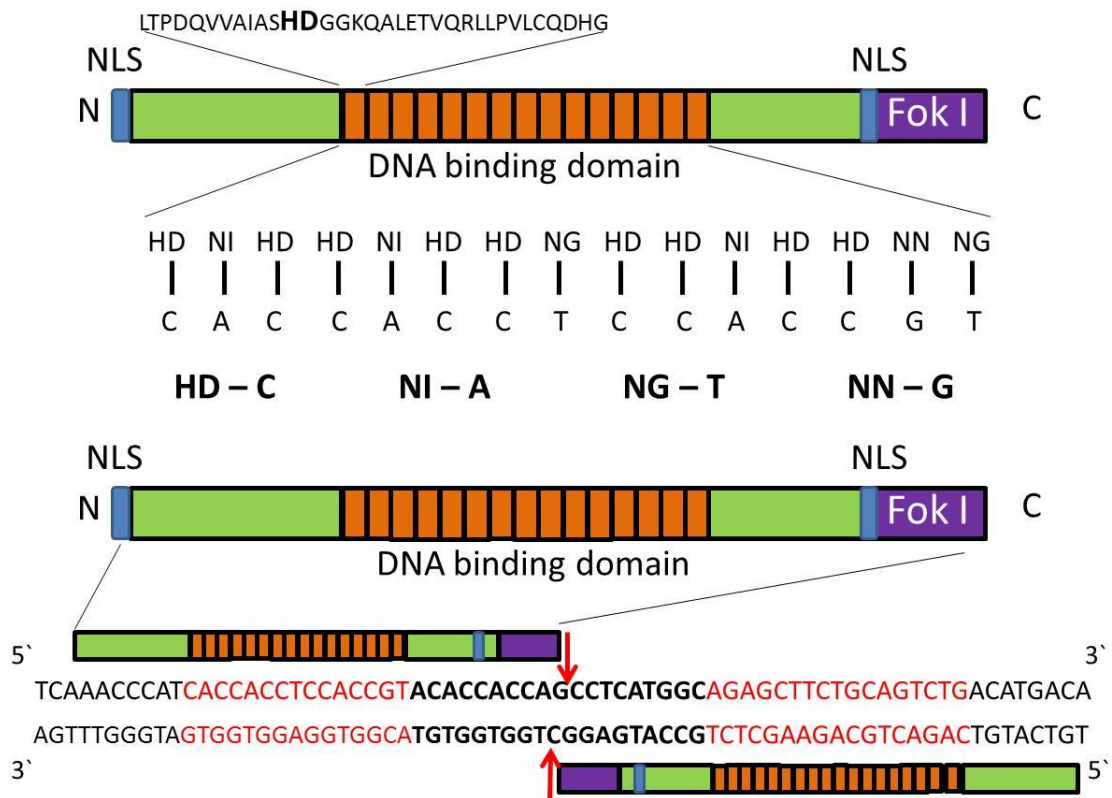


Figure 2.4 Structure of a TALEN

Structure of *klf2a*-specific right TALEN subunit (top part of the figure) with target *klf2a* genomic sequence (bottom part of the figure) is shown. This TALEN was used in *klf2a* mutagenesis described in this thesis. Right *klf2a* TALEN subunit contains 15 repeat-variable di-residues (RVDs) and left *klf2a* TALEN subunit contains 17 RVDs. DNA binding domain (in orange) consists of tandem, 33-35 AA repeats followed by a truncated 20 AA repeat. Primary sequence of one of the AA repeats is shown at the top. AAs at the position 12 and 13 (in bold) represent the repeat-variable di-residue (RVD) and determine the nucleotide binding specificity of the AA repeat. The four most common RVDs used in TALEN design are shown together with the nucleotides they bind to (HD → C; NI → A; NG → T; NN → G). Both right and left TALEN subunits are required to meet at the target site so that the Fok1 endonuclease can dimerize and cleave DNA as indicated by the red arrows. Abbreviations: NLS: nuclear localization signal. Figure after (Cermak, Doyle et al. 2011).

2.7.2 TALEN assembly

TALEN assembly is done in two stages using Golden Gate Assembly (NEB) with type IIS restriction endonucleases BsaI or Esp3I (both NEB) that cleave outside their recognition sites and leave 4bp overhangs. Thus digesting and ligating of all constituent plasmids that are needed for a particular assembly can be done in a single reaction (Engler, Kandzia et al. 2008; Engler, Gruetzner et al. 2009; Cermak, Doyle et al. 2011).

2.7.2.1 TALEN assembly stage 1

At this stage the left and right TALEN subunit were each constructed in two parts named A and B. A part contains first 10 RVDs, B part contains remaining RVDs apart from the last truncated RVD which was added in stage 2. Parts A and B were assembled from constituent plasmids, each of which contains a specific RVD for a particular position in the assembly. All constituent plasmids came from the AddGene non-profit repository. The plasmids were labelled according to the plate key on <http://www.addgene.org/TALeffector/goldengate/voytas/Plate1/>.

All 4 Golden Gate reactions were assembled separately. For each A part mix 1µl each RVD plasmid (150ng/µl), 1µl pFusA plasmid (150ng/µl), 2µl T4 DNA ligase (NEB), 2µl 10x T4 DNA ligase buffer (NEB), 1µl BsaI, 4µl miliQ water. For each B part mix 1µl each RVD plasmid (150ng/µl), 1µl pFusB plasmid (150ng/µl), 2µl T4 DNA ligase, 2µl 10x T4 DNA ligase buffer 1µl BsaI, miliQ water up to 20µl. All 4 reactions were then incubated for 10x (37°C/5min + 16°C/10min) + 50°C/5min + 80°C/5min. After completion 1µl of plasmid-safe ATP-dependent DNase + 0.3µl of 25mM ATP (both from EPICENTRE) were added and incubated at 37°C for 1 hour.

Assembly plasmids were then transformed into NEB 10-beta competent *E.coli* (NEB) following the manufacturer's protocol exactly and grown in selective media

(spectinomycin + Xgal) at 37°C overnight and purified using the QIAprep Spin Miniprep kit (QIAGEN).

2.7.2.2 TALEN assembly stage 2

A and B part of each subunit were first tested with a double restriction enzyme digest with NheI and XbaI (both NEB). The expected band sizes were 2132bp, 1050bp and 266bp for A plasmid and 2132bp, 266bp and 500-1100bp (depending on number of RVDs) for B part.

A and B part from R and L subunit were combined together with the last truncated RVD and cloned into a backbone plasmid in following reaction: 4µl of each purified plasmids A and B, 1µl E4 plasmid (150ng/µl), 1µl pCAGT7TALEN plasmid, 2µl 10x T4 DNA ligase buffer, 2µl T4 DNA ligase, 1µl Esp3I, 5µl miliQ water. Both reactions were then incubated for 10x (37°C/5min+16°C/10min) + 50°C/5min + 80°C/5min.

L and R subunit plasmids were transformed into 10-beta competent *E.coli* (NEB) following the manufacturer's protocol exactly and grown in selective media (carbenicillin + Xgal) at 37°C overnight and purified using the NucleoBond® Xtra Midi/Maxi kit (MACHEREY-NAGEL).

Both L and R plasmids were sent for sequencing using TAL_R2 and SeqTALEN_5-1 primers (**Table 2**). L and R plasmids were also checked with a double restriction enzyme digest with BamHI and XbaI (NEB).

2.7.3 Capped mRNA synthesis and injections into zebrafish embryos

L and R plasmids were linearized in following reaction: 6µg of each L and R plasmid, 30µl 10x NEB3 buffer, 3µl BSA (NEB), 2.5µl NotI, miliQ water up to 300µl.

Capped TALEN mRNA was synthesized from the NotI linearized plasmids using MessageMAX T7 ARCA-capped Message Transcription kit (EPICENTRE) following the manufacturer's protocol exactly and subsequently purified using RNeasy MinElute Cleanup kit (QIAGEN).

Capped TALEN mRNA was injected into one-cell stage zebrafish embryos in various amounts either neat or mixed with phenol red to determine the dose which gives many, but not all embryos free of toxic effects at 24hpf. Typical toxic effects would be death, dorsalisation and small heads. Thus the highest possible capped mRNA injection dose was established and this dose was then injected to maximise the mutagenesis rate.

2.7.4 Mutation analysis of injected embryos

Genomic DNA was extracted from individual embryos injected with capped TALEN mRNA at 3-4dpf. Somatic mutation rate induced by the TALEN was assessed by subsequent PCR across the target site and restriction enzyme digest with a wide spanning restriction enzyme.

2.7.4.1 PCR and restriction enzyme test used in *klf2a* TALEN mutagenesis

klf2a TAL XcmI L1 and R1 primers (**Table 2**) amplified a 281bp region. Following reaction was set up: *klf2a* TAL XcmI L1 and R1 primers (10 μ M): 1 μ l each, 2xBioMix (BIOLINE): 10 μ l, genomic DNA: 1-2 μ l, milliQ water: up to final volume of 20 μ l. PCR programme used in this reaction is detailed in **Table 6**.

Following the PCR 0.5 μ l of XcmI restriction enzyme (NEB) was added into each reaction and reaction was incubated for 3 hours at 37 $^{\circ}$ C. 15 μ l of the enzymatic digest was then separated via agarose gel electrophoresis using a 2.5% LE agarose (LONZA)

gel. Detection of an uncut 281bp band showed the occurrence of site-targeted mutagenesis.

Table 6. PCR programme used for genotyping in *klf2a* TALEN mutagenesis

Step	Temperature	Time
8. Initialisation	94°C	2min
9. Denaturation	94°C	20 sec
10. Annealing	52.5°C	20 sec
11. Elongation	72°C	45 sec
12. Cycle to step 2 – 34x		
13. Final elongation	72 °C	3min
14. Final hold	4 °C	hold

2.7.5 Screening for founder fish

Once the injected embryos were grown up, a proportion of them had mosaic germlines such that some of their offspring were carried for a TALEN induced mutation. In order to identify such founder fish they were outcrossed and put into individual tanks. The progeny of this outcross was then tested using a PCR and restriction enzyme test. From each potential founder, 8x3 = 24 embryos at 72hpf were analysed by PCR and restriction enzyme digest. Only the progeny of fish found to transmit any mutant allele (identified by the presence of an uncut band) were raised.

2.7.6 Screening for F1 generation of heterozygous carriers

The progeny of mosaic germ line founder fish included fish that are carriers of mutant allele. Once the F1 generation of fish reached sexual maturity (2-3 months of age),

they were identified by PCR and restriction enzyme digest. Larger insertions and deletions can be seen on the agarose gel without the need for a restriction enzyme test as long as primers are designed to give a small amplicon (<150bp). All fish identified to carry any mutation were genotyped by PCR and subsequent sequencing. Fish identified to carry identical mutant allele were put into a separate tank. Heterozygous carriers for a particular mutant allele were further outcrossed to other transgenic lines. Alternatively, incross of two F1 heterozygous carriers for a particular mutant allele gave rise to a F2 generation progeny of which 25% was homozygous carriers and 50% heterozygous carriers and the remaining 25% wild type. These embryos can be used for experiments up to 5.2dpf or can be raised. F2 generation embryos used for experiments will require subsequent genotyping unless the homozygous or heterozygous carriers exhibit an obvious easily detectable phenotype.

2.7.7 Experiments on F2 and F3 generation of *klf2a* mutant line

Homozygous carriers for a particular allele from F2 generation were incrossed once they reached sexual maturity (2-3 months of age). The progeny represented an F3 generation which will be a maternal mutant line without any possible maternal zygotic contribution. Additionally, no further genotyping of such a progeny was necessary since 100% of progeny were homozygous mutants. Another way of excluding maternal zygotic contribution was an incross of a female homozygous carrier for a particular mutant allele with a heterozygous male carrier. In this case 50% of progeny was maternal mutants and 50% heterozygous carriers and genotyping was necessary.

2.8 Klf2a protein analysis

2.8.1 Western blot analysis

Protein was extracted from previously genotyped zebrafish embryos at 5dpf (4 embryos per group) using RIPA lysis buffer (SIGMA-ALDRICH) with added Halt Protease and Phosphatase inhibitor cocktail (THERMO SCIENTIFIC). Embryos were homogenised using Eppendorf pestle (SIGMA-ALDRICH) and left on ice for 30min. Lysate was centrifuged at 14000rpm for 10min at 4°C and the resulting supernatant was separated and protein amounts quantified using a standard Bradford assay. Protein samples were then mixed with 1M dithiothreitol (DTT) (SIGMA-ALDRICH) and NuPAGE LDS Sample Buffer (LIFE TECHNOLOGIES) heated to 95°C for 5min and loaded onto a NuPAGE NOVEX 4-12% Bis-Tris gel (LIFE TECHNOLOGIES). After the electrophoretic separation, proteins were transferred to Immobilon-P PVDF transfer membranes (MILLIPORE) using the Xcell II Blot Module (LIFE TECHNOLOGIES). After blocking with 5% non-fat milk for 1 hour at RT, transfer membranes were incubated with rabbit anti-mouse Klf2a polyclonal antibody (1:500) (MILLIPORE) which use on zebrafish was previously published (Wang, Zhang et al. 2011) or with antibodies against housekeeper genes – either with a rabbit anti-human glyceraldehyde-3-phosphate dehydrogenase (GAPDH) monoclonal antibody (1:1000) (CELL SIGNALLING) or a rabbit anti-human β -actin antibody (1:10000) (CELL SIGNALLING) overnight. Membranes were washed in TBSTw (Tris buffer saline plus Tween 20: 136,8mM NaCl, 24.8mM Tris, 0.1% Tween 20 (vol/vol) (all from SIGMA), pH 7.6) for 3x5min on a rocker and then incubated with a secondary antibody (goat anti-rabbit polyclonal antibody with conjugated horseradish peroxidase (HRP), 1:1000) (DAKO) for 45min on a rocker. After thorough washing of the membranes, immobilised

proteins were detected by the EZ-ECL Chemiluminescence Detection Kit (BIOLOGICAL INDUSTRIES).

2.8.2 Klf2a protein immunoprecipitation (IP)

Protein extract from approximately 130 Nacre WT 5dpf old zebrafish embryos was used for Klf2a protein immunoprecipitation in order to detect the Klf2a protein via following MS. Protein concentration in the lysate was estimated by a standard Bradford assay to be 3.37 $\mu\text{g}/\mu\text{l}$. A total volume of 890 μl of this lysate was used, giving the total amount of protein to be 3 mg. In parallel, the same amount of lysate was used for a control Immunoglobulin G (IgG) IP. Following the overnight incubation of the lysate with 30 μl of neat rabbit anti-mouse Klf2a polyclonal antibody (MILLIPORE) or with 7.5 μl of non-specific Normal rabbit IgG antibody (CELL SIGNALLING), IP samples were incubated with 60 μl Protein G-coupled Sepharose beads (produced locally in the centre) 50% slurry mixed with RIPA lysis buffer (SIGMA-ALDRICH) for 60min at 4°C on a rotator. IP samples were then washed in RIPA lysis buffer (SIGMA-ALDRICH) and centrifuged at 14000rpm for 1min. IP supernatants from both samples were carefully removed and kept for further analysis. Remaining IP precipitates were mixed with 30 μl of 2x SDS sample buffer (LIFE TECHNOLOGIES) with 100 μM DTT (SIGMA-ALDRICH) and boiled at 100°C for 5min. Samples were centrifuged at 14000rpm for 30 seconds and supernatants with eluted Klf2a protein were removed. These samples, together with IP supernatants were run on a Klf2a Western blot to check for the correct precipitation of Klf2a and IgG proteins. IP protein samples were stored at -20°C before they were used for the Mass Spectrometry (MS).

2.8.3 Mass Spectrometry

Protein samples were extracted and electrophoretically separated on a polyacrylamide gel in parallel to Western blot as described in the Western blot section. Protein bands were then visualised using SimplyBlue Safe Stain (LIFE TECHNOLOGIES). Bands identified to contain proteins of interest (according to their molecular weight) were cut out from the gel in a laminar fume hood using a clean scalpel blade (WORLD PRECISION INSTRUMENTS), put into siliconized Eppendorf tubes (EPPENDORF) and de-stained. Following the reduction and alkylation of proteins, gel pieces were washed and dried in a vacuum concentrator (H.SAUR). Proteins embedded in the gel were then subjected to an overnight digest with Chymotrypsin (PROMEGA). Digested peptides were extracted from the gel and slowly dried down (overnight at 37°C) in the vacuum concentrator. Such samples were submitted for MS. MS and subsequent MS data analysis was performed by Dr Richard Beniston at the Biomedical Mass Spectrometry Facility (biOMICS) of the University of Sheffield using the Orbitrap Elite mass spectrometer and the Proteome Discoverer software (both from THERMO SCIENTIFIC).

Chapter 3

***klf2a* expression patterns and morpholino - mediated *klf2a* knockdown experiments**

3.1 Introduction

Spatial and temporal patterns of *klf2a* expression in developing zebrafish embryos from earliest stages up to 48hpf have been previously studied using WISH protocols (Oates, Pratt et al. 2001; Kotkamp, Mossner et al. 2014). Some scattered data on *klf2a* expression patterns at later stages come from other groups (Parmar, Larman et al. 2006; Vermot, Forouhar et al. 2009; Nicoli, Standley et al. 2010; Wang, Zhang et al. 2011), but a thorough analysis of *klf2a* expression patterns beyond 48hpf has not been available so far. Endothelial early expression of *klf2a* in zebrafish vasculature has been shown to be blood flow dependent however (Parmar, Larman et al. 2006; Nicoli, Standley et al. 2010; Wang, Zhang et al. 2011). I therefore went on to examine *klf2a* expression patterns in zebrafish embryos up to 5dpf and sought to confirm that *klf2a* endothelial expression is blood flow dependent by using several ways to interfere with embryonic blood flow.

Methods of reverse genetics used in *klf2a* studies in zebrafish have relied exclusively on morpholino-mediated *klf2a* knockdown so far. I therefore started my *klf2a* studies by using previously published *klf2a* morpholinos (Vermot, Forouhar et al. 2009; Nicoli, Standley et al. 2010; Wang, Zhang et al. 2011). Our research group have previously shown that several endothelial factors and signalling cascades such as *cxcr4a* and Notch signalling are downregulated by blood flow (Packham, Gray et al. 2009; Watson, Novodvorsky et al. 2013). I hypothesised that *klf2a* as one of the major endothelial mechanosensitive transcription factors might play a role in these processes.

3.2 Results

3.2.1 *klf2a* expression patterns in developing zebrafish embryos

I *de novo* synthesised a *klf2a* riboprobe in order to study *klf2a* expression patterns in developing zebrafish embryos. As shown in **Figure 3.1**, at 24hpf *klf2a* expression is present in the cloaca, in cells lateral to the most posterior notochord and faint signal becomes detectable in pronephric ducts, but no expression is detected in axial vessels. From 36hpf onwards *klf2a* becomes detectable in the heart and in the vasculature - mainly in ISVs but also in DA, caudal vein (CV) and posterior cardinal vein (PCV) and head vessels (**Figure 3.1**). This corresponds with the fact zebrafish embryos develop a contracting heart and therefore blood circulation at approximately 24-26hpf (Kimmel, Ballard et al. 1995). At 48hpf vascular expression becomes much stronger and appears also in the DLAV. From 48hpf onwards *klf2a* mRNA becomes also expressed in pectoral fins (**Figure 3.1**). The expression patterns from 24 to 48hpf therefore correspond to previously published data (Oates, Pratt et al. 2001; Vermot, Forouhar et al. 2009; Wang, Zhang et al. 2011). At 72hpf *klf2a* mRNA becomes detectable in trunk vasculature (DA, ISVs, DLAV, CV, PCV) and also in subintestinal veins (**Figure 3.2**). *klf2a* continues to be expressed in the heart region, pectoral fin, cloaca and cells lateral to the most posterior notochord (**Figure 3.2**). At 72hpf *klf2a* becomes also expressed in neuromasts. Neuromasts form a lateral line sensory organ located within the skin epithelium that is stimulated by local water vibrations (Raible and Kruse 2000). From 4dpf onwards vascular *klf2a* mRNA signal becomes significantly reduced (**Figure 3.2**). At 4dpf *klf2a* expression in the heart region, pectoral fins, neuromasts and cells lateral to the most posterior notochord becomes weaker, but remains strongly expressed in the cloaca. Strong *klf2a* mRNA signal from cloaca is present at 5dpf as well, but *klf2a*

expression in the heart and in cells lateral to the most posterior notochord is almost lost at this stage (**Figure 3.2**). *klf2a* mRNA signal becomes also detectable in the developing hepatic portal vein (green arrow in **Figure 3.2**, image of 5dpf old embryo). Next I performed cross sections on AB WT zebrafish embryos following *klf2a* WISH at 48hpf. This was done to prove that the vascular staining pattern of *klf2a* WISH described above really represents *klf2a* mRNA expression in endothelial cells. These cross sections clearly demonstrate *klf2a* expression in the DA, parachordal vessel, ISVs and DLAV at several anatomical locations (**Figure 3.3**).

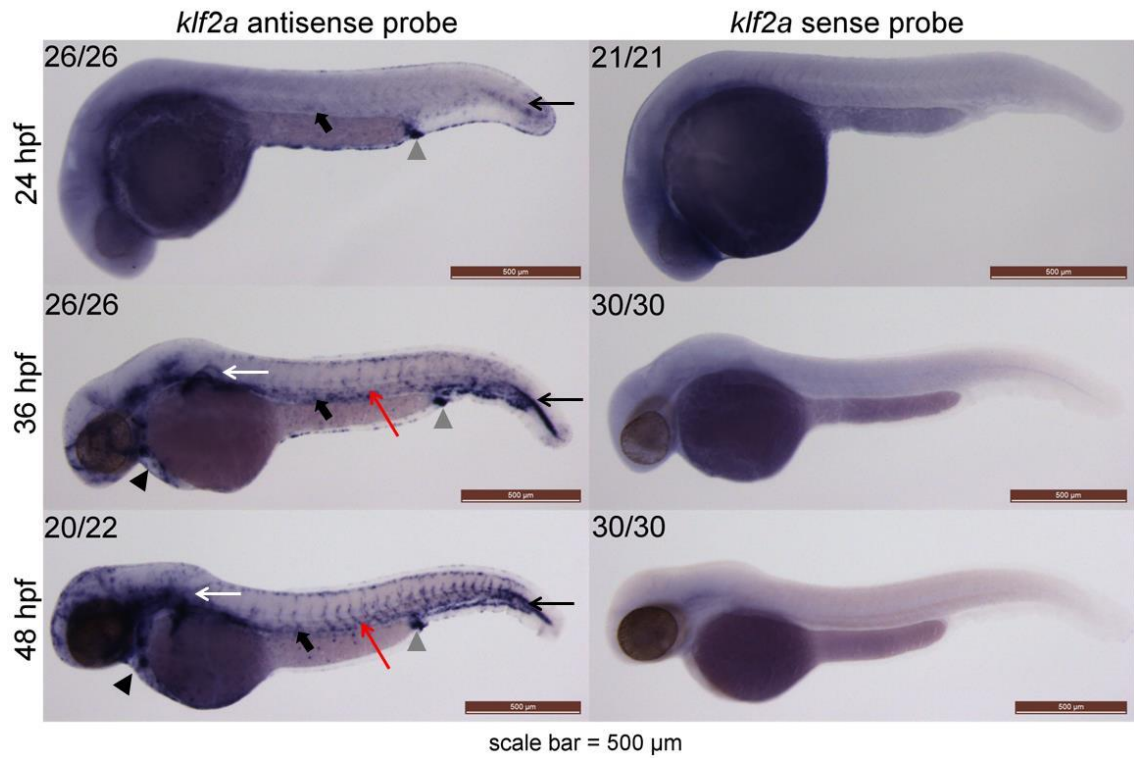


Figure 3.1 *klf2a* expression patterns in AB WT embryos at 24 to 48hpf.

klf2a antisense riboprobe was used to visualise *klf2a* expression patterns. *klf2a* sense riboprobe was used as a negative control. Red arrow points at trunk vasculature, black arrow points at cells lateral to the most posterior notochord, thick black arrow points at pronephric ducts, black arrow points at cells lateral to the most posterior notochord, black arrowhead points at the heart region, grey arrowhead points at the cloaca. Numbers in top right corners indicate number of embryos with identical staining patterns out of total number of embryos examined. Scale bar = 500 μ m.

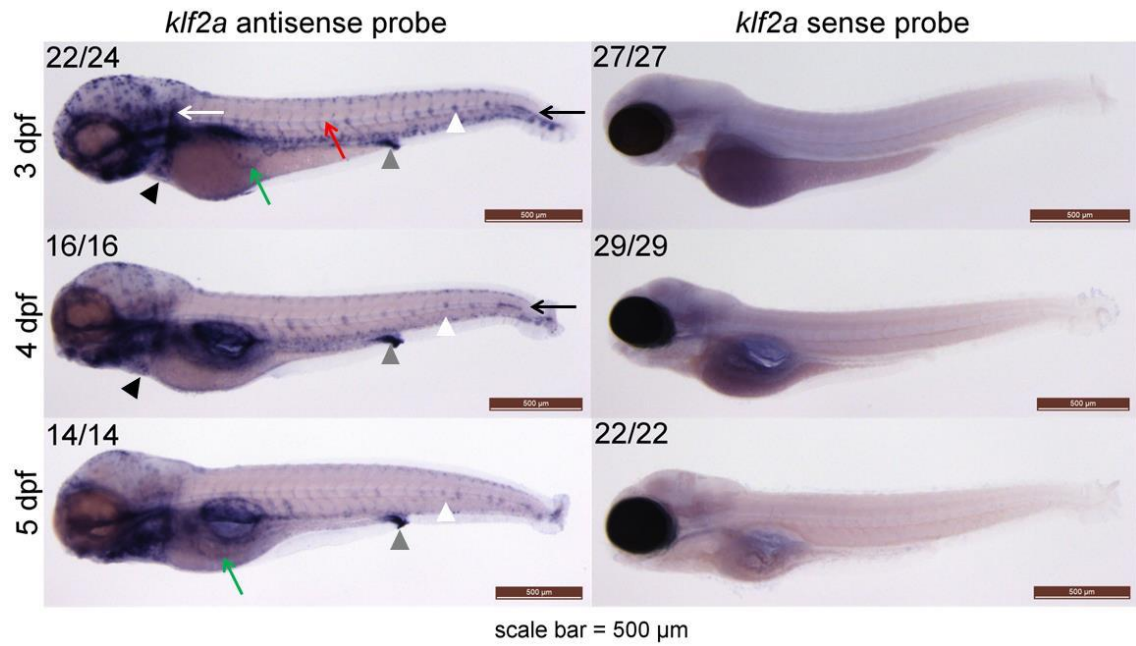


Figure 3.2 *klf2a* expression patterns in AB WT embryos at 3 to 5 dpf.

klf2a antisense riboprobe was used to visualise *klf2a* expression patterns. *klf2a* sense riboprobe was used as a negative control. Red arrow points at trunk vasculature, green arrow points at subintestinal veins (3dpf) and hepatic portal vein (5dpf), black arrow points at cells lateral to the most posterior notochord. Thick black arrow points at pronephric ducts, black arrow points at cells lateral to the most posterior notochord, black arrowhead points at the heart region, grey arrowhead points at cloaca and white arrowhead points at neuromasts. Numbers in top right corners indicate number of embryos with identical staining patterns out of total number of embryos examined. Scale bar = 500µm.

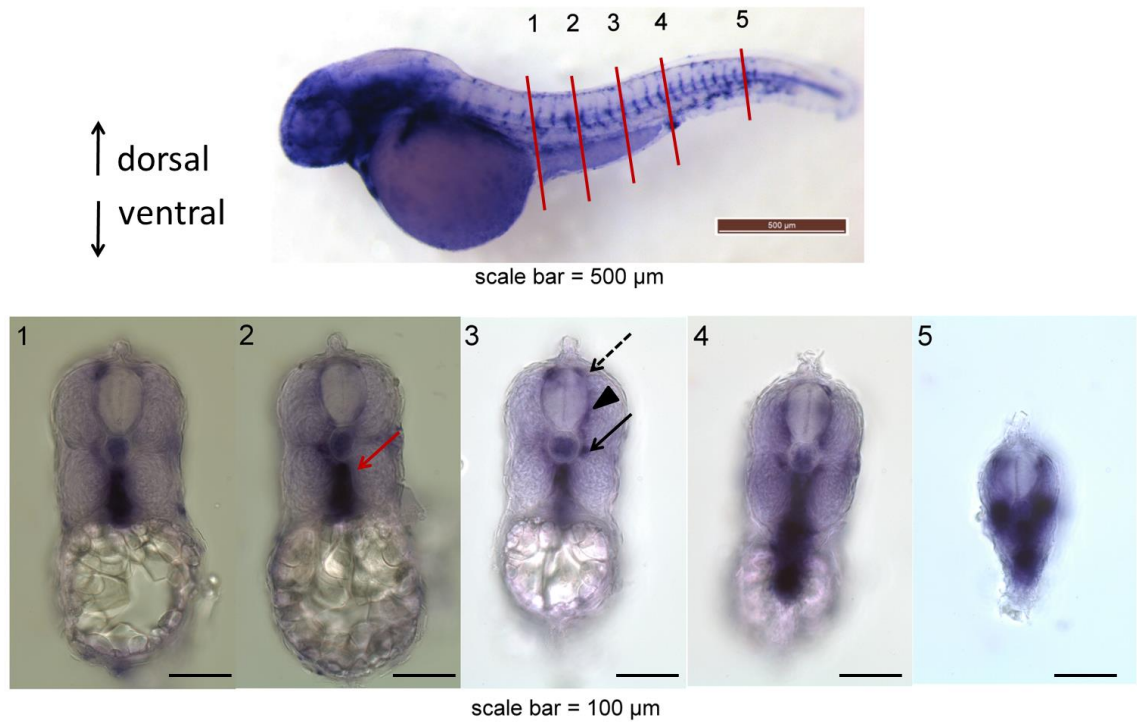


Figure 3.3 Cross sections of an AB WT zebrafish embryo at 48hpf after *klf2a* WISH.

Red lines indicate anatomical positions of sections 1 to 5. Red arrow points at dorsal aorta (DA) black arrow points at parachordal vessel, black arrowhead points at one of the intersegmental vessels (ISVs) and dotted black arrow points at dorsal longitudinal anastomotic vessel (DLAV). On the cross section images dorsal is up and ventral is down as indicated by the arrows in top left corner. Scale bar = 500 μ m (top panel) or 100 μ m (bottom panel).

3.2.2 *klf2a* vascular expression is blood flow dependent

Next I wanted to confirm that endothelial *klf2a* expression in developing zebrafish embryos is blood flow dependent. I performed 3 experiments in which blood flow in trunk vasculature is either permanently or temporarily hindered. I performed *klf2a* WISH at 48hpf on these embryos alongside a batch of wild type embryos at the same developmental stage. 48hpf time point was chosen because *klf2a* vascular expression in a wild type embryo is strongest at this stage.

Initially, I used *gridlock* mutants with proximal occlusion of the dorsal aorta. These mutants experience no blood flow distal to the occlusion until collateral vessels form and bypass the occlusion (up to 80% of embryos develop collaterals by 5dpf) (Zhong, Rosenberg et al. 2000; Gray, Packham et al. 2007). As shown in **Figure 3.4**, *klf2a* vascular expression in *gridlock* mutants is completely abolished whilst *klf2a* expression in the heart, in pectoral fins, in the cloaca and the cells lateral to the most posterior notochord remains unchanged.

Secondly I used *tnnt2* morphants which experience no cardiac contraction and therefore have no flow due to blockage of expression of one of the key elements of cardiac contractile apparatus troponin t2 (*tnnt2*) by a morpholino (Stainier, Fouquet et al. 1996). *klf2a* vascular expression in *tnnt2* MO morphants is significantly decreased (**Figure 3.4**) with preserved *klf2a* expression in the heart, in pectoral fins, in the cloaca and the cells lateral to the most posterior notochord.

Lastly, I temporarily stopped cardiac contraction with local anaesthetic Tricaine from 32hpf onwards. These embryos experienced blood flow from its onset at 24-26hpf until 32hpf, but Tricaine treatment resulted in significantly reduced *klf2a* vascular expression at 48hpf (**Figure 3.4**). Interestingly Tricaine treatment also significantly reduced *klf2a* expression in the heart and in the cells lateral to the most posterior notochord. *klf2a* expression in pectoral fins and in the cloaca remained unchanged (**Figure 3.4**).

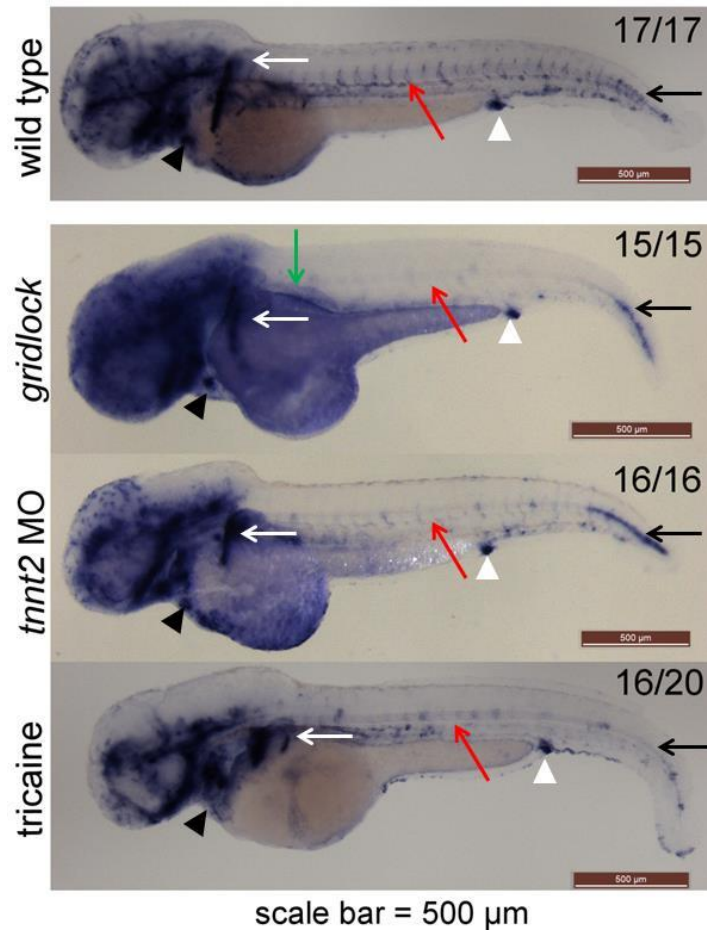


Figure 3.4 *klf2a* vascular expression is blood flow dependent.

klf2a is expressed in zebrafish embryonic vasculature of a WT embryo at 48hpf. Cessation of blood flow in the truncal vasculature by an occlusion of proximal aorta in the *gridlock* mutants (indicated by a green arrow) results in a complete loss of *klf2a* vascular expression distally to the occlusion. Blockage of embryonic heart contractions by *tnnt2* MO results in significantly decreased *klf2a* vascular expression. Pharmacological inhibition of heart contractions by Tricaine from 32 to 48hpf results in significantly decreased *klf2a* vascular expression. Interestingly Tricaine also reduces *klf2a* expression in the heart region and in the cells lateral to the most posterior notochord. Red arrow points at truncal vasculature, black arrow points at the cells lateral to most posterior notochord, white arrow points at pectoral fins, black arrowhead points at the heart region and white arrowhead points at cloaca. Numbers in top right corners indicate the number of embryos with identical staining pattern out of all embryos examined. *klf2a* riboprobe used. Scale bar = 500μm.

3.2.2.1 SB *klf2a* MO and ATG *klf2a* MO do not impair cardiac performance of zebrafish embryos at 48hpf

Heart rates and blood flow velocities in DA were measured in morphants injected with SB *klf2a* MO and ATG *klf2a* MO compared to cont MO injected embryos at 48hpf prior to their experimental use. As shown in **Figure 3.5**, SB *klf2a* MO and ATG *klf2a* MO injected at doses mentioned in **Table 1** (Chapter 2: Materials and Methods) do not cause any significant impairment of heart rates or blood flow velocities in DA at 48hpf when compared to controls. Additionally, all SB *klf2a* MO, ATG *klf2a* MO and cont MO morphants that were used in experiments described in this thesis were checked for the presence of functional blood circulation under dissecting microscope.

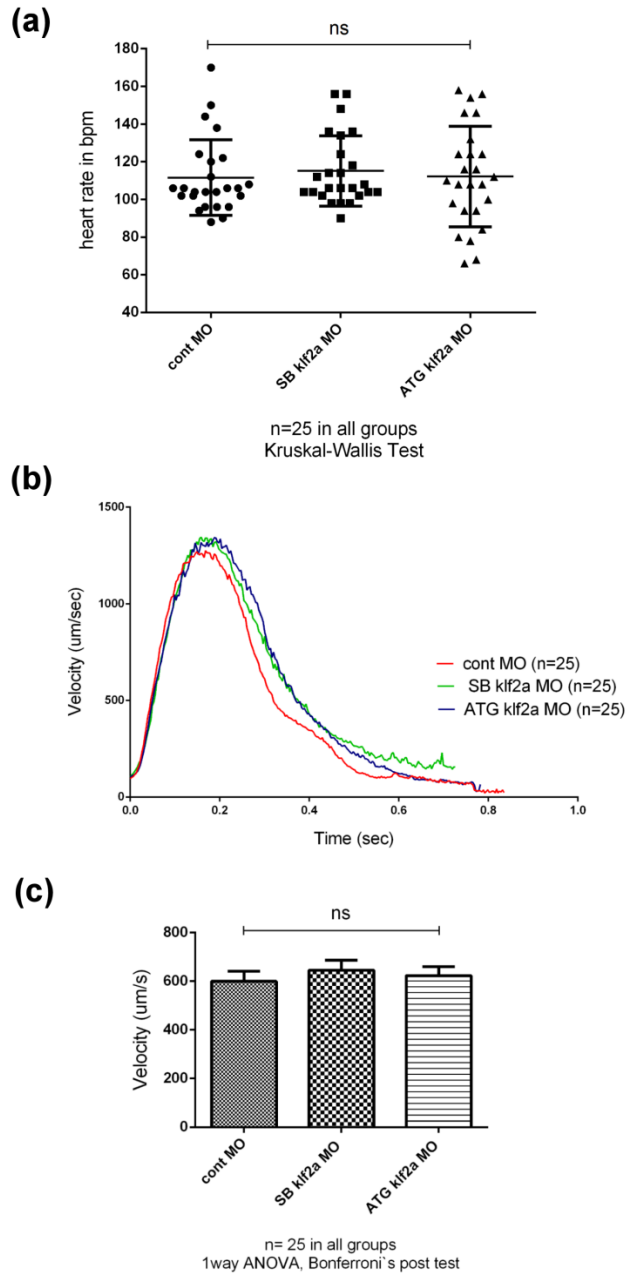


Figure 3.5 Comparison of heart rates and blood flow velocities of cont MO, SB *klf2a* MO and ATG *klf2a* MO morphants at 48hpf

(a) There are no significant differences in heart rates between the cont MO, SB *klf2a* MO and ATG *klf2a* MO morphants at 48hpf. **(b)** Instantaneous blood flow velocities were measured throughout a single cardiac cycle individually in altogether 25 embryos from each group. These values were then averaged and plotted on a graph as a single velocity curve. Velocity curves of cont MO, SB *klf2a* MO and ATG *klf2a* MO morphants are almost identical at 48hpf. **(c)** Bar graph shows an average velocity from all measured instantaneous blood flow velocities during a single cardiac cycle for cont MO, SB *klf2a* MO and ATG *klf2a* MO morphants. No statistically significant differences in average blood flow velocities could be detected at 48hpf. Summary of 3 independent experiments. In total 25 embryos were examined per group.

3.2.3 *cxcr4a* vascular expression is upregulated in a proportion of SB *klf2a* MO and ATG *klf2a* MO injected morphants at 48hpf

Our group previously showed that at 36hpf *cxcr4a* is expressed in zebrafish embryonic vasculature at similar levels in both control MO and *tnnt2* MO morphants. Later on *cxcr4a* is rapidly downregulated in the control group whereas *cxcr4a* continues to be expressed in the vasculature in the absence of blood flow up to 48hpf and beyond and mediates collateral vessel formation (Packham, Gray et al. 2009). The exact mechanism by which endothelial cells sense blood flow as mechanical force leading to downregulation of *cxcr4a* expression after 36hpf remains unclear. I hypothesised that the flow dependent regulation of *cxcr4a* expression in endothelium could be mediated via *klf2a*.

In order to test this hypothesis I performed WISH for *cxcr4a* in SB *klf2a* MO and ATG *klf2a* MO morphants at 48hpf. As shown in **Figure 3.6**, a proportion of both SB *klf2a* MO and ATG *klf2a* MO injected embryos showed increased vascular presence of *cxcr4a* up to the levels observed in *tnnt2* MO morphants that do not experience any blood flow. WISH experiments were repeated several times with reproducible results and similar proportions of SB *klf2a* MO and ATG *klf2a* MO morphants showing increased vascular *cxcr4a* expression were detected each time.

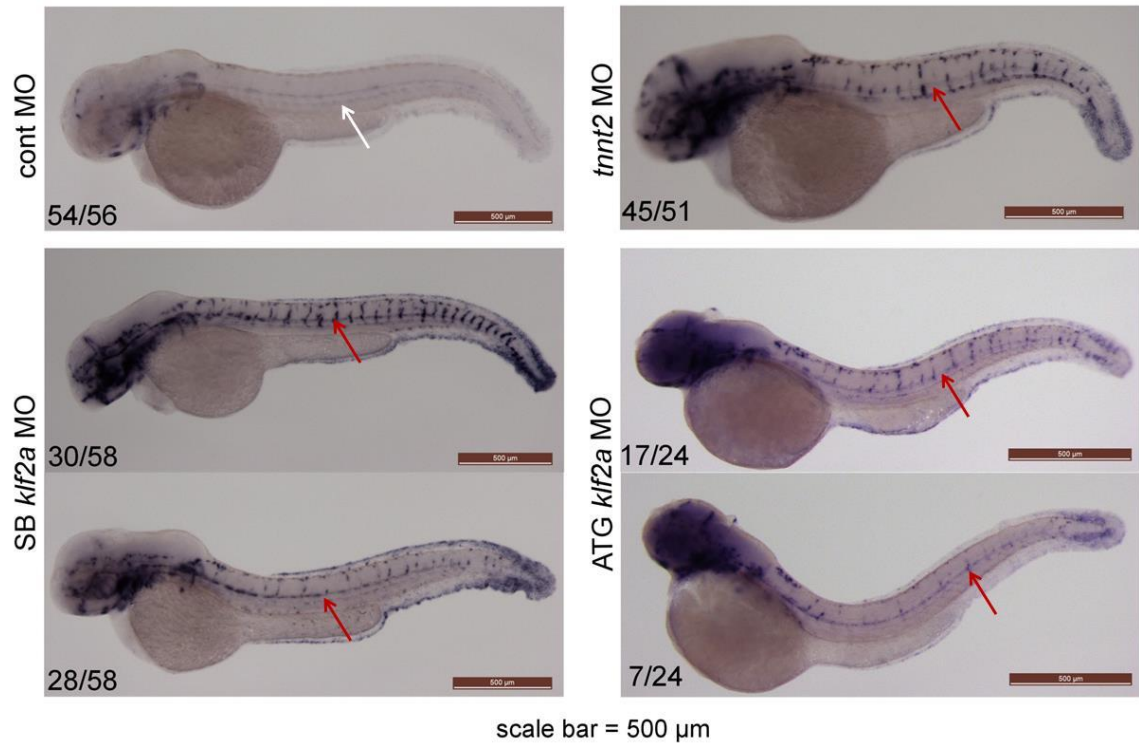


Figure 3.6 *cxcr4a* vascular expression is upregulated in a proportion of SB *kif2a* MO and ATG *kif2a* MO morphants at 48hpf.

Vascular expression of *cxcr4a* is downregulated in control MO morphants (white arrow) at 48hpf but remains highly expressed in *tnnt2* MO morphants (red arrow). SB *kif2a* MO and ATG *kif2a* MO morphants exhibit various levels of increased *cxcr4a* expression when compared to controls (red arrows). Numbers in bottom left corner indicate the number of embryos with identical staining patterns out of total number of embryos examined. Representative images from a total of 4 (cont MO, *tnnt2* MO, SB *kif2a* MO) or 2 (ATG *kif2a* MO) independent experiments are shown. Scale bar = 500µm.

3.2.3.1 RT-qPCR data do not show any significant increase in relative *cxcr4a* expression in SB *klf2a* MO and ATG *klf2a* MO morphants at 48hpf

I used RT-qPCR performed on whole-embryo cDNA to quantify the observed upregulation of *cxcr4a* vascular expression in the proportion of SB *klf2a* MO and ATG *klf2a* MO morphants. As expected, *cxcr4a* expression was upregulated in *tnnt2* MO morphants by approximately 2.5-fold thus representing a positive control (**Figure 3.7**). Uninjected embryos were also examined for relative *cxcr4a* expression to demonstrate that injections of control MO have no real effect on *cxcr4a* expression levels (**Figure 3.7**). Surprisingly, neither SB *klf2a* MO nor ATG *klf2a* MO morphants showed any significant increase of relative *cxcr4a* expression when compared to controls (**Figure 3.7**).

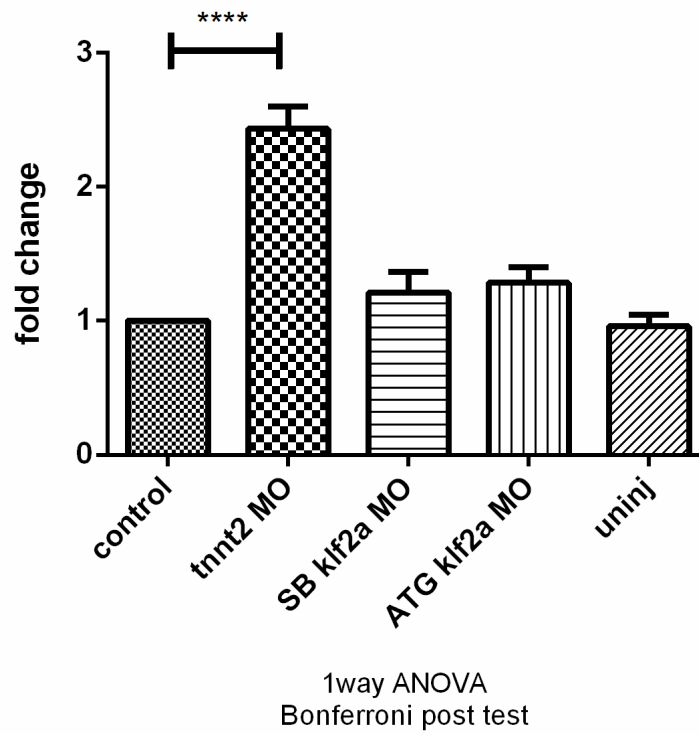


Figure 3.7 RT-qPCR from whole embryonic cDNA comparing relative expression of *cxcr4a* at 48hpf.

RT-qPCR performed in duplicate on 3 independent experiments (3 separate pools of 20 embryos). Elongation factor 1 (*ef1*) used as a reference gene. *cxcr4a* expression in control MO morphants taken as a reference sample (control). Pfaffl method of relative quantification used. Error bars represent mean \pm SEM. **** = $p < 0.0001$.

3.2.4 Does *klf2a* play a role in flow dependent regulation of Notch signalling in embryonic zebrafish vasculature?

Our group has shown that blood flow suppresses vascular Notch signalling in developing zebrafish embryos via suppressing vascular *dll4* expression. Cessation of blood flow in zebrafish embryos caused increased vascular *dll4* expression resulting in increased activity of Notch signalling pathway at 48hpf and 72hpf. (Watson, Novodvorsky et al. 2013).

This was for the first time that blood flow as a mechanical force has been found to alter Notch signalling *in vivo* and I aimed to find out whether *klf2a* plays a role in this process. I performed a WISH for *dll4* on SB *klf2a* MO and ATG *klf2a* MO morphants at 48hpf (**Figure 3.8**). As expected, increased vascular *dll4* expression was detected in *tnnt2* MO morphants confirming our previously published data. Interestingly, increased vascular *dll4* expression was noticed also in a large proportion of SB *klf2a* MO and ATG *klf2a* MO morphants (**Figure 3.8**). This suggests that the flow-mediated regulation of endothelial Notch signalling in embryonic zebrafish vasculature might be mediated by *klf2a*.

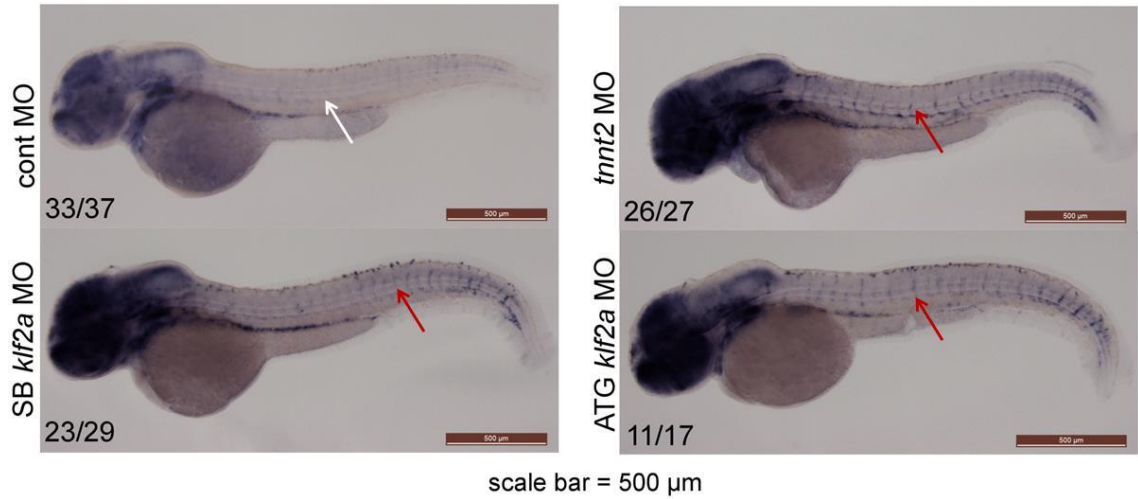
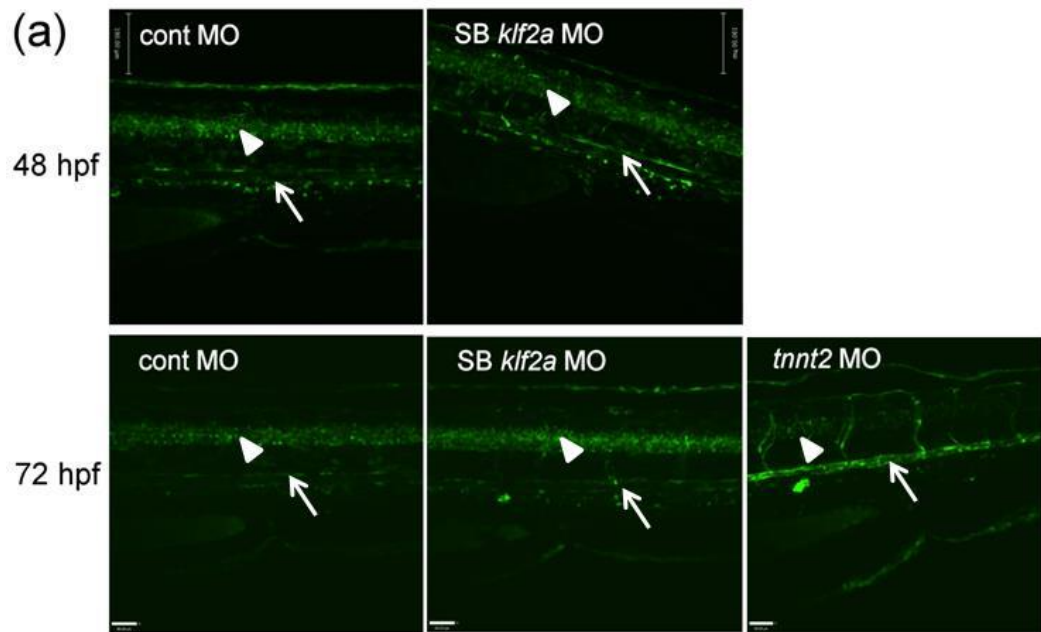


Figure 3.8 *dlla4* vascular expression is upregulated in a proportion of SB *kif2a* MO and ATG *kif2a* MO morphants at 48hpf.

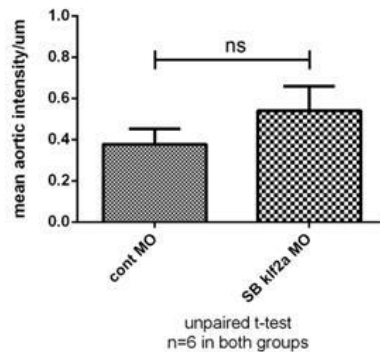
dlla4 vascular expression is downregulated at 48hpf in the presence of blood flow (white arrow) as shown in the control MO injected embryos, but increases in the absence of blood flow - *tnnt2* MO morphants (red arrow). A significant proportion of SB *kif2a* MO and ATG *kif2a* MO morphants exhibit increased vascular *dlla4* expression when compared to controls (red arrows). Numbers in left bottom corners indicate the number of embryos with identical staining patterns out of total number of embryos examined. Representative images from 3 independent experiments are shown. Scale bar = 500µm.

3.2.4.1 *klf2a* MO morphants do not exhibit increased CSL:venus fluorescence in DA at 48hpf and 72hpf

I wanted to examine whether the increased *dll4* expression in the vasculature of SB *klf2a* MO morphants at 48hpf resulted in increased vascular Notch activity. I therefore examined the activity of CSL in SB *klf2a* MO morphants using the *Tg(CSL:venus)qmc61* line that expresses the yellow fluorescent protein derivative venus under the control of CSL. *Tg(CSL:venus)qmc61* zebrafish adults were outcrossed to wild type zebrafish line. Progeny of such an outcross were then injected with control MO or SB *klf2a* MO. Embryos coming from a particular pair of parents were kept separate and were screened for fluorescence at 48hpf. The fact that around 50% of the progeny displayed fluorescence (the remaining 50% showed no fluorescence) was considered as a confirmation that the fluorescent fish contained only a single copy of the transgene. Mean intensity of venus fluorescence in dorsal wall of DA was measured at 2dpf and 3dpf as detailed in Section 2.5.6. As shown in **Figure 3.9**, SB *klf2a* MO morphants do not show any significant difference in aortic venus fluorescence at this stages when compared to controls. Increased venus fluorescence could be confirmed in *tnnt2* MO morphants without flow at 3dpf confirming previously published data (Watson, Novodvorsky et al. 2013) (data not shown).



(b) 48 hpf



(c) 72 hpf

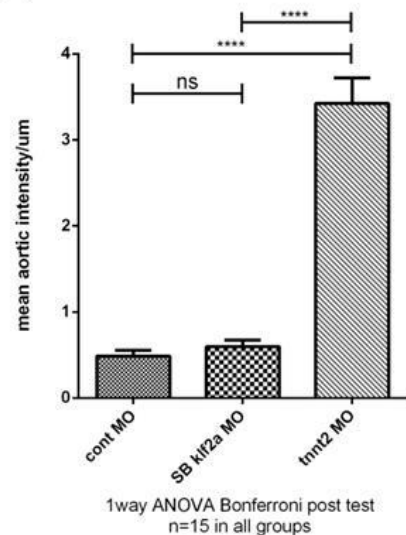


Figure 3.9 Comparison of the mean venus fluorescence in dorsal wall of DA between SB *klf2a* MO and cont MO morphants at 48hpf and 72hpf.

(a) Representative images show a region around the cloaca which was chosen for the fluorescence measurements. White arrows point at dorsal aortae and white arrowheads point at neural tubes. Scale bar = 190µm (48hpf) or 80µm (72hpf). (b)-(c) Quantification of venus fluorescence in dorsal wall of DA normalised to the fluorescence of neural tube. SB *klf2a* MO morphants do not show any significant difference in this parameter when compared to controls at 48hpf or 72hpf. *tnnt2* MO morphants exhibit increased mean venus fluorescence at 72hpf in keeping with previously published data. Unpaired t-test (48hpf) or 1way ANOVA with Bonferroni post test used (72hpf). Error bars represent mean ± SEM. **** = p<0.0001.

3.3 Discussion

I reproduced and extended the studies on spatial and temporal *klf2a* expression patterns in developing zebrafish embryos especially beyond 72hpf. I achieved this by performing a series of whole mount in situ hybridisations (WISH) using a *de novo* synthesized *klf2a* riboprobe. For the first time I detected *klf2a* expression in subintestinal veins and hepatic portal vein as well as in neuromast cells forming the lateral line organ. I reproducibly detected *klf2a* vascular expression from 36hpf until 72hpf. It is very likely that *klf2a* is expressed in vasculature also in later developmental stages, but the riboprobe penetration into zebrafish tissues beyond 48hpf has been reported to be problematic and represents one of the main limitations of the WISH technique (Thisse and Thisse 2008). The rather strong vascular signal I was able to detect at 72hpf is a result of optimised WISH protocol with extended proteinase K treatments.

By performing cross sections on a fixed 48hpf embryo following a *klf2a* WISH I proved that the *klf2a* mRNA signal from the trunk is truly vascular in origin. I was able to localise not only the major embryonic trunk vessels such as DA or DLAV, but also vessels such as ISVs and parachordal vessels.

Next I confirmed that *klf2a* expression in endothelial cells of developing zebrafish embryos is blood flow dependent by showing the loss of *klf2a* vascular expression in three different zebrafish models of hindered blood flow. Initially I used *gridlock* mutants with occlusion of the proximal DA. Secondly I achieved complete cessation of cardiac contractions by knocking down troponin t2 by a specific morpholino (*tnnt2* MO morphants). Thirdly I stopped cardiac contractions pharmacologically with local anaesthetic Tricaine. Vascular *klf2a* expression was abolished or significantly reduced in all three cases. In *gridlock* mutants and *tnnt2* MO morphants, *klf2a* expression in all

other anatomical locations remained unchanged. Tricaine treatment resulted in decreased *klf2a* expression in the heart region and in the cells lateral to the most posterior notochord. This descriptive name denotes cells within the posterior somites from which later posterior myotomes develop. It is currently not known what function *klf2a* has in these cells and I can equally not explain why *klf2a* expression diminished in these cells following treatment with Tricaine. In general, embryos were treated with the lowest possible dose of Tricaine that would visibly stop erythrocyte movements in the DA from 32hpf to 48hpf. Weak cardiac contractions were still present in these embryos. These contractions were apparently strong enough to maintain *klf2a* expression in the heart at a detectable level.

For morpholino-mediated *klf2a* knockdown studies I used two previously published *klf2a* MOs (Vermot, Forouhar et al. 2009; Nicoli, Standley et al. 2010; Wang, Zhang et al. 2011).

The splice-blocking *klf2a* morpholino I used (SB *klf2a* MO) is intended to cause an inclusion of intron 2 in the *klf2a* mRNA (Nicoli, Standley et al. 2010). In the original work, SB *klf2a* MO could only cause an incomplete knockdown even in the case of the highest dose of MO injected per embryo (2.5ng) as shown by the subsequent RT-PCR (Supplementary Figure 7 in the original work and also **Figure 2.1**). This level of *klf2a* knockdown was however reported to be sufficient to cause a biological effect and subsequent *klf2a* RT-qPCR demonstrated decreased levels of wild type *klf2a* transcript when compared to controls (Supplementary Figure 7 in the original work and also **Figure 2.1**) In my hands, SB *klf2a* MO proved to be very difficult to work with due to its unpredictable toxicity levels. Due to this fact, lower than previously published doses had to be used (1.1ng per embryo).

Another *klf2a* MO I used is intended to block initiation of *klf2a* translation by binding to and around the translational start of the *klf2a* mRNA. On closer examination of the ATG

klf2a MO sequence I found out that it binds to a region 74bp 3' downstream from the translational start of *klf2a* mRNA at the 5' end of *klf2a* exon 2 and would therefore not be able to interfere with *klf2a* translation (GENE TOOLS). I was able to detect a putative alternative translational start for *klf2a* mRNA downstream to the ATG *klf2a* MO binding site. It is unlikely that this ATG in primary gene structure represents a true alternative translational start for two reasons. Firstly, the 34 AA-polypeptide coded by *klf2a* mRNA sequence between the original and putative translational starts is highly conserved among the species. It is therefore unlikely to be missed out by using the alternative translational start. Secondly, this putative translational start is not present in mouse or human *KLF2/Klf2* genomic sequence in this region which makes the possibility of a simple mistake more likely. Given the above circumstances it is rather surprising that I could observe changes in vascular expression levels of *cxcr4a* and *dll4* and these changes were in keeping with my previously postulated hypotheses. This made me to further examine the possible mechanism of action for this morpholino. Given the fact that the ATG *klf2a* MO binds closely to the intron 1 - exon 2 splice junction site, I performed an RT-PCR spanning *klf2a* exon 1 and exon 3 to see whether ATG *klf2a* MO interferes with *klf2a* pre-mRNA splicing. I could indeed detect the presence of additional bands in ATG *klf2a* morphants indicating a possible partial and total inclusion of *klf2a* intron 1. Similar changes in vascular expression of *cxcr4a* and *dll4* seen in SB *klf2a* MO and ATG *klf2a* MO morphants would be in keeping with these findings.

In my studies I sought to distinguish between the effects of blood flow as mechanical force and the specific effects of *klf2a* as one of the main endothelial mechanosensitive transcription factors. It was therefore of great importance to make sure that the injections of both *klf2a* morpholinos did not cause impairment of cardiac output and subsequent reduction of blood flow by the mechanism of simple morpholino toxicity. I

confirmed that heart rates and blood flow velocities in SB *klf2a* MO and ATG *klf2a* MO morphants did not differ significantly when compared to the control MO morphants. This suggests that the observed changes in gene expression levels are not caused by morpholino-mediated impairment of cardiovascular performance.

The SDF chemokine receptor *CXCR4* has 2 zebrafish paralogs. One of them, *cxcr4a* was shown by our group to be negatively regulated by blood flow in the developing zebrafish vasculature and to contribute to collateral vessel formation (Packham, Gray et al. 2009). I found that a significant proportion (approximately 50%) of both SB *klf2a* MO and ATG *klf2a* MO morphants had increased vascular *cxcr4a* expression at 48hpf despite intact blood flow. I therefore hypothesised that *klf2a* could play a role as a negative regulator of *cxcr4a* in the vasculature. In this scenario, *klf2a* gets upregulated in the presence of blood flow and subsequently inhibits *cxcr4a* expression. In the absence of blood flow, the inhibitory function of *klf2a* diminishes and this allows for increased *cxcr4a* vascular expression and its contribution towards formation of the collateral vessels. Surprisingly the RT-qPCR data did not confirm a significant increase in relative *cxcr4a* expression in *klf2a* MOs morphants as it was the case in *tnnt2* MO morphants without flow. The calculated *cxcr4a* TaqMan probe efficiency was 105.4% which is within the acceptable range (90-110%). I hypothesised that the changes in *klf2a* expression in endothelial cells are not sufficient to cause a statistically significant difference when cDNA from whole embryos is used as a template for RT-qPCR in the case of *klf2a* MO morphants. I therefore performed an RT-qPCR on cDNA isolated from trunks of zebrafish embryos. Unfortunately, I was not able to demonstrate significantly increased levels of relative *cxcr4a* expression even in the *tnnt2* MO morphants that should represent a positive control in this experiment. A possible explanation in this case is a technical error, because the calculated efficiency of *cxcr4a* TaqMan probe in this case was 122.8% which is outside acceptable levels. The

intensity of *cxcr4a* signal in the vasculature of a significant proportion of SB *klf2a* MO morphants is clearly comparable to the intensity of *cxcr4a* signal in *tnnt2* MO morphants (**Figure 3.6**). The discrepancy between the *in situ* data and the RT-qPCR data could be addressed by simply repeating the RT-qPCR from the cDNA of whole embryos and the cDNA isolated from the trunks of embryos. If no technical difficulties occurred and similarly discrepant results were detected a different *cxcr4a* TaqMan probe could be used to address this issue further. At that stage of my project, I generated a stable *klf2a* mutant line and sought for a definitive answer to this hypothesis by performing the experiments on this mutant line.

One potential link between *klf2a* and *cxcr4a* could be *miR-150*. *miR-150* expression is known to be stimulated by KLF2 in HUVEC (Hergenreider, Heydt et al. 2012) and stimulates endothelial cell migration (Zhang, Liu et al. 2010). Interestingly, *Cxcr4* was found to be downregulated by *miR-150*. Under the hypoxic conditions of myocardial infarction model in mouse, *miR-150* expression is downregulated and results in an increase of *Cxcr4* positive mononuclear cells in bone marrow as well as in peripheral blood (Tano, Kim et al. 2011).

Another work that connects CXCR4 and KLF2 was performed by Uchida et al. They showed that Vesnarinone, a chemotherapeutic agent used in treatment of oral squamous cell carcinoma in humans was found to downregulate *CXCR4* expression in several human oral cancer cell lines. Vesnarinone increases *KLF2* expression and potentiates direct binding of KLF2 to the *CXCR4* promoter (Uchida, Onoue et al. 2009).

When I examined the effects of *klf2a* on Notch signalling pathway I found increased endothelial expression of Notch ligand *dll4* in most SB *klf2a* MO and ATG *klf2a* MO morphants at 48hpf. The increase in *dll4* expression was similar to the levels seen in the embryos without blood flow - *tnnt2* MO morphants. Subsequent RT-qPCR on cDNA from the trunks of embryos unfortunately could not detect any significant increase in

relative *dll4* expression even in the positive controls (*tnnt2* MO morphants) and could not be therefore be interpreted. I am not sure what could be the cause of this failure since the technique of extracting RNA from the trunks of zebrafish embryos has been used successfully in our group in the past. Calculated TaqMan probe efficiencies were within the acceptable limits (97% for *dll4* and 110% for *ef1*) this time. A *dll4* RT-qPCR from whole-embryo cDNA was not performed because brain tissues contain high amounts of active Notch signalling throughout the embryonic development and could therefore interfere with the assay (Cau and Blader 2009). Again, as in the case of *cxcr4a*, a repeated RT-qPCR on cDNA from the trunks of zebrafish embryos could be tried to exclude other potential technical errors or different *dll4* TaqMan probe could be used to address this discrepancy.

For further studies of *klf2a* involvement in Notch signalling cascade I used a fluorescent transgenic reporter line *Tg(CSL-venus)qmc61*. This line expresses yellow fluorescent protein venus under direct control of the canonical Notch transcription factor CSL. I examined whether the increased vascular expression of the canonical Notch ligand *dll4* seen in SB *klf2a* MO morphants resulted in increased vascular Notch activity. This would be reflected by increased vascular venus fluorescence in this model. Although I could see a trend towards increased venus fluorescence in the SB *klf2a* MO morphants at 48hpf, this was not significant. At 3dpf this trend was reversed, but not significant either. Increased venus aortic fluorescence was detected in *tnnt2* MO morphants at 3dpf confirming previously published data (Watson, Novodvorsky et al. 2013). Instead of repeating the above experiments using *klf2a* morpholinos, I chose to perform these experiments on the *klf2a* mutant zebrafish line which I generated around that time. To my knowledge no direct link between Notch signalling and *KLF2/Klf2/klf2a* has been established so far.

In the next chapter I detail my generation of stable *klf2a* mutants to extend these studies.

Chapter 4

Generation of a stable *klf2a* mutant line

4.1 Introduction

The advent of new techniques and protocols for site-targeted mutagenesis in recent years has made it possible to generate mutations in genes of choice. A significant number of mutant lines has now been generated this way, driven by the problems associated with morpholino use, mainly time-limited and incomplete knockdown and off-target effects. Generation of a stable *klf2a* mutant line would enable comparison with the data obtained by the morpholino-mediated *klf2a* knockdown. It would equally represent an excellent tool for studying the role of *klf2a* in vascular biology exploiting the advantages the zebrafish model has to offer in this field.

4.2 Results

4.2.1 *klf2a* targeted mutagenesis by Transcription Activator-Like Effector Nucleases (TALEN)

The TALEN approach to genome-wide editing has been recently published and made available for wide laboratory use (Cermak, Doyle et al. 2011). One of the main advantages of TALENs when compared to CoDA ZFN protocols is the availability of candidate cleavage sites. Whereas a potential CoDA ZFN target site can be found only every 400bp in a protein coding transcript (Sander, Dahlborg et al. 2011), TALEN candidate cleavage sites were reported to be found on average every 35bp in 9 genes initially tested (Cermak, Doyle et al. 2011). A design of a *klf2a*-specific TALEN was therefore chosen as a next step towards generation of a stable *klf2a* mutant line.

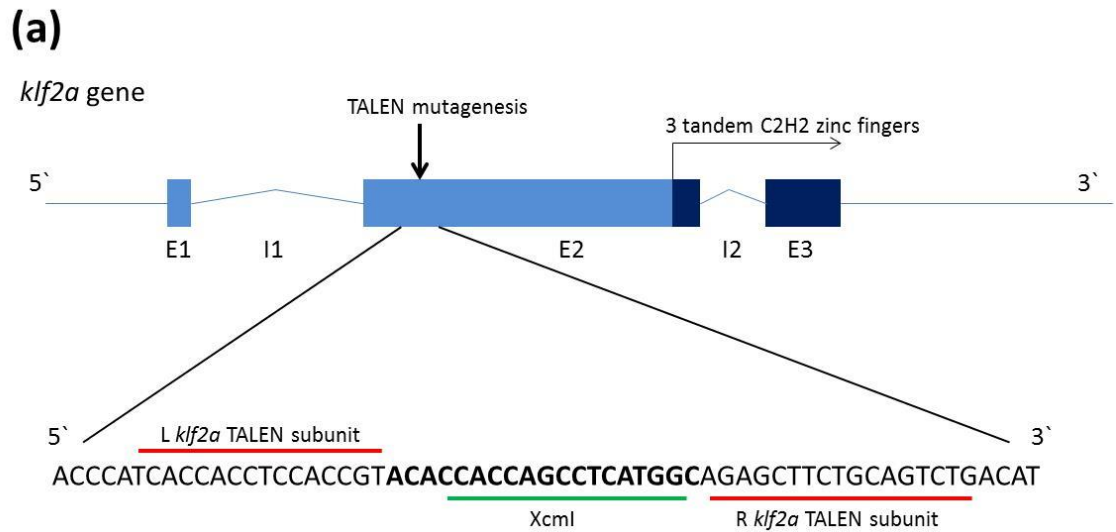
4.2.1.1 *klf2a* TALEN design

A detailed general protocol for TALEN mutagenesis is included in the Materials and Methods chapter. Here are presented the important steps and results in the *klf2a* TALEN mutagenesis. All enzymes used in this project were purchased from New England Biolabs (NEB).

From the designs suggested by the TALEN targeter software, a TALEN was chosen that comprises of 15 RVDs in the R subunit and of 17 RVDs in the L subunit and has got a 19bp long spacer with a wide-spanning restriction enzyme XcmI site within it (**Figure 4.1**). This TALEN binds to a sequence in *klf2a* Exon 2 closer to its 5' end that is upstream of the three tandem zinc fingers coding sequence as indicated in **Figure 4.1**. Any missense mutation in the gene region would cause a premature stop codon resulting in a translation of a truncated Klf2a protein without its key DNA binding motif – the 3 tandem zinc fingers.

4.2.1.2 Test PCR across the *klf2a* TALEN target site and XcmI digest

Before the actual TALEN assembly was started, a pair of PCR primers (named as *klf2a* TAL XcmI L1 and *klf2a* TAL XcmI R1) was designed to span a 281bp region around the *klf2a* TALEN mutagenesis target site. Genomic DNA from WT zebrafish embryos was used as template for the PCR. Following the PCR, a restriction enzyme digest with XcmI was set up. As shown in **Figure 4.2**, this PCR produced a single band of expected size and subsequent XcmI digest for 1 hour at RT resulted in complete digest of the PCR product leaving 2 products of 180bp and 101bp size respectively. This was important because this PCR and XcmI digest were to be used as a test of *klf2a* TALEN efficiency and also for further genotyping of mutant embryos and adult zebrafish



(b)

L *klf2a* TALEN RVDs: HD NI HD HD NI HD HD NG HD HD NI HD HD NN NG

R *klf2a* TALEN RVDs: HD NI NN NI HD NG NN HD NI NN NI NI NN HD NG HD NG

Figure 4.1 *klf2a* TALEN mutagenesis

(a) Schematic structure of *klf2a* gene. Dark blue colour of the 3' end of Exon 2 and the whole Exon 3 highlights the coding sequence for 3 tandem C2H2 zinc-fingers which represent the DNA binding motif of KLF family of transcription factors. Black arrow indicates the site of *klf2a* TALEN mutagenesis. Below, sequence of the + strand of *klf2a* gene at the site of mutagenesis is shown with L and R *klf2a* TALEN subunit binding sites marked with red lines and XcmI restriction enzyme site of general structure CCANNNNNNNTGG (N represents any nucleotide) underlined in green. 19bp spacer between the L and R *klf2a* TALEN binding sites is highlighted in bold. **(b)** AA structure of the RVDs in the *klf2a* TALEN of choice. RVDs determine the nucleotide binding specificity of each AA repeat of the array (see also **Figure 2.4**).

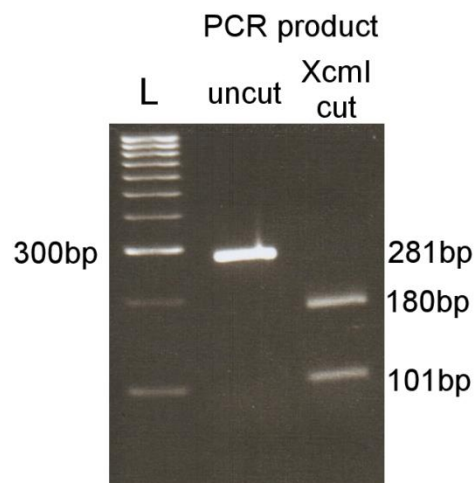


Figure 4.2 Test PCR across *klf2a* TALEN mutagenesis target site

PCR across *klf2a* TALEN target site with a wild type zebrafish genomic DNA confirmed a single 281bp product. Subsequent XcmI digest resulted in a complete PCR product digest leaving 2 bands of 180bp and 101bp. Abbreviations: L: Hyperladder IV (NEB).

4.2.1.3 *klf2a* TALEN assembly and mRNA synthesis

Following the stage 1 assembly A and B parts of L and R TALEN subunit were checked by a double restriction enzyme digest with NheI (NEB) and XbaI (NEB) which confirmed the predicted sizes of products (**Figure 4.3a**). Similarly, after the assembly stage 2, the double restriction enzyme digest with BamHI (NEB) and XbaI (NEB) was run alongside the NotI (NEB) linearized L and R TALEN plasmids and the correct band sizes were confirmed (**Figure 4.3b**). Additionally, sequencing confirmed the correct assembly of all RVDs within the expression plasmids and capped *klf2a* TALEN mRNA could be synthesized. Following the synthesis and purification the presence of *klf2a* TALEN mRNA was checked by agarose gel electrophoresis (**Figure 4.3c**).

4.2.1.4 *klf2a* TALEN mRNA injections and mutation analysis of injected embryos

The optimal injection dose of *klf2a* TALEN mRNA was established to be approximately 1.5ng per embryo. Injected embryos were raised and genomic DNA from individual injected embryos together with DNA from uninjected littermates was extracted at 3dpf. PCR across the *klf2a* TALEN target site and subsequent XcmI restriction enzyme digest showed the presence of an uncut 281bp band in PCR products from *klf2a* TALEN mRNA injected embryos suggesting loss of XcmI restriction site caused by *klf2a* TALEN induced mutagenesis (**Figure 4.4**).

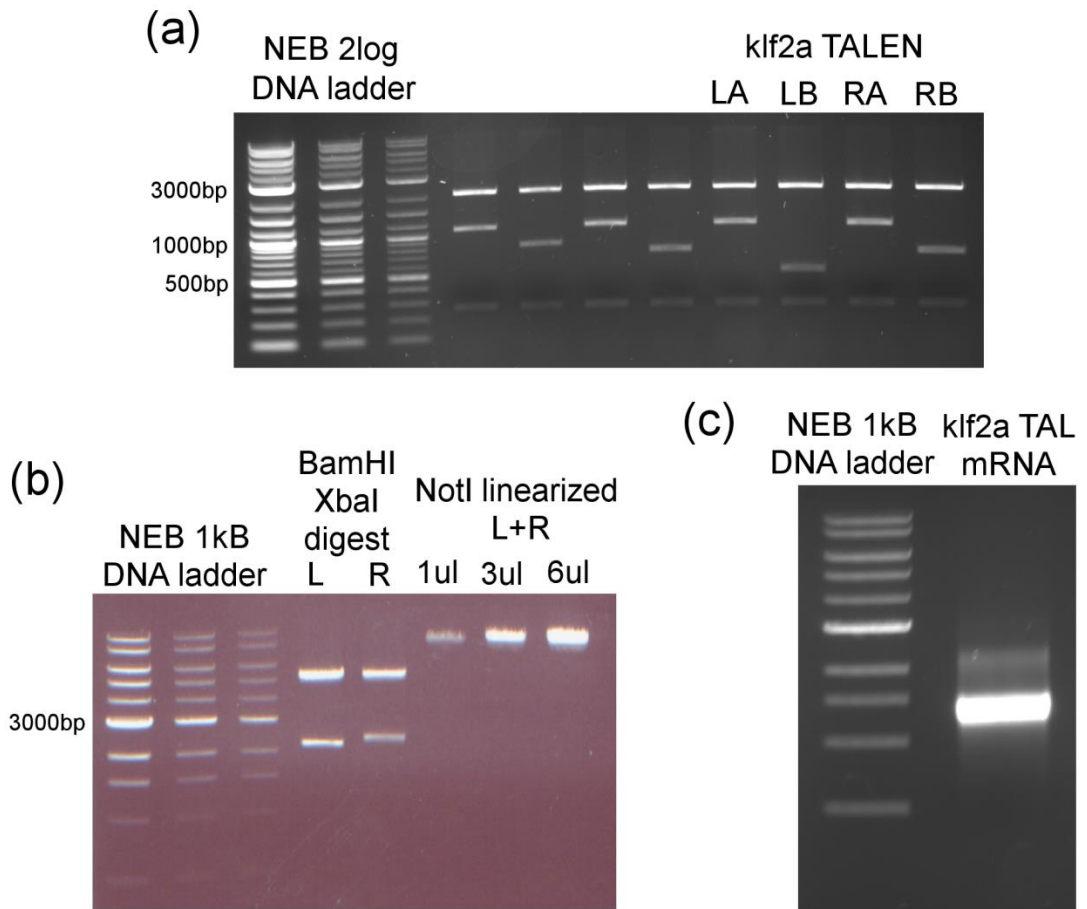


Figure 4.3 *klf2a* TALEN assembly. Control enzymatic digests and capped mRNA synthesis

(a) NheI and XbaI digest of LA, LB, RA and RB parts of *klf2a* TALEN showed bands at 2132bp, 1100bp and 266bp (LA and RA), at 2132bp, 550bp and 266bp (LB) and at 2132bp, 770bp and 266bp (RB). (b) BamHI and XbaI digest of L and R *klf2a* TALEN expression plasmids showed bands at 5323bp and 2207bp (L) and bands at 5323bp and 2411bp (R). NotI linearization bands are a mixture of L (7530bp) and R (7743bp) linearized plasmids. (c) Capped *klf2a* TALEN mRNA visualised on an agarose gel.

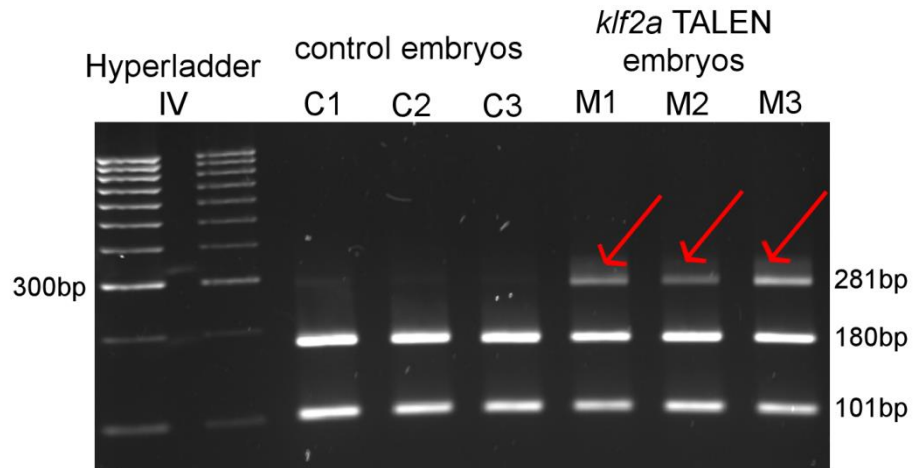


Figure 4.4 *klf2a* TALEN F0 generation mutation analysis.

klf2a TALEN mRNA injected embryos (M1-M3) exhibit the presence of a 281bp uncut band (red arrows) following a PCR across the mutagenesis site and restriction enzyme digest with XcmI suggesting the loss of restriction enzyme site due to *klf2a* TALEN targeted mutagenesis. PCR across the same region with subsequent XcmI digest on genomic DNA from control embryos (C1-C3) resulted in a complete digest and detection of 180bp and 101bp bands. Genomic DNA was extracted at 3dpf.

4.2.1.5 Screening for potential founder fish and identification of 4 *klf2a* mutant alleles

A proportion of *klf2a* TALEN mRNA injected embryos (F0 generation) had mosaic germlines so that some of their offspring would be carriers for the *klf2a* TALEN induced mutations. Once the F0 generation reached sexual maturity (2-3 months), individual fish were outcrossed to Nacre WT adults. F0 generation fish that produced progeny were kept in individual tanks and their progeny were tested at 3dpf with a PCR and XcmI restriction digest. In total 29 F0 generation fish were pair-mated with Nacre WT out of which 20 produced progeny which was subsequently tested. Altogether 6 out of 20 fish annotated as T1, T2, T15, T18, T20 and T27 were founders that passed the mutations to some of their offspring (**Figure 4.5**). The remaining 14 fish were euthanised. Undigested bands from the progeny of fish T1, T2, T15, T18, T20 and T27 were cut out from the gel, purified and sequenced. Fish T20 and T27 transmitted an allele with 3bp and 6bp deletion that would not cause a frame shift and were therefore euthanised. Sequencing confirmed an allele with 1bp deletion in the T1 progeny, another 1bp deletion in progeny of T2 and T15 fish and several alleles (3bp deletion, 14bp deletion, 1bp substitutions and other not clearly identifiable mutations) in T18 progeny. These alleles were named: *klf2a*^{sh306} and *klf2a*^{sh307} carry different 1bp deletions, *klf2a*^{sh317} carries a 14bp deletion and *klf2a*^{sh310} carries a 7bp deletion which - as found out later re-created the XcmI restriction enzyme site sequence preventing easy genotyping by PCR and XcmI restriction enzyme digest. Sequences of mutant alleles, translated proteins and predicted molecular weights are shown in **Figure 4.6**.

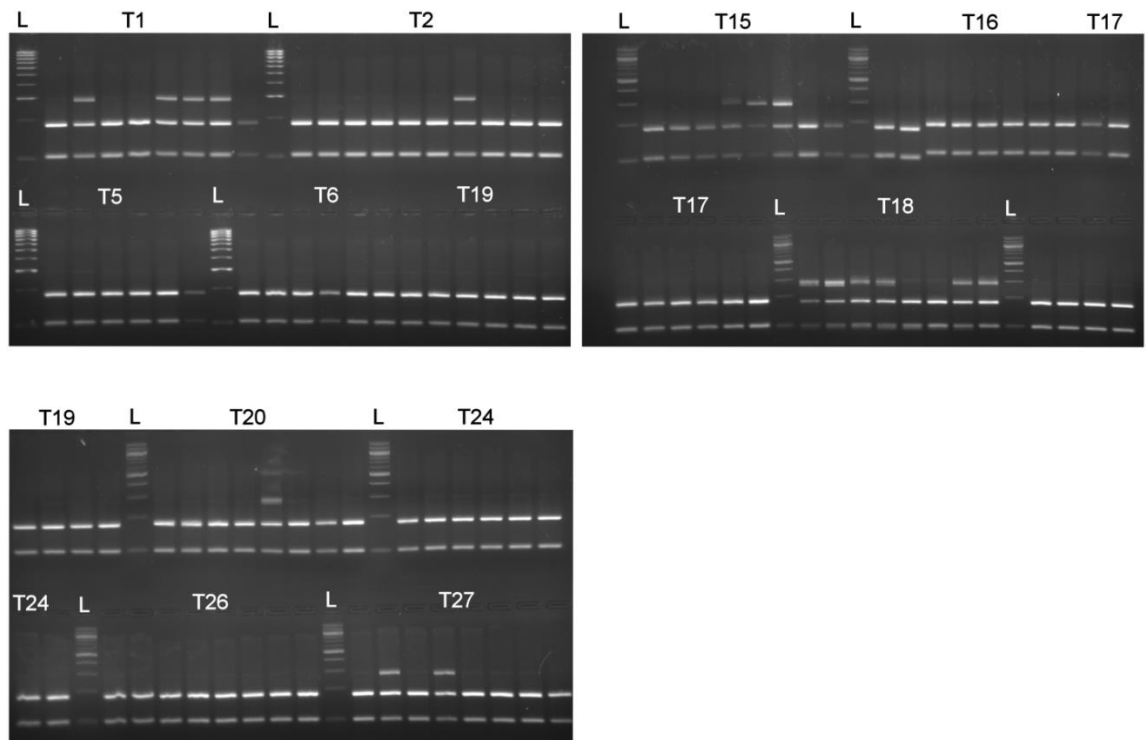


Figure 4.5 Screening for potential *klf2a* TALEN founder fish.

T1-T27 *klf2a* TALEN F0 generation fish were outcrossed with Nacre WT fish and their progeny were tested for the presence of any mutant *klf2a* allele. Each sample well contains genomic DNA from 3 embryos following a genomic DNA extraction at 3dpf, PCR and restriction enzyme test with XcmI. Up to 3x8 i.e. 24 embryos were tested per fish or all embryos produced if that was less than 24. Fish T1, T2, T15, T18, T20 and T27 were found to pass mutant *klf2a* allele(s) to a proportion of their progeny as indicated by the presence of an uncut 281bp band in some of the wells. Abbreviations: L: Hyperladder IV (NEB).

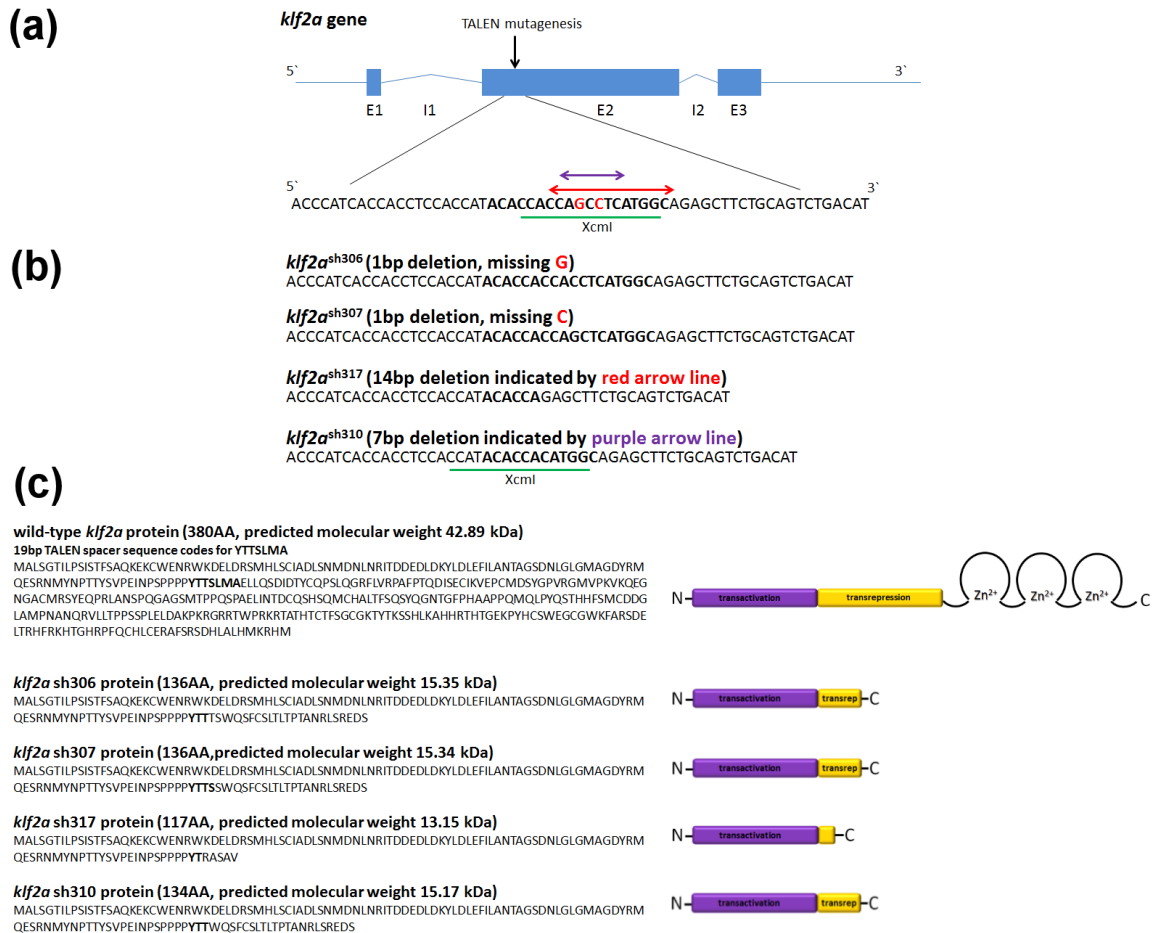


Figure 4.6 Identification of 4 *klf2a* mutant alleles

(a) Wild type *klf2a* gene, genetic code at the site of mutagenesis with indicated *klf2a* TALEN 19bp spacer in bold. XcmI restriction site is underlined in green. In *klf2a*^{sh310} allele a new XcmI restriction site of general structure CCANNNNNNNNTGG was generated due to the 7bp deletion **(b)** *klf2a* mutant alleles identified by sequencing of the progeny of a *klf2a* TALEN F0 generation outcross with Nacre WT fish. Mutations are indicated by the base pairs highlighted in red or by the red and purple arrow lines in the wild type sequence **(a)**. **(c)** Primary protein structure of Klf2a wild type and mutant proteins with indicated AA lengths, predicted molecular weights in kilodaltons (kDa) (free public domain http://www.bioinformatics.org/sms/prot_mw.html) and schematic drawing of protein domains.

4.2.1.6 Generation of *klf2a* TALEN mutant lines

F0 generation founder fish T1, T2, T15 and T18 transmitting frame shift mutations were outcrossed to Nacre WT to generate an F1 generation of *klf2a* mutant fish in WT background without skin pigmentation that was to be used for WISH experiments. *klf2a* TALEN founder fish were also outcrossed to *Tg(CSL:venus)qmc61* and *Tg(kdrl:HRAS-mCherry;flk1:EGFP-nls)* zebrafish to generate transgenic lines in *klf2a* mutant background as tools for studying the role of *klf2a* in vascular development.

Once the F1 generation of fish reached sexual maturity, individual fish were genotyped by fin-clipping and subsequent PCR and XcmI restriction digest. All individual fish that were shown to be heterozygous carriers for any *klf2a* mutant allele (50% of the progeny) were also confirmed to carry a mutant *klf2a* allele by sequencing. This was absolutely necessary in the progeny of T18 fish which transmitted several mutant alleles some of which did not cause frame shifts. An example of such genotyping is shown in **Figure 4.7a**. Heterozygous carriers for a particular *klf2a* allele in a particular genetic background were put into separate fish tanks and appropriately labelled. WT siblings of F1 fish were euthanised. Heterozygous F1 fish were then ready to be used for experiments. An incross of 2 such fish would give rise to 25% homozygous carriers, 50% heterozygous carriers and 25% WT fish in the F2 generation. These F2 generation fish would have to be genotyped following any experiment performed on them. WT siblings would represent an important negative control in experiments carried out on these fish.

A proportion of F2 generation of fish were raised and genotyped when they reached sexual maturity. An example of such genotyping is shown in **Figure 4.7b**. Homozygous carriers for a particular allele in any given genetic background were separated from heterozygous carriers, put into separate fish tanks and labelled appropriately. These

fish were then incrossed and produced an F3 generation of mutant zebrafish embryos which were used in experiments. Progeny of an incross of F2 generation homozygous carriers for particular *klf2a* allele (i.e. the F3 generation) would represent a maternal mutant line without any possible maternal zygotic mRNA or protein contribution.

F2 generation *klf2a*^{sh317} mutant fish were outcrossed to *Tg(vhl*^{hu2117+/-} *;fli1:eGFP)* zebrafish line. Once this progeny reached sexual maturity, they were fin-clipped and genotyped for both *klf2a*^{sh317} and *vhl*^{hu2117} alleles. Heterozygous carriers for both mutant alleles were kept separate and used for further experiments as detailed in Chapter 5.

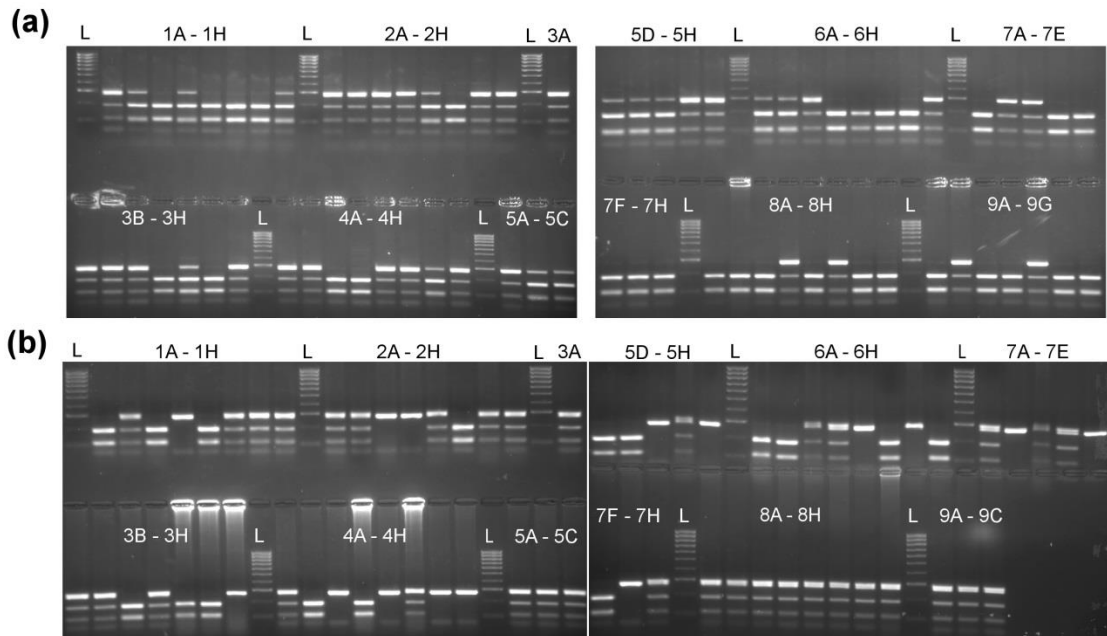


Figure 4.7 Genotyping of *klf2a* mutant zebrafish

Fin clips from individual F1 or F2 generation zebrafish were labelled according to their position in a 96-well plate. Following genomic DNA extraction, genotyping was done via PCR and XcmI restriction enzyme digest. **(a) Genotyping of F1 generation of *klf2a* mutant zebrafish** Heterozygous F1 carriers were identified by the presence of 3 bands, the uncut 281bp band and two 180bp and 101bp bands. PCR products from gDNA from WT siblings underwent a complete XcmI digest indicated by the absence of an uncut 281bp band. **(b) Genotyping of F2 generation of *klf2a* mutant zebrafish.** Homozygous carriers for a mutant *klf2a* allele were identified by the presence of a single 281bp uncut band. Heterozygous carriers were identified by the presence of 3 bands, the uncut 281bp band and two 180bp and 101bp bands. PCR products from gDNA from WT siblings underwent a complete XcmI digest indicated by the absence of an uncut 281bp band. Abbreviations: L: Hyperladder IV (NEB).

4.2.2 Assessment of the effects of *klf2a* mutation on *klf2a* mRNA transcription and Klf2a protein translation

Predicted sequences for all F1 generation heterozygous carriers of any of the 4 *klf2a* mutant alleles were confirmed by sequencing as described above. Apart from the confirmation of altered primary DNA sequence I sought to confirm that the mutations in *klf2a* gene resulted in transcription of altered *klf2a* mRNA and translation of altered, truncated Klf2a protein.

4.2.2.1 *klf2a*^{sh317} cDNA sequencing

Whole embryo RNA from 30 pooled embryos from the F3 generation of homozygous carriers of *klf2a*^{sh317} allele was extracted at 4dpf. In the following step cDNA was synthesised and *klf2a* coding sequence (cgs) was PCR amplified. *klf2a* cgs was then cloned into a pGEM-Teasy vector and transformed into bacterial cells. 24 well-separated colonies were picked up, grown in selective media and submitted for sequencing with SP6 and T7 primers (**Table 2**) to ensure that the whole *klf2a* cgs would get sequenced. Sequencing of 23 colonies confirmed the expected sequence for *klf2a*^{sh317} mRNA without any additional sequences thus reliably excluding the presence of any *klf2a* splice variants (**Figure 4.8**).

(a) Wild-type *klf2a* sequence around the *klf2a* TALEN mutagenesis site (19bp spacer in bold)

5' ACCCATCACCACCTCCACCAT**ACACCACCGCCTCATGGC**AGAGCTTCTGCAGTCTGACAT 3'

(b) *klf2a*^{sh317} sequence (14bp deletion indicated by red arrow line)

5' ACCCATCACCACCTCCACCAT**ACACC**AGAGCTTCTGCAGTCTGACAT 3'

(c) *klf2a*^{sh317} sequence confirmation

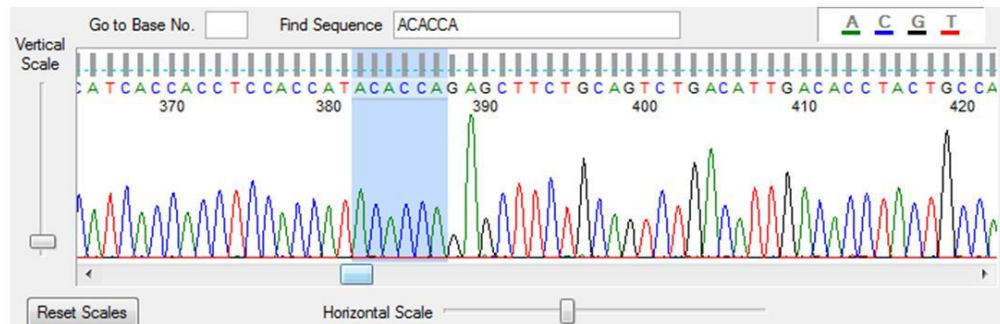


Figure 4.8 *klf2a*^{sh317} cDNA sequencing

(a) Wild type *klf2a* genomic sequence around the *klf2a* TALEN mutagenesis site. *klf2a* TALEN 19bp spacer in bold. *klf2a*^{sh317} 14bp deletion indicated by red arrow line. **(b)** *klf2a*^{sh317} genomic sequence around the region where *klf2a* TALEN mutagenesis took place. **(c)** *klf2a*^{sh317} cDNA sequencing confirmed the expected sequence.

4.2.2.2 Klf2a Western blot

I sought to find out whether the confirmed changes in *klf2a* DNA and mRNA structure induced by TALEN mutagenesis resulted in translation of incomplete, truncated Klf2a protein. I performed Western blot (WB), firstly on the whole embryo protein extracted from F2 generation of homozygous carriers of *klf2a*^{sh317} allele and secondly on the protein extracted from the F3 generation of homozygous *klf2a*^{sh317} mutants with similar results. As shown in **Figure 4.9**, a significant reduction of the intensity of a 43 kilodalton (kDa) band was detected in *klf2a*^{sh317} homozygous carriers. This band represents a full-length Klf2a protein. Additionally two new bands that run at approximately 33kDa (or at 24kDa – WB on F2 generation of *klf2a*^{sh317} homozygotes – data not shown) have been detected in the *klf2a*^{sh317} homozygous mutants that could represent the truncated Klf2a protein.

4.2.2.3 Identification of Klf2a proteins by Mass spectrometry analysis

Klf2a WB performed on the *klf2a*^{sh317} homozygous embryos showed significantly decreased intensities of the 43kDa band representing the full-length Klf2a protein and detected a new 24-33kDa band that could represent the truncated Klf2a protein. The predicted molecular mass of the *klf2a*^{sh317} protein is 13.15kDa and I therefore wanted to verify that this band really represents the predicted truncated Klf2a protein by performing MS analysis. Unfortunately, no Klf2a protein could be detected via MS in the protein samples from *klf2a*^{sh317} homozygous embryos or Nacre WT zebrafish. Given the fact that Klf2a is a transcription factor that might be present in cells in low abundance, increased numbers of 5dpf old Nacre WT embryos (approximately 140) were used for whole-embryo protein extraction in the next step. Additionally, Klf2a immunoprecipitation (IP) was used prior to MS in order to concentrate Klf2a wild type

protein. Unfortunately, due to technical difficulties the IP did not work optimally and the following MS could not detect any Klf2a protein in these samples either.

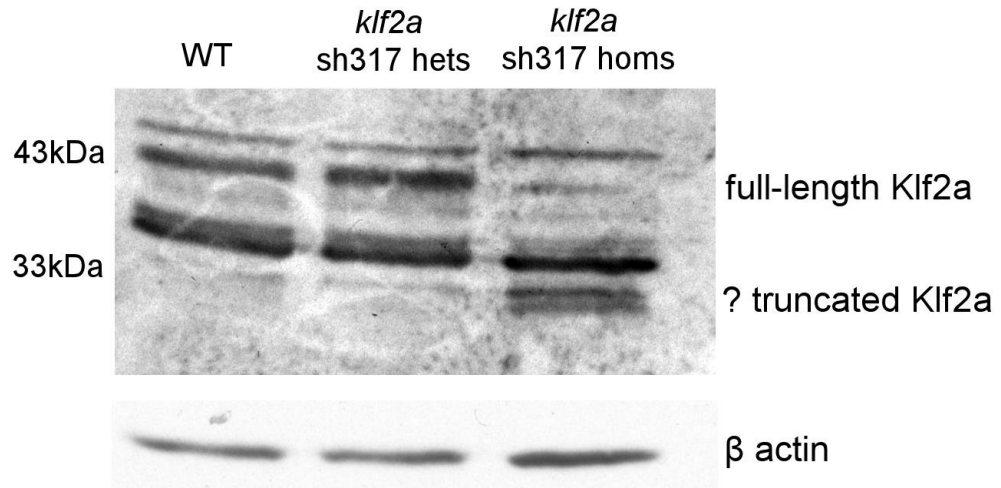


Figure 4.9 Klf2a Western blot

Substantial reduction of a 43kDa band representing the full-length Klf2a protein can be seen in a Western blot performed on whole-embryo protein sample extracted from the F3 generation of *klf2a*^{sh317} mutant embryos at 5dpf when compared to Western blot on WT embryos and heterozygous *klf2a*^{sh317} carriers. Additionally, two bands that run at approximately 33kDa of have been detected in *klf2a*^{sh317} mutants that could represent the truncated Klf2a protein. β actin Western blot used as a loading control.

4.2.2.4 Maternal *klf2a* mRNA is not present in unfertilised zebrafish eggs

Lastly, I wanted to assess whether there is any maternal *klf2a* mRNA present in zebrafish embryos prior to the activation of zygotic transcription - the maternal to zygotic transition (MZT) (Kane and Kimmel 1993; Harvey, Sealy et al. 2013).

RNA from a pool of unfertilised wild type eggs was extracted and reversely transcribed into a cDNA. *klf2a* cds L and R primers (**Table 2**) amplify the whole *klf2a* cds giving a 1155bp PCR product. In case of genomic DNA contamination, primers would amplify a 1674bp product due to the presence of *klf2a* intronic sequences in gDNA. As shown in **Figure 4.10**, no 1155bp PCR product representing maternal *klf2a* mRNA was detected in the cDNA sample from unfertilised zebrafish eggs thus ruling out the presence of maternal *klf2a* mRNA in zebrafish embryos. The absence of a 1674bp PCR product in this sample ruled out gDNA contamination. On the contrary, *gapdh* mRNA was detected in the unfertilised embryos being a positive control (**Figure 4.10**).

The fact that maternal *klf2a* mRNA is not present in zebrafish embryos is important in regards to experiments performed on F2 generation of *klf2a* mutant zebrafish embryos. These embryos are progeny of an incross of two F1 generation heterozygous carriers of a particular *klf2a* mutant allele. If *klf2a* mRNA was detected prior to MZT, the wild type *klf2a* mRNA from the heterozygous mother could influence embryonic development in the genotypically homozygous *klf2a* mutant embryos. Due to the absence of maternal *klf2a* mRNA homozygous *klf2a* mutants from F2 generation could be considered equal to the *klf2a* maternal zygotic mutants from the F3 generation.

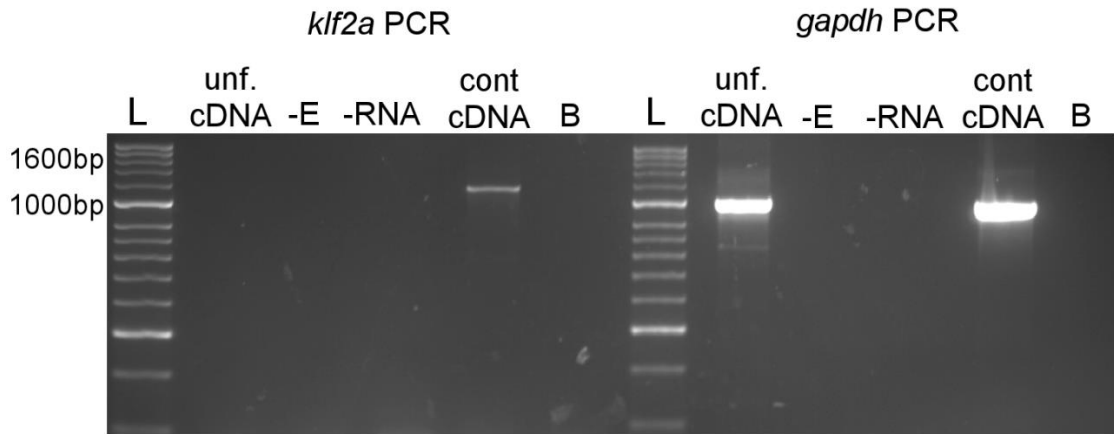


Figure 4.10 Test for the presence of maternal mRNA in unfertilised zebrafish eggs

klf2a cds F1 and R1 primers were used to amplify *klf2a* coding sequence giving a 1155bp PCR product. No band was detected in the sample with cDNA from unfertilised embryos (unf. cDNA) suggesting the absence of maternal *klf2a* mRNA in unfertilised embryos. On contrary, a band of expected size was detected in the sample with control cDNA originating from 48hpf wild type zebrafish embryos (cont cDNA). No 1674bp band was detected in unf. cDNA or cDNA sample confirming the absence of genomic DNA contamination of the samples (explanation in the text). *gapdh* primers that amplify a 1019bp PCR product were used as a positive control. A band of expected size was detected in both the unfertilised eggs cDNA and control cDNA lanes indicating the presence of maternal *gapdh* mRNA in unfertilised zebrafish eggs. Abbreviations: -E: negative control with no reverse transcriptase added during reverse transcription (RT). -RNA: negative control with no RNA added during RT. B: blank, no template added to the PCR reaction. Abbreviations: L: Hyperladder II (NEB).

4.3 Discussion

Recent advances in targeted genome editing made novel mutagenesis techniques available to broad research community. Despite these advances targeted mutagenesis still remains a time consuming process with uncertain outcome. In my pursuit for a stable *klf2a* mutant line I initially used ZFN engineering by CoDA (Sander, Dahlborg et al. 2011) and designed altogether 3 distinct *klf2a* ZFN constructs. Genomic DNA from 30 pooled embryos injected with the ZFN capped mRNA construct was isolated and submitted for 454 sequencing to The Centre of Genomic Research in The University of Liverpool. In the case of the first *klf2a* ZFN construct, although essentially functional, the mutagenesis rate was too low to make the identification of individual zebrafish embryos carrying the mutant alleles in their germlines feasible. The following two *klf2a* ZFN constructs were designed alongside the *klf2a* TALEN construct. *klf2a* TALEN mutagenesis design did not require any 454 sequencing step. Once the *klf2a* TALEN construct was established to be functional (via the loss of XcmI restriction enzyme site), I did not proceed with *klf2a* ZFN mutagenesis and focused on the characterisation of this TALEN induced mutant line.

The TALEN mutagenesis site was chosen upstream of the 3 tandem zinc fingers coding sequence. The spacer between the binding sites of both *klf2a* TALEN heterodimers contained a XcmI wide-spanning restriction enzyme site so that the targeted mutagenesis could be easily confirmed by the loss of restriction enzyme site as mentioned above. The chosen *klf2a* TALEN construct was found to be functional and effective enough to generate a stable *klf2a* mutant line. 4 novel *klf2a* mutant alleles with frame shift mutations causing changes in the reading frame were identified. I chose the *klf2a*^{sh317} allele with 14bp deletion for further validation and experiments

however some experiments were performed using the other mutant alleles as described in Chapter 5.

In the next step I wanted to ascertain that the mutation in *klf2a* could not be overcome by a generation of an alternative *klf2a* transcript in the mutants. Sequencing of 23 full-length *klf2a* cDNA clones made from RNA from *klf2a*^{sh317} homozygous mutants confirmed the presence of predicted mutant *klf2a* mRNA in all cases. No other cDNA sequences indicating alternative *klf2a* splicing that would result in novel Klf2a protein isoform were detected.

Recent experience with generation of mutant zebrafish lines in our centre has shown that zebrafish possess the ability to overcome missense mutations by employing alternative pre-mRNA splicing of the paralog gene to the gene affected by the mutation. In this particular case a mutagenesis in transactive response DNA-binding protein gene (*tardpb*) causes alternative splicing of a paralog gene *tardpb*-like (*tardpbl*). This alternative splicing includes *tardpbl* intronic sequence that is almost identical to the coding sequences of *tardpb* lost by the mutagenesis. The alternatively spliced paralog translates into a protein almost identical to the wild type protein and rescues the phenotype expected from the original gene mutation (Hewamadduma, Grierson et al. 2013). The *in silico* analysis of *klf2b* intronic sequences could exclude this possibility.

Next I wanted to find out whether the *klf2a*^{sh317} allele translated into a truncated Klf2a protein. I used a polyclonal rabbit anti-mouse KLF2 antibody which was recently published to detect zebrafish Klf2a protein by WB (Wang, Zhang et al. 2011). To my knowledge this has been the only published zebrafish Klf2a WB so far. WB was initially performed on the F2 generation of *klf2a*^{sh317} homozygous and heterozygous carriers and on their WT siblings. In order to do so I used a novel zebrafish embryonic fin-clipping protocol developed in our centre (Wilkinson, Elworthy et al. 2013). Zebrafish embryos were genotyped at 3dpf before zebrafish embryonic proteins were extracted

at 5dpf. Secondly I repeated Klf2a WB on the *klf2a*^{sh317} maternal zygotic mutants from the F3 generation. In both experiments I saw a substantial reduction of the intensity of the 43kDa band representing the full-length Klf2a protein in the *klf2a*^{sh317} homozygous fish. The fact that a 43kDa band can still be detected in the mutant fish samples is likely to be explained by the polyclonal character of the anti-mouse KLF2 antibody used and might be a background band (indeed several other likely nonspecific bands were seen). Additionally two bands of increased intensity were detected in *klf2a*^{sh317} mutants. These bands have an apparent molecular weight of approximately 33kDa (WB on F3 generation of *klf2a*^{sh317} mutants). WB on F2 generation of *klf2a*^{sh317} mutants showed a single band with apparent molecular weight of 24kDa (data not shown). The predicted molecular mass for Klf2a sh317 protein is approximately 13.15kDa, Discrepancies between the apparent and predicted molecular masses could be explained by posttranslational modifications of this novel protein, such as phosphorylation or ubiquitination. Secondly, SDS-PAGE is not a reliable method for accurately determining molecular weight of proteins and its accuracy depends on the uniform binding of the SDS to the protein which can differ significantly among various proteins (as per QIAGEN).

Given the above discrepancies a mass spectrometry approach was taken to confirm the presence of the Klf2a peptides in the 43kDa and 33kDa bands. Unfortunately no Klf2a peptides could be detected either in the WT nor the mutant zebrafish samples. Immunoprecipitation of Klf2a protein from a protein sample extracted from approximately 140 WT embryos did not result in increased concentration of Klf2a protein (data not shown) and the subsequent repeated attempt to detect Klf2a protein via MS was again unsuccessful. It is likely that the Klf2a protein as a transcription factor is present in the cells in low number of copies and a more robust and therefore more costly approach would be necessary in order to detect any Klf2a peptides via MS.

Lastly, I proved that maternal *klf2a* mRNA is not present in zebrafish embryos by demonstrating its absence in unfertilised zebrafish eggs. This was important, because it showed that the zygotic *klf2a* mutants that arise from an incross of 2 adults from the F1 generation of heterozygous carriers for a *klf2a* mutant allele can be considered to be equal to maternal zygotic mutants from the F3 generation of fish that arise from an incross of 2 homozygous mutants. There is however a possibility of a *klf2a* maternal effect that is caused by maternal Klf2a protein deposited in the egg during oocyte maturation and the presence of such protein in the zygote has not been excluded at this stage. The existence of any maternal zygotic contribution in case of *klf2a* is rather unlikely given that there was no phenotypical difference between zygotic *klf2a* mutant embryos from the F2 generation and maternal zygotic mutants from the F3 generation of *klf2a* mutant fish in any of the experiments I have performed so far as detailed in the next chapter.

To my knowledge no data on any *klf2a* mutant line have been published so far. However, I am aware some other research groups are pursuing generation of a *klf2a* mutant line.

In the next chapter I evaluate the phenotype of this novel mutant line.

Chapter 5

Characterisation of the *klf2a* mutant zebrafish line

5.1 Introduction

Following the generation of 4 *klf2a* mutant lines and their outcrossing to several transgenic lines I went on to characterise the effects of *klf2a* mutation on developing zebrafish embryo and adult zebrafish especially with regards to cardiovascular system.

5.2 Results

Much of my characterisation of a *klf2a* mutant line has been done on *klf2a*^{sh317} allele. It was this particular mutant line that has been used in the experiments required for validation of *klf2a* mutant lines as described in previous chapter. Carriers of this allele have also been crossed with several transgenic lines useful in characterisation of zebrafish cardiovascular system. However, there are no reasons to believe that any other from the 3 remaining alleles would have different phenotypic effects on zebrafish embryos than the *klf2a*^{sh317} allele.

5.2.1 *klf2a* mutant zebrafish do not show any morphological abnormalities

Homozygous carriers of all 4 *klf2a* mutant alleles are viable to adulthood and fertile. As shown in **Figure 5.1**, *klf2a* mutant embryos do not have any morphological abnormalities or differences when compared to WT embryos and there were no differences noticed beyond 5dpf up to adulthood either. In particular, no formation of pericardial oedema has been noted at 72hpf or at any other developmental stage contradicting the previously published data (Lee, Yu et al. 2006). Importantly, *klf2a* mutant fish do not morphologically differ in anatomical locations where *klf2a* expression is high during early developmental stages, such as cloaca or pectoral fins (**Figure 5.2**).

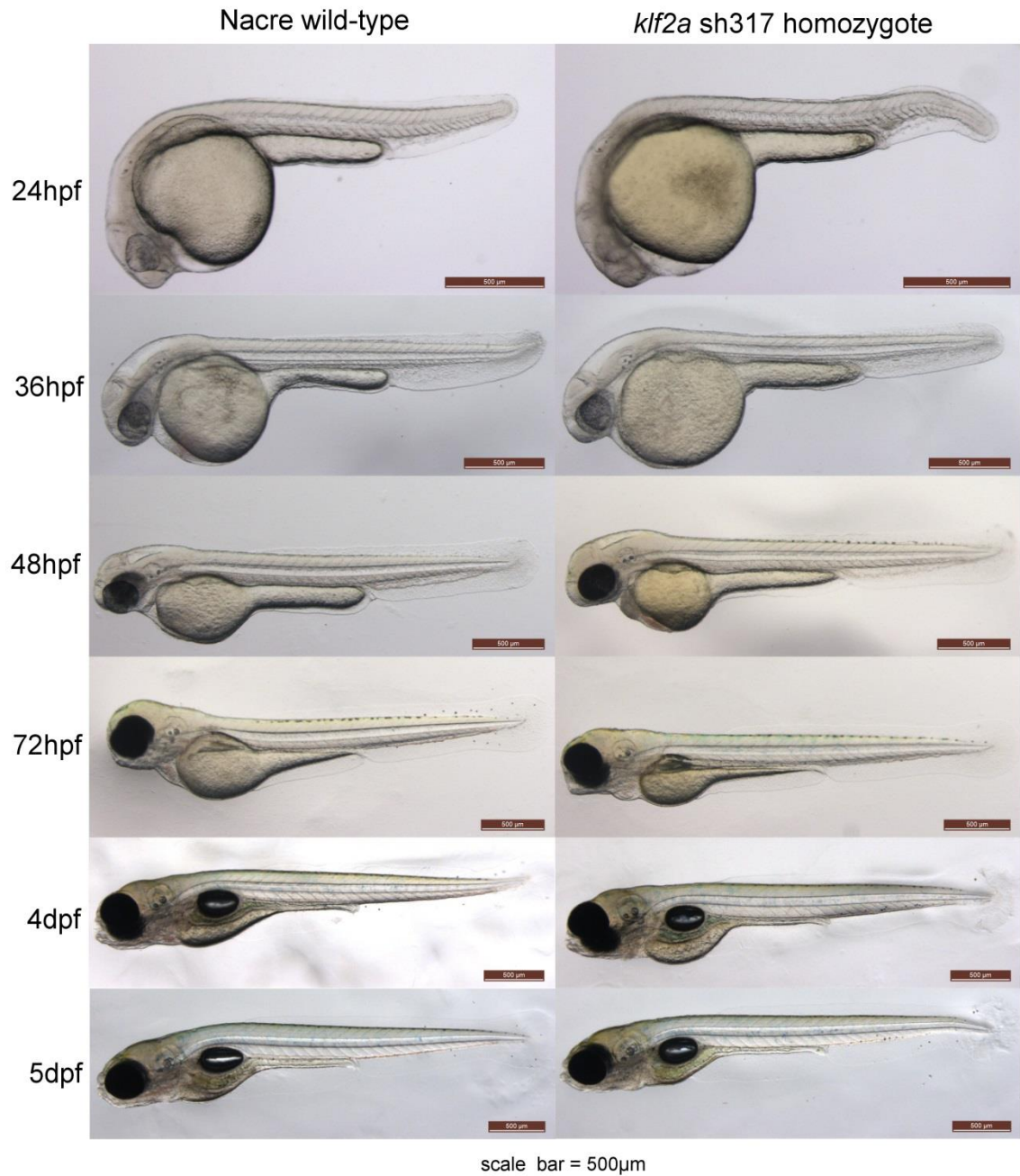


Figure 5.1 Comparison of wild type and *klf2a* mutant zebrafish embryos

There are no obvious morphological differences between Nacre WT zebrafish embryos and *klf2a*^{sh317} mutant embryos in Nacre background until 5dpf and also beyond (not shown). Scale bar = 500µm.

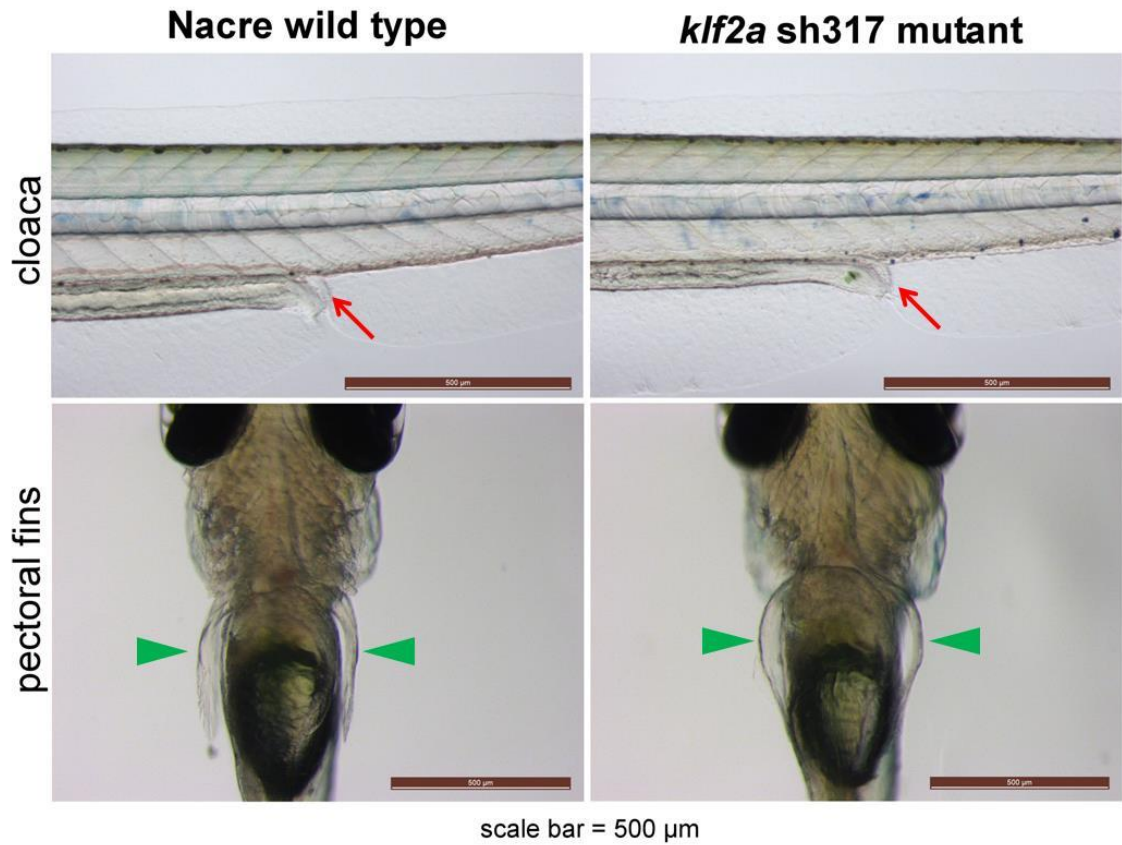


Figure 5.2 Comparison of morphology of zebrafish embryonic structures with high *klf2a* expression

Nacre WT and *klf2a*^{sh317} mutant embryos compared at 5dpf. *klf2a*^{sh317} embryos do not show any obvious morphological abnormalities in regions with previously detected high *klf2a* expression such as cloaca (top panel, red arrow points at cloaca, longitudinal view) or pectoral fins (bottom panel, green arrowheads point at pectoral fins, ventral view). Representative images shown. Scale bar = 500µm.

5.2.2 Characterisation of cardiovascular system

Next I aimed to characterise cardiovascular system of *klf2a* mutant embryos in more detail. Previous works suggested grossly normal vascular patterning in *klf2a* MO injected zebrafish embryos, apart from the formation of a small connecting vessel between the 5th and 6th aortic arch vessels, the so-called AA5x vessel which formation was postulated to be *klf2a*-dependent (Lee, Yu et al. 2006; Nicoli, Standley et al. 2010). Functionally, high-output cardiac failure with increased aortic blood flow velocities (measured at 54hpf) and presence of pericardial oedema (at 72hpf) were described in *klf2a* MO morphants (Lee, Yu et al. 2006).

5.2.2.1 *klf2a* mutant embryos exhibit normal vascular patterning

klf2a^{sh317} mutant embryos were observed under dissecting microscope at several developmental stages (1-5dpf) and compared to WT embryos. No obvious vascular defects were detected and circulating erythrocytes were observed in both wild type and *klf2a*^{sh317} embryos in the axial vasculature, ISVs and head vessels in corresponding developmental stages as expected. *Tg(kdrl:HRAS-mCherry;flk1:EGFP-nls)* embryos in WT or *klf2a*^{sh317} mutant background were imaged at 3dpf on confocal microscope and a compound figure was made showing the entire vascular anatomy of these embryos. As shown in **Figure 5.3**, vascular patterning of both WT and *klf2a*^{sh317} mutants is identical and no gross vascular abnormalities can be seen in the *klf2a*^{sh317} embryos.

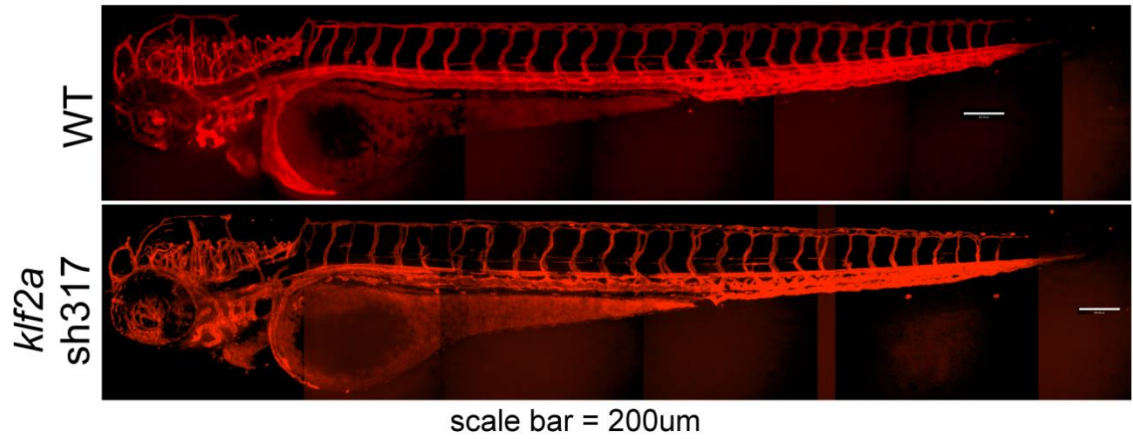


Figure 5.3 Vascular anatomy of a WT and *klf2a*^{sh317} embryo at 3dpf

Tg(kdr1:HRAS-mCherry;flk1:EGFP-nls) embryos in WT or *klf2a*^{sh317} mutant background imaged at 3dpf. Normal vascular patterning could be detected in *klf2a*^{sh317} embryos. Representative images shown. Scale bar = 200µm.

5.2.2.2 *klf2a* mutants exhibit normal AA5x angiogenesis

Nicoli et al. report that the formation of a connecting vessel between the 5th and 6th aortic arch (further referred to as AA5x) occurs via angiogenesis that is blood flow dependent as well as *klf2a* - dependent (Nicoli, Standley et al. 2010).

I initially verified that AA5x formation is blood flow dependent. I used 2 different ways of preventing blood flow in developing zebrafish embryos. Firstly I treated the *Tg(kdrl:HRAS-mCherry;flk1:EGFP-nls)* zebrafish embryos with local anaesthetic Tricaine in a concentration (0.66 mg/ml) and at developmental stage (46-65hpf) identical to published data (Nicoli, Standley et al. 2010). As shown in **Figure 5.4b**, cessation of embryonic blood flow due to the arrest of heart contractions by Tricaine prevented formation of AA5x vessels bilaterally as opposed to control non-treated embryos. Secondly, embryos were treated with the myosin ATPase inhibitor BDM (15mM, 46-65hpf) and cessation of flow caused by BDM identically resulted in abrogation of AA5x formation (**Figure 5.4b**). These experiments confirmed that AA5x angiogenesis is blood flow dependent as described before (Nicoli, Standley et al. 2010).

Next I examined AA5x formation in *klf2a*^{sh317} mutant embryos. As shown in **Figure 5.4c**, all *klf2a*^{sh317} mutant embryos examined formed AA5x vessels bilaterally suggesting that AA5x formation is *klf2a*-independent contradicting the previously published data (Nicoli, Standley et al. 2010).

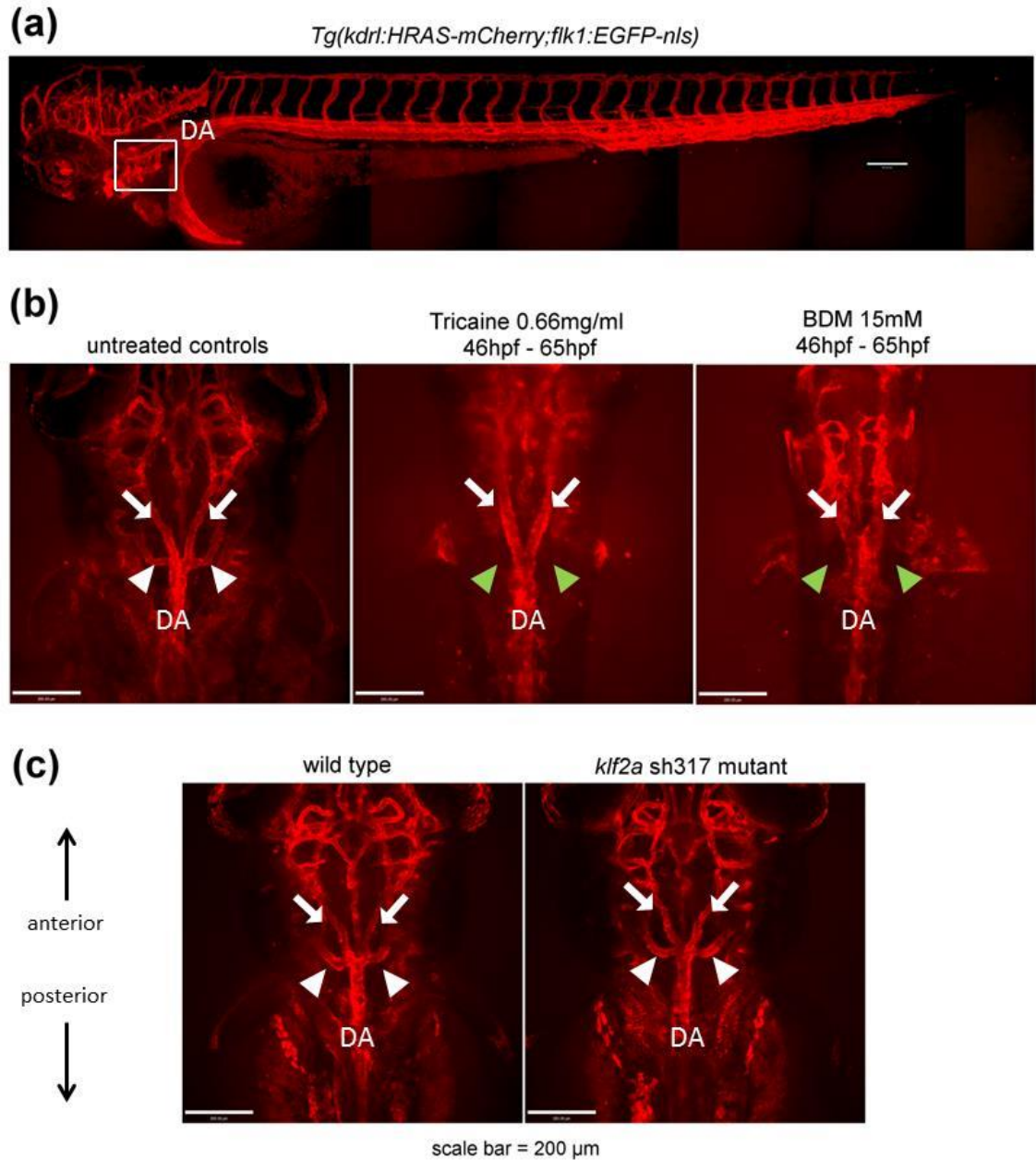


Figure 5.4 AA5x angiogenesis is blood flow dependent but is unaffected in *klf2a*^{sh317} mutants

(a) Vascular anatomy of a zebrafish embryo at 3dpf. Anatomical location of 3rd – 6th aortic arch (AAs) is indicated by the white rectangle. DA indicates location of dorsal aorta. **(b)** AA5x vessel formation is blood flow dependent. Presence of AA5x is indicated by white arrowheads. Cessation of flow, with Tricaine or with BDM results in abrogation of AA5x formation as published before (Nicoli, Standley et al. 2010). Absence of AA5x is indicated by green arrowheads. White arrows point at lateral dorsal aortae. DA indicates location of dorsal aorta. **(c)** All *klf2a*^{sh317} mutants examined formed AA5x vessel bilaterally suggesting AA5x formation is *klf2a*-independent. Presence of

AA5x is indicated by white arrowheads. White arrows point at lateral dorsal aortae. DA indicates location of dorsal aorta.

Summary of 3 biological replicates (except BDM - 2 biological replicates). Total number of embryos examined: n=23 (untreated controls), n=15 (Tricaine), n=5 (BDM), n=9 (WT embryos), n=16 (*klf2a*^{sh317} mutants). *Tg(kdrl:HRAS-mCherry;flk1:EGFP-nls)* zebrafish line in WT or in *klf2a*^{sh317} mutant background used (**(a)** is a lateral view, **(b)-(c)** are dorsal views. Representative images of all groups of embryos are shown at 3dpf. Scale bar = 200µm.

5.2.2.3 *klf2a* mutation does not affect endothelial cell numbers in ISVs and DLAV

Our group has recently shown that blood flow cessation significantly reduces endothelial cell nuclei numbers (and therefore endothelial cell numbers) in ISVs and DLAV of *vhl* mutants (*vhl*^{-/-}) which exhibit excessive hypoxia-driven angiogenesis, although it has no effect on endothelial cell numbers in WT embryos (Watson, Novodvorsky et al. 2013). I was therefore interested whether the *klf2a* had any effect on endothelial cell numbers in this region. In order to do so I used a double-transgenic line *Tg(kdrl:HRAS-mCherry;flk1:EGFP-nls)* (where *flk1* labels endothelial nuclei green with GFP and *kdrl* labels endothelial membrane red with red fluorescent protein (RFP) derivative mCherry) in *klf2a*^{sh317} mutant background. I counted endothelial nuclei dorsally of DA in a 3 somite region in the middle of the trunk, including 4 ISVs and a corresponding region of DLAV. As shown in **Figure 5.5**, *klf2a* mutation had no effect on endothelial cell numbers in ISVs and DLAV in a developing zebrafish embryo.

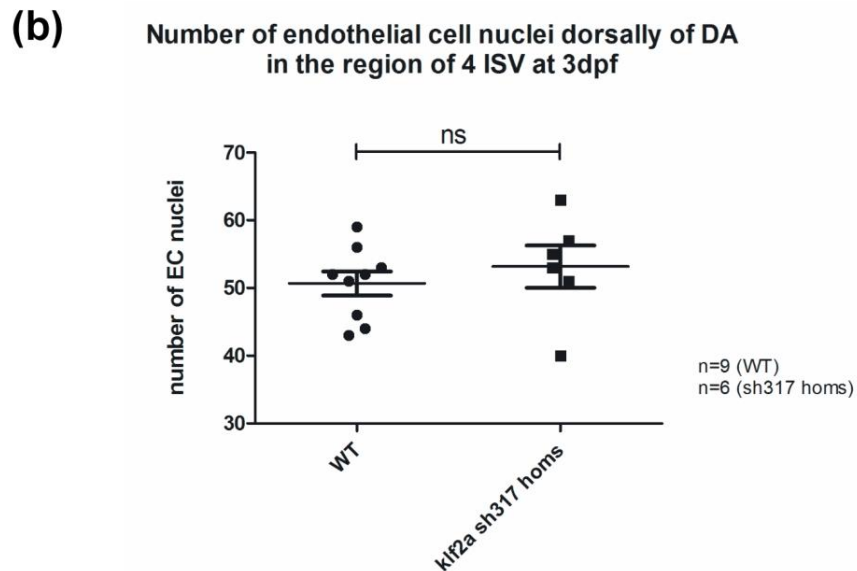
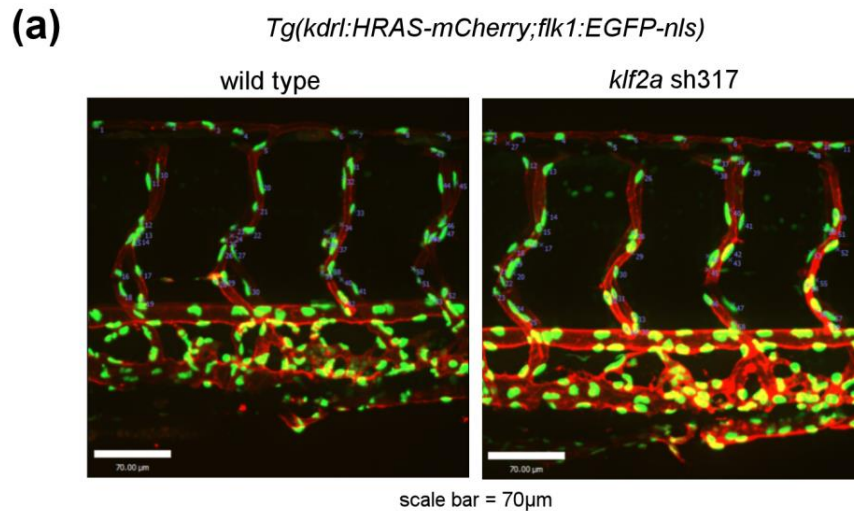


Figure 5.5 Quantification of endothelial cell nuclei in a region of 4 ISVs and corresponding part of DLAV: *klf2a*^{sh317} versus WT at 3dpf

(a) Representative images of a wild type and *klf2a*^{sh317} embryos in a double transgenic background *Tg(kdrl:HRAS-mCherry;flk1:EGFP-nls)*. 4 ISVs closest to cloacal opening and a corresponding region of DLAV were chosen for endothelial nuclei counting. Only endothelial nuclei dorsally from DA were included. **(b)** Quantification and comparison of endothelial nuclei numbers between wild type and *klf2a*^{sh317} embryos did not show any significant differences. Error bars represent mean ± SEM; unpaired t test used. Scale bar = 70µm.

5.2.2.4 *klf2a* mutant embryos exhibit decreased blood flow velocities and increased heart rates at 72hpf.

Comparison of heart rates and blood flow velocities in DA throughout a single cardiac cycle showed no differences between *klf2a*^{sh317} mutants and WT embryos at 48hpf (**Figure 5.6**).

At 72hpf significantly slower blood flow velocities in DA were detected in *klf2a*^{sh317} mutants and this was accompanied by increased heart rates when compared to WT embryos (**Figure 5.7**). Generally, there is a trend towards slower blood flow velocities and higher heart rates at 72hpf when compared to 48hpf even in the WT embryos. This trend is more accentuated in *klf2a*^{sh317} mutants than in WT embryos at 72hpf with resulting significant differences at this developmental stage.

These data together with the previously described absence of pericardial oedemas in *klf2a*^{sh317} mutants exclude the high output cardiac failure phenotype previously described in *klf2a* MO morphants (Lee, Yu et al. 2006). It is important to mention that WT embryos represent an independent cross to maternal *klf2a* mutant embryos in this experiment. Although both WT and *klf2a*^{sh317} embryos were in the same genetic background (Nacre WT), detected heart rate and blood flow velocity differences at 3dpf might simply reflect variability between two independent crosses.

Another, more interesting explanation for decreased aortic blood flow velocities detected in *klf2a*^{sh317} mutants at 3dpf would be the abnormal valvulogenesis which has been described in *klf2a* MO morphants before (Vermot, Forouhar et al. 2009). Valve dysgenesis would thus cause increased blood regurgitation from ventricle into the atrium with resulting decreased blood volumes propelled into the aorta and decreased blood flow velocities. My preliminary data shown in **Figure 5.8** are not suggestive of this however. A much stronger line of evidence against valve dysgenesis in *klf2a* mutants is the fact that they are viable and fertile and do not suffer from heart failure.

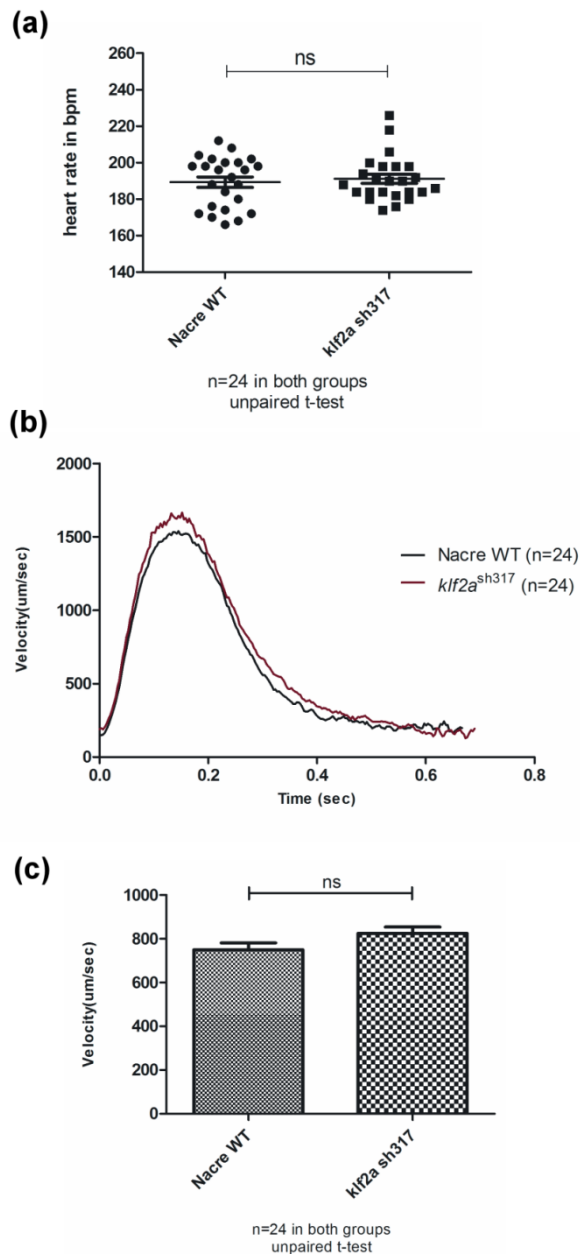


Figure 5.6 Comparison of heart rates and blood flow velocities of Nacre WT and *klf2a*^{sh317} mutants at 48hpf

(a) There are no significant differences in heart rates between the Nacre WT embryos and *klf2a*^{sh317} mutants at 48hpf. **(b)** Instantaneous blood flow velocities were measured throughout a single cardiac cycle individually in altogether 24 embryos from each group. These values were then averaged and plotted on a graph as a single velocity curve. Velocity curves from Nacre WT and *klf2a*^{sh317} embryos are almost identical at this stage. **(c)** Bar graph shows an average velocity from all measured instantaneous blood flow velocities during a single cardiac cycle for Nacre WT and *klf2a*^{sh317} embryos. No statistically significant differences in average blood flow velocities could be detected at 48hpf. Summary of 3 independent experiments. In total 24 embryos examined per group.

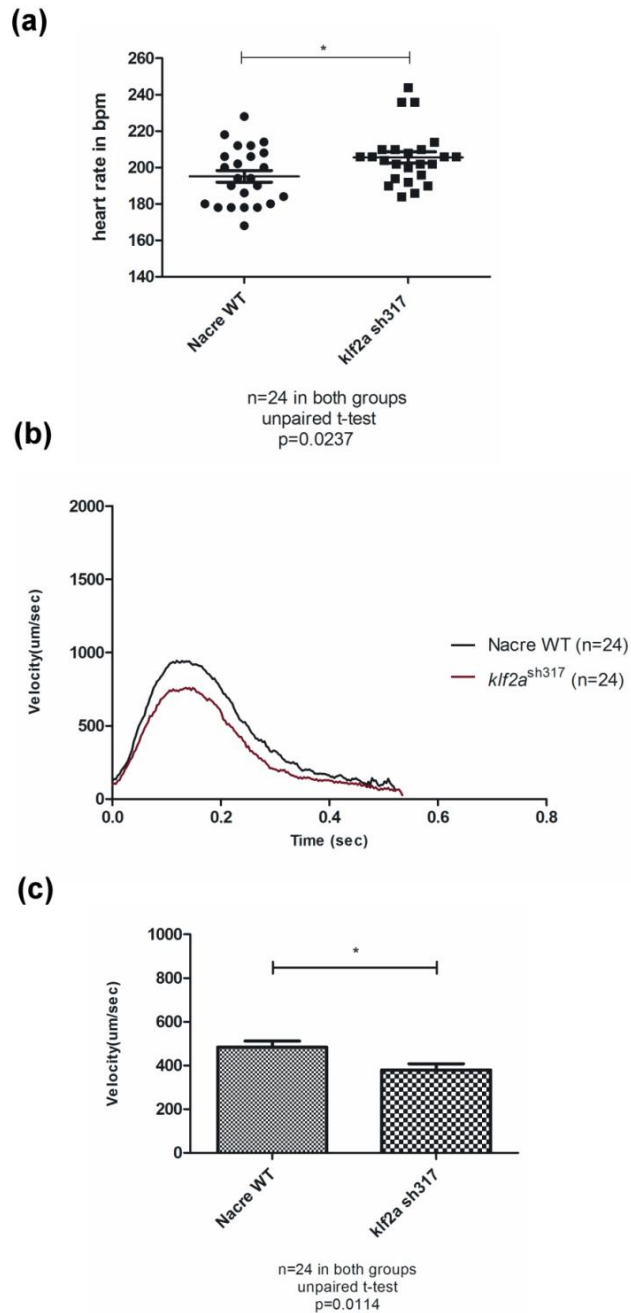


Figure 5.7 Comparison of heart rates and blood flow velocities of Nacre WT and *klf2*^{sh317} mutants at 72hpf

(a) *klf2a*^{sh317} mutants show significantly higher heart rates when compared to Nacre WT at 72hpf. **(b)** Instantaneous blood flow velocity curves show differences between velocities at each stage of cardiac cycle - lower systolic velocities could be observed in *klf2a*^{sh317} mutants when compared to Nacre WT embryos **(c)** Bar graph reflects the differences observed in velocity curves - lower average blood flow velocity was observed in *klf2*^{sh317} mutants when compared to Nacre WT embryos at 72hpf. Summary of 3 independent experiments. In total 24 embryos were examined per group.

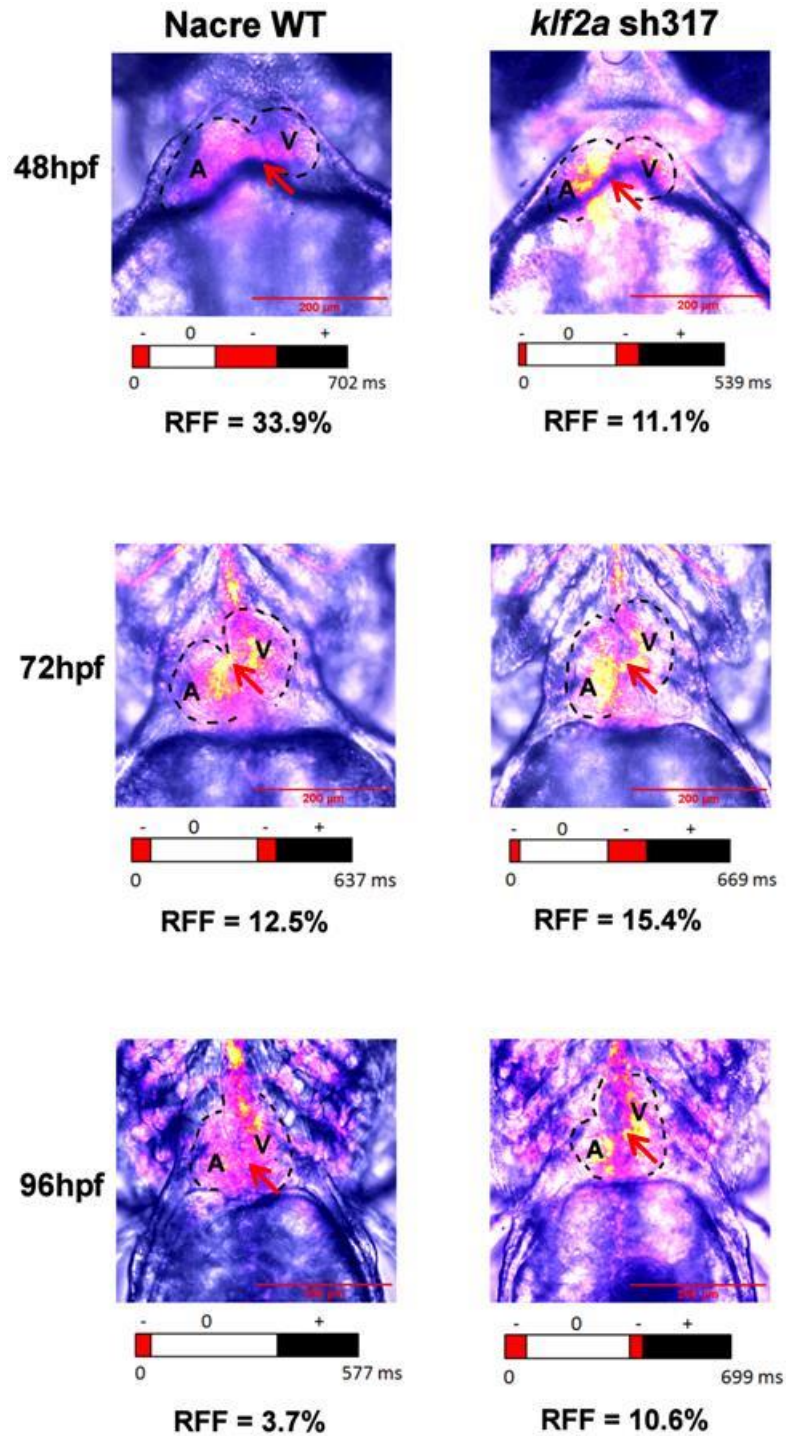


Figure 5.8 Comparison of transvalvular blood flow patterns in Nacre WT and *klfa2*^{sh317} embryos with retrograde flow fraction (RFF) quantifications

Embryos were imaged on a high-speed camera (300fps) and angiograms were constructed using ImageJ software. The shape of embryonic hearts is indicated by the black lines. A indicates cardiac atrium and V indicates cardiac ventricle. The site of flow direction measurements was the AV canal which location is indicated by red arrows.

Average transvalvular flow directions throughout single cardiac cycle are summarised in the flow diagrams below each figure. Retrograde flow from ventricle to atrium is shown in red (-), no flow in AV canal is shown in white (0) and anterograde flow from atrium to ventricle is shown in black (+). Retrograde flow fractions (RFF) indicate the duration of retrograde flows through AV canal relative to the duration of a single cardiac cycle which length is shown in milliseconds (ms) below the actual figure. Preliminary data, 3 embryos per group examined. Scale bar = 200 μ m.

5.2.2.5 *klf2a* mutant embryos do not show increased vascular *cxcr4a* expression

Earlier I detected increased vascular *cxcr4a* expression in SB *klf2a* MO and ATG *klf2a* MO morphants at 48hpf up to the levels seen in *tnnt2* MO morphants which experience no blood flow. Increased vascular *cxcr4a* expression could not be confirmed by subsequent RT-qPCR. I therefore aimed to repeat the *cxcr4a* WISH on *klf2a* mutant embryos to assess the role of *klf2a* in regulation of vascular *cxcr4a* expression.

I performed a WISH with *cxcr4a* riboprobe on 3 different *klf2a* mutant lines (*klf2a*^{sh334}, *klf2a*^{sh307} and *klf2a*^{sh317}) and on Nacre WT embryos at 48hpf. I also included control MO or *tnnt2* MO injected embryos at 48hpf as positive and negative controls respectively. Increased *cxcr4a* vascular expression was detected in *tnnt2* MO morphants as expected but *cxcr4a* mRNA could not be detected in vasculature of *klf2a* mutant embryos. *klf2a* mutant embryos showed *cxcr4a* staining pattern identical to the one seen in Nacre WT embryos at 48hpf (**Figure 5.9**). These results obtained from *klf2a* mutant embryos thus do not support the previously postulated hypothesis that *klf2a* might mediate the flow dependent *cxcr4a* regulation of its vascular expression.

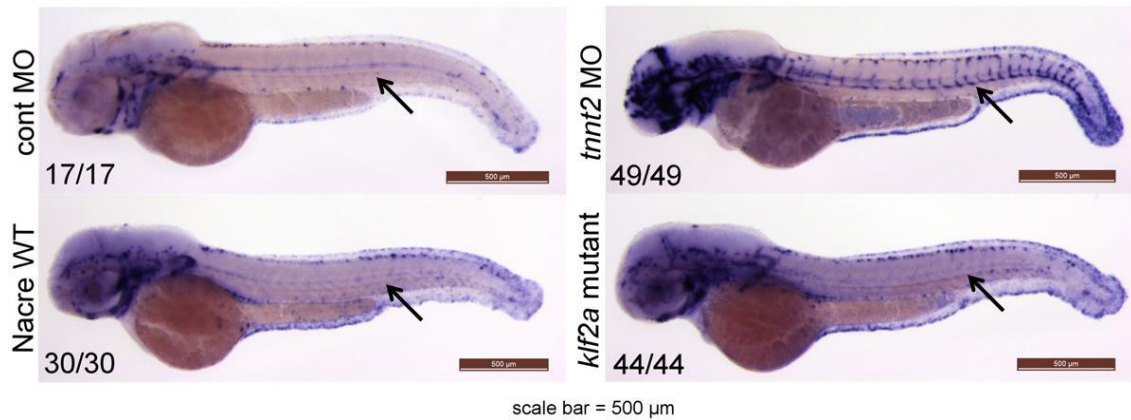


Figure 5.9 *klf2a*^{sh317} mutant embryos do not show increased *cxcr4a* vascular expression at 48hpf.

Vascular *cxcr4a* expression in all imaged embryos is indicated by black arrows. *cxcr4a* expression in vasculature is inhibited by flow in both control MO morphants and in Nacre WT embryos. *cxcr4a* vascular expression in *klf2a*^{sh317} mutants is also inhibited and the *cxcr4a* staining pattern is identical to Nacre WT and cont MO injected embryos. *tnnt2* MO morphants with no blood flow were previously shown to have increased vascular expression of *cxcr4a* (Packham, Gray et al. 2009) and represent a positive control. Number of embryos with identical staining patterns out of total number of embryos examined is shown in bottom left corner of each image. Summary of 3 independent experiments. Representative images shown. Scale bar = 500μm.

5.2.2.6 Flow dependent regulation of Notch signalling is not affected in *klf2a* mutant zebrafish embryos

Our group has recently shown that blood flow influences Notch signalling in zebrafish embryos. *tnt2* morphants lacking blood flow exhibited increased activity of *csf* transcription factor and showed increased vascular staining for one of the canonical Notch ligands *dll4* (Watson, Novodvorsky et al. 2013). *klf2a* MO morphants also showed increased vascular staining for *dll4* at 48hpf although the activity of *csf* transcription factor was unchanged compared to controls. I therefore examined whether a similar response was seen in *klf2a* mutants.

Male zebrafish from *Tg(CSL:venus)qmc61* line in *klf2a*^{sh306} heterozygous background were crossed with *klf2a*^{sh317} homozygous females. This cross was done due to high levels of variability of venus fluorescence in progeny of different adult carriers of single copy of *(CSL:venus)qmc61* transgene. Thus it was made sure that fluorescence of only a progeny of a single pair of fish would be compared. Equally there were no *klf2a*^{sh306} homozygous adult fish available at the time and *klf2a*^{sh317} were used instead. Progeny of each pair of this cross were kept separate and screened for fluorescence at 48hpf prior to imaging. Numbers of fluorescent and non-fluorescent embryos were approximately equal in each pair tested confirming the presence of a single copy of *(CSL:venus)qmc61* transgene in the parents. Multiple and different numbers of *(CSL:venus)qmc61* copies would prevent correct measurement and subsequent comparison of fluorescence between the groups. Following confocal microscope imaging all embryos were genotyped for the *klf2a* mutant status. As shown in **Figure 5.10**, *klf2a*^{sh306/sh317} mutant embryos did not show any significant difference in the CSL venus activity in DA when compared to the *klf2a*^{sh306} heterozygous siblings.

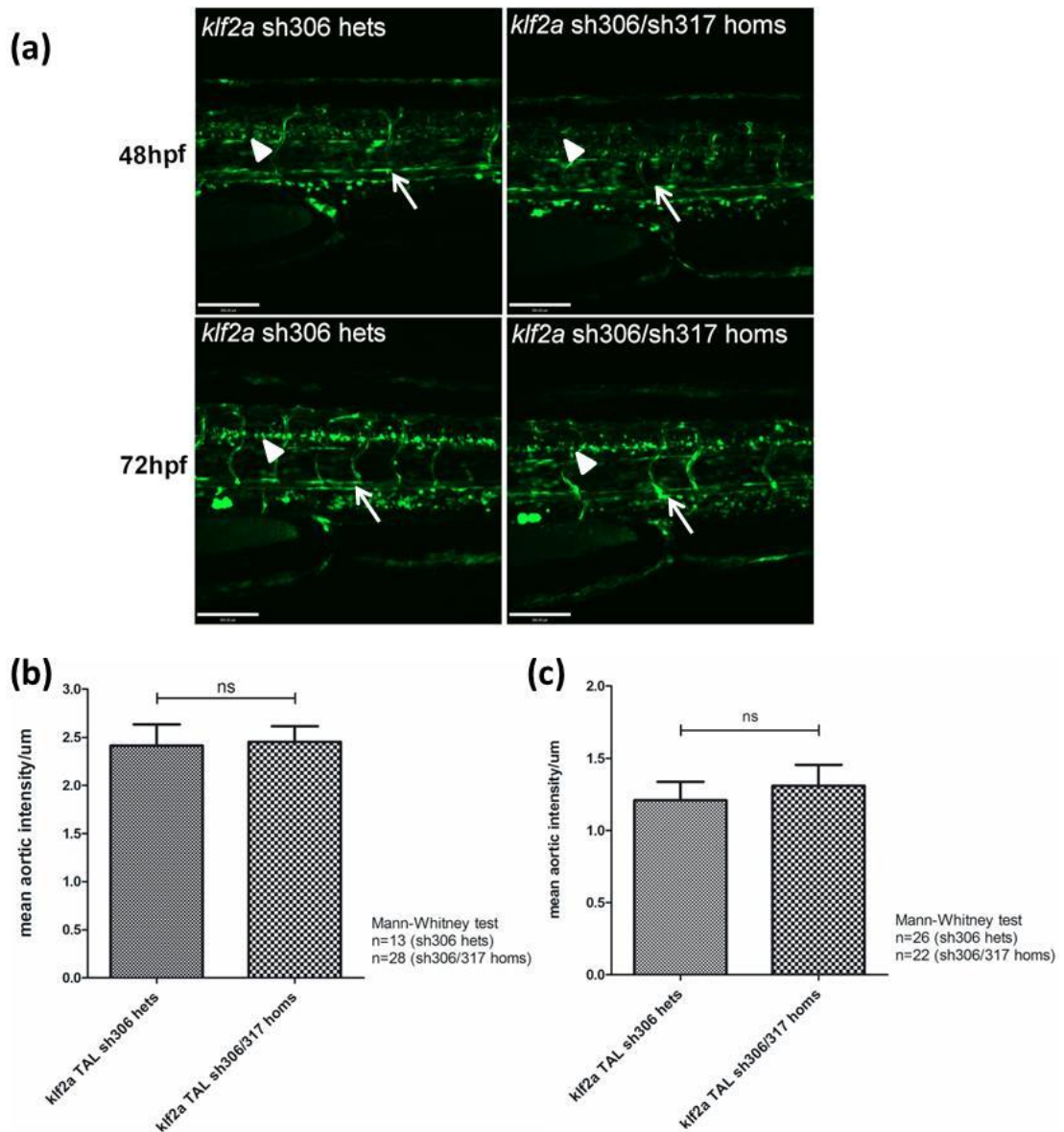


Figure 5.10 *klf2a*^{sh306/sh317} mutant embryos do not show any changes in vascular activity of Notch transcription factor CSL Venus.

(a) Confocal images of *klf2a*^{sh306} heterozygotes and *klf2a*^{sh306/sh317} mutants. White arrows point at dorsal aortae and white arrowheads point at neural tubes of imaged embryos. Representative images shown. Scale bar = 80µm. **(b)-(c)** (*CSL:venus*)*qmc61* fluorescence was measured at 48hpf **(b)** and at 72hpf **(c)** and normalised to the fluorescence of neural tube. No significant differences have been observed at these developmental stages. Summary of 3 independent experiments. Total numbers of embryos per group are indicated by the n numbers in the graphs. Error bars represent mean ± SEM.

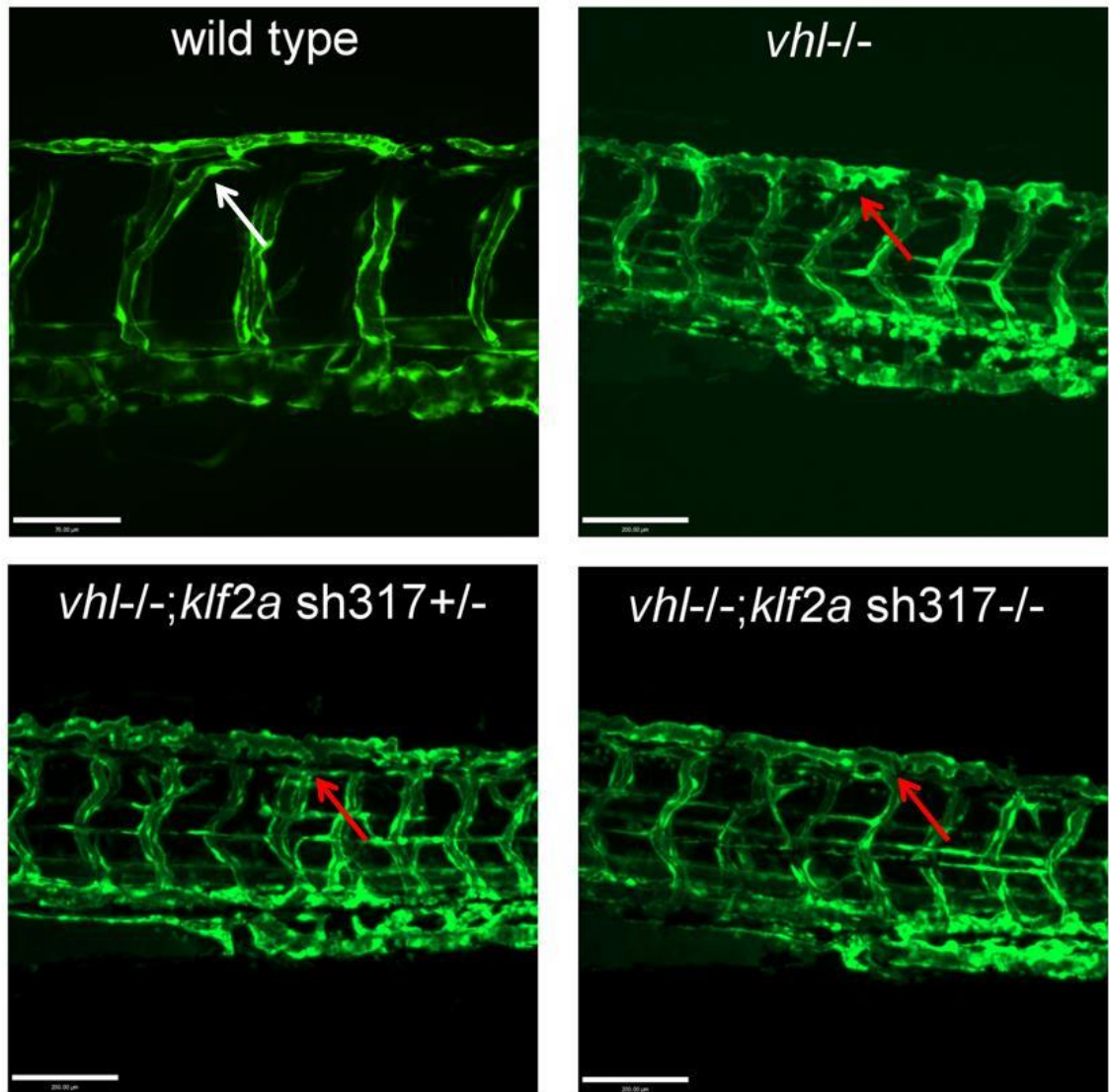


Figure 5.11 *klf2a*^{sh317} mutant embryos do not show increased *dll4* vascular expression at 48hpf

Vascular expression of *dll4* in *klf2a*^{sh317} mutant embryos is not detectable at 48hpf and is identical to *dll4* staining pattern observed in Nacre WT embryos (indicated by black arrows in both figures). Embryos lacking flow (*tnnt2* MO morphants) were included as positive control - *dll4* vascular expression in *tnnt2* MO morphants is upregulated (indicated by a red arrow) when compared to control MO injected embryos (indicated by a black arrow) as published before (Watson, Novodvorsky et al. 2013). Number of embryos with identical staining patterns out of total number of embryos examined is shown in bottom left corner of each image. Summary of 3 independent experiments. Representative images shown. Scale bar = 500µm.

5.2.2.7 Blood flow mechanotransduction critical for aberrant angiogenic phenotype of *vhl* mutants is not affected in *klf2a* mutant zebrafish embryos

vhl mutant embryos (*vhl*^{-/-}) have constitutively activated HIF-mediated hypoxic signalling. This results in excessive and aberrant angiogenic sprouting of the ISVs that can be observed from 3dpf onwards. Oliver Watson from our group recently showed that this excessive angiogenesis is blood flow dependent (Watson, Novodvorsky et al. 2013). The exact mechanism of how blood flow induces this effect remains to be elucidated. I was therefore interested whether *klf2a* as one of the major mechanosensitive endothelial transcription factors was involved in this process. I incrossed zebrafish heterozygous for *klf2a*^{sh317} and *vhl*^{hu2117} in *Tg(fli1:eGFP)* background. 1/16 of a progeny of such cross would be double mutants and I wanted to find out whether these double mutant zebrafish embryos still exhibited the aberrant angiogenic phenotype. Embryos were initially sorted out for fluorescence and the easily observed *vhl*^{-/-} vascular phenotype under fluorescence microscope at 3dpf. 16 *vhl*^{hu2117} *vhl*^{-/-}; *Tg(fli1:eGFP)* embryos were imaged using confocal microscope and subsequently genotyped for *klf2a*^{sh317} mutant status. Out of these 16, 2 were WT, 10 were *klf2a*^{sh317} *klf2a*^{+/+} and 4 were *klf2a*^{sh317} mutants. The presence of *vhl*^{-/-} angiogenic phenotype in *klf2a*^{sh317} mutant background in expected numbers suggests that the blood flow mechanotransduction critical for *vhl*^{-/-} angiogenic phenotype is *klf2a* - independent (Figure 5.12).



scale bar = 70 μm (wild type)
 scale bar = 200 μm (the rest)

Figure 5.12 Blood flow mechanotransduction critical for *vhl*^{-/-} angiogenic phenotype is unaffected in *klf2a*^{sh317} mutant embryos

Confocal images of *Tg(fli1:eGFP)* zebrafish embryos in various genetic backgrounds at 3dpf. Wild type embryos exhibit angiogenesis typical for this developmental stage (top left panel, white arrow). *vhl*^{-/-} embryos show enlargement of vessels (ISVs and DLAV) with increased tortuosity and looping of the DLAV (top right panel, right arrow). The same vascular phenotype can be observed in *vhl*^{-/-} embryos in *klf2a*^{sh317} mutant phenotype (bottom right panel, right arrow). Representative images shown. Scale bar = 70 μm (wild type) or 200 μm (all other figures).

5.2.2.8 Blood flow dependent HSC maturation is not affected in *klf2a* mutant zebrafish embryos

It has been postulated that HSC maturation in zebrafish embryos is a blood flow dependent process mediated by *klf2a*/NO signalling cascade (Wang, Zhang et al. 2011). I wanted to examine this in *klf2a* mutant embryos. WISH on Nacre WT and *klf2a*^{sh317} mutant embryos (in Nacre background) were performed for HSC markers *runx1* and *cmyb* at 36hpf. As shown in **Figure 5.13**, removal of blood flow by *tnnt2* knockdown reduced *runx1* expression in AGM confirming previously published data (Wang, Zhang et al. 2011). Expression of *runx1* in AGM however did not differ between the Nacre WT and *klf2a*^{sh317} mutant embryos (**Figure 5.13**). Expression of another HSC marker *cmyb* in AGM and CHT was also reduced in *tnnt2* morphants in keeping with previously published data (Wang, Zhang et al. 2011) (**Figure 5.14**). Again, I could not detect any difference in *cmyb* expression between Nacre WT and *klf2a*^{sh317} mutant embryos (**Figure 5.14**).

Cont MO and *tnnt2* MO morphants in these experiments were in AB WT genetic background. *runx1* and *cmyb* expression in these embryos cannot be therefore directly compared to *runx1* and *cmyb* expression in Nacre WT or *klf2a*^{sh317} mutant embryos (also in Nacre WT background). Nevertheless, these data suggest that HSC maturation in zebrafish embryos is dependent on blood flow, but is not affected in *klf2a* mutant embryos.

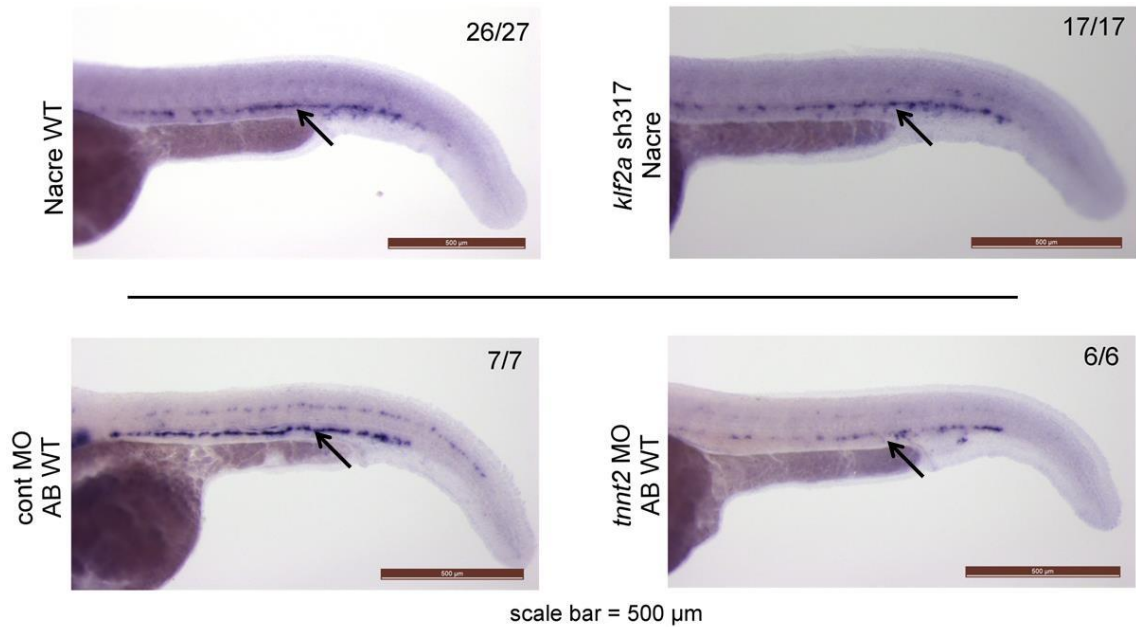


Figure 5.13 *klf2a* mutants do not show differences in expression of HSC marker *runx1* at 36hpf

Expression of HSC marker *runx1* in AGM region (indicated by black arrows in all 4 images) does not differ between Nacre WT and *klf2a*^{sh317} mutant embryos (top panel). Expression of *runx1* is significantly diminished in *tnnt2* MO morphants lacking blood flow when compared to cont MO morphants (bottom panel). Cont MO and *tnnt2* MO morphants are in AB WT genetic background and therefore *runx1* expression in these cannot be directly compared to *runx1* expression in Nacre WT or *klf2a*^{sh317} embryos which are in Nacre WT background. This is indicated by the black line between the top and bottom panel. Figures in top right corner indicate the number of embryos with identical staining patterns out of total number of embryos examined. Scale bar = 500µm.

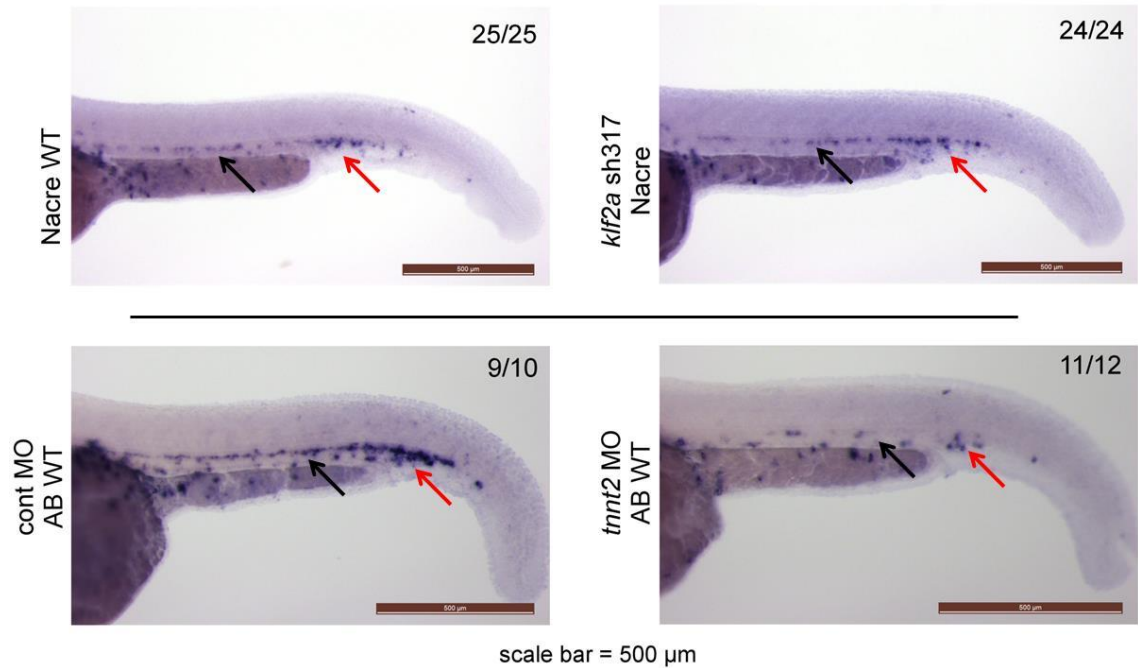


Figure 5.14 *klf2a* mutants do not show differences in expression of HSC marker *cmyb* at 36hpf

Expression of HSC marker *cmyb* in AGM (indicated by black arrows) and CHT (indicated by red arrows) does not differ between Nacre WT and *klf2a*^{sh317} mutant embryos (top panel). Expression of *cmyb* is significantly diminished in *tnnt2* MO morphants that do not experience blood flow when compared to control MO morphants (bottom panel). Control MO and *tnnt2* MO morphants are in AB WT genetic background and *cmyb* expression in these cannot be therefore directly compared to *cmyb* expression in Nacre WT or *klf2a*^{sh317} embryos which are in Nacre WT background. This is indicated by the black line between top and bottom panel. Figures in top right corner indicate the number of embryos with identical staining patterns out of total number of embryos examined. Scale bar = 500μm.

5.2.2.9 *klf2b* is detected in vasculature of a proportion of WT and *klf2a* mutant zebrafish embryos

All experiments performed on the *klf2a* mutant embryos so far failed to reproduce the previously published data obtained by morpholino-mediated *klf2a* knockdown studies. Equally, data obtained by myself using MO-mediated *klf2a* knockdown described in Chapter 3 could not be reproduced in *klf2a* mutants. This leads to a possibility that zebrafish are able to compensate for the loss of function of *klf2a* by a yet unknown mechanism. In the first instance I tried to assess the role of the *klf2a* paralog *klf2b* in *klf2a* mutant embryos. I wanted to find out whether *klf2b* compensates for potential *klf2a* loss of function in the vasculature via expression in endothelial cells. In order to do so I *de novo* synthesised a *klf2b* ISH riboprobe and performed WISH on WT and *klf2a* mutant embryos at 48hpf and 72hpf. These developmental stages were chosen because vascular expression of genes studied could be easily detected at these stages. Additionally, most experiments performed so far were done using zebrafish at these developmental stages.

As shown in **Figure 5.15**, *klf2b* signal could be detected in the pectoral fin, in the cleithrum and some epidermal *klf2b* signal could be detected in the Nacre WT embryos as well confirming previously published data (Oates, Pratt et al. 2001; Thisse 2001). With longer staining time epidermal presence of *klf2b* could be detected also in *klf2a*^{sh317} mutant embryos. Additionally, *klf2b* mRNA was detected in the heart quite early in both the Nacre WT and the *klf2a*^{sh317} mutant embryos. In a small proportion of both Nacre WT and *klf2a*^{sh317} mutants, *klf2b* mRNA could be detected in ISVs as shown in **Figure 5.15c**. The proportion of embryos with vascular staining for *klf2b* mRNA was higher in Nacre WT embryos than in *klf2a*^{sh317} mutants. This is for the first time that *klf2b* expression was reported in the heart and in the vasculature of zebrafish embryos.

Admittedly only a small number of embryos have been studied so far and some degree of variability in staining of embryos has been noted as well.

At 72hpf, *klf2b* expression patterns in Nacre WT and *klf2a*^{sh317} embryos did not show any differences either. *klf2b* mRNA could be initially detected in the mesenchyme of pectoral fins and some signal was also detected from the area of aortic arch arteries for the first time (**Figure 5.16**, top panel). With longer staining time more *klf2b* signal could be detected in the epidermis in the majority of the embryos examined. Small proportion of both Nacre WT and *klf2a*^{sh317} embryos clearly exhibited *klf2b* mRNA in the ISVs and also in the subintestinal veins (SIVs) which has not been reported before. There was however no concordance in *klf2b* mRNA presence in ISVs and SIVs. All 4 combinations of *klf2b* staining patterns (no vascular staining, *klf2b* detected only in ISVs, *klf2b* detected only in SIVs, *klf2b* detected in both ISVs and SIVs) could be seen in both Nacre WT and *klf2a*^{sh317} embryos (**Figure 5.16**, bottom panel).

Overall, I did not detect increased *klf2b* vascular expression in *klf2a* mutant embryos in comparison to WT embryos of the same developmental stage. I cannot exclude however that low levels of *klf2b* expression suffice to rescue any *klf2a* mutant phenotype.

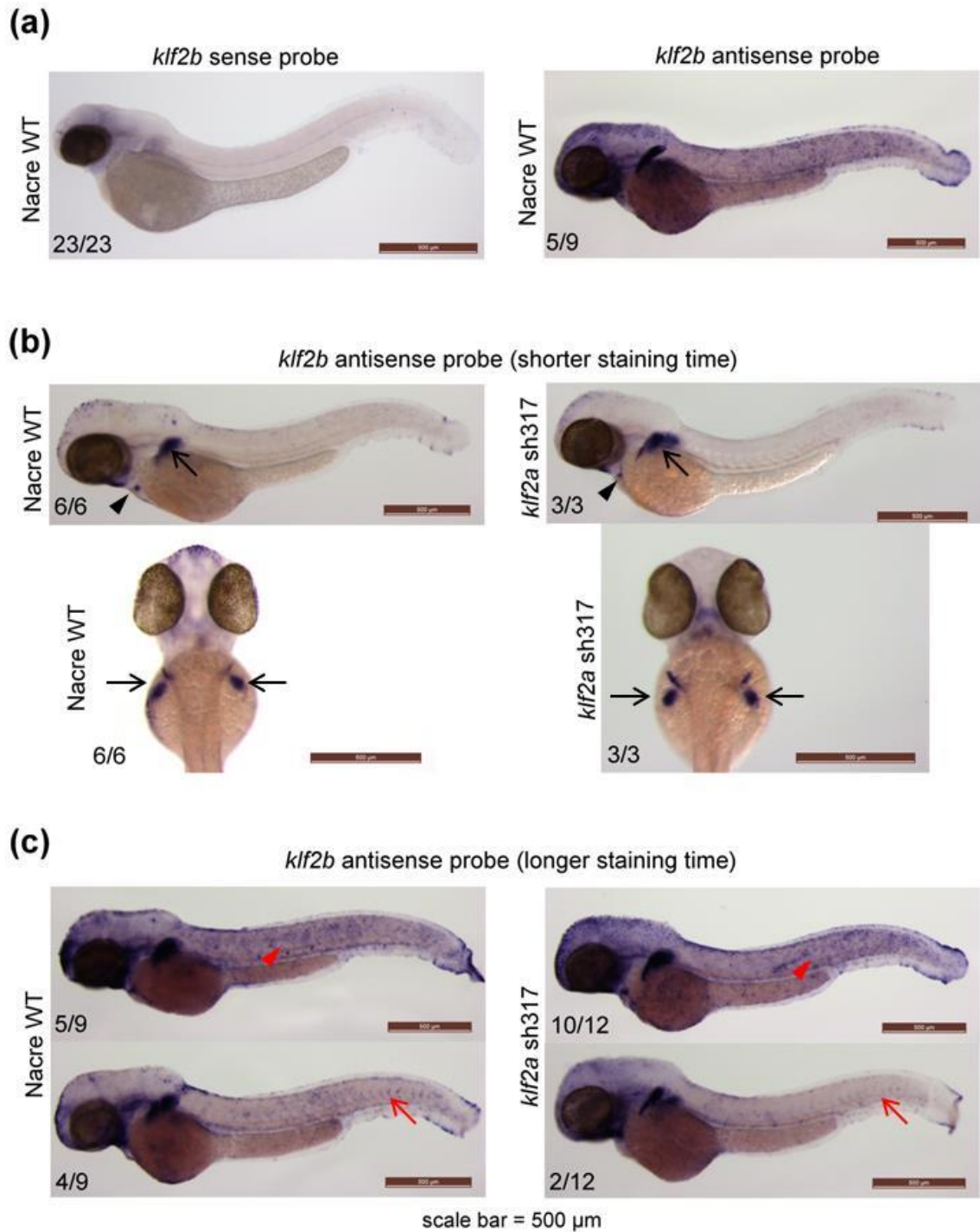


Figure 5.15 *klf2b* expression patterns in Nacre WT and *klf2a*^{sh317} mutants at 48hpf
(a) Comparison of WISH staining patterns for *klf2b* using a *de novo* synthesised *klf2b* sense (left) and *klf2b* antisense (right) riboprobe. **(b)** *klf2b* expression patterns in Nacre WT and *klf2a*^{sh317} embryos at 48hpf do not show any differences. A proportion of zebrafish embryos were stained for less time to study the staining patterns in more detail. *klf2b* mRNA can be detected in the cleithrum and mesenchyme of pectoral fins

(black arrows) as well as in developing heart (black arrowheads) Top panel represents lateral view, bottom panel represents dorsal view. **(c)** Remaining embryos were stained for longer period of time. A significant proportion of embryos showed *klf2b* expression (apart from the above described anatomical structures) on the surface (red arrowheads) most likely representing epidermal cells as described before. A smaller proportion of both Nacre WT and *klf2a*^{sh317} embryos clearly exhibited *klf2b* mRNA presence in distal ISVs (red arrows). Figures in bottom left corner of each image indicate the number of embryos with identical staining patterns out of total number of embryos examined. Scale bar = 500µm.

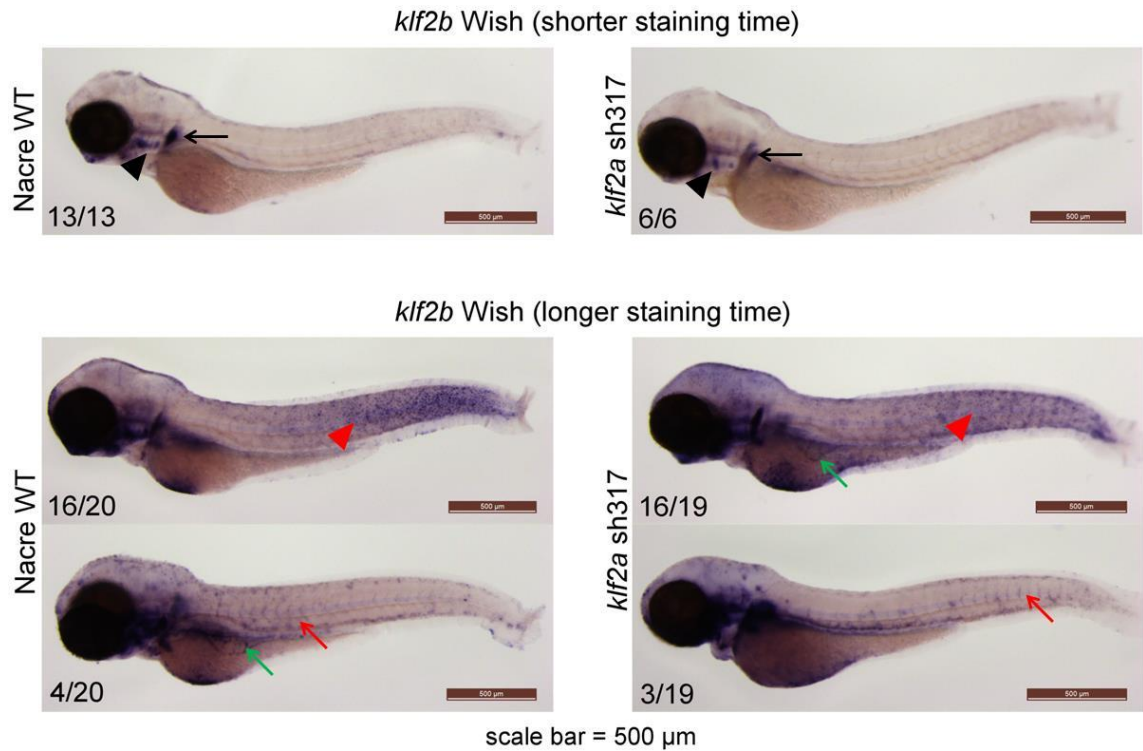


Figure 5.16 *klf2b* expression patterns in Nacre WT and *klf2a*^{sh317} mutants at 72hpf *klf2b* expression patterns in Nacre WT and *klf2a*^{sh317} embryos at 72hpf do not show any differences. A proportion of zebrafish embryos were stained for shorter time (top part of the figure) to study the staining patterns in more detail. *klf2b* mRNA could be initially detected in the mesenchyme of pectoral fins (black arrows) and some signal came from the area of aortic arch arteries (black arrowheads). With longer staining times (bottom part of the figure), more *klf2b* signal could be detected in the epidermis (red arrowheads) in the majority of the embryos examined. Small proportion of both Nacre WT and *klf2a*^{sh317} embryos clearly exhibited *klf2b* mRNA in the ISVs (red arrows) and also in the subintestinal veins (SIVs)(green arrow). There was however no concordance in *klf2b* mRNA presence in ISVs and SIVs in Nacre WT or *klf2a*^{sh317} embryos. Figures in bottom left corner of each image indicate the number of embryos with identical staining patterns out of total number of embryos examined. Scale bar = 500 μ m.

5.2.2.10 AA5x angiogenesis is not affected in *klf2a*^{sh317} mutant embryos injected with *klf2b* MO

Vascular *klf2b* expression was observed in some of the Nacre WT and *klf2a*^{sh317} embryos. I was therefore interested whether *klf2b* knockdown in *klf2a* mutant background could prevent AA5x vessel angiogenesis. For *klf2b* knockdown I used a *klf2b* morpholino that binds to E111 splice donor site and should therefore cause partial or total inclusion of *klf2b* intron 1. These were the last experiments I managed to do in this project and due to shortage of time I did not check for the level of *klf2b* knockdown caused by the *klf2b* MO via RT-PCR. I tested several *klf2b* MO doses and used the highest dose that did not haemodynamically compromise the embryos. As shown in **Figure 5.17a**, injection of 2.1ng of *klf2b* MO into *klf2a*^{sh317} heterozygous embryos does not cause any significant changes in heart rate when compared to control MO injected siblings at 48hpf or 72hpf. In relation to AA5x vessel formation, *klf2b* knockdown in *klf2a* mutant embryos does not cause any disruption in AA5x angiogenesis in any of the embryos examined (**Figure 5.17b**).

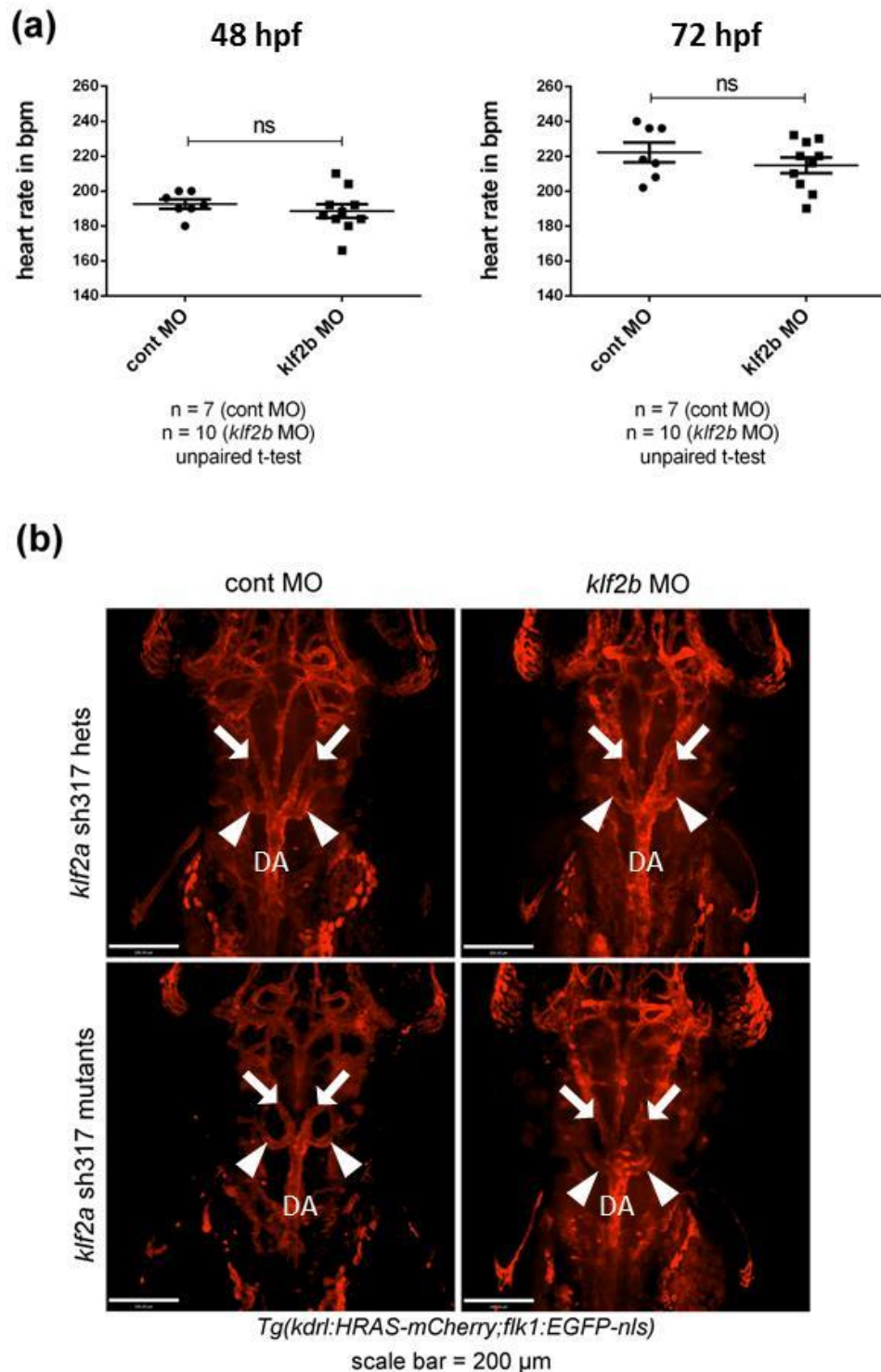


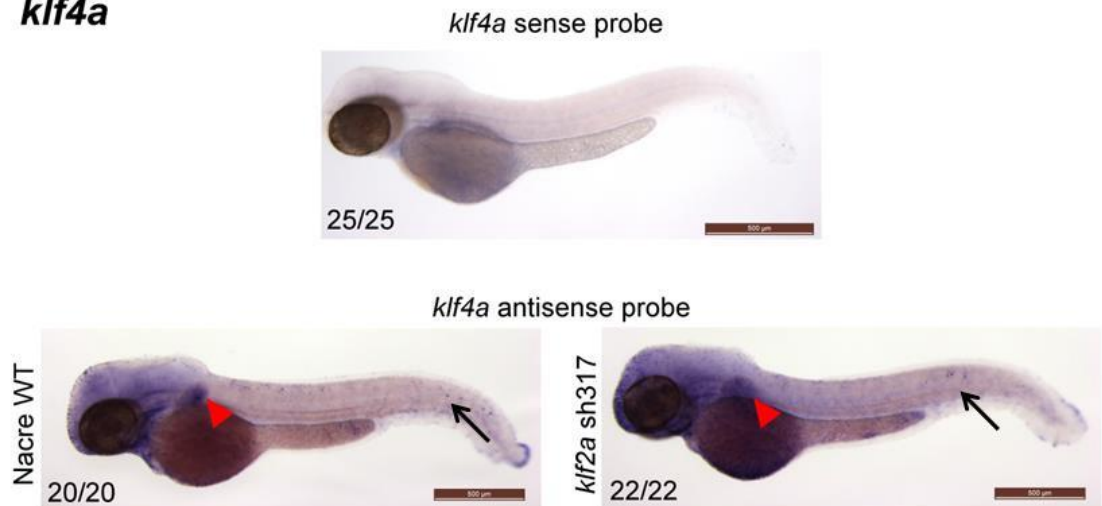
Figure 5.17 Comparison of heart rates and AA5x angiogenesis in *kif2b* MO injected homozygous and heterozygous *kif2a*^{sh317} carriers

(a) Heart rates of control MO and *kif2b* MO injected *kif2a*^{sh317} heterozygotes do not differ significantly at 48hpf or 72hpf. Error bars represent mean \pm SEM. **(b)** AA5x vessel (white arrowheads) angiogenesis is intact in all *kif2b* MO injected *kif2a*^{sh317} mutant embryos examined. White arrows indicate lateral dorsal aortae. DA stands for dorsal aorta. Scale bar = 200 μ m.

5.2.2.11 *klf4a* and *biklf/klf4b/klf17* are not expressed in the vasculature of wild type or *klf2a* mutant embryos

KLF4/Klf4 is expressed in human and murine vasculature and its effects are similar to those of *KLF2/Klf2* as detailed in Section 1.8 of this thesis. I therefore examined whether any of the 2 zebrafish *KLF4* paralogs - *klf4a* or *biklf/klf4b/klf17* could compensate for the loss of *klf2a* function in the vasculature of the *klf2a*^{sh317} mutant embryos. In order to do so I performed WISH for *klf4a* and *biklf/klf4b/klf17* on Nacre WT and *klf2a*^{sh317} mutants at 48hpf with *de novo* synthesised *klf4a* and *biklf/klf4b/klf17* ISH probes. This developmental stage was chosen because vascular expression of genes studied could be easily detected at this time point. As shown in **Figure 5.18**, *klf4a* mRNA could not be detected in the vasculature of Nacre WT or *klf2a*^{sh317} mutants at this stage. *klf4a* mRNA was detected in the epidermis and pectoral fins in keeping with previously published data (Li, Chan et al. 2011). Similarly, *biklf/klf4b/klf17* expression could not be detected in the vasculature of Nacre WT or *klf2a*^{sh317} mutants at 48hpf. *biklf/klf4b/klf17* expression was detected in the neuromast cells that form the lateral line organ and in the hatching gland (**Figure 5.18**), again in keeping with previously published data (Oates, Pratt et al. 2001; Gardiner, Daggett et al. 2005).

klf4a



biklf/klf4b/klf17

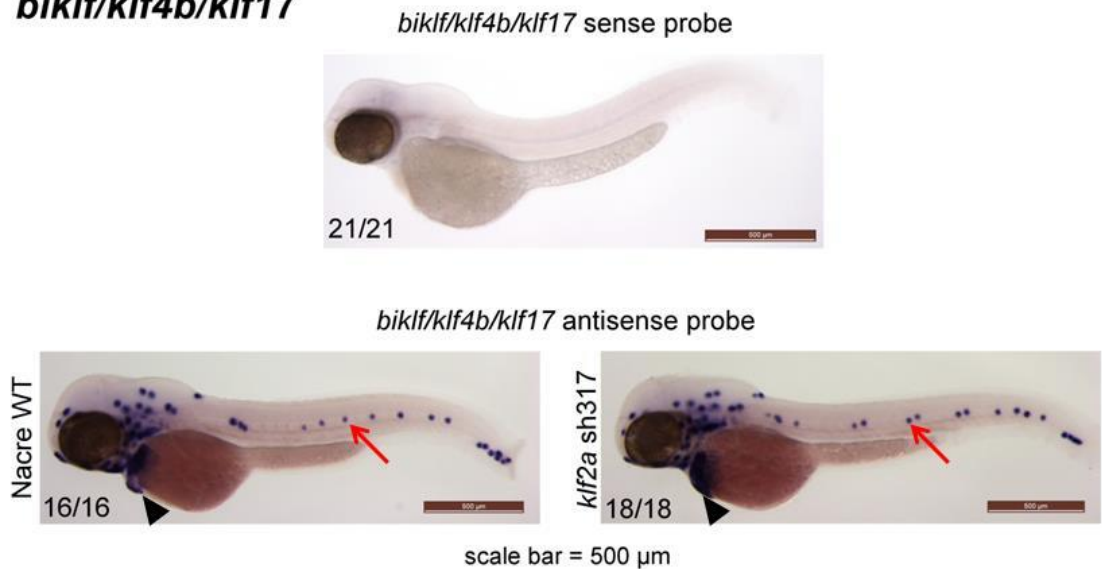


Figure 5.18 Expression patterns of *klf4a* and *biklf/klf4b/klf17* in Nacre WT and *klf2a*^{sh317} mutants at 48hpf

klf4a expression was detected in epidermis (black arrows) and pectoral fins (red arrowheads) of both Nacre WT and *klf2a*^{sh317} mutants in keeping with previously published data. No *klf4a* vascular expression could be detected in any of the Nacre WT or *klf2a*^{sh317} mutants examined. *biklf/klf4b/klf17* expression was detected in neuromasts of lateral line organ (red arrows) and in hatching glands (black arrowheads) of both Nacre WT and *klf2a*^{sh317} mutants in keeping with previously published data. No *biklf/klf4b/klf17* vascular expression could be detected in any of the Nacre WT or *klf2a*^{sh317} mutants examined. Figures in bottom left corner of each image indicate the number of embryos with identical staining patterns out of total number of embryos examined. Scale bar = 500μm.

5.3 Discussion

I created a stable *klf2a* mutant zebrafish line which is viable to adulthood and fertile in its homozygous state. This alone represents a contradiction to previously published work which suggest that MO-mediated *klf2a* knockdown causes high-output cardiac failure with pericardial oedema in early developmental stages of zebrafish embryos (Lee, Yu et al. 2006). Although the authors do not comment on the long-term effects of these observed features it is difficult to imagine that embryos with such severe impairment of cardiovascular system would be viable to adulthood and fertile.

Another confirmation of the absence of this phenotype in *klf2a* mutants comes from the direct morphological observations and measurements of heart rates and blood flow velocities. *klf2a* mutant embryos do not morphologically differ from WT embryos at any developmental stage, nor do the adult mutant zebrafish differ from adult WT zebrafish. There is no pericardial oedema detected in the *klf2a* mutant embryos and there are no morphological differences in the anatomical areas with previously detected high *klf2a* expression such as cloaca or pectoral fin. Heart rates and blood flow velocities in DA in WT and *klf2a* mutants are identical at 48hpf. At 72hpf blood flow velocities in DA generally tend to slow down in both WT and *klf2a* mutants. This trend is much stronger in *klf2a* mutants so that a significant difference in this parameter can be detected at this stage when compared to WT embryos. Comparatively heart rates of both WT and *klf2a* mutant embryos get faster at 72hpf when compared to 48hpf but this trend is again more accentuated in *klf2a* mutants. It is reasonable to think that *klf2a* mutant embryos compensate for slower blood flow velocities with increased heart rates to maintain the cardiac output level with the WT embryos of the same stage. This is therefore another argument against a high-output heart failure phenotype at this stage which is around the time when the high-output cardiac failure features were observed in the *klf2a* MO morphants. It should be noted however that WT embryos and maternal *klf2a* mutant

embryos in this experiment represent two independent crosses. Despite the fact that both WT embryos and *klf2a* mutants are in Nacre WT background the observed changes could be explained by variability between two independent crosses. In order to exclude this possibility, this experiment needs to be repeated on a progeny of 2 heterozygous carriers for *klf2a* mutant allele. I did not manage to carry out this experiment due to the shortage of time. It would be interesting to measure heart rates and blood flow velocities beyond 72hpf, but this might be technically challenging. Heart rates and blood flow velocities at 48hpf and 72hpf were measured by direct observation without the need for light Tricaine anaesthesia which itself influences these parameters. Embryos older than 72hpf have more developed nervous system and would require anaesthesia to stop them moving for a period of time necessary for the measurements. This would thus introduce another significant variable into this experiment.

An interesting theory that could explain the differences in blood flow velocities observed in *klf2a* mutant embryos at 72hpf comes from the previously published data suggesting a role of *klf2a* in AV valve development (Vermot, Forouhar et al. 2009). *klf2a* knockdown was reported to cause AV valve dysgenesis (scored at 4dpf) and resulting dysfunctional valve. Valve dysgenesis causes increased RFF which would manifest itself as slower blood flow in DA. Unfortunately, in the original work, there were no RFF measurements on *klf2a* MO morphants performed at 4dpf. RFFs were only measured at 48hpf and they did not differ significantly between WT and *klf2a* MO morphants at this stage (Vermot, Forouhar et al. 2009). Given these inaccuracies in the original work, I went on to ascertain whether there was any valve dysgenesis in *klf2a* mutant zebrafish embryos at various developmental stages. So far, I only examined a limited number of embryos and cardiac cycles. My preliminary data show differences in RFF between WT and *klf2a* mutant zebrafish at 48, 72 and 96hpf. At 72hpf when the difference in blood flow velocity was noticed, RFF in WT and *klf2a* embryos seems to

be very similar. Certainly, more cardiac cycles and more embryos need to be examined before any conclusion can be made in this respect. Again, a strong argument against any significant valve dysgenesis in *kif2a* mutant zebrafish is the fact that they are viable and fertile in the adulthood and do not suffer from heart failure.

To my knowledge mouse represents the only species in which homozygous *Klf2* deficiency has been described so far. Homozygous *Klf2* deficient mice die between E12.5-14.5 from intraembryonic and intraamniotic haemorrhaging associated with endothelial necrosis, cuboidal VSMCs, abnormally thin tunica media and aneurysms. Defective VSMC and pericyte migration to endothelial tubes result in the loss of their stabilising and modulatory functions and failure to organize into a compact tunica media (Kuo, Veselits et al. 1997; Wu, Bohanan et al. 2008). Experiments on mouse embryos with conditional *Klf2* knockout in various tissues confirm that it is the endothelial *Klf2* deletion that is responsible for the embryonic mortality around E14 (Lee, Yu et al. 2006). This group did not report the VSMC defects or haemorrhages however. The cause of death was reported to be cardiac defects and high-output cardiac failure caused by loss of smooth muscle tone and vasodilation (Lee, Yu et al. 2006).

Zebrafish adult VSMCs develop from vascular mural cells (MCs). MCs found in zebrafish embryos share many of the characteristics of embryonic VSMCs and pericytes found in higher vertebrates (Santoro, Pesce et al. 2009). Specific MC markers such as *acta2* and *transgelin* can be found in the perivascular regions of the zebrafish vasculature from 72hpf. At 20dpf several layers of undifferentiated VSMCs can be observed around DA and at 3 months a thick layer of fully differentiated VSMCs surround endothelial cells of DA (Santoro, Pesce et al. 2009). It is therefore interesting that *kif2a* mutation in zebrafish does not appear to have any significant effect on the development of VSMC given the viability and fertility of adult *kif2a* mutants. It would be

interesting to perform sections of adult *klf2a* mutants and investigate the morphology and molecular markers of the VSMC layer in *klf2a* mutants in more detail.

Further examination of cardiovascular system in *klf2a* mutant embryos revealed normal vascular patterning and circulatory patterns which is in concordance with previously reported data obtained by MO-mediated *klf2a* knockdown (Nicoli, Standley et al. 2010). This group however reported that a formation of a tiny vessel connecting the 5th and 6th aortic arch termed AA5x is dependent on blood flow which effects are mediated by the flow dependent transcription factor *klf2a*. *klf2a* then induces *miR-126* that inhibits Vegfa inhibitor *spred-1* thus allowing Vegf-mediated angiogenesis to proceed. My data indicate that AA5x angiogenesis is blood flow dependent but is not affected in *klf2a*^{sh317} mutants. All *klf2a*^{sh317} mutants examined formed AA5x vessel bilaterally. Additionally, my preliminary data on *klf2a* mutant embryos where *klf2b* was knocked down by *klf2b* MO show that AA5x angiogenesis is intact in these morphants as well. It has to be said that due to the shortage of time I did not manage to check for the actual level of *klf2b* knockdown and simply used the highest non-toxic *klf2b* MO dose. With respect to the original work it would be interesting to find out whether AA5x angiogenesis is really dependent on *miR-126* and *spred-1* as originally suggested (Nicoli, Standley et al. 2010).

Next I was interested whether *klf2a* mutation has any effect on the number of endothelial cells in the developing zebrafish vasculature. This hypothesis comes from an observation that the *vhl*^{-/-} phenotype of excessive and aberrant hypoxia-driven angiogenesis with increased vessel length and increased endothelial cell numbers was found to be blood flow dependent (Watson, Novodvorsky et al. 2013). I showed that *klf2a* mutation does not have any effect on endothelial cell number at the very early stages of zebrafish embryonic development.

The actual fact that the above mentioned *vhl*^{-/-} phenotype of aberrant angiogenesis was dependent on blood flow as mechanical force led me to investigate whether the *klf2a* mutation in *vhl*^{-/-} background would similarly result in the abrogation of *vhl*^{-/-} angiogenic phenotype. *vhl*^{-/-} fish are not viable beyond 11dpf (van Rooijen, Voest et al. 2010) and therefore I incrossed double heterozygous line *klf2a*^{sh317+/-} ; *vhl*^{hu2117+/-} in *Tg(fli1:eGFP)* background. 1/16 of the progeny of such cross would be double mutants *klf2a*^{sh317-/-} ; *vhl*^{hu2117-/-} and I was interested whether or not these embryos exhibited the typical *vhl*^{-/-} angiogenic phenotype. The easily observed *vhl*^{-/-} vascular phenotype was examined under fluorescent microscope and thus *vhl*^{hu2117-/-} ; *Tg(fli1:eGFP)* embryos could be sorted out. A group of these embryos were then imaged and subsequently genotyped for *klf2a* mutant status. Out of 16 embryos examined 4 were in *klf2a*^{sh317} mutant background suggesting that mutation of *klf2a* does not abrogate formation of excessive angiogenic phenotype in *vhl* mutant embryos. This indicates that *klf2a* is unlikely to be the crucial link between blood flow and angiogenic *vhl*^{-/-} phenotype which thus remains to be identified yet.

I was also interested to find out whether *klf2a* plays any role in blood flow dependent regulation of *cxcr4a* expression. My initial observation of increased vascular *cxcr4a* mRNA presence in SB *klf2a* MO and ATG *klf2a* MO morphants could not be confirmed via qRT-PCR from whole embryonic cDNA. I could not detect any increased *cxcr4a* vascular expression in *klf2a* mutant embryos at 48hpf. *cxcr4a* expression in *klf2a* mutants remains suppressed to the level seen in WT embryos. I was able to repeatedly confirm that removal of blood flow increases *cxcr4a* vascular expression but the actual mechanosensation in this pathway is likely to be mediated via a different mechanism than *klf2a*.

Similarly I wanted to clarify whether *klf2a* is involved in the recently discovered blood flow mediated regulation of canonical Notch signalling (Watson, Novodvorsky et al.

2013). Initial observations suggested that *dll4* expression was increased in SB *klf2a* MO and ATG *klf2a* MO morphants at 48hpf, although this did not reflect in increased activity of Notch transcription factor CSL. Surprisingly, *dll4* vascular expression remained unchanged in *klf2a* mutants when compared to controls at 48hpf. Removal of blood flow resulted in increased vascular *dll4* expression confirming previous data. Additionally, CSL activity in DA measured via fluorescence of YFP derivative venus using *Tg(CSL:venus)qmc61* transgenic reporter line remained unchanged in *klf2a* mutants at 48 and 72hpf. This again suggests that *klf2a* is not involved in mechanosensation related to vascular Notch signalling cascade.

Another recent work on zebrafish related to *klf2a* linked HSC maturation to a blood flow dependent *klf2a*-NO signalling cascade (Wang, Zhang et al. 2011). Blood flow has been shown to be indispensable for the maintenance of HSC programming. Expression of HSC markers *runx1* and *cmyb* significantly decreased when blood flow was removed. Similar reduction of *runx1* and *cmyb* expression was reported in ATG *klf2a* MO morphants. I therefore performed WISH for *runx1* and *cmyb* on *klf2a* mutant embryos. I could not detect any diminished expression of any of these HSC markers, but I noticed a degree of variability in the levels of *runx1* and *cmyb* staining among embryos of the same group. Consistent with previous results, HSC markers were diminished in *tnt2* MO morphants without blood flow. This group claimed that they could partially rescue the diminished *runx1* and *cmyb* by injecting a full-length capped *klf2a* mRNA (Wang, Zhang et al. 2011). I have been kindly donated the expression plasmid that was supposed to contain the full-length *klf2a* cDNA sequence. Unfortunately when I sequenced this expression plasmid I found out that the whole *klf2a* exon 1 and initial parts of exon 2 were missing. This truncated *klf2a* cDNA still contained an 'in frame' ATG which happens to be the same ATG that the ATG *klf2a*

MO is targeting. The functional relevance of this ATG remains questionable due to the reasons I explained elsewhere in this thesis.

The lack of phenotype in the *klf2a* mutant zebrafish (apart from the changes in heart rate and blood flow velocity at 3dpf) as well as the fact that experiments on *klf2a* mutant embryos failed to confirm previous data obtained by MO-mediated *klf2a* knockdown made me to investigate whether zebrafish embryos possess any mechanism by which the *klf2a* mutation could be compensated. Following the exclusion of alternative *klf2a* splicing, my attention moved towards *klf2a* paralog *klf2b*. *klf2b* has been very little investigated so far and its vascular expression has not been reported yet. I managed to reproduce and extend the studies on spatial and temporal *klf2b* expression patterns by performing a series of WISH experiments. I confirmed *klf2b* expression in the epidermis, cleithrum and pectoral fin bud at 48hpf. I extended *klf2b* expressional studies by detecting *klf2b* expression in the hearts and ISVs in a proportion of both WT and *klf2a* mutant embryos at 48hpf. Later on at 72hpf, *klf2b* vascular expression persisted in ISVs and extended also to the area of aortic arches and subintestinal veins in a small proportion of embryos examined. Altogether I could not detect any differences in *klf2b* staining patterns between WT and *klf2a* mutant embryos. Despite these data, I can not exclude the possibility that low levels of endothelial *klf2b* expression, non-detectable via WISH technique compensate for any *klf2a* mutant phenotype. Preliminary data from MO-mediated *klf2b* knockdown in *klf2a* mutant embryos did not show any difference in the phenotype in relation to embryonic morphology, heart rates or vascular patterning. A generation of *klf2b* mutant line and subsequent phenotyping of a double *klf2a/klf2b* mutant line would bring the definitive answer to the issue of gene redundancy in this case.

KLF4 was identified as another blood flow dependent transcription factor in human and murine endothelial cells (McCormick, Eskin et al. 2001; Hamik, Lin et al. 2007). *KLF4*

endothelial expression is similarly to *KLF2* upregulated by laminar shear stress and statins, but is also upregulated by proinflammatory cytokines (Hamik, Lin et al. 2007; Ohnesorge, Viemann et al. 2010). *KLF2* and *KLF4* thus have many overlapping functions in ECs (Bieker 2001). I therefore considered *KLF4* as another relevant candidate gene which could compensate for the loss of *klf2a* function in zebrafish vasculature. Zebrafish have two *KLF4* paralogs termed *klf4a* and *klf4b*, however *klf4b* has been recently named *klf17* (Kotkamp, Mossner et al. 2014). WISH for *klf4a* and *biklf/klf4b/klf17* confirmed previously published staining patterns for these genes (Oates, Pratt et al. 2001; Gardiner, Daggett et al. 2005; Li, Chan et al. 2011). I observed identical staining patterns for *klf4a* and *biklf/klf4b/klf17* in WT and *klf2a* mutant embryos. I could not detect any vascular expression of *klf4a* and *biklf/klf4b/klf17* in any WT or *klf2a* mutant embryos examined. Thus it seems unlikely that any of the two zebrafish *KLF4* paralogs compensate for the *klf2a* mutation in the vasculature of *klf2a* mutant embryos, although again I can not exclude the possibility that low levels of endothelial *klf4a* or *biklf/klf4b/klf17* expression, non-detectable via WISH technique compensate for any *klf2a* mutant phenotype.

Chapter 6

General discussion

In the first part of this project I reproduced and extended the previous studies on spatial and temporal *klf2a* expression patterns in developing zebrafish embryos. I detected *klf2a* expression in subintestinal veins, hepatic portal vein and in neuromasts for the first time. It is not certain what functions *klf2a* has in anatomical locations such as neuromasts, pectoral fin, cloaca or cells in the posterior somites lateral to the most posterior notochord in which *klf2a* expression is high during early developmental stages. However, as detailed later, all these parts and organs seem to develop normally in *klf2a* mutant fish. In my project I focused on *klf2a* function in the vasculature. It was therefore important that I localised *klf2a* expression to the vasculature by performing cross sections on fixed zebrafish embryos following WISH for *klf2a*. I also confirmed that endothelial *klf2a* expression in zebrafish embryos is blood flow dependent using three distinct models of altered blood flow.

In the next part of the project I used methods of reverse genetics to study the functions of *klf2a* in zebrafish vasculature. At the start of this project, the morpholino (MO) antisense technology represented the gold standard for reverse genetics studies in zebrafish. I therefore used two previously published *klf2a* MOs (Vermot, Forouhar et al. 2009; Nicoli, Standley et al. 2010; Wang, Zhang et al. 2011) to achieve a temporarily knockdown of *klf2a* expression. The use of both SB *klf2a* and ATG *klf2a* morpholinos proved to be technically challenging and also led to detection of a potentially different mechanism of action in the case of ATG *klf2a* MO as detailed in the discussion to Chapter 3 of this thesis.

I detected increased vascular expression of *cxcr4a* in a significant proportion of SB *klf2a* MO and ATG *klf2a* MO morphants at 48hpf. The levels of *cxcr4a* expression were comparable to the levels seen in *tnnt2* MO morphants lacking blood flow. This finding would be in keeping with the hypothesis that the flow dependent transcription factor *klf2a* acts as a negative regulator of vascular *cxcr4a* expression.

When I examined the effects of *klf2a* on Notch signalling pathway I found increased endothelial expression of Notch ligand *dll4* in most of the SB *klf2a* MO and ATG *klf2a* MO morphants at 48hpf. The increase in *dll4* expression was similar to the levels seen in *tnnt2* MO morphants without flow. Surprisingly, the increased levels of *dll4* expression in the vasculature of SB *klf2a* MO and ATG *klf2a* MO morphants did not result in increased vascular Notch activity measured by the aortic venus fluorescence in the transgenic reporter line *Tg(CSL-venus)qmc61*.

The subsequent RT-qPCR was not able to detect any significantly increased relative expression of *cxcr4a* or *dll4* in *klf2a* MO morphants and this discrepancy is discussed elsewhere in this thesis.

I found significant discrepancies between the observed effects of MO-mediated *klf2a* knockdown and the phenotype of the *klf2a* mutant line. Although there are several hypotheses that could account for the 'lack of phenotype' in the *klf2a* mutant line as detailed later in this discussion, it is also necessary to comment on the effects seen in the SB *klf2a* MO and ATG *klf2a* MO morphants. Based on my findings it is possible that both *klf2a* morpholinos I used in this project interfere with *klf2a* pre-mRNA splicing. Their effect on *cxcr4a* and *dll4* expression is similar and these effects can not be seen in the *klf2a* mutants. It is therefore likely that both SB *klf2a* MO and ATG *klf2a* MO induce expressional changes not only in *klf2a* but also in other off-target genes such as p53 and other unknown genes and the resulting morphants represent a 'compound knockdown' phenotype. Clearly, further work needs to be done to better understand and explain these differences.

In the next part of this project I generated a stable *klf2a* mutant line using a TALEN mutagenesis technique. I isolated 4 novel *klf2a* mutant alleles with frame shift mutations causing changes in the reading frame. I proved that the mutations in *klf2a* gene resulted in the transcription of predicted mutant *klf2a* mRNA. I could exclude

alternative mRNA splicing as a compensation mechanism for the loss of non-mutant *klf2a* sequence. By performing a Western blot I saw a substantial reduction of the intensity of the 43kDa band representing the full-length Klf2a protein in *klf2a* mutants. Additionally I detected the presence of smaller bands most likely representing the truncated Klf2a protein. Lastly I proved that maternal *klf2a* mRNA is not present in zebrafish embryos by demonstrating its absence in unfertilised zebrafish eggs.

klf2a mutant zebrafish are viable to adulthood and fertile. They exhibit normal development of cardiovascular system based on the observations I managed to accomplish so far with the exception of slower blood flow velocities and increased heart rates at 72hpf. Notably no high-output cardiac failure or pericardial oedema were detected which contradicts previously published data (Lee, Yu et al. 2006). The formation of AA5x vessel was intact in all *klf2a* mutants examined, but I could confirm that AA5x angiogenesis was blood flow dependent which therefore partially contradicts another work in this field (Nicoli, Standley et al. 2010). My preliminary data also indicate that the previously reported *klf2a* function in AV valve development (Vermot, Forouhar et al. 2009) might not be reproduced in *klf2a* mutant embryos. Based on these findings I conclude that *klf2a* mutations at the genomic sites I generated do not affect vasculogenesis and angiogenesis in early stages of embryonic zebrafish development.

The blood flow dependent *vhl*^{-/-} phenotype of excessive and aberrant hypoxia-driven angiogenesis is not affected by *klf2a* mutation. This is indicated by the existence of double mutant *klf2a*^{sh317-/-}; *vhl*^{hu2117-/-} zebrafish embryos with this phenotype in expected numbers following an incross of zebrafish lines heterozygous for *klf2a*^{sh317} and for *vhl*^{hu2117}. Experiments into the role of *klf2a* in *cxcr4a* regulation of expression show that *klf2a* mutation does not affect vascular *cxcr4a* expression. These findings thus do not confirm my previous observations made on *klf2a* MO morphants. Similarly, experiments into the role of *klf2a* in the recently discovered blood flow mediated

regulation of canonical Notch signalling suggest that *klf2a* is not involved in mechanosensation related to vascular Notch signalling cascade. Notably, vascular *dll4* expression in *klf2a* mutant embryos does not differ from WT controls at 48hpf. This again contradicts my data obtained from *klf2a* MO morphants.

Despite the well known role of *KLF2* in endothelial biology as described in the introduction to this thesis, only several works have been published on the role of *KLF2* zebrafish ortholog *klf2a* in zebrafish vascular biology (Oates, Pratt et al. 2001; Lee, Yu et al. 2006; Parmar, Larman et al. 2006; Vermot, Forouhar et al. 2009; Nicoli, Standley et al. 2010; Wang, Zhang et al. 2011). One of them links HSC maturation to a blood flow dependent *klf2a*-NO signalling cascade (Wang, Zhang et al. 2011). Experiments on *klf2a* mutant embryos could not establish a link between *klf2a* nonsense mutation and difference in expression of HSC markers *runx1* and *cmyb* as described before yet again contradicting the previously published data. Flow dependent regulation of these markers could be confirmed, however.

To summarize, *klf2a* mutant does not exhibit any phenotype apart from changes in the heart rate and blood flow velocity at 3dpf. On one side this lack of phenotype is rather surprising given the previously published data based on MO-mediated *klf2a* knockdown. On the other hand, in the light of the most recently published works on large-scale phenotyping of zebrafish mutants, these findings appear to be less of a surprise. The zebrafish mutation project (ZMP) aims to identify and phenotype disruptive (nonsense or missense) mutations in every protein coding gene (Kettleborough, Busch-Nentwich et al. 2013). So far they were able to identify potentially disruptive mutations in approximately 40% of all zebrafish protein-coding genes. 1216 alleles were further analysed for phenotype. Only around 6% of alleles were found to have a phenotype within the first 5dpf in their homozygous state (Kettleborough, Busch-Nentwich et al. 2013). This number is surprisingly low even when taking into account that only morphological and behavioural changes in the first

5dpf were examined. The authors of the project discuss that some more phenotypes might be detected on closer observation and phenotypic analysis of older zebrafish larvae. Gene redundancy due to partial genome duplication as an explanation for the lack of phenotypes in some of the mutant genes is also mentioned. Data generated by this group are freely available. In relation to *klf2a* they report identification of a nonsense mutation (A→T) in exon 3 of *klf2a* gene in the F1 generation (http://www.sanger.co.uk/projects/D_rerio/zmp).

In my search for a gene that could compensate for the potential loss of *klf2a* function I analysed vascular expression of several candidate genes in *klf2a* mutant background. The candidate genes were chosen based on their phylogenetic proximity to *klf2a* (**Figure 6.1**). Firstly I assessed vascular expression of *klf2a* paralog *klf2b*. I was able to detect *klf2b* mRNA in the vasculature of some WT and *klf2a* mutant embryos, but vascular presence of *klf2b* mRNA in *klf2a* mutant embryos was by no means more intense than the one detected in WT embryos. These findings however do not exclude the possibility that low levels of *klf2b* mRNA in the vasculature compensate for any *klf2a* mutant phenotype. Given more time I would strive for a generation of a *klf2b* mutant line. Subsequent phenotypisation of a double *klf2a/klf2b* mutant line would answer the question of gene redundancy in this case. Next I examined vascular expression of both zebrafish *KLF4* paralogs *klf4a* and *biklf/klf4b/klf17* because apart from *klf2b*, these 2 genes are phylogenetically closest to *klf2a* (**Figure 6.1**). *KLF4* vascular expression has been well described in other species as detailed in the introduction to this thesis. I confirmed the previously described expression patterns for both of these transcription factors at 48hpf. I could not detect any vascular expression of *klf4a* and *biklf/klf4b/klf17* neither in WT nor in *klf2a* mutant embryos at 48hpf. It is possible that the gene X that compensates for the potential loss of *klf2a* function in *klf2a* mutant background exists, but I have not managed to identify it. Despite the initial

negative results, *klf2b* still remains the most likely candidate. A zebrafish-specific member of *KLF* gene family, *klfd* could represent another candidate (**Figure 6.1**) (Oates, Pratt et al. 2001). *klfd* is highly expressed in haematopoietic system of developing zebrafish embryo and plays a role in embryonic zebrafish α -globin synthesis (Oates, Pratt et al. 2001; Fu, Du et al. 2009). *klfd* could therefore compensate for some *klf2a* functions related to HSC development (Oates, Pratt et al. 2001; Wang, Zhang et al. 2011). To my knowledge *klfd* vascular expression has not been described.

It is also possible that *klf2a* mutants retain functions that might be not mediated by the 3 tandem zinc fingers of the Klf2a protein, but rather by the N-terminal part of the Klf2a protein that is not affected by the induced mutation. To confirm these conclusions a total knockout of *klf2a* would be required in order to establish whether or not there is residual *klf2a* function in the *klf2a* mutant alleles I examined.

Alternatively it is possible that zebrafish possess an as yet unidentified mechanism by which they are able to compensate for the loss of function of a single gene. If I had more time, I would perform RNA sequencing profile in *klf2a* mutant and WT embryos thus comparing the transcriptomes of both groups. I am sure that this would shed more light into the functions of *klf2a* in zebrafish in general and also help in identifying candidate genes that could compensate for the potential loss of *klf2a* function in *klf2a* mutants if such gene(s) exist.

Overall, the most important scientific question of this project remains the discrepancy between the phenotypes observed by other research groups and by myself achieved by MO-mediated *klf2a* knockdown and the phenotype (or the lack of one) observed in the *klf2a* mutant line so far. I have therefore briefly summarised both main approaches in reverse genetics studies currently used – the morpholino antisense technology and the more novel approaches including TALENs and CRISPR/Cas9 system. This is

followed by recommendations for future reverse genetics studies in zebrafish based on the experience I have gained during this project.

Morpholino oligonucleotides have been introduced to zebrafish research in 2000 (Nasevicius and Ekker 2000) and in following years became the most widely used tool for reverse genetics studies in zebrafish. Their use is not without potential caveats however. Off-target effects of MOs have been well described (Eisen and Smith 2008; Bill, Petzold et al. 2009). Off-target effect means that the MO inhibits the function of an irrelevant gene instead of, or in addition to the intended gene. This might also relate to the fact the amount of MO typically injected into the 1-cell stage embryo (1ng) is in a vast molar excess (approx. 2×10^4 -fold) to the amount of available target mRNA so the likelihood of binding other RNA is rather high (Schulte-Merker and Stainier 2014). A very common off-target effect is activation of p53-induced apoptosis observed in 15-20% of all MOs (Robu, Larson et al. 2007). Some researchers have therefore used the *p53* MO in addition to the MO against the gene of interest. The interpretation of a gene knockdown phenotype in a p53-deficient background might be difficult though (Schulte-Merker and Stainier 2014). One method to distinguish between an off-target and a specific MO effect is the usage of two non-overlapping MOs against the same gene. Both of them might be causing an off-target effect, but the chance of the two off-target effects being the same is considerably lower (Eisen and Smith 2008). There are also other ways how to distinguish between off-target and specific MOs effects such as co-injection of 2 MOs at low levels or a rescue experiment with synthetic mRNA encoding the protein from the targeted locus (Eisen and Smith 2008). With the advent of new genome editing technologies (ZFNs, TALENs and CRISPR/Cas9) a generation of several mutant zebrafish lines has been described in which – similarly to the *klf2a* – the phenotype observed in MO knockdown studies could not be reproduced in the mutants (van Impel, Zhao et al. 2014). This means that any future report of a 'gene-specific' knockdown based solely on MO knockdown should be viewed very critically

(Schulte-Merker and Stainier 2014). On the other hand, there are examples of morpholinos that work very well and appear to work specifically, such as the *tnnt2* MO I used in this project. Even in the times of CRISPR/Cas9 systems, morpholinos are still the easiest, quickest and cheapest method for gene knockdown studies in zebrafish.

The novel techniques for site-specific mutagenesis, especially TALENs and CRISPR/Cas9 have only become available for the wide research community in recent years (Cermak, Doyle et al. 2011; Hwang, Fu et al. 2013). These platforms enable generation of capped mRNA constructs within two weeks (TALENs) or even within one week in case of CRISPR/Cas9 that can be injected to zebrafish embryos. TALENs and CRISPR/Cas9 systems have certain common features. They use constructs which consist of specific sequences that bind to genomic region of interest (TAL effectors in TALENs or gRNA in CRISPR/Cas9) and of an endonuclease – dimeric Fok1 in case of TALENs and monomeric Cas9 in case of CRISPR/Cas9. These constructs cause double stranded DNA breakdowns which get repaired by error-prone non-homologous end joining (NHEJ) resulting in genomic mutations (Cermak, Doyle et al. 2011; Hwang, Fu et al. 2013). The current opinion is that TALENs and CRISPR/Cas9 systems do have only minimal off-target effects in comparison to morpholinos (Hruscha, Krawitz et al. 2013) although non-specific binding has been described in both platforms (Reyon, Tsai et al. 2012; Fu, Sander et al. 2014). The numerous candidate cleavage sites available for both platforms enable generation of multiple mutant alleles for genes studied. This means that we can study and compare the phenotypes of different mutant alleles and thus gain more information about the functional domains of the protein coded by the studied gene. On the other hand the process of generating a stable mutant line is, and will always be quite time consuming. Although some TALEN and CRISPR/Cas9 constructs are reported to be efficient enough to cause phenotypes in F0 generation of fish, these will inevitably be mosaics for induced mutations and are likely to contain different mutations in different cell populations. This can make interpretation of the

phenotypes difficult. To overcome this one would need to wait for the F1 generation to reach sexual maturity which will be 4-6 months at best. In the case of a need for a maternal mutant (F3 generation) this will be even 2-3 months longer. Thirdly the recent experience of our group with generating CRISPR/Cas9 constructs is that by far not all constructs do work as expected for various and yet unknown reasons.

Based on the above considerations if one was to study a function of a zebrafish gene using methods of reverse genetics my recommendations would be following: A method of choice based on local expertise and experience - either TALENs or CRISPR/Cas9 systems should be employed to generate several mutant alleles in different genomic sites of the gene studied. This would be based - if known - on the existence of any functional domains in the studied gene. Additionally, given the partial genome duplication in zebrafish, the generation of a mutant for a paralog gene should be attempted at the same time. Simultaneously a pair of morpholinos, ideally those which interfere with pre-mRNA splicing should be obtained and injected using all standard controls. The phenotypes observed in the mutants should be compared with the ones observed in the morpholino morphants. If there is concordance, the morpholino can be used for further studies due to easier manipulation and possibility to inject into transgenic lines of choice. If there is discrepancy the interpretation of the phenotypes becomes more difficult and there is currently no clear answer to this question. The next step I suggest is to study the phenotype of the double mutant line generated by an incross of mutant lines for both paralog genes. I suspect however that the gene redundancy won't be an answer to all the differences between morphants and mutants and only the future will bring a definitive answer to this issue.

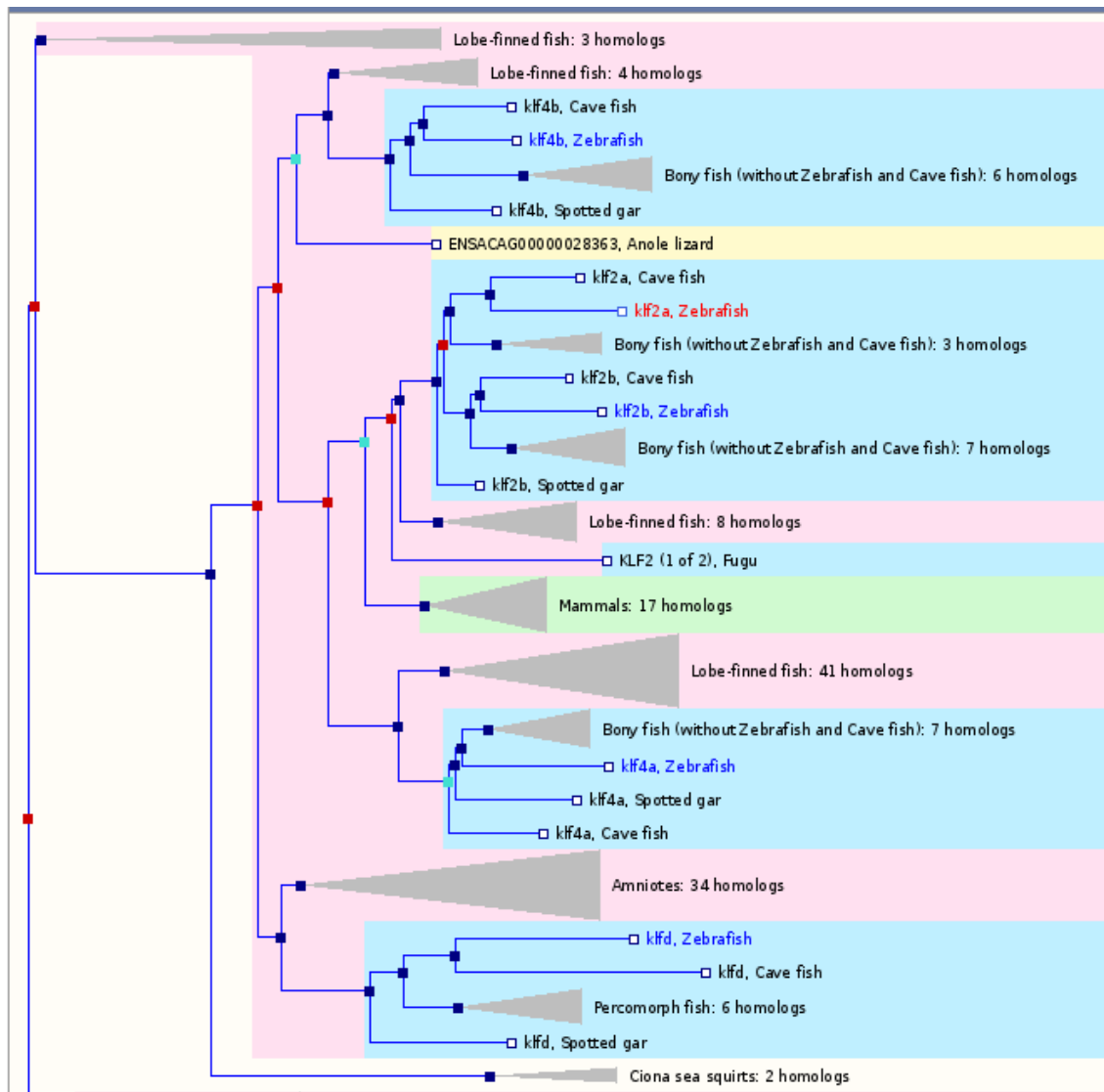


Figure 6.1 Gene tree showing phylogenetic relations of zebrafish *klf2a*

Zebrafish *klf2a* gene (in red) is most closely related to its zebrafish paralog *klf2b* as far as zebrafish genes concerned. Other closely related zebrafish genes are *klf4a* and *klf4b* (now renamed to *biklf/klf17*) and a zebrafish-specific member of *KLF* gene family *klfd*. Zebrafish genes are in blue. Genes from other species are in black. Adapted from Ensembl (<http://www.ensembl.org/index.html>).

Chapter 7 References

- Ait-Oufella, H., B. L. Salomon, et al. (2006). "Natural regulatory T cells control the development of atherosclerosis in mice." *Nat Med* **12**(2): 178-180.
- Ali, F., S. S. Hamdulay, et al. (2007). "Statin-mediated cytoprotection of human vascular endothelial cells: a role for Kruppel-like factor 2-dependent induction of heme oxygenase-1." *J Thromb Haemost* **5**(12): 2537-2546.
- Allen, K. L., A. Hamik, et al. (2011). "Endothelial cell activation by antiphospholipid antibodies is modulated by Kruppel-like transcription factors." *Blood* **117**(23): 6383-6391.
- Anderson, K. P., C. B. Kern, et al. (1995). "Isolation of a gene encoding a functional zinc finger protein homologous to erythroid Kruppel-like factor: identification of a new multigene family." *Mol Cell Biol* **15**(11): 5957-5965.
- Andersson, E. R., R. Sandberg, et al. (2011). "Notch signaling: simplicity in design, versatility in function." *Development* **138**(17): 3593-3612.
- Ando, J. and K. Yamamoto (2009). "Vascular mechanobiology: endothelial cell responses to fluid shear stress." *Circ J* **73**(11): 1983-1992.
- Ang, S. O., H. Chen, et al. (2002). "Disruption of oxygen homeostasis underlies congenital Chuvash polycythemia." *Nat Genet* **32**(4): 614-621.
- Arai, M., T. Ohashi, et al. (1998). "Human T-cell leukemia virus type 1 Tax protein induces the expression of lymphocyte chemoattractant SDF-1/PBSF." *Virology* **241**(2): 298-303.
- Armstrong, E. J. and J. Bischoff (2004). "Heart valve development: endothelial cell signaling and differentiation." *Circ Res* **95**(5): 459-470.
- Asahara, T., T. Murohara, et al. (1997). "Isolation of putative progenitor endothelial cells for angiogenesis." *Science* **275**(5302): 964-967.
- Atkins, G. B., Y. Wang, et al. (2008). "Hemizygous deficiency of Kruppel-like factor 2 augments experimental atherosclerosis." *Circ Res* **103**(7): 690-693.
- Banerjee, S. S., M. W. Feinberg, et al. (2003). "The Kruppel-like factor KLF2 inhibits peroxisome proliferator-activated receptor-gamma expression and adipogenesis." *J Biol Chem* **278**(4): 2581-2584.
- Barrionuevo, W. R. and W. W. Burggren (1999). "O₂ consumption and heart rate in developing zebrafish (*Danio rerio*): influence of temperature and ambient O₂." *Am J Physiol* **276**(2 Pt 2): R505-513.
- Bartel, D. P. (2004). "MicroRNAs: genomics, biogenesis, mechanism, and function." *Cell* **116**(2): 281-297.
- Bartel, D. P. (2009). "MicroRNAs: target recognition and regulatory functions." *Cell* **136**(2): 215-233.
- Baur, J. A. and D. A. Sinclair (2006). "Therapeutic potential of resveratrol: the in vivo evidence." *Nat Rev Drug Discov* **5**(6): 493-506.
- Bellosta, S., N. Ferri, et al. (2000). "Non-lipid-related effects of statins." *Ann Med* **32**(3): 164-176.
- Berk, B. C., J. I. Abe, et al. (2001). "Endothelial atheroprotective and anti-inflammatory mechanisms." *Ann N Y Acad Sci* **947**: 93-109; discussion 109-111.
- Bhattacharya, R., S. Senbanerjee, et al. (2005). "Inhibition of vascular permeability factor/vascular endothelial growth factor-mediated angiogenesis by the Kruppel-like factor KLF2." *J Biol Chem* **280**(32): 28848-28851.
- Bieker, J. J. (2001). "Kruppel-like factors: three fingers in many pies." *J Biol Chem* **276**(37): 34355-34358.

- Bill, B. R., A. M. Petzold, et al. (2009). "A primer for morpholino use in zebrafish." Zebrafish **6**(1): 69-77.
- Bleul, C. C., M. Farzan, et al. (1996). "The lymphocyte chemoattractant SDF-1 is a ligand for LESTR/fusin and blocks HIV-1 entry." Nature **382**(6594): 829-833.
- Blum, Y., H. G. Belting, et al. (2008). "Complex cell rearrangements during intersegmental vessel sprouting and vessel fusion in the zebrafish embryo." Dev Biol **316**(2): 312-322.
- Boch, J., H. Scholze, et al. (2009). "Breaking the code of DNA binding specificity of TAL-type III effectors." Science **326**(5959): 1509-1512.
- Bogdanove, A. J., S. Schornack, et al. (2010). "TAL effectors: finding plant genes for disease and defense." Curr Opin Plant Biol **13**(4): 394-401.
- Bonauer, A., G. Carmona, et al. (2009). "MicroRNA-92a controls angiogenesis and functional recovery of ischemic tissues in mice." Science **324**(5935): 1710-1713.
- Boon, R. A., J. O. Fledderus, et al. (2007). "KLF2 suppresses TGF-beta signaling in endothelium through induction of Smad7 and inhibition of AP-1." Arterioscler Thromb Vasc Biol **27**(3): 532-539.
- Boon, R. A., T. A. Leyen, et al. (2010). "KLF2-induced actin shear fibers control both alignment to flow and JNK signaling in vascular endothelium." Blood **115**(12): 2533-2542.
- Boon, R. A., C. Urbich, et al. (2011). "Kruppel-like factor 2 improves neovascularization capacity of aged proangiogenic cells." Eur Heart J **32**(3): 371-377.
- Brouard, S., L. E. Otterbein, et al. (2000). "Carbon monoxide generated by heme oxygenase 1 suppresses endothelial cell apoptosis." J Exp Med **192**(7): 1015-1026.
- Brunt, K. R., K. K. Fenrich, et al. (2006). "Protection of human vascular smooth muscle cells from H₂O₂-induced apoptosis through functional codependence between HO-1 and AKT." Arterioscler Thromb Vasc Biol **26**(9): 2027-2034.
- Bu, D. X., M. Tarrío, et al. (2010). "Statin-induced Kruppel-like factor 2 expression in human and mouse T cells reduces inflammatory and pathogenic responses." J Clin Invest **120**(6): 1961-1970.
- Buckley, A. F., C. T. Kuo, et al. (2001). "Transcription factor LKLF is sufficient to program T cell quiescence via a c-Myc--dependent pathway." Nat Immunol **2**(8): 698-704.
- Busse, R., G. Trogisch, et al. (1985). "The role of endothelium in the control of vascular tone." Basic Res Cardiol **80**(5): 475-490.
- Bussmann, J. and S. Schulte-Merker (2011). "Rapid BAC selection for tol2-mediated transgenesis in zebrafish." Development **138**(19): 4327-4332.
- Carlson, C. M., B. T. Endrizzi, et al. (2006). "Kruppel-like factor 2 regulates thymocyte and T-cell migration." Nature **442**(7100): 299-302.
- Cau, E. and P. Blader (2009). "Notch activity in the nervous system: to switch or not switch?" Neural Dev **4**: 36.
- Cermak, T., E. L. Doyle, et al. (2011). "Efficient design and assembly of custom TALEN and other TAL effector-based constructs for DNA targeting." Nucleic Acids Res **39**(12): e82.
- Chakroborty, D., C. Sarkar, et al. (2011). "Dopamine stabilizes tumor blood vessels by up-regulating angiopoietin 1 expression in pericytes and Kruppel-like factor-2 expression in tumor endothelial cells." Proc Natl Acad Sci U S A **108**(51): 20730-20735.
- Chauhan, S. D., H. Nilsson, et al. (2003). "Release of C-type natriuretic peptide accounts for the biological activity of endothelium-derived hyperpolarizing factor." Proc Natl Acad Sci U S A **100**(3): 1426-1431.
- Chekulaeva, M. and W. Filipowicz (2009). "Mechanisms of miRNA-mediated post-transcriptional regulation in animal cells." Curr Opin Cell Biol **21**(3): 452-460.
- Chen, J. N., P. Haffter, et al. (1996). "Mutations affecting the cardiovascular system and other internal organs in zebrafish." Development **123**: 293-302.

- Chico, T. J., P. W. Ingham, et al. (2008). "Modeling cardiovascular disease in the zebrafish." *Trends Cardiovasc Med* **18**(4): 150-155.
- Chiplunkar, A. R., T. K. Lung, et al. (2013). "Kruppel-like factor 2 is required for normal mouse cardiac development." *PLoS One* **8**(2): e54891.
- Clifton, J. D., E. Lucumi, et al. (2010). "Identification of novel inhibitors of dietary lipid absorption using zebrafish." *PLoS One* **5**(8): e12386.
- Conkright, M. D., M. A. Wani, et al. (2001). "Lung Kruppel-like factor contains an autoinhibitory domain that regulates its transcriptional activation by binding WWP1, an E3 ubiquitin ligase." *J Biol Chem* **276**(31): 29299-29306.
- D'Souza, B., L. Meloty-Kapella, et al. (2010). "Canonical and non-canonical Notch ligands." *Curr Top Dev Biol* **92**: 73-129.
- Das, H., A. Kumar, et al. (2006). "Kruppel-like factor 2 (KLF2) regulates proinflammatory activation of monocytes." *Proc Natl Acad Sci U S A* **103**(17): 6653-6658.
- Davies, P. F. (1997). "Overview: temporal and spatial relationships in shear stress-mediated endothelial signalling." *J Vasc Res* **34**(3): 208-211.
- Davies, P. F. (2009). "Hemodynamic shear stress and the endothelium in cardiovascular pathophysiology." *Nat Clin Pract Cardiovasc Med* **6**(1): 16-26.
- Davies, P. F., K. A. Barbee, et al. (1997). "Spatial relationships in early signaling events of flow-mediated endothelial mechanotransduction." *Annu Rev Physiol* **59**: 527-549.
- De Caterina, R., P. Libby, et al. (1995). "Nitric oxide decreases cytokine-induced endothelial activation. Nitric oxide selectively reduces endothelial expression of adhesion molecules and proinflammatory cytokines." *J Clin Invest* **96**(1): 60-68.
- De Martin, R., M. Hoeth, et al. (2000). "The transcription factor NF-kappa B and the regulation of vascular cell function." *Arterioscler Thromb Vasc Biol* **20**(11): E83-88.
- De, S., O. Razorenova, et al. (2005). "VEGF-integrin interplay controls tumor growth and vascularization." *Proc Natl Acad Sci U S A* **102**(21): 7589-7594.
- Dekker, R. J., R. A. Boon, et al. (2006). "KLF2 provokes a gene expression pattern that establishes functional quiescent differentiation of the endothelium." *Blood* **107**(11): 4354-4363.
- Dekker, R. J., S. van Soest, et al. (2002). "Prolonged fluid shear stress induces a distinct set of endothelial cell genes, most specifically lung Kruppel-like factor (KLF2)." *Blood* **100**(5): 1689-1698.
- Dekker, R. J., J. V. van Thienen, et al. (2005). "Endothelial KLF2 links local arterial shear stress levels to the expression of vascular tone-regulating genes." *Am J Pathol* **167**(2): 609-618.
- dela Paz, N. G., T. E. Walshe, et al. (2012). "Role of shear-stress-induced VEGF expression in endothelial cell survival." *J Cell Sci* **125**(Pt 4): 831-843.
- Drexler, H. and B. Hornig (1999). "Endothelial dysfunction in human disease." *J Mol Cell Cardiol* **31**(1): 51-60.
- Egorova, A. D., M. C. DeRuiter, et al. (2012). "Endothelial colony-forming cells show a mature transcriptional response to shear stress." *In Vitro Cell Dev Biol Anim* **48**(1): 21-29.
- Egorova, A. D., K. Van der Heiden, et al. (2011). "Tgfbeta/Alk5 signaling is required for shear stress induced klf2 expression in embryonic endothelial cells." *Dev Dyn* **240**(7): 1670-1680.
- Eisen, J. S. and J. C. Smith (2008). "Controlling morpholino experiments: don't stop making antisense." *Development* **135**(10): 1735-1743.
- Engler, C., R. Gruetzner, et al. (2009). "Golden gate shuffling: a one-pot DNA shuffling method based on type IIs restriction enzymes." *PLoS One* **4**(5): e5553.
- Engler, C., R. Kandzia, et al. (2008). "A one pot, one step, precision cloning method with high throughput capability." *PLoS One* **3**(11): e3647.

- Ferrara, N., H. P. Gerber, et al. (2003). "The biology of VEGF and its receptors." *Nat Med* **9**(6): 669-676.
- Fledderus, J. O., R. A. Boon, et al. (2008). "KLF2 primes the antioxidant transcription factor Nrf2 for activation in endothelial cells." *Arterioscler Thromb Vasc Biol* **28**(7): 1339-1346.
- Fledderus, J. O., J. V. van Thienen, et al. (2007). "Prolonged shear stress and KLF2 suppress constitutive proinflammatory transcription through inhibition of ATF2." *Blood* **109**(10): 4249-4257.
- Folkman, J. and C. Haudenschild (1980). "Angiogenesis in vitro." *Nature* **288**(5791): 551-556.
- Fu, Y., J. D. Sander, et al. (2014). "Improving CRISPR-Cas nuclease specificity using truncated guide RNAs." *Nat Biotechnol* **32**(3): 279-284.
- Fu, Y. F., T. T. Du, et al. (2009). "Mir-144 selectively regulates embryonic alpha-hemoglobin synthesis during primitive erythropoiesis." *Blood* **113**(6): 1340-1349.
- Fukuhara, S., K. Sako, et al. (2008). "Differential function of Tie2 at cell-cell contacts and cell-substratum contacts regulated by angiopoietin-1." *Nat Cell Biol* **10**(5): 513-526.
- Fukumura, D., D. G. Duda, et al. (2010). "Tumor microvasculature and microenvironment: novel insights through intravital imaging in pre-clinical models." *Microcirculation* **17**(3): 206-225.
- Gardiner, M. R., D. F. Daggett, et al. (2005). "Zebrafish KLF4 is essential for anterior mesendoderm/pre-polyester differentiation and hatching." *Dev Dyn* **234**(4): 992-996.
- Gardiner, M. R., M. M. Gongora, et al. (2007). "A global role for zebrafish klf4 in embryonic erythropoiesis." *Mech Dev* **124**(9-10): 762-774.
- Ghysen, A. and C. Dambly-Chaudiere (2004). "Development of the zebrafish lateral line." *Curr Opin Neurobiol* **14**(1): 67-73.
- Gimbrone, M. A., Jr. (1999). "Endothelial dysfunction, hemodynamic forces, and atherosclerosis." *Thromb Haemost* **82**(2): 722-726.
- Gleadle, J. M., B. L. Ebert, et al. (1995). "Regulation of angiogenic growth factor expression by hypoxia, transition metals, and chelating agents." *Am J Physiol* **268**(6 Pt 1): C1362-1368.
- Goerdt, S. and C. E. Orfanos (1999). "Other functions, other genes: alternative activation of antigen-presenting cells." *Immunity* **10**(2): 137-142.
- Gracia-Sancho, J., H. Garcia-Caldero, et al. (2013). "Simvastatin maintains function and viability of steatotic rat livers procured for transplantation." *J Hepatol* **58**(6): 1140-1146.
- Gracia-Sancho, J., L. Russo, et al. (2011). "Endothelial expression of transcription factor Kruppel-like factor 2 and its vasoprotective target genes in the normal and cirrhotic rat liver." *Gut* **60**(4): 517-524.
- Gracia-Sancho, J., G. Villarreal, Jr., et al. (2010). "Activation of SIRT1 by resveratrol induces KLF2 expression conferring an endothelial vasoprotective phenotype." *Cardiovasc Res* **85**(3): 514-519.
- Gray, C., I. M. Packham, et al. (2007). "Ischemia is not required for arteriogenesis in zebrafish embryos." *Arterioscler Thromb Vasc Biol* **27**(10): 2135-2141.
- Gridley, T. (2010). "Notch signaling in the vasculature." *Curr Top Dev Biol* **92**: 277-309.
- Gu, H. and B. G. Neel (2003). "The "Gab" in signal transduction." *Trends Cell Biol* **13**(3): 122-130.
- Haase, V. H. (2005). "The VHL tumor suppressor in development and disease: functional studies in mice by conditional gene targeting." *Semin Cell Dev Biol* **16**(4-5): 564-574.
- Hamik, A., Z. Lin, et al. (2007). "Kruppel-like factor 4 regulates endothelial inflammation." *J Biol Chem* **282**(18): 13769-13779.
- Hamzah, J., M. Jugold, et al. (2008). "Vascular normalization in Rgs5-deficient tumours promotes immune destruction." *Nature* **453**(7193): 410-414.

- Hanahan, D. and J. Folkman (1996). "Patterns and emerging mechanisms of the angiogenic switch during tumorigenesis." *Cell* **86**(3): 353-364.
- Harvey, S. A., I. Sealy, et al. (2013). "Identification of the zebrafish maternal and paternal transcriptomes." *Development* **140**(13): 2703-2710.
- Hay, N. and N. Sonenberg (2004). "Upstream and downstream of mTOR." *Genes Dev* **18**(16): 1926-1945.
- Heitzler, P. (2010). "Biodiversity and noncanonical Notch signaling." *Curr Top Dev Biol* **92**: 457-481.
- Helbing, T., R. Rothweiler, et al. (2011). "BMP activity controlled by BMPER regulates the proinflammatory phenotype of endothelium." *Blood* **118**(18): 5040-5049.
- Hergenreider, E., S. Heydt, et al. (2012). "Atheroprotective communication between endothelial cells and smooth muscle cells through miRNAs." *Nat Cell Biol* **14**(3): 249-256.
- Hewamadduma, C. A., A. J. Grierson, et al. (2013). "Tardbp splicing rescues motor neuron and axonal development in a mutant tardbp zebrafish." *Hum Mol Genet* **22**(12): 2376-2386.
- Hierck, B. P., K. Van der Heiden, et al. (2008). "Primary cilia sensitize endothelial cells for fluid shear stress." *Dev Dyn* **237**(3): 725-735.
- Higuchi, K., Y. Nakaoka, et al. (2012). "Endothelial Gab1 deletion accelerates angiotensin II-dependent vascular inflammation and atherosclerosis in apolipoprotein E knockout mice." *Circ J* **76**(8): 2031-2040.
- Hogan, B. M., F. L. Bos, et al. (2009). "Ccbe1 is required for embryonic lymphangiogenesis and venous sprouting." *Nat Genet* **41**(4): 396-398.
- Hruscha, A., P. Krawitz, et al. (2013). "Efficient CRISPR/Cas9 genome editing with low off-target effects in zebrafish." *Development* **140**(24): 4982-4987.
- Huddleson, J. P., N. Ahmad, et al. (2006). "Up-regulation of the KLF2 transcription factor by fluid shear stress requires nucleolin." *J Biol Chem* **281**(22): 15121-15128.
- Huddleson, J. P., N. Ahmad, et al. (2005). "Induction of KLF2 by fluid shear stress requires a novel promoter element activated by a phosphatidylinositol 3-kinase-dependent chromatin-remodeling pathway." *J Biol Chem* **280**(24): 23371-23379.
- Huddleson, J. P., S. Srinivasan, et al. (2004). "Fluid shear stress induces endothelial KLF2 gene expression through a defined promoter region." *Biol Chem* **385**(8): 723-729.
- Hwang, W. Y., Y. Fu, et al. (2013). "Efficient genome editing in zebrafish using a CRISPR-Cas system." *Nat Biotechnol* **31**(3): 227-229.
- Iomini, C., K. Tejada, et al. (2004). "Primary cilia of human endothelial cells disassemble under laminar shear stress." *J Cell Biol* **164**(6): 811-817.
- Jain, R. K. (2005). "Normalization of tumor vasculature: an emerging concept in antiangiogenic therapy." *Science* **307**(5706): 58-62.
- Jin, H. K., S. H. Ahn, et al. (2009). "Rapamycin down-regulates inducible nitric oxide synthase by inducing proteasomal degradation." *Biol Pharm Bull* **32**(6): 988-992.
- Jing, L. and L. I. Zon (2011). "Zebrafish as a model for normal and malignant hematopoiesis." *Dis Model Mech* **4**(4): 433-438.
- Just, S., I. M. Berger, et al. (2011). "Protein kinase D2 controls cardiac valve formation in zebrafish by regulating histone deacetylase 5 activity." *Circulation* **124**(3): 324-334.
- Kaelin, W. G. (2005). "Proline hydroxylation and gene expression." *Annu Rev Biochem* **74**: 115-128.
- Kaelin, W. G. (2005). "The von Hippel-Lindau tumor suppressor protein: roles in cancer and oxygen sensing." *Cold Spring Harb Symp Quant Biol* **70**: 159-166.

- Kalev-Zylinska, M. L., J. A. Horsfield, et al. (2002). "Runx1 is required for zebrafish blood and vessel development and expression of a human RUNX1-CBF2T1 transgene advances a model for studies of leukemogenesis." *Development* **129**(8): 2015-2030.
- Kaminski, A., C. B. Pohl, et al. (2004). "Up-regulation of endothelial nitric oxide synthase inhibits pulmonary leukocyte migration following lung ischemia-reperfusion in mice." *Am J Pathol* **164**(6): 2241-2249.
- Kane, D. A. and C. B. Kimmel (1993). "The zebrafish midblastula transition." *Development* **119**(2): 447-456.
- Katz, J. P., N. Perreault, et al. (2005). "Loss of Klf4 in mice causes altered proliferation and differentiation and precancerous changes in the adult stomach." *Gastroenterology* **128**(4): 935-945.
- Katz, J. P., N. Perreault, et al. (2002). "The zinc-finger transcription factor Klf4 is required for terminal differentiation of goblet cells in the colon." *Development* **129**(11): 2619-2628.
- Kaunas, R., S. Usami, et al. (2006). "Regulation of stretch-induced JNK activation by stress fiber orientation." *Cell Signal* **18**(11): 1924-1931.
- Kawahara, A. and I. B. Dawid (2001). "Critical role of biklf in erythroid cell differentiation in zebrafish." *Curr Biol* **11**(17): 1353-1357.
- Kawanami, D., G. H. Mahabeleshwar, et al. (2009). "Kruppel-like factor 2 inhibits hypoxia-inducible factor 1alpha expression and function in the endothelium." *J Biol Chem* **284**(31): 20522-20530.
- Kettleborough, R. N., E. M. Busch-Nentwich, et al. (2013). "A systematic genome-wide analysis of zebrafish protein-coding gene function." *Nature* **496**(7446): 494-497.
- Kietzmann, T., U. Roth, et al. (1999). "Induction of the plasminogen activator inhibitor-1 gene expression by mild hypoxia via a hypoxia response element binding the hypoxia-inducible factor-1 in rat hepatocytes." *Blood* **94**(12): 4177-4185.
- Kim, C. H. and H. E. Broxmeyer (1999). "Chemokines: signal lamps for trafficking of T and B cells for development and effector function." *J Leukoc Biol* **65**(1): 6-15.
- Kim, D. W., B. L. Langille, et al. (1989). "Patterns of endothelial microfilament distribution in the rabbit aorta in situ." *Circ Res* **64**(1): 21-31.
- Kim, I., S. O. Moon, et al. (2001). "Vascular endothelial growth factor expression of intercellular adhesion molecule 1 (ICAM-1), vascular cell adhesion molecule 1 (VCAM-1), and E-selectin through nuclear factor-kappa B activation in endothelial cells." *J Biol Chem* **276**(10): 7614-7620.
- Kimmel, C. B., W. W. Ballard, et al. (1995). "Stages of embryonic development of the zebrafish." *Dev Dyn* **203**(3): 253-310.
- Kinderlerer, A. R., F. Ali, et al. (2008). "KLF2-dependent, shear stress-induced expression of CD59: a novel cytoprotective mechanism against complement-mediated injury in the vasculature." *J Biol Chem* **283**(21): 14636-14644.
- Klevit, R. E. (1991). "Recognition of DNA by Cys2,His2 zinc fingers." *Science* **253**(5026): 1367, 1393.
- Knaut, H., C. Werz, et al. (2003). "A zebrafish homologue of the chemokine receptor Cxcr4 is a germ-cell guidance receptor." *Nature* **421**(6920): 279-282.
- Kobus, K., J. Kopycinska, et al. (2012). "Angiogenesis within the duodenum of patients with cirrhosis is modulated by mechanosensitive Kruppel-like factor 2 and microRNA-126." *Liver Int* **32**(8): 1222-1232.
- Kotkamp, K., R. Mossner, et al. (2014). "A Pou5f1/Oct4 dependent Klf2a, Klf2b, and Klf17 regulatory sub-network contributes to EVL and ectoderm development during zebrafish embryogenesis." *Dev Biol* **385**(2): 433-447.
- Kracht, M. and J. Saklatvala (2002). "Transcriptional and post-transcriptional control of gene expression in inflammation." *Cytokine* **20**(3): 91-106.

- Kryczek, I., A. Lange, et al. (2005). "CXCL12 and vascular endothelial growth factor synergistically induce neoangiogenesis in human ovarian cancers." *Cancer Res* **65**(2): 465-472.
- Kumar, A., T. A. Hoffman, et al. (2009). "Transcriptional repression of Kruppel like factor-2 by the adaptor protein p66shc." *FASEB J* **23**(12): 4344-4352.
- Kumar, A., C. S. Kim, et al. (2011). "p53 impairs endothelial function by transcriptionally repressing Kruppel-Like Factor 2." *Arterioscler Thromb Vasc Biol* **31**(1): 133-141.
- Kumar, A., S. Kumar, et al. (2013). "Histone and DNA methylation-mediated epigenetic downregulation of endothelial Kruppel-like factor 2 by low-density lipoprotein cholesterol." *Arterioscler Thromb Vasc Biol* **33**(8): 1936-1942.
- Kumar, A., Z. Lin, et al. (2005). "Tumor necrosis factor alpha-mediated reduction of KLF2 is due to inhibition of MEF2 by NF-kappaB and histone deacetylases." *Mol Cell Biol* **25**(14): 5893-5903.
- Kuo, C. T., M. L. Veselits, et al. (1997). "The LKLF transcription factor is required for normal tunica media formation and blood vessel stabilization during murine embryogenesis." *Genes Dev* **11**(22): 2996-3006.
- Kuo, C. T., M. L. Veselits, et al. (1997). "LKLF: A transcriptional regulator of single-positive T cell quiescence and survival." *Science* **277**(5334): 1986-1990.
- Kwak, B. R., F. Mulhaupt, et al. (2002). "Altered pattern of vascular connexin expression in atherosclerotic plaques." *Arterioscler Thromb Vasc Biol* **22**(2): 225-230.
- Kyaw, T., C. Tay, et al. (2011). "B1a B lymphocytes are atheroprotective by secreting natural IgM that increases IgM deposits and reduces necrotic cores in atherosclerotic lesions." *Circ Res* **109**(8): 830-840.
- Kyaw, T., A. Winship, et al. (2013). "Cytotoxic and proinflammatory CD8+ T lymphocytes promote development of vulnerable atherosclerotic plaques in apoE-deficient mice." *Circulation* **127**(9): 1028-1039.
- Lawson, N. D., A. M. Vogel, et al. (2002). "sonic hedgehog and vascular endothelial growth factor act upstream of the Notch pathway during arterial endothelial differentiation." *Dev Cell* **3**(1): 127-136.
- Lawson, N. D. and B. M. Weinstein (2002). "In vivo imaging of embryonic vascular development using transgenic zebrafish." *Dev Biol* **248**(2): 307-318.
- Lee, D. Y., C. I. Lee, et al. (2012). "Role of histone deacetylases in transcription factor regulation and cell cycle modulation in endothelial cells in response to disturbed flow." *Proc Natl Acad Sci U S A* **109**(6): 1967-1972.
- Lee, H. Y., S. W. Youn, et al. (2013). "FOXO1 impairs whereas statin protects endothelial function in diabetes through reciprocal regulation of Kruppel-like factor 2." *Cardiovasc Res* **97**(1): 143-152.
- Lee, H. Y., S. W. Youn, et al. (2012). "Kruppel-like factor 2 suppression by high glucose as a possible mechanism of diabetic vasculopathy." *Korean Circ J* **42**(4): 239-245.
- Lee, J. S., Q. Yu, et al. (2006). "Klf2 is an essential regulator of vascular hemodynamic forces in vivo." *Dev Cell* **11**(6): 845-857.
- Leslie, J. D., L. Ariza-McNaughton, et al. (2007). "Endothelial signalling by the Notch ligand Delta-like 4 restricts angiogenesis." *Development* **134**(5): 839-844.
- Leung, D. W., G. Cachianes, et al. (1989). "Vascular endothelial growth factor is a secreted angiogenic mitogen." *Science* **246**(4935): 1306-1309.
- Levine, A. J. (1997). "p53, the cellular gatekeeper for growth and division." *Cell* **88**(3): 323-331.
- Li, I. C., C. T. Chan, et al. (2011). "Zebrafish kruppel-like factor 4a represses intestinal cell proliferation and promotes differentiation of intestinal cell lineages." *PLoS One* **6**(6): e20974.

- Li, M., X. Wang, et al. (2011). "CD4+CD25+Foxp3+ regulatory T cells protect endothelial function impaired by oxidized low density lipoprotein via the KLF-2 transcription factor." Cell Physiol Biochem **28**(4): 639-648.
- Libby, P. (2002). "Inflammation in atherosclerosis." Nature **420**(6917): 868-874.
- Lin, Z., A. Hamik, et al. (2006). "Kruppel-like factor 2 inhibits protease activated receptor-1 expression and thrombin-mediated endothelial activation." Arterioscler Thromb Vasc Biol **26**(5): 1185-1189.
- Lin, Z., A. Kumar, et al. (2005). "Kruppel-like factor 2 (KLF2) regulates endothelial thrombotic function." Circ Res **96**(5): e48-57.
- Lin, Z., V. Natesan, et al. (2010). "Kruppel-like factor 2 regulates endothelial barrier function." Arterioscler Thromb Vasc Biol **30**(10): 1952-1959.
- Lingrel, J. B., R. Pilcher-Roberts, et al. (2012). "Myeloid-specific Kruppel-like factor 2 inactivation increases macrophage and neutrophil adhesion and promotes atherosclerosis." Circ Res **110**(10): 1294-1302.
- Lister, J. A., C. P. Robertson, et al. (1999). "nacre encodes a zebrafish microphthalmia-related protein that regulates neural-crest-derived pigment cell fate." Development **126**(17): 3757-3767.
- Liu, Y., S. R. Cox, et al. (1995). "Hypoxia regulates vascular endothelial growth factor gene expression in endothelial cells. Identification of a 5' enhancer." Circ Res **77**(3): 638-643.
- Luscher, T. F., J. Steffel, et al. (2007). "Drug-eluting stent and coronary thrombosis: biological mechanisms and clinical implications." Circulation **115**(8): 1051-1058.
- Ma, Q., X. Nie, et al. (2012). "Rapamycin regulates the expression and activity of Kruppel-like transcription factor 2 in human umbilical vein endothelial cells." PLoS One **7**(8): e43315.
- Maharaj, A. S. and P. A. D'Amore (2007). "Roles for VEGF in the adult." Microvasc Res **74**(2-3): 100-113.
- Malek, A. M., A. L. Greene, et al. (1993). "Regulation of endothelin 1 gene by fluid shear stress is transcriptionally mediated and independent of protein kinase C and cAMP." Proc Natl Acad Sci U S A **90**(13): 5999-6003.
- Mallat, Z., S. Taleb, et al. (2009). "The role of adaptive T cell immunity in atherosclerosis." J Lipid Res **50** Suppl: S364-369.
- Mammoto, A., T. Mammoto, et al. (2012). "Mechanosensitive mechanisms in transcriptional regulation." J Cell Sci **125**(Pt 13): 3061-3073.
- Mantovani, A., C. Garlanda, et al. (2009). "Macrophage diversity and polarization in atherosclerosis: a question of balance." Arterioscler Thromb Vasc Biol **29**(10): 1419-1423.
- McCormick, S. M., S. G. Eskin, et al. (2001). "DNA microarray reveals changes in gene expression of shear stressed human umbilical vein endothelial cells." Proc Natl Acad Sci U S A **98**(16): 8955-8960.
- McGuinness, B. and P. Passmore (2010). "Can statins prevent or help treat Alzheimer's disease?" J Alzheimers Dis **20**(3): 925-933.
- Meadows, S. M., M. C. Salanga, et al. (2009). "Kruppel-like factor 2 cooperates with the ETS family protein ERG to activate Flk1 expression during vascular development." Development **136**(7): 1115-1125.
- Methe, H., M. Balcells, et al. (2007). "Vascular bed origin dictates flow pattern regulation of endothelial adhesion molecule expression." Am J Physiol Heart Circ Physiol **292**(5): H2167-2175.
- Migliaccio, E., M. Giorgio, et al. (1999). "The p66shc adaptor protein controls oxidative stress response and life span in mammals." Nature **402**(6759): 309-313.

- Miller, I. J. and J. J. Bieker (1993). "A novel, erythroid cell-specific murine transcription factor that binds to the CACCC element and is related to the Kruppel family of nuclear proteins." *Mol Cell Biol* **13**(5): 2776-2786.
- Mor, A., D. Planer, et al. (2007). "Role of naturally occurring CD4+ CD25+ regulatory T cells in experimental atherosclerosis." *Arterioscler Thromb Vasc Biol* **27**(4): 893-900.
- Moscou, M. J. and A. J. Bogdanove (2009). "A simple cipher governs DNA recognition by TAL effectors." *Science* **326**(5959): 1501.
- Muldowney, J. A., 3rd, J. R. Stringham, et al. (2007). "Antiproliferative agents alter vascular plasminogen activator inhibitor-1 expression: a potential prothrombotic mechanism of drug-eluting stents." *Arterioscler Thromb Vasc Biol* **27**(2): 400-406.
- Napoli, C., I. Martin-Padura, et al. (2003). "Deletion of the p66Shc longevity gene reduces systemic and tissue oxidative stress, vascular cell apoptosis, and early atherogenesis in mice fed a high-fat diet." *Proc Natl Acad Sci U S A* **100**(4): 2112-2116.
- Nasevicius, A. and S. C. Ekker (2000). "Effective targeted gene 'knockdown' in zebrafish." *Nat Genet* **26**(2): 216-220.
- Nauli, S. M., Y. Kawanabe, et al. (2008). "Endothelial cilia are fluid shear sensors that regulate calcium signaling and nitric oxide production through polycystin-1." *Circulation* **117**(9): 1161-1171.
- Nicoli, S., C. Standley, et al. (2010). "MicroRNA-mediated integration of haemodynamics and Vegf signalling during angiogenesis." *Nature* **464**(7292): 1196-1200.
- Nie, X. M., L. X. Su, et al. (2013). "Kruppel-like factor 2 might mediate the rapamycin-induced arterial thrombosis in vivo: implications for stent thrombosis in patients." *Chin Med J (Engl)* **126**(14): 2636-2640.
- Novodvorsky, P., M. M. J. Da Costa, et al. (2012). "Zebrafish-based small molecule screens for novel cardiovascular drugs." *Drug Discovery Today: Technologies*(0).
- Oates, A. C., S. J. Pratt, et al. (2001). "The zebrafish klf gene family." *Blood* **98**(6): 1792-1801.
- Oh, H., H. Takagi, et al. (1999). "Hypoxia and vascular endothelial growth factor selectively up-regulate angiopoietin-2 in bovine microvascular endothelial cells." *J Biol Chem* **274**(22): 15732-15739.
- Ohnesorge, N., D. Viemann, et al. (2010). "Erk5 activation elicits a vasoprotective endothelial phenotype via induction of Kruppel-like factor 4 (KLF4)." *J Biol Chem* **285**(34): 26199-26210.
- Otterbein, L. E., B. S. Zuckerbraun, et al. (2003). "Carbon monoxide suppresses arteriosclerotic lesions associated with chronic graft rejection and with balloon injury." *Nat Med* **9**(2): 183-190.
- Pacini, S., M. Pellegrini, et al. (2004). "p66SHC promotes apoptosis and antagonizes mitogenic signaling in T cells." *Mol Cell Biol* **24**(4): 1747-1757.
- Packham, I. M., C. Gray, et al. (2009). "Microarray profiling reveals CXCR4a is downregulated by blood flow in vivo and mediates collateral formation in zebrafish embryos." *Physiol Genomics* **38**(3): 319-327.
- Parmar, K. M., H. B. Larman, et al. (2006). "Integration of flow-dependent endothelial phenotypes by Kruppel-like factor 2." *J Clin Invest* **116**(1): 49-58.
- Parmar, K. M., V. Nambudiri, et al. (2005). "Statins exert endothelial atheroprotective effects via the KLF2 transcription factor." *J Biol Chem* **280**(29): 26714-26719.
- Peal, D. S., R. W. Mills, et al. (2011). "Novel chemical suppressors of long QT syndrome identified by an in vivo functional screen." *Circulation* **123**(1): 23-30.
- Peiser, L. and S. Gordon (2001). "The function of scavenger receptors expressed by macrophages and their role in the regulation of inflammation." *Microbes Infect* **3**(2): 149-159.

- Peled, A., I. Petit, et al. (1999). "Dependence of human stem cell engraftment and repopulation of NOD/SCID mice on CXCR4." *Science* **283**(5403): 845-848.
- Pelster, B. and W. W. Burggren (1996). "Disruption of hemoglobin oxygen transport does not impact oxygen-dependent physiological processes in developing embryos of zebra fish (*Danio rerio*)." *Circ Res* **79**(2): 358-362.
- Perry, H. M., T. P. Bender, et al. (2012). "B cell subsets in atherosclerosis." *Front Immunol* **3**: 373.
- Peters, K. G., C. D. Kontos, et al. (2004). "Functional significance of Tie2 signaling in the adult vasculature." *Recent Prog Horm Res* **59**: 51-71.
- Pfaffl, M. W. (2001). "A new mathematical model for relative quantification in real-time RT-PCR." *Nucleic Acids Res* **29**(9): e45.
- Pfenniger, A., C. Wong, et al. (2012). "Shear stress modulates the expression of the atheroprotective protein Cx37 in endothelial cells." *J Mol Cell Cardiol* **53**(2): 299-309.
- Poelmann, R. E., K. Van der Heiden, et al. (2008). "Deciphering the endothelial shear stress sensor." *Circulation* **117**(9): 1124-1126.
- Quaife, N. M., O. Watson, et al. (2012). "Zebrafish: an emerging model of vascular development and remodelling." *Curr Opin Pharmacol* **12**(5): 608-614.
- Raible, D. W. and G. J. Kruse (2000). "Organization of the lateral line system in embryonic zebrafish." *J Comp Neurol* **421**(2): 189-198.
- Rand, J. H. (2003). "The antiphospholipid syndrome." *Annu Rev Med* **54**: 409-424.
- Razani, B., J. A. Engelman, et al. (2001). "Caveolin-1 null mice are viable but show evidence of hyperproliferative and vascular abnormalities." *J Biol Chem* **276**(41): 38121-38138.
- Reyon, D., S. Q. Tsai, et al. (2012). "FLASH assembly of TALENs for high-throughput genome editing." *Nat Biotechnol* **30**(5): 460-465.
- Riley, J. L., M. Mao, et al. (2002). "Modulation of TCR-induced transcriptional profiles by ligation of CD28, ICOS, and CTLA-4 receptors." *Proc Natl Acad Sci U S A* **99**(18): 11790-11795.
- Roberts, O. L., K. Holmes, et al. (2009). "ERK5 and the regulation of endothelial cell function." *Biochem Soc Trans* **37**(Pt 6): 1254-1259.
- Robu, M. E., J. D. Larson, et al. (2007). "p53 activation by knockdown technologies." *PLoS Genet* **3**(5): e78.
- Ross, R. (1999). "Atherosclerosis--an inflammatory disease." *N Engl J Med* **340**(2): 115-126.
- Rossi, J., L. Rouleau, et al. (2010). "Effect of simvastatin on Kruppel-like factor2, endothelial nitric oxide synthase and thrombomodulin expression in endothelial cells under shear stress." *Life Sci* **87**(3-4): 92-99.
- Ruppert, J. M., K. W. Kinzler, et al. (1988). "The GLI-Kruppel family of human genes." *Mol Cell Biol* **8**(8): 3104-3113.
- Russo, L., J. Gracia-Sancho, et al. (2012). "Addition of simvastatin to cold storage solution prevents endothelial dysfunction in explanted rat livers." *Hepatology* **55**(3): 921-930.
- Ryter, S. W., J. Alam, et al. (2006). "Heme oxygenase-1/carbon monoxide: from basic science to therapeutic applications." *Physiol Rev* **86**(2): 583-650.
- Saez, J. C., V. M. Berthoud, et al. (2003). "Plasma membrane channels formed by connexins: their regulation and functions." *Physiol Rev* **83**(4): 1359-1400.
- Saharinen, P., L. Eklund, et al. (2008). "Angiopoietins assemble distinct Tie2 signalling complexes in endothelial cell-cell and cell-matrix contacts." *Nat Cell Biol* **10**(5): 527-537.
- Sako, K., S. Fukuhara, et al. (2009). "Angiopoietin-1 induces Kruppel-like factor 2 expression through a phosphoinositide 3-kinase/AKT-dependent activation of myocyte enhancer factor 2." *J Biol Chem* **284**(9): 5592-5601.

- Sander, J. D., E. J. Dahlborg, et al. (2011). "Selection-free zinc-finger-nuclease engineering by context-dependent assembly (CoDA)." *Nat Methods* **8**(1): 67-69.
- Santoro, M. M., G. Pesce, et al. (2009). "Characterization of vascular mural cells during zebrafish development." *Mech Dev* **126**(8-9): 638-649.
- Schleef, R. R., M. P. Bevilacqua, et al. (1988). "Cytokine activation of vascular endothelium. Effects on tissue-type plasminogen activator and type 1 plasminogen activator inhibitor." *J Biol Chem* **263**(12): 5797-5803.
- Schrader, A. J., O. Lechner, et al. (2002). "CXCR4/CXCL12 expression and signalling in kidney cancer." *Br J Cancer* **86**(8): 1250-1256.
- Schulte-Merker, S. and D. Y. Stainier (2014). "Out with the old, in with the new: reassessing morpholino knockdowns in light of genome editing technology." *Development* **141**(16): 3103-3104.
- Segre, J. A., C. Bauer, et al. (1999). "Klf4 is a transcription factor required for establishing the barrier function of the skin." *Nat Genet* **22**(4): 356-360.
- Sehnert, A. J., A. Huq, et al. (2002). "Cardiac troponin T is essential in sarcomere assembly and cardiac contractility." *Nat Genet* **31**(1): 106-110.
- Semenza, G. L. and G. L. Wang (1992). "A nuclear factor induced by hypoxia via de novo protein synthesis binds to the human erythropoietin gene enhancer at a site required for transcriptional activation." *Mol Cell Biol* **12**(12): 5447-5454.
- Sen-Banerjee, S., S. Mir, et al. (2005). "Kruppel-like factor 2 as a novel mediator of statin effects in endothelial cells." *Circulation* **112**(5): 720-726.
- SenBanerjee, S., Z. Lin, et al. (2004). "KLF2 Is a novel transcriptional regulator of endothelial proinflammatory activation." *J Exp Med* **199**(10): 1305-1315.
- Senger, D. R., S. J. Galli, et al. (1983). "Tumor cells secrete a vascular permeability factor that promotes accumulation of ascites fluid." *Science* **219**(4587): 983-985.
- Serbedzija, G. N., E. Flynn, et al. (1999). "Zebrafish angiogenesis: a new model for drug screening." *Angiogenesis* **3**(4): 353-359.
- Shaik, S. S., T. D. Soltau, et al. (2009). "Low intensity shear stress increases endothelial ELR+ CXC chemokine production via a focal adhesion kinase-p38 β MAPK-NF- κ B pathway." *J Biol Chem* **284**(9): 5945-5955.
- Shi, H., B. Sheng, et al. (2013). "Kruppel-like factor 2 protects against ischemic stroke by regulating endothelial blood brain barrier function." *Am J Physiol Heart Circ Physiol* **304**(6): H796-805.
- Shields, J. M., R. J. Christy, et al. (1996). "Identification and characterization of a gene encoding a gut-enriched Kruppel-like factor expressed during growth arrest." *J Biol Chem* **271**(33): 20009-20017.
- Shioyama, W., Y. Nakaoka, et al. (2011). "Docking protein Gab1 is an essential component of postnatal angiogenesis after ischemia via HGF/c-met signaling." *Circ Res* **108**(6): 664-675.
- Simantov, R., J. M. LaSala, et al. (1995). "Activation of cultured vascular endothelial cells by antiphospholipid antibodies." *J Clin Invest* **96**(5): 2211-2219.
- Slater, S. C., R. D. Ramnath, et al. (2012). "Chronic exposure to laminar shear stress induces Kruppel-like factor 2 in glomerular endothelial cells and modulates interactions with co-cultured podocytes." *Int J Biochem Cell Biol* **44**(9): 1482-1490.
- Stainier, D. Y. (2001). "Zebrafish genetics and vertebrate heart formation." *Nat Rev Genet* **2**(1): 39-48.
- Stainier, D. Y., B. Fouquet, et al. (1996). "Mutations affecting the formation and function of the cardiovascular system in the zebrafish embryo." *Development* **123**: 285-292.

- Strazielle, N., J. F. Gherzi-Egea, et al. (2000). "In vitro evidence that beta-amyloid peptide 1-40 diffuses across the blood-brain barrier and affects its permeability." J Neuropathol Exp Neurol **59**(1): 29-38.
- Taichman, R. S., C. Cooper, et al. (2002). "Use of the stromal cell-derived factor-1/CXCR4 pathway in prostate cancer metastasis to bone." Cancer Res **62**(6): 1832-1837.
- Tano, N., H. W. Kim, et al. (2011). "microRNA-150 regulates mobilization and migration of bone marrow-derived mononuclear cells by targeting Cxcr4." PLoS One **6**(10): e23114.
- Tarbell, J. M., S. Weinbaum, et al. (2005). "Cellular fluid mechanics and mechanotransduction." Ann Biomed Eng **33**(12): 1719-1723.
- Taylor, J. S., I. Braasch, et al. (2003). "Genome duplication, a trait shared by 22000 species of ray-finned fish." Genome Res **13**(3): 382-390.
- Thisse, B., Pflumio, S., Fürthauer, M., Loppin, B., Heyer, V., Degraeve, A., Woehl, R., Lux, A., Steffan, T., Charbonnier, X.Q. and Thisse, C. (2001). Expression of the zebrafish genome during embryogenesis ZFIN Direct Data Submission, ZFIN.
- Thisse, C. and B. Thisse (2008). "High-resolution in situ hybridization to whole-mount zebrafish embryos." Nat Protoc **3**(1): 59-69.
- Thompson, M. A., D. G. Ransom, et al. (1998). "The cloche and spadetail genes differentially affect hematopoiesis and vasculogenesis." Dev Biol **197**(2): 248-269.
- Topper, J. N. and M. A. Gimbrone, Jr. (1999). "Blood flow and vascular gene expression: fluid shear stress as a modulator of endothelial phenotype." Mol Med Today **5**(1): 40-46.
- Tuomisto, T. T., H. Lumivuori, et al. (2008). "Simvastatin has an anti-inflammatory effect on macrophages via upregulation of an atheroprotective transcription factor, Kruppel-like factor 2." Cardiovasc Res **78**(1): 175-184.
- Turner, J. and M. Crossley (1999). "Mammalian Kruppel-like transcription factors: more than just a pretty finger." Trends Biochem Sci **24**(6): 236-240.
- Tzima, E., M. A. Del Pozo, et al. (2002). "Activation of Rac1 by shear stress in endothelial cells mediates both cytoskeletal reorganization and effects on gene expression." EMBO J **21**(24): 6791-6800.
- Tzima, E., M. A. del Pozo, et al. (2001). "Activation of integrins in endothelial cells by fluid shear stress mediates Rho-dependent cytoskeletal alignment." EMBO J **20**(17): 4639-4647.
- Tzima, E., M. Irani-Tehrani, et al. (2005). "A mechanosensory complex that mediates the endothelial cell response to fluid shear stress." Nature **437**(7057): 426-431.
- Tziros, C. and J. E. Freedman (2006). "The many antithrombotic actions of nitric oxide." Curr Drug Targets **7**(10): 1243-1251.
- Uchida, D., N. M. Begum, et al. (2003). "Possible role of stromal-cell-derived factor-1/CXCR4 signaling on lymph node metastasis of oral squamous cell carcinoma." Exp Cell Res **290**(2): 289-302.
- Uchida, D., T. Onoue, et al. (2009). "Vesnarinone downregulates CXCR4 expression via upregulation of Kruppel-like factor 2 in oral cancer cells." Mol Cancer **8**: 62.
- van Agtmaal, E. L., R. Bierings, et al. (2012). "The shear stress-induced transcription factor KLF2 affects dynamics and angiopoietin-2 content of Weibel-Palade bodies." PLoS One **7**(6): e38399.
- van Impel, A., Z. Zhao, et al. (2014). "Divergence of zebrafish and mouse lymphatic cell fate specification pathways." Development **141**(6): 1228-1238.
- van Rooijen, E., E. E. Voest, et al. (2010). "von Hippel-Lindau tumor suppressor mutants faithfully model pathological hypoxia-driven angiogenesis and vascular retinopathies in zebrafish." Dis Model Mech **3**(5-6): 343-353.
- van Rooijen, E., E. E. Voest, et al. (2009). "Zebrafish mutants in the von Hippel-Lindau tumor suppressor display a hypoxic response and recapitulate key aspects of Chuvash polycythemia." Blood **113**(25): 6449-6460.

- van Thienen, J. V., J. O. Fledderus, et al. (2006). "Shear stress sustains atheroprotective endothelial KLF2 expression more potently than statins through mRNA stabilization." Cardiovasc Res **72**(2): 231-240.
- van Tits, L. J., R. Stienstra, et al. (2011). "Oxidized LDL enhances pro-inflammatory responses of alternatively activated M2 macrophages: a crucial role for Kruppel-like factor 2." Atherosclerosis **214**(2): 345-349.
- van Vliet, J., L. A. Crofts, et al. (2006). "Human KLF17 is a new member of the Sp/KLF family of transcription factors." Genomics **87**(4): 474-482.
- Vasa, M., S. Fichtlscherer, et al. (2001). "Number and migratory activity of circulating endothelial progenitor cells inversely correlate with risk factors for coronary artery disease." Circ Res **89**(1): E1-7.
- Vermot, J., A. S. Forouhar, et al. (2009). "Reversing blood flows act through klf2a to ensure normal valvulogenesis in the developing heart." PLoS Biol **7**(11): e1000246.
- Waltenberger, J., L. Claesson-Welsh, et al. (1994). "Different signal transduction properties of KDR and Flt1, two receptors for vascular endothelial growth factor." J Biol Chem **269**(43): 26988-26995.
- Wang, L., P. Zhang, et al. (2011). "A blood flow-dependent klf2a-NO signaling cascade is required for stabilization of hematopoietic stem cell programming in zebrafish embryos." Blood **118**(15): 4102-4110.
- Wang, N., H. Miao, et al. (2006). "Shear stress regulation of Kruppel-like factor 2 expression is flow pattern-specific." Biochem Biophys Res Commun **341**(4): 1244-1251.
- Wang, W., C. H. Ha, et al. (2010). "Fluid shear stress stimulates phosphorylation-dependent nuclear export of HDAC5 and mediates expression of KLF2 and eNOS." Blood **115**(14): 2971-2979.
- Wang, X. Q., P. Nigro, et al. (2012). "Thioredoxin interacting protein promotes endothelial cell inflammation in response to disturbed flow by increasing leukocyte adhesion and repressing Kruppel-like factor 2." Circ Res **110**(4): 560-568.
- Wani, M. A., M. D. Conkright, et al. (1999). "cDNA isolation, genomic structure, regulation, and chromosomal localization of human lung Kruppel-like factor." Genomics **60**(1): 78-86.
- Wani, M. A., R. T. Means, Jr., et al. (1998). "Loss of LKLF function results in embryonic lethality in mice." Transgenic Res **7**(4): 229-238.
- Watson, O., P. Novodvorsky, et al. (2013). "Blood flow suppresses vascular Notch signalling via dll4 and is required for angiogenesis in response to hypoxic signalling." Cardiovasc Res **100**(2): 252-261.
- Weinstein, B. M., D. L. Stemple, et al. (1995). "Gridlock, a localized heritable vascular patterning defect in the zebrafish." Nat Med **1**(11): 1143-1147.
- White, C. R. and J. A. Frangos (2007). "The shear stress of it all: the cell membrane and mechanochemical transduction." Philos Trans R Soc Lond B Biol Sci **362**(1484): 1459-1467.
- Wilkinson, R. N. (2008). Hedgehog and TGF-beta family signalling in zebrafish blood and endothelial development, University of Oxford.
- Wilkinson, R. N., S. Elworthy, et al. (2013). "A method for high-throughput PCR-based genotyping of larval zebrafish tail biopsies." Biotechniques **55**(6): 314-316.
- Wong, A. L., Z. A. Haroon, et al. (1997). "Tie2 expression and phosphorylation in angiogenic and quiescent adult tissues." Circ Res **81**(4): 567-574.
- Wong, C. W., T. Christen, et al. (2006). "Connexin37 protects against atherosclerosis by regulating monocyte adhesion." Nat Med **12**(8): 950-954.
- Wu, C., F. Li, et al. (2013). "Abeta(1-42) disrupts the expression and function of KLF2 in Alzheimer's disease mediated by p53." Biochem Biophys Res Commun **431**(2): 141-145.

- Wu, J., C. S. Bohanan, et al. (2008). "KLF2 transcription factor modulates blood vessel maturation through smooth muscle cell migration." *J Biol Chem* **283**(7): 3942-3950.
- Yamawaki, H., S. Pan, et al. (2005). "Fluid shear stress inhibits vascular inflammation by decreasing thioredoxin-interacting protein in endothelial cells." *J Clin Invest* **115**(3): 733-738.
- Yang, L., X. Zhou, et al. (2013). "Role of Kruppel-like factor 2 and protease-activated receptor-1 in vulnerable plaques of ApoE(-/-) mice and intervention with statin." *Can J Cardiol* **29**(8): 997-1005.
- Yet, S. F., M. M. McA'Nulty, et al. (1998). "Human EZF, a Kruppel-like zinc finger protein, is expressed in vascular endothelial cells and contains transcriptional activation and repression domains." *J Biol Chem* **273**(2): 1026-1031.
- Yokoi, H., Y. L. Yan, et al. (2009). "Expression profiling of zebrafish sox9 mutants reveals that Sox9 is required for retinal differentiation." *Dev Biol* **329**(1): 1-15.
- Young, A., W. Wu, et al. (2009). "Flow activation of AMP-activated protein kinase in vascular endothelium leads to Kruppel-like factor 2 expression." *Arterioscler Thromb Vasc Biol* **29**(11): 1902-1908.
- Zhang, X., S. V. Srinivasan, et al. (2004). "WWP1-dependent ubiquitination and degradation of the lung Kruppel-like factor, KLF2." *Biochem Biophys Res Commun* **316**(1): 139-148.
- Zhang, Y., D. Liu, et al. (2010). "Secreted monocytic miR-150 enhances targeted endothelial cell migration." *Mol Cell* **39**(1): 133-144.
- Zhong, T. P., M. Rosenberg, et al. (2000). "gridlock, an HLH gene required for assembly of the aorta in zebrafish." *Science* **287**(5459): 1820-1824.
- Zou, Y. R., A. H. Kottmann, et al. (1998). "Function of the chemokine receptor CXCR4 in haematopoiesis and in cerebellar development." *Nature* **393**(6685): 595-599.